

# Experiments in hydrologic solute transport

THÈSE N° 6688 (2015)

PRÉSENTÉE LE 28 AOÛT 2015

À LA FACULTÉ DE L'ENVIRONNEMENT NATUREL, ARCHITECTURAL ET CONSTRUIT  
LABORATOIRE D'ÉCOHYDROLOGIE  
PROGRAMME DOCTORAL EN GÉNIE CIVIL ET ENVIRONNEMENT

ÉCOLE POLYTECHNIQUE FÉDÉRALE DE LAUSANNE

POUR L'OBTENTION DU GRADE DE DOCTEUR ÈS SCIENCES

PAR

Pierre Claude Jean QUELOZ

acceptée sur proposition du jury:

Prof. A. Berne, président du jury  
Prof. A. Rinaldo, directeur de thèse  
Dr Y. van der Velde, rapporteur  
Prof. M. Hrachowitz, rapporteur  
Prof. P. Perona, rapporteur



ÉCOLE POLYTECHNIQUE  
FÉDÉRALE DE LAUSANNE

Suisse  
2015



In rivers, the water that you touch is the last of what has passed  
and the first of that which comes; so with present time.  
— Leonardo da Vinci

To my mother...



# Acknowledgements

First of all, I express my deepest gratitude to my supervisor Professor Andrea Rinaldo, for his trust and continuous support during these four years, for his enthusiasm and great personality. Thanks for having taken me on board on this sturdy ship which has allowed me to end my long journey at EPFL pleasantly and safely.

A special thanks to Enrico Bertuzzo and Luca Carraro whose modeling expertise has been a very important contribution to my thesis. I also thank Bernard Sperandio, for the uncountable amount of time he spent collecting data on the field, helping with the lysimeter experiments or filtering my samples when I was ~~on-vacation~~ at conferences. Thanks to Bettina Schaepli for not having kicked my students out after I sent them knocking on her door to get some support on SEHR-ECHO. Our lab would have been bankrupted many times (. . . my experiments considerably contributing to this end) without the wise management of Anna Rothenbühler, to whom I am also very grateful. Many thanks to all other former and current colleagues and friends Andrea Giometto, Sylvia Zaoli, Lorenzo Mari, Jean-Marc Fröhlich, Serena Ceola, Francesco Carrara, Lorenzo Righetto, Javier Perez, Nathalie Ceperley, Theo Mande, Flavio Finger, Allyn Knox and Ana Clara Santos for their essential contribution to the nice working atmosphere in the lab and the good moments shared on the slopes.

I would like to thank the Central Environmental Laboratory (CEL) in EPFL, and particularly Dominique Grandjean and Michaël Bensimon, who have carried out countless chemical analyses of my samples and for their technical support. Thanks also to Htet Kyi Wynn from the ECOL laboratory who has lent me quite some equipment for extended periods.

I am also deeply grateful to Professor Suresh Rao for his support already since my first steps in this PhD, the inspiring, enthusiastic and catalytic discussions we shared (and a great visit of Verona!) and thanks to his former PhD student, now Professor Heather Gall for her kindness and warm welcome at Purdue University. Thanks to Franco Miglietta and his innovative ideas and insights, who showed me that experiments can actually be fun (between two inundations) and shared his fishing spots and fascinating anecdotes. I also thank Professor Gianluca Botter and Paolo Benettin for their expert contributions and welcome in Padova.

Many thanks to all students who contributed in this work, particularly Luca Carraro, Pascal Stalder and Federico Crocci and to my civilists Basile Perrenoud, Jo Besuchet and Ian Schori

## Acknowledgements

---

who brought their competences and allowed me to diversify my job. Many thanks to Belinda Bates, who spent several hours to considerably improve the writing of this thesis (and desperately tried to "britishize" my english!).

I would also like to thank the Swiss National Science Foundation for the generous financial support of this thesis.

Ma thèse n'aurait pas été si enrichissante sans mes amis de parcours, avec qui nous avons partagé tant de séminaires scientifiques (à Sat ou à la cafèt'): Sylvain, virtuose en son art (mais entouré de piètres disciples), Lorenzo et son inaltérable humour (néanmoins discutable), Antoine, toujours en quête d'aventures (en tous genres) et Flavio, suisse-allemand finalement bien adapté au laxisme romand (et aux us et coutumes jurassiennes; il ne partira pas avant une dernière damassine).

Un merci particulier aux coureurs "d'en-dessous" Tristan, Raph, Francesco, Marc et M. Matthe avec qui quelques paires de semelles ont été éparpillées le long de la Venoge (fébrilement remplacées au Sport Basement de San Francisco). Merci aux membres du laboratoire EFLUM/CRYOS pour tous les bons moments partagés lors de conférences ou à Sat. Je remercie également tous les autres amis de l'institut IIE, qui m'ont rendu ces quatre années très agréables et enrichissantes.

Cette thèse m'a également permis de consolider et de former d'incroyables amitiés à travers de nombreuses activités comme l'escalade, le ski ou la voile (sans oublier quelques apéros et repas !). Merci donc à mes anciens (et très anciens) collocataires Benoit Le B., Jakob et Gaudenz. Merci à Jakob et Patrick avec qui je pense partager la même vision du sport, mais surtout celle du réconfort que l'on trouve tout de suite après à la Bossette. Merci à mes amis ascendeurs et descendeurs, en particulier Evelyne, Jo et Fried et Marc H. Merci à tous les autres amis qui se reconnaîtront sans aucun doute ici et avec qui j'ai partagé d'innombrables expériences. Je leur suis tout autant reconnaissant.

Je remercie également de fond du cœur ma famille qui m'a toujours soutenu dans mes choix de vie, en particulier ma maman pour son amour et sa constante préoccupation pour mon bien-être, son compagnon François qui m'a ouvert les yeux sur la nature il y a déjà bien longtemps, et mon frère Antonin, pour toutes les moments que l'on a partagés, partage, et partagera encore longtemps.

Enfin, la plus belle découverte que j'ai pu faire pendant ces quelques années de recherche n'était finalement pas où je l'ai cherchée. Mille mercis à toi Belinda, pour ton amour et ta gentillesse. Merci pour avoir toujours respecté mes choix et pour m'avoir tant soutenu dans toutes mes entreprises, professionnelles et personnelles (et merci pour les bons gateaux !).

*Lausanne, May 6, 2015*

Pierre Q.

# Summary

This thesis deal with experimental, field and modeling studies on reactive solute transport within hydrologic control volumes. The substances used in open environments for plant protection and other purposes are likely to be flushed by rainfall and enter into the hydrologic system if they are not disposed of through a sewage network. This represents a significant hazard for receiving ecosystems. The concentrations observed in surface waters are often highly dynamic, because of the variability of the hydrologic drivers controlling solute transport. This makes surface water monitoring particularly laborious, thus calling for a better understanding, and description of hydrologic transport at relevant spatial and temporal scales.

The features of hydrologic transport are investigated under controlled conditions in a large weighing lysimeter, where all input (rainfall) and output (evapotranspiration and bottom discharge) fluxes are closely monitored. Random rainfall and large evapotranspiration (ET) fluxes dictated by two willows induce highly variable hydrologic conditions in the system. Fluorobenzoic acids (FBAs) as well as isotopically labeled water were used to unequivocally mark selected rainfall events. Chemical analyses were performed on samples of discharge and soil water collected through sampling ports in order to estimate the breakthrough curves of each tracer. Besides revealing unreported reactive behavior of the FBAs, these results demonstrate non stationary tracer responses that not only result from the transient precipitation forcing, but also from the variability in the ET-induced water deficits and how the output fluxes sample the water and solutes in storage under the prevalent moisture conditions.

The experimental data were further explored using a model based on travel time distributions (TTDs). Describing hydrologic transport using TTDs is becoming increasingly common in catchment hydrology, because it allows a collective measurement of many processes (climate forcing, internal mixing, flow pathways, etc.) into a single stochastic descriptor, therefore removing the need to estimate numerous physical parameters and circumventing the limited applicability of point-scale laws for structurally complex and heterogenous environments. This parsimonious model is able to reproduce the different tracer responses by keeping track of the age composition of the stored water and assessing the ways ET and discharge sample the available water ages in time. The results emphasize the effects of ET on solute transport, because it samples water of different ages (i.e. residence times) in the transport volume in regards to discharge and thereby strongly modifies the resulting TTDs. In this way it is possible to compare the respective roles of the hydrologic variability and reactivity attributes (namely plant uptake and microbial degradation) which affect the tracer responses and prevent a direct interpretation of the experimental breakthrough curves as TTDs.

## Summary

---

These experimental and modeled results highlight the importance of non stationary transport, often overlooked to interpret tracer data in catchment hydrology. This thesis demonstrates the benefits of tracer experiments towards the understanding of hydrologic systems undergoing reactive transport.

**Key words:** hydrology, solute transport, hydrologic transport, travel time, residence time, age, non stationarity, transport model, tracer, lysimeter.



# Résumé

Un nombre croissant de substances anthropogènes souvent issues des activités agricoles (pesticides, fertilisants, etc.) ou des zones urbaines (par ex. biocides) se retrouvent dans les eaux de surface. Utilisés dans des environnements ouverts, ces produits sont en général lessivés lors de précipitations et rentrent dans le cycle hydrologique naturel lorsqu'ils ne sont pas évacués dans le réseau d'eaux usées, ce qui peut présenter un risque potentiel pour les écosystèmes récepteurs. Les concentrations observées dans les eaux de surface sont souvent fortement dynamiques, ceci dû à la variabilité des processus hydrologiques qui contrôlent le transport de ces substances. Le suivi continu de la qualité des eaux de surface est donc une tâche particulièrement laborieuse, qui appelle à une meilleure compréhension et description du transport hydrologique à des échelles temporelles et spatiales appropriées afin de développer des outils d'évaluation et de prédiction.

Dans cette thèse, les caractéristiques du transport hydrologique sont examinées en conditions contrôlées dans un grand lysimètre de précision permettant la mesure des flux entrants (précipitation) et sortants (écoulement et évapotranspiration). La stochasticité des précipitations générées ainsi qu'une évapotranspiration conséquente provoquée par deux saules plantés dans le lysimètre induisent des conditions hydrologiques fortement variables. Plusieurs acides fluorobenzoïques (AFBs) et de l'eau avec une composition isotopique ( $^{18}\text{O}$  and  $^2\text{H}$ ) spécifique permettent le marquage non-équivoque de précipitations sélectionnées. Des échantillons d'eau du sol et de l'écoulement ont été analysés afin d'estimer la répartition des traceurs dans le temps et de calculer leurs courbes de restitution. En plus de révéler un comportement plus réactif des AFBs que ce qui peut être trouvé dans la littérature scientifique (examiné en détails par des expériences *ad hoc*), limitant ainsi leur intérêt et leur interprétation en tant que traceurs conservatifs, les résultats ont démontré que les réponses du système en terme de restitution de traceurs sont fortement non-stationnaires. Cette variabilité se manifeste non seulement à cause du caractère aléatoire des contraintes climatiques, mais également suite aux déficits hydriques induits par un flux d'évapotranspiration changeant et à la manière avec laquelle les flux sortants prélèvent l'eau et les substances dissoutes dans le système selon les conditions ambiantes d'humidité.

Les données expérimentales obtenues ont été ensuite examinées à l'aide d'un modèle de transport basé sur des distributions de temps de résidence hydrologique. Cette démarche est devenue de plus en plus fréquente en hydrologie de bassins versants, car elle permet d'intégrer tous les processus hydrologiques (forcing climatique, stocks et mélanges dans le bassin, trajectoires d'écoulement, etc.) en un unique descripteur stochastique. Cela permet d'éviter

## Résumé

---

l'estimation de nombreux paramètres physiques, qui limitent souvent l'applicabilité des lois physiques utilisées lors que l'on a affaire à des environnements complexes et caractérisés par une hétérogénéité prononcée. Ce modèle simple permet de reproduire convenablement les différentes réponses des traceurs en suivant l'évolution de la composition du stock interne en terme d'âge hydrologique (càd. le temps qu'une particule d'eau a passé à l'intérieur du système depuis son introduction) et en estimant la manière dont les flux d'évapotranspiration et d'écoulement prélèvent l'eau disponible du stock dans le temps. Ces résultats soulignent en particulier les conséquences importantes de l'évapotranspiration sur le transport de substances solubles, puisque l'eau prélevée est constituée d'âges diamétralement opposés à ceux qui constituent l'écoulement, ce qui modifie fortement les temps de résidence hydrologique qui en résultent. Cet exercice permet également de distinguer les effets des processus transitoires de transport hydrologique par rapport aux artefacts émanant de la réactivité spécifique de chaque traceur (à savoir phytoaccumulation/dégradation et dégradation microbienne) sur les différentes réponses observées.

Ces résultats expérimentaux et de modélisation attirent en particulier l'attention sur l'importance de l'instabilité temporelle des phénomènes de transport, bien souvent négligée en hydrologie de bassin versant afin de faciliter l'interprétation de données provenant de traceurs environnementaux. Cette thèse démontre les bénéfices apportés par l'utilisation de traceurs pour la compréhension et la description de systèmes hydrologiques. L'intérêt des traceurs est toutefois relativisé à cause de l'absence de candidat au comportement "idéal" (càd. identique au comportement de l'eau, également discuté pour les isotopes stables), ce qui nécessite le support de modèles appropriés permettant une évaluation correcte des processus intervenant dans le transport des substances solubles.

**Mots-clés :** hydrologie, transport de substances, transport hydrologique, temps de transit, temps de résidence, âge, instationarité, modèle de transport, traceur, lysimètre.

# Zusammenfassung

Die Anzahl und Menge von Menschenhand gemachter chemischer Verbindungen, oftmals landwirtschaftlicher (Pestizide, Dünger, usw.) oder urbaner (z.B. Biozide) Herkunft, die in Oberflächengewässer gelangen, nimmt stetig zu. Diese im Freien applizierten Substanzen werden vom Regen leicht ausgewaschen und gelangen, falls sie nicht durch Kanalsationssysteme aufgefangen werden, in den hydrologischen Kreislauf. Dort stellen sie eine mögliche Gefahr für die flussabwärts gelegenen Ökosysteme dar. Die in Oberflächengewässern gemessenen Konzentrationen sind, aufgrund der Dynamik der hydrologischen Prozesse kraft welcher das Wasser gelöste Stoffe transportiert, oft äusserst variabel. Aus diesem Grund ist die Überwachung von Oberflächengewässern äusserst aufwändig. Daher ist ein besseres Verständnis des hydrologischen Stofftransports in relevanten räumlichen und zeitlichen Auflösungen und die Entwicklung geeigneter Modelle notwendig.

In dieser Doktorarbeit werden die Eigenschaften des hydrologischen Stofftransports unter kontrollierten Bedingungen in grossen Lysimetern, in denen alle Zu- (regen) und Abflüsse (Verdunstung und Grundwasserabfluss) überwacht werden, untersucht. Zufällig generierte Regenfälle und hohe Verdunstung durch zwei in den Lysimetern gepflanzte Weiden führen zu höchst variablen Bedingungen im hydrologischen System. Mittels mehrerer Tracer aus der Familie der Fluorobenzoessäuren sowie Isotopen ( $^{18}\text{O}$  and  $^2\text{H}$ ) markiertes Wasser wurden benutzt um ausgewählte Regenereignisse zu kennzeichnen. Wasserproben aus verschiedenen Tiefen und dem Grundwasserabfluss wurden chemisch analysiert um die Durchbruchkurven jedes Tracers zu bestimmen. Die Resultate zeigen, neben bisher unbekanntem Verhalten der Fluorobenzoessäuren, instationäres Verhalten, das nicht lediglich auf den unregelmässigen Regen, sondern auch auf die Variabilität des verdunstungsbedingten Wasserdefizits und auf die zeitliche Abfolge in der Wasser und gelöste Stoff unter den herrschenden Bodenfeuchtigkeitsbedingungen in den Abfluss gelangen, zurückzuführen ist.

Mittels eines auf der Verteilung der Durchflusszeit basierenden Modells wurden die experimentellen Daten weiter analysiert. Aufgrund der Möglichkeit verschiedenste Prozesse (klimatische Einflüsse, interne Speicherung und Durchmischung, Abflusswege, usw.) mittels ein und derselben stochastischen Beschreibung zu kombinieren, weshalb die Abschätzung verschiedenster physikalischer Parameter entfällt und die beschränkte Anwendbarkeit von einfachen physikalischen Beziehungen für strukturell komplexe und heterogene Milieus umgangen wird, werden hydrologische Transportphänomene je länger je mehr durch Durchflusszeitverteilungen beschrieben. Dieses einfache Modell erlaubt eine angemessene Beschreibung des ungleichen Verhaltens der verschiedenen Tracer mittels der Verfolgung der Alterszusammensetzung des

## Zusammenfassung

---

gespeicherten Wassers und der Charakterisierung der Art und Weise wie sich die verfügbaren Wasseralter in Abfluss und Verdunstung wiederfinden. Die Resultate heben insbesondere den Einfluss der Verdunstung auf den Stofftransport hervor, weil Wasser völlig anderen Alters als jenes das durch den Grundwasserabfluss entweicht verdunstet wird. Die resultierenden, äusserst variablen Durchflusszeitsverteilungen werden dadurch stark verändert. Das Modell ermöglicht zudem die Abgrenzung der Auswirkungen der hydrologischen Transportprozesse von jenen der spezifischen Reaktionen der einzelnen Tracer (namentlich die Aufnahme durch Pflanzen und der mikrobiologische Abbau) welche den Abtransport der Tracer aus dem System beeinflussen und eine direkte Interpretation als eigentliche Durchflusszeitsverteilung der experimentellen Durchbruchkurven verunmöglichen.

Die Resultate der Experimente und Modelle unterstreichen die Wichtigkeit instationärer Transportphänomene, welche in der Hydrologie für lange Zeit vernachlässigt wurden um die Interpretation von Tracertests zu vereinfachen. Diese Doktorarbeit hebt die Wichtigkeit von Tracerexperimenten für das Verständnis und die Beschreibung hydrologischer Systeme hervor. Diese Experimente werden jedoch durch das Fehlen eines idealen Tracers (auch im Fall von stabilen Isotopen) erschwert, was geeignete Modelle unerlässlich macht.

**Stichwörter:** Hydrologie, Stofftransport, hydrologischer Transport, Laufzeit, Verweildauer, Alter, Instationarität, Transportmodell, Tracer, Lysimeter

## Riassunto

Un numero sempre maggiore di sostanze chimiche, spesso provenienti da attività agricole (pesticidi, fertilizzanti, ecc.) o aree urbane, viene riscontrato nelle acque superficiali. Queste sostanze, utilizzate in ambienti aperti, vengono dilavate dalle precipitazioni atmosferiche e, quando non opportunamente evacuate dalla rete fognaria, possono entrare nel ciclo idrologico e rappresentare una potenziale minaccia per gli ecosistemi riceventi. Le concentrazioni osservate nelle acque superficiali sono fortemente dinamiche, a causa della variabilità dei processi idrologici che ne governano il trasporto. Di conseguenza il monitoraggio delle acque superficiali è particolarmente laborioso e richiede una miglior comprensione del trasporto idrologico a scale spaziali e temporali appropriate, e lo sviluppo di specifici modelli.

In questa tesi, le caratteristiche del trasporto idrologico sono esaminate in condizioni controllate in un grande lisimetro, nel quale tutti i flussi entranti (precipitazioni atmosferiche) ed uscenti (evaporazione, percolazione) sono opportunamente misurati. Precipitazioni casuali e grandi tassi di evaporazione (grazie a due salici piantati nel lisimetro) determinano condizioni molto variabili nel sistema. Diversi acidi fluorobenzoidici (FABs) e dell'acqua con una combinazione isotopica specifica ( $^{18}\text{O}$  and  $^2\text{H}$ ) sono stati utilizzati per identificare univocamente gli eventi meteorici simulati. Sono state eseguite analisi chimiche su campioni d'acqua percolata al fine di determinare la distribuzione dei traccianti nel tempo e calcolarne le relative curve di distribuzione. Oltre a rivelare un comportamento più reattivo da parte degli FABs (analizzato in dettaglio attraverso esperimenti *ad hoc*) rispetto a quanto riportato in letteratura, i risultati hanno mostrato che la risposta del sistema in termini di restituzione dei traccianti è fortemente non-stazionaria. Questa non-stazionarietà si manifesta non solamente a causa del carattere aleatorio delle precipitazioni, ma anche del deficit idrico indotto dal tasso d'evapotraspirazione variabile e della maniera con la quale i flussi uscenti portano con se acqua e sostanze disciolte nel sistema in funzione delle condizioni d'umidità.

I dati sperimentali così ottenuti sono stati in seguito esaminati per mezzo di un modello di trasporto basato sulle distribuzioni dei tempi di residenza. Questo approccio è diventato sempre più frequente nello studio dell'idrologia dei bacini, poiché permette d'integrare tutti i processi idrologici (forzanti climatiche, volumi accumulati e miscelati nei bacini, traiettorie di deflusso, ecc.) in un unico descrittore stocastico. Questo permette di evitare la stima di diversi parametri fisici, che di fatto limitano l'applicabilità delle leggi fisiche utilizzate in presenza di ambienti complessi e caratterizzati da pronunciata eterogeneità.

Questo semplice modello permette di riprodurre adeguatamente le diverse risposte dei traccianti seguendo l'evoluzione della composizione del volume d'acqua interno in termini di

## Riassunto

---

età idrologica (il tempo che una particella d'acqua necessita per percorrere l'intero sistema) et stimando il modo con il quale i flussi d'evapotraspirazione e percolazione evolvono nel tempo. Questi risultati evidenziano le importanti conseguenze che l'evapotraspirazione ha sul trasporto delle sostanze disciolte, poiché l'acqua prelevata contiene età idrologiche molto diverse a quelle della percolazione, fatto che modifica radicalmente i tempi di residenza idrologici risultanti. Tale esercizio permette inoltre di distinguere gli effetti dei processi transitori di trasporto idrologico da quelli derivanti dalla reattività specifica di ogni tracciante (fitoaccumulazione/degradazione e degradazione biologica).

Questi risultati sperimentali e modellistici sottolineano l'importanza dell'instabilità temporale dei fenomeni di trasporto, spesso trascurati nell'idrologia dei bacini al fine di semplificare l'interpretazione dei dati provenienti da traccianti ambientali. Questa tesi evidenzia l'importanza dell'utilizzo di traccianti nella comprensione e descrizione dei sistemi idrologici. L'opportunità di utilizzare tali traccianti è tuttavia condizionata dall'assenza di un candidato dal comportamento "ideale" e dunque dalla necessità di avere il supporto di modelli adeguati, che consentano una valutazione corretta dei processi di trasporto relativi alle sostanze disciolte.

**Parole chiave :** idrologia, trasporto solido, trasporto idrologico, tempo di transito, tempo di residenza, età, non stazionarietà, modello di trasporto, tracciante, lisimetro.

# Contents

<b>Acknowledgements</b>	<b>i</b>
<b>Summary (English/Français/Deutsch/Italiano)</b>	<b>iii</b>
<b>1 Introduction</b>	<b>1</b>
1.1 Motivation and context . . . . .	1
1.2 Hydrologic flow and transport modeling . . . . .	2
1.3 Travel time distributions . . . . .	4
1.4 Tracers . . . . .	10
1.5 Lysimeters as hydrologic systems . . . . .	13
1.6 Research questions and structure of the thesis . . . . .	14
<b>2 Transport of fluorobenzoate tracers in a vegetated hydrologic control volume: Experimental results</b>	<b>17</b>
2.1 Introduction . . . . .	18
2.2 Materials and methods . . . . .	20
2.2.1 System setup . . . . .	20
2.2.2 Selection of suitable tracers . . . . .	22
2.2.3 Tracer analysis . . . . .	24
2.2.4 Tracer sampling . . . . .	25
2.2.5 Rainfall and tracer applications . . . . .	25
2.2.6 Tracer validation by leaching test . . . . .	26
2.2.7 <i>Post hoc</i> tracer reactivity testing . . . . .	27
2.3 Results . . . . .	31
2.3.1 Hydrologic fluxes . . . . .	31
2.3.2 Tracer dynamics and fluxes . . . . .	36
2.4 Discussion . . . . .	40
2.4.1 Temporally displaced injections . . . . .	40
2.4.2 Sequenced multiple tracer injections . . . . .	42
2.4.3 On reactivity . . . . .	44
2.5 Conclusions . . . . .	47

## Contents

---

<b>3</b>	<b>Transport of fluorobenzoate tracers in a vegetated hydrologic control volume: Theoretical inferences and modeling</b>	<b>49</b>
3.1	Introduction . . . . .	50
3.2	Methods . . . . .	51
3.2.1	Experimental data . . . . .	51
3.2.2	Travel-time formulation of transport and age-selection schemes . . . . .	51
3.2.3	Solute transport . . . . .	55
3.2.4	Application to fluorobenzoate transport . . . . .	56
3.2.5	Details on analytical and numerical methods . . . . .	57
3.2.6	Model calibration . . . . .	58
3.3	Results . . . . .	59
3.4	Discussion . . . . .	63
3.5	Conclusions . . . . .	65
<b>4</b>	<b>Water stable isotopes: a transport experiment</b>	<b>67</b>
4.1	Introduction . . . . .	68
4.2	Theory . . . . .	69
4.2.1	Basic definitions . . . . .	69
4.2.2	Isotopic fractionation . . . . .	70
4.3	Material and methods . . . . .	72
4.3.1	General experimental set-up . . . . .	72
4.3.2	Preparation and application of the isotopically labelled pulse . . . . .	72
4.3.3	Sampling, conditioning and isotope analysis . . . . .	73
4.3.4	Evaporation model . . . . .	73
4.4	Results . . . . .	74
4.4.1	Isotopes and difluorobenzoic acids breakthrough . . . . .	74
4.4.2	Evaporation estimation . . . . .	75
4.4.3	Pulse contribution in the discharge by accounting for evaporation enrichment . . . . .	78
4.5	Discussion . . . . .	82
4.6	Conclusions . . . . .	83
<b>5</b>	<b>Catchment-scale experimental site and pesticides dynamics screening</b>	<b>85</b>
5.1	Introduction . . . . .	86
5.2	Agricultural practices . . . . .	86
5.3	Catchment gauging . . . . .	90
5.3.1	Water-level gages . . . . .	90
5.3.2	Flow gauging and rating curves . . . . .	90
5.3.3	Rain gauges . . . . .	92
5.4	Pesticide sampling campaigns . . . . .	92
5.5	Results and discussion . . . . .	94
5.5.1	Rating curves . . . . .	94
5.5.2	Discharge and rainfall . . . . .	94



5.5.3 Pesticide concentrations . . . . .	97
5.6 Detailed chemographs . . . . .	100
5.7 Conclusions . . . . .	113
<b>6 Conclusions and perspectives</b>	<b>115</b>
<b>A Details of the lysimeter experiment</b>	<b>121</b>
A.1 Lysimeter filling . . . . .	122
A.2 Load cells . . . . .	123
A.3 Willow development . . . . .	126
<b>B FDR installation and soil specific calibration</b>	<b>127</b>
B.1 Description of the equipment . . . . .	127
B.2 Calibration procedure . . . . .	128
<b>C Lysimeter discharge flow measurement and sampling details</b>	<b>131</b>
C.1 Description of the discharge device . . . . .	131
C.2 Soil water sampling . . . . .	133
<b>D Experimental details on the leaching test</b>	<b>135</b>
<b>E Development of a wireless controller for flexible sampling strategies based on real-time flow monitoring</b>	<b>137</b>
E.1 Context . . . . .	137
E.2 Prototype concept . . . . .	137
E.3 Sampling model . . . . .	139
E.4 Technical equipment . . . . .	141
<b>Bibliography</b>	<b>157</b>
<b>Publications and conference proceedings</b>	<b>159</b>
<b>Curriculum Vitae</b>	<b>163</b>



# 1 Introduction

## 1.1 Motivation and context

Due to a variety of human activities, surface waters are exposed to many anthropogenic compounds such as nutrients, biocides, pharmaceuticals or personal care products (PPCPs). While pharmaceuticals and PPCPs are normally released to the environment in urban areas through water network overflows and waste water effluents, nutrients and biocides (englobing herbicides, pesticides and fungicides) mainly originate from agricultural activities. Both classes of pollutants originate from non-point source and belong to some of the most harmful substances for the natural environment as they are specifically designed to kill, repel or inactivate living organisms (*Chèvre et al.*, 2006). Although they are usually designed to take action where they are applied, they are easily mobilized by rainfall (or directly by spraying solutions) and carried through the hydrologic cycle. Due to the persistence of some of these substances, drainage and runoff on agricultural areas readily transport them to receiving surface waters such as streams, rivers and ultimately lakes and seas, thus posing a threat to aquatic ecosystems. Laboratory studies have demonstrated the toxicological effects of many biocides on living organisms (e.g. *El-Sheekh et al.*, 1994; *Ma et al.*, 2002; *Vallotton et al.*, 2009), and eutrophication due to nutrient excess is commonplace. Nevertheless, today's yield-focused agriculture still largely relies on the use of fertilizers and crop protection products of various kinds, increasing the stress on natural environments.

Due to an increasing number of available commercial products with various chemical components affecting their persistence, mobility and toxicity, assessing the exposure and the risk for downstream ecosystems is an urgent challenge. The concentration of such compounds in surface waters is often highly spatially and temporally variable, due to local and one-time applications and to the variability of the climatic forcing which controls their transport (Figure 1.1). In such a context, the estimation of total export (i.e. the substance loss, from the farmer's point of view) is a good indicator of the environmental risk, yet it is insufficient for accurate analysis of the impacts on exposed organisms as they may be differently susceptible to acute, chronic or sequential exposure (see e.g. *Vallotton et al.*, 2009).

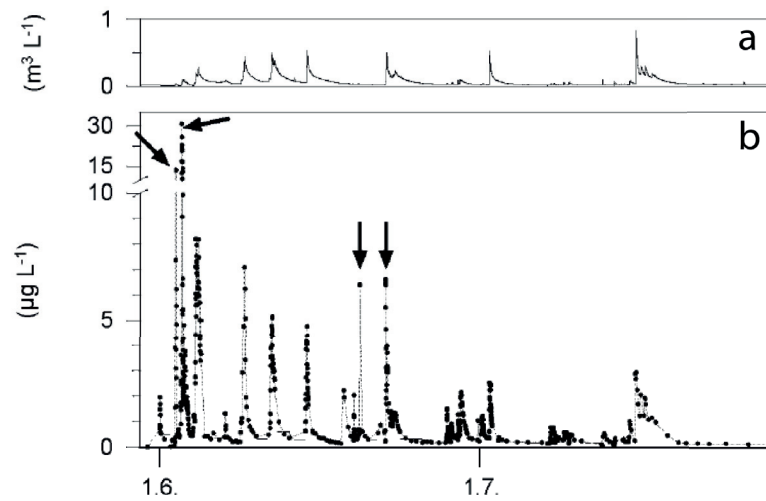


Figure 1.1: Discharge flow (a) and atrazine concentration dynamics (b) in June and July in a small agricultural catchment near Lake Greifensee (Switzerland). The arrows indicate the timing of atrazine applications (from *Leu*, 2003).

Although recent progresses in analytical technologies have improved and facilitated the measurements of water contaminants, they remain costly. Further, monitoring of a site requires intensive and long-term sampling in order to obtain kinetics of the order of the hydrologic lead time and seasonal variations. In this framework, modeling is particularly useful, because it may be applied to arbitrary geomorphologic and climatic settings and to substances affected by specific biogeochemical reactions. In this way, modeling serves as an ecological risk assessment (e.g. to identify sensitive areas, evaluate concentration dynamics) or as a management tool elaborating agricultural strategies to minimize substance losses. However, acknowledging the relevance of short-term dynamics for the quantification of environmental impacts, models should be based on hydrologic transport processes (main and common carriers for these substances) at pertinent scales in order to reproduce these fluctuations. The limitations of the applicability of point-scale physical laws for the movement of water due to the structural complexity and heterogeneity of subsurface environments signal a need for the development and proof of a more general theory to describe hydrologic and solute transport at larger spatial scales, which has been the main focus of this thesis. This is also likely the reason why dynamic modeling of biocides at catchment scale has rarely been done until now (e.g. *Squillace and Thurman*, 1992; *Luo et al.*, 2008; *Zanardo et al.*, 2012; *Bertuzzo et al.*, 2013), focusing essentially on limited parts of the catchment whose substance export contribution to surface water is the highest (e.g. *Rao et al.*, 1974; *Flury*, 1995; *Leu et al.*, 2004; *Freitas et al.*, 2008; *Frey et al.*, 2009).

## 1.2 Hydrologic flow and transport modeling

Models to assess surface water quality by predicting runoff, erosion and chemical transport began to be developed in 1970 after the U.S. Clean Water Act. The modeling at that time

## 1.2. Hydrologic flow and transport modeling

---

was based on deterministic approaches (see e.g. *Knisel*, 1980; *Leonard and Knisel*, 1987), such as the more recent and still largely used SWAT model (e.g. *Arnold et al.*, 1993; *Luo et al.*, 2008; *Lam et al.*, 2010; *Setegn et al.*, 2010; *Talebizadeh et al.*, 2010). These models are usually limited to rainfall-driven solute transport, because percolation in the subsurface is based on the saturated hydraulic conductivity of the soil layer (*Arnold et al.*, 1993) and fast transport through preferential flowpaths (e.g. macropores) is therefore not taken into account (*Frey et al.*, 2009; *Zanardo et al.*, 2012). Multiple studies have emphasized the event-driven character of herbicide losses in surface water (e.g. *Leu et al.*, 2005, 2010), which is deemed crucial for an accurate prediction of concentration dynamics and load export in stream water, considering the sparse and season-dependent applications of these products (*Kladivko et al.*, 2001).

Acknowledging the importance of macropore flow for the rapid movement of solutes through soils (see e.g. *Beven and Germann*, 1982), so-called dual-domain models became popular (*Simunek et al.*, 1998; *Christiansen et al.*, 2004; *Malone et al.*, 2004; *Larsbo et al.*, 2005), adding a supplementary fast-flow component to the hydrologic transport domain due to preferential flow pathways. This addition has considerably improved the ability to reproduce the observed breakthrough of solutes in the outflow (e.g. *Larsson et al.*, 2007). However, these models are characterized by a large number of (mainly physical) parameters, which are not always easy to measure and may not be representative of a complete setting with pronounced heterogeneity at large scales. This limits their applicability in natural environments, in particular for prediction purposes (*Tiktak et al.*, 2006).

In order to overcome these problems of so many unknown parameters (and their resulting uncertainty) of deterministic models, simpler models were developed as screening tools to assess catchment vulnerability to diffuse herbicide loss based on the premise that most export loads occur through fast-flow bypasses. Based on long-term data, the ratio of fast-flow to total discharge is used as an indicator for herbicide losses (*Siber et al.*, 2009; *Leu et al.*, 2010). Although such models were able to explain interannual and spatial variability only by relying on long-term discharge data, they are limited to the ranking of catchment vulnerability and are thus unable to predict concentration dynamics at short time-scales. The latter is typically vital for toxicological studies.

More recently, water quality models have used the bulk hydrologic response of catchments as the transport component of substances. This theory, first proposed by *Rinaldo and Marani* (1987), introduces mass response function (MRF) as the probability density function (pdf) describing the random retention time of water particles conditional on the input time in a hydrologic system (Figure 1.2). This approach, later refined and leading to the emergence of time-variant travel time distributions (TTDs, see section 1.3), has been largely discussed in its various forms over the last decade, but only applied to a limited number of solutes transported at catchment scales (*Botter et al.*, 2006; *van der Velde et al.*, 2010; *Zanardo et al.*, 2012; *Bertuzzo et al.*, 2013). The reason is that despite the great advantage of combining physical, chemical or biological processes affecting transport into a single probability distribution (e.g. *McGuire et al.*, 2007; *Beven*, 2012), the form of the ensuing pdf is highly variable and remains difficult to

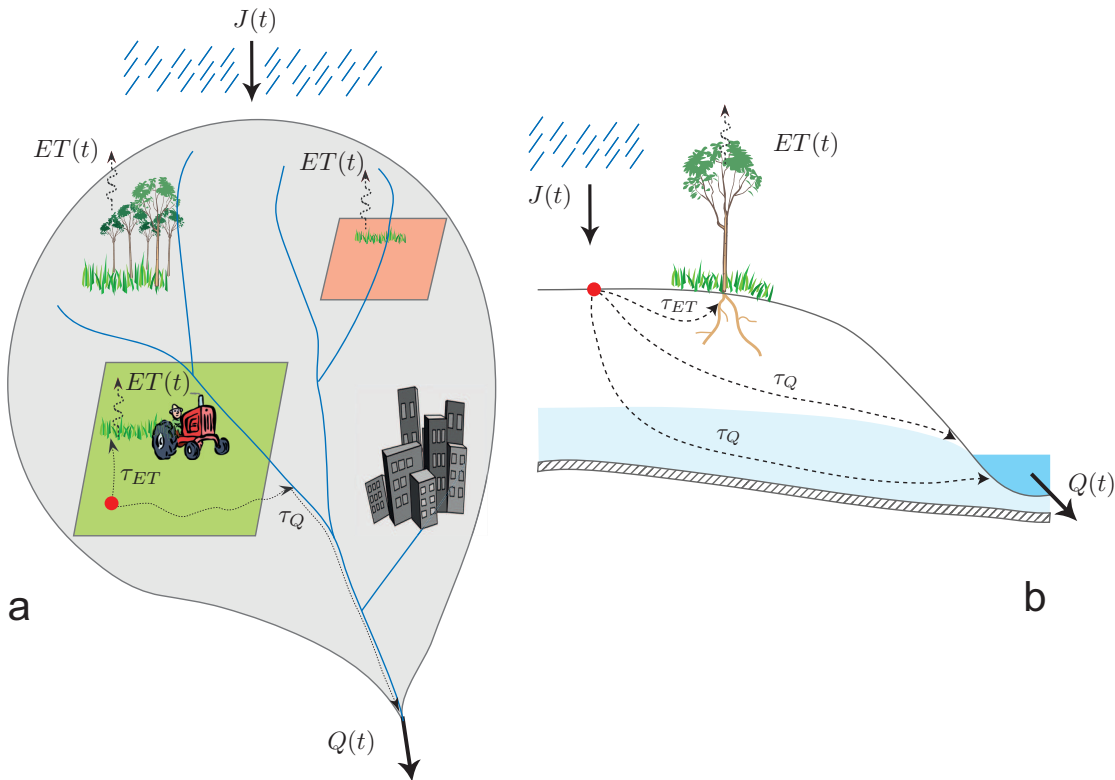


Figure 1.2: Schematic illustration of the concept of travel time ( $\tau = t - t_i$ ) of a particle in a catchment (a) and in a hillslope (b).  $\tau_Q$  and  $\tau_{ET}$  defines the travel time of the particles exiting the system in the discharge or in the evapotranspiration flux respectively. Based on Botter et al. (2010).

measure in a real hydrologic system (e.g. Rinaldo and Marani, 1987; Rinaldo et al., 2006a,b; Fiori and Russo, 2008; Darracq et al., 2010; Hrachowitz et al., 2009a, 2010a, 2013; van der Velde et al., 2010, 2012, 2014). Besides, it has lately been recognized that variability of climatic forcing and the pronounced non linearity of some catchment processes can cause the TTDs to show a significant time variance (e.g. Fiori and Russo, 2008; Botter et al., 2010; Hrachowitz et al., 2010a; van der Velde et al., 2010; Botter, 2012; Harman, 2015). Thus, current pitfalls still prevent the expression of a general form for TTDs. This thesis explores the TTDs of reactive transport to progress towards more efficient water quality models.

### 1.3 Travel time distributions

Travel time is defined as the time elapsed since injection of a particle (e.g. a water parcel or a solute molecule) into a hydrologic system until its exit through an output flux (e.g., discharge or evapotranspiration) (Figure 1.2). This concept has gained particular relevance in light of the so-called *old-water paradox*, which notes the significant contribution of water originating from antecedent rainfall events into the current discharge. A sizable part of the discharge

### 1.3. Travel time distributions

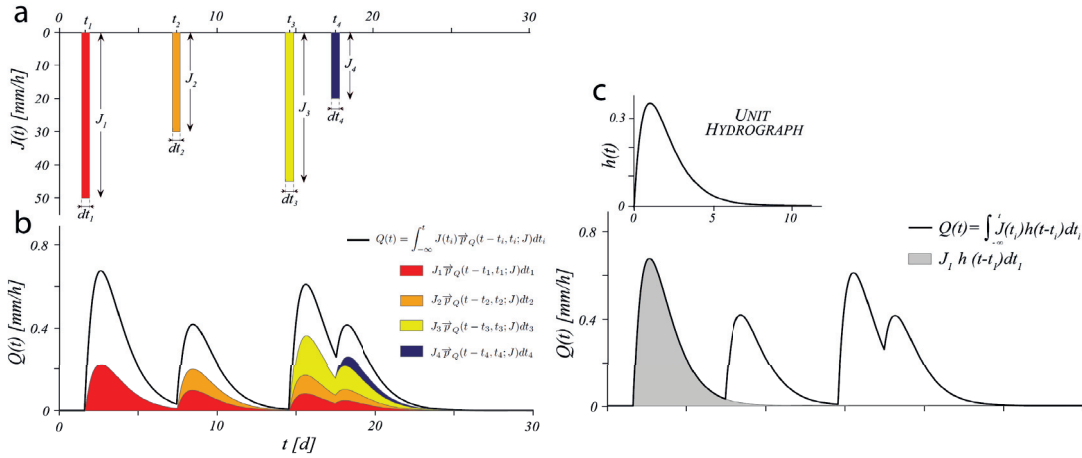


Figure 1.3: Graphical representation of the meaning of water ages and travel time  $\bar{p}_Q(t - t_i, t_i; J)$ . For every time  $t$ , the discharge  $Q(t)$  (b) is composed by water of different ages ( $t - t_i$ ) depending on the time the water particles have been injected ( $t_i = t_{1,2,3,4}$ ) through rainfall (a). The white area in (b) represents the contribution of water injected earlier than  $t_1$ . The comparison with the unit hydrograph (c) which does not distinguish the age structure of exiting particles is provided (adapted from *Botter et al., 2010*).

volume is already contained in the storage prior to the event, i.e. "older" water (*Kirchner, 2003; McDonnell et al., 2010*). It differs from the "conventional hydrologic response", i.e. the discharge response to a given rainfall, in as much as the latter is controlled by the celerity of the pressure wave induced by a precipitation event, whereas travel time looks in a lagrangian framework at the actual velocities of each individual particle contained in a pulse (*Beven, 1981*). The combination of water of different ages simultaneously exiting the system in the discharge is quantitatively equivalent to the hydrologic response at the same time, as illustrated in Figure 1.3, but the later does not allow the identification of the water ages that compose the flux. This is obviously relevant when the different ages in the storage are characterized by specific chemical attributes.

Travel time distributions are very efficient descriptors of catchment-scale transport processes, as they describe into a single attribute the effects of climate forcing, sources, storages or flow pathways on the transfer of a water (or solute) pulse from the input to the output of a hydrologic system (e.g. *McGuire and McDonnell, 2006; McGuire et al., 2007; Beven, 2012*). These effects are relevant to models of the hydrologic response (Figure 1.3), and become particularly important for solute transport schemes at catchment scale. Here, the chemical composition of the water particles released from any source zone through rainfall is significantly affected by their travel times to the control section. For non-reactive solutes, travel times are the direct transfer functions from input to output chemical fluxes. Conversely, for reactive solutes, travel times are in addition the drivers of chemical, physical or biological mass exchange processes like e.g. degradation/removal processes occurring along the hydrologic pathways. The effects of geomorphology, soils, climate and vegetation are directly reflected in the TTDs

## Chapter 1. Introduction

---

(e.g. *Rodriguez-Iturbe and Valdes*, 1979; *Rinaldo and Marani*, 1987; *Rinaldo et al.*, 1989; *Weiler et al.*, 2003; *McGuire et al.*, 2007; *Fiori and Russo*, 2008; *Hrachowitz et al.*, 2009a,b). Yet the effects of certain physical processes on the temporary storage and release of water are still poorly understood, in particular because they show non linear and non-stationary behaviors (*Weiler and McDonnell*, 2006; *Botter et al.*, 2010). The non-stationarity of the TTDs emerges due to the transient behavior of the hydrologic forcing, originating from the time variability of the rainfall forcing. Simply speaking, a water pulse injected at a given time  $t_i$  will stay longer within a hydrologic control volume  $V$  if no further significant rainfall occurs (resulting in a long mean travel time). Then if a long sequence of rainfall follows the injection, forcing the pulse through the volume and therefore leading to a shorter mean travel time. Further, evaporation and transpiration (often combined and referred to as evapotranspiration or ET for short) can induce a soil water deficit and therefore also affect the resulting hydrologic fluxes and travel times. It is worth noting that ET samples available stored water differently from how discharge does, requiring to describe both the travel times of water exiting as discharge and ET (*Botter et al.*, 2010). Recent studies have also stressed the importance of internal mixing dynamics, which control the availability of water pools of a given age for discharge or ET and which shape the TTDs (*Hrachowitz et al.*, 2009b; *Botter et al.*, 2011; *Hrachowitz et al.*, 2011; *Rinaldo et al.*, 2011; *Botter*, 2012; *van der Velde et al.*, 2012; *Benettin et al.*, 2013a; *Hrachowitz et al.*, 2013; *van der Velde et al.*, 2014). In a physical sense, catchment mixing should be seen as the functioning state of the various flow pathways in a hydrologic system which determines the overall combination of "old" water traveling along slow or tortuous pathways with "new" water shortcutting through faster transport channels. As the activation or deactivation of transport processes and flow pathways are closely related to wetness conditions (e.g. *Beven and Germann*, 1982, and references therein), mixing may also be a time-variant process (see e.g. *van der Velde et al.*, 2014).

The stochastic forcing and the pronounced non-linearity and non-stationarity of hydrologically relevant processes suggests strong variability in the TTDs which gives rise to the distinction between forward and backward TTDs. Forward TTDs, denoted by the symbol  $\bar{p}$  hereafter, describe the TTD associated with a water parcel injected at a given time  $t_i$ . In contrast, backward TTDs ( $\bar{p}$ ) describe the pdf of the time spent by a water parcel in the hydrological volume exiting through a control section (e.g. as discharge or ET) at a given time  $t$  (*Niemi*, 1977; *Rinaldo et al.*, 2011; *Cvetkovic et al.*, 2012). One can further define the residence time distribution (RTD), referred to as  $p_S$ , which characterizes the distribution of ages of all water particles contained within the volume  $V$  at time  $t$ . Hence, travel time coincides to residence time at the exit of the control volume. Forward and backward TTDs would only coincide under unrealistic hydrologic settings prompting time invariance and rainfall-runoff transformations (*Botter et al.*, 2011; *Rinaldo et al.*, 2011). Chapter 3 gives more detail about the differences between these distributions, using a case study for their derivation.

The theoretical framework defining the different forms of travel and residence time has been set and refined in various papers (e.g. *Botter et al.*, 2010, 2011; *Hrachowitz et al.*, 2010a; *Rinaldo et al.*, 2011; *Botter*, 2012; *van der Velde et al.*, 2012, 2014; *Harman*, 2015, and references



therein), but it is worth summarizing the most important mathematical relations and clarify the notation used as an introduction to this thesis.

To illustrate the concepts above, let us assume a control volume  $V$  which represents a catchment, a hillslope, or any hydrologic system with defined boundaries (note that routing through channel networks is neglected, which limits a direct application to small basins). Identifying rainfall  $J(t)$  as the only input flux, with discharge  $Q(t)$  and evapotranspiration  $ET(t)$  as the output fluxes, the water balance for the water storage  $S(t)$  contained in  $V$  is:

$$\frac{dS(t)}{dt} = J(t) - Q(t) - ET(t). \quad (1.1)$$

A water particle entering  $V$  at time  $t_i$  and exiting the system at  $t$  has an exit time of  $\tau = t - t_i$ . Treating the transport of water particles through  $V$  as a stochastic process, the exit time  $\tau$  is random variable whose pdf is written  $p_{ex}$ . As detailed above, the pdf of the exit time is likely to depend on the state of the system at the time of injection  $t_i$  and the evolution of this state until the particle exits the system. This leads to a more explicit notation of the pdf as  $\vec{p}_{ex}(t - t_i, t_i; J)$ . The probability that a particle injected at time  $t_i$  is still within  $V$  at time  $t$  is the cumulative density function:

$$\vec{P}_{ex}(t - t_i, t_i; J) = 1 - \int_0^{t-t_i} \vec{p}_{ex}(x, t_i; J) dx. \quad (1.2)$$

The total storage at time  $t$  is consequently the addition of all injections at  $t_i < t$  that are still in storage at time  $t$ :

$$S(t) = \int_{-\infty}^t J(t_i) \vec{P}_{ex}(t - t_i, t_i; J) dt_i. \quad (1.3)$$

Using Leibniz's rule, the change in storage  $S(t)$  is described as:

$$\frac{dS(t)}{dt} = J(t) - \int_{-\infty}^t J(t_i) \vec{p}_{ex}(t - t_i, t_i; J) dt_i, \quad (1.4)$$

which becomes, with the substitution in Eq. 1.1:

$$Q(t) + ET(t) = \int_{-\infty}^t J(t_i) \vec{p}_{ex}(t - t_i, t_i; J) dt_i. \quad (1.5)$$

Eq. 1.5 describes the output fluxes in terms of the input flux, with a time-variant transfer function  $\vec{p}_{ex}$ .  $ET(t)$  and  $Q(t)$  can only be distinguished if two new random variables describing the respective exit time to one or the other output flux is defined. For any time  $t_i$ , there will be a fraction  $\theta(t_i)$  of the particles injected at this time that will ultimately leave the system as discharge  $Q(t)$ , with the remaining part  $(1 - \theta(t_i))$  leaving as evapotranspiration  $ET(t)$ :

$$\vec{p}_{ex}(t - t_i, t_i; J) = \theta(t_i) \vec{p}_Q(t - t_i, t_i; J) + [1 - \theta(t_i)] \vec{p}_{ET}(t - t_i, t_i; J), \quad (1.6)$$

Here  $\vec{p}_Q$  is the forward TTD of the particles leaving in  $Q(t)$  and  $\vec{p}_{ET}$  of the particles leaving in

## Chapter 1. Introduction

---

$ET(t)$ . The respective output fluxes can now be expressed individually:

$$Q(t) = \int_{-\infty}^t J(t_i)\theta(t_i)\vec{p}_Q(t-t_i, t_i; J)dt_i; \quad (1.7a)$$

$$ET(t) = \int_{-\infty}^t J(t_i)[1-\theta(t_i)]\vec{p}_{ET}(t-t_i, t_i; J)dt_i. \quad (1.7b)$$

Note the resemblance of Eq. 1.7a to the unit hydrograph (*Sherman*, 1932):

$$Q(t) = \int_{-\infty}^t J(t_i)h(t-t_i)dt_i. \quad (1.8)$$

Eq. 1.8 assumes linearity and invariance (or stationarity) of the transfer function which can therefore be seen as a convolution operator. However, there is no requirement that the water exiting the system at  $t$  is the same as that which entered at  $t_i$ , which is a limiting factor when water quality is at stake, and strongly reduces the significance of non-stationary transport processes. This is the reason why the unit hydrograph can be successfully applied in a number of cases. Instead, the transfer function of Eq. 1.7a, is dependent on the injection time  $t_i$  and on the entire rainfall sequence that follows the injection, and keeps track of each individual water particle in terms of injection and exit time.

Now, let us consider a reactive solute already dissolved in the water when injected (i.e. non-point source) whose solute mass balance reads:

$$\frac{dM(t)}{dt} = \phi_J(t) - \phi_Q(t) - \phi_{ET}(t) + \left(\frac{dM(t)}{dt}\right)_r, \quad (1.9)$$

where  $\phi_X(t) = C_X(t)X(t)$  is the mass flux associated with rainfall  $J$ , discharge  $Q$  or evapotranspiration  $ET$ .  $X(t)$  represents the flow magnitude at time  $t$  of each flux and  $C_X(t)$  the corresponding flux concentration at  $t$ .  $(dM(t)/dt)_r$  is the soluble mass loss owing to biological, chemical or physical degradation/removal processes. Similarly to Eq. 1.3, the stored solute mass in storage  $M(t)$  can be described as the mass that has not yet exited  $V$  at time  $t$  given the cumulative density function of the exit time:

$$M(t) = \int_{-\infty}^t J(t_i)C(t-t_i, t_i)\vec{P}_{ex}(t-t_i, t_i; J)dt_i, \quad (1.10)$$

where  $C(t-t_i, t_i)$  denotes the concentration associated with the injection at  $t_i$  evaluated at  $t-t_i$ . Differentiating Eq. 1.10 with respect to  $t$  gives:

$$\begin{aligned} \frac{dM(t)}{dt} = J(t)C_J(t) - \int_{-\infty}^t J(t_i)C(t-t_i, t_i)\vec{p}_{ex}(t-t_i, t_i; J)dt_i \\ + \int_{-\infty}^t J(t_i)\vec{P}_{ex}(t-t_i, t_i; J)\frac{dC(t-t_i, t_i)}{dt}dt_i. \end{aligned} \quad (1.11)$$

At this stage, it is assumed that the change in solute concentration  $C(t-t_i, t_i)$  within  $V$  is only

due to biogeochemical reaction processes:

$$\left(\frac{dM(t)}{dt}\right)_r = \int_{-\infty}^t J(t_i) \vec{P}_{ex}(t-t_i, t_i; J) \frac{dC(t-t_i, t_i)}{dt} dt_i. \quad (1.12)$$

Note that this assumption is later relaxed in order to account for a specific affinity of ET for the solute which can lead to evapoconcentration effects (see Chapter 3). Combining Eqs. 1.1, 1.11 and 1.12, one obtains:

$$\phi_Q(t) + \phi_{ET}(t) = \int_{-\infty}^t J(t_i) C(t-t_i, t_i) \vec{p}_{ex}(t-t_i, t_i; J) dt_i, \quad (1.13)$$

the counterpart of Eq. 1.5 for the solute output fluxes. Hence, the respective fluxes for  $Q$  and  $ET$  can be described analogously:

$$\phi_Q(t) = \int_{-\infty}^t J(t_i) \theta(t_i) C(t-t_i, t_i) \vec{p}_Q(t-t_i, t_i; J) dt_i; \quad (1.14a)$$

$$\phi_{ET}(t) = \int_{-\infty}^t J(t_i) [1 - \theta(t_i)] C(t-t_i, t_i) \vec{p}_{ET}(t-t_i, t_i; J) dt_i; \quad (1.14b)$$

The above sets out the theoretical framework for the description of hydrologic and solute transport in terms of travel time distributions. It is important to note that in Eqs. 1.7a, 1.7b, 1.14a and 1.14b, the forward TTDs  $\vec{p}_Q$  and  $\vec{p}_{ET}$  depend not only on the injection time  $t_i$  and the sequence of events that follow ( $J$ ), but also on the connectivity of the inherent flow pathway, which control how the discharge  $Q$  and evapotranspiration  $ET$  sample water among the available "ages" within  $V$ . The concentration  $C(t-t_i, t_i)$  assigned to each water age depends on the degradation/removal processes taking place, while the pulse injected at  $t_i$  is still in  $V$  but can be affected if an output flux (physically only relevant for  $ET$ ) operates a concentration discrimination (e.g., if a plant cannot withdraw a specific substance, it will concentrate the remaining concentration of any water age it is sampling). Analytical expressions have been derived for specific mixing schemes (random sampling, old water first) and solute reactivity assumptions (Botter *et al.*, 2010; Fenicia *et al.*, 2010; Botter, 2012; van der Velde *et al.*, 2012; Benettin *et al.*, 2013a; Carraro, 2014; van der Velde *et al.*, 2014). Those relevant to the modeling carried out in this thesis are further detailed in Chapter 3.

The implications of mixing, internal mass degradation/removal and selective affinity of evapotranspiration make the experimental measurement of travel times particularly difficult. As water molecules cannot be tracked individually, the most direct way to estimate travel times in a hydrologic system is to use soluble tracers. However, the breakthrough curves (BTCs) that one observes (usually at the discharge outlet, as  $ET$  flux is difficult to monitor) are the combination of all those processes, and are only a direct measurement of forward travel time if degradation/mass removal can be disregarded and if  $ET$  uptake is non-selective. If not, the interpretation of BTCs may be subject to the equifinality (see Beven, 2012) of different combinations of processes and potential behaviors.

### 1.4 Tracers

The main advantage of using TTDs as a proxy of contact time between fixed and mobile phases in the hydrologic response compared to conventional methods such as the unit hydrograph (Sherman, 1932; Beven, 2012) is that in addition to providing a quantitative output response to a given input sequence, it is possible to keep track of each single input pulse characterized by a specific injection time through storage and output fluxes. This is crucial when the concern is on water quality or pollutant transport, because solutes travel at velocities equal or similar to those of water particles (the carrier) rather than at the celerity of the pressure wave induced, e.g., by a rainfall event (Beven, 1981; Kirchner, 2003). As presented in the previous section, the analytical description of TTDs is difficult, because they implicitly encompass many processes whose interactions and impacts on the distributions are not clearly signaled. In addition, assumptions must be made, which have significant implications, in particular regarding the internal mixing and/or sampling within the hydrologic system, in order to derive analytical expressions for the TTDs.

The experimental measurement of TTDs is thus a prerequisite in efforts to describe any real-life hydrologic system with this framework, and potentially verify simplifying assumptions towards modeling. However, measuring the input and output fluxes of a system's water budget (see Eq. 1.1) is simply insufficient, specifically because information about the age composition of a flux is lost. Tracers provide a good — indeed the only — solution because, as indicated by their designation, they are substances or molecules that can be used to "track" a marked water parcel. Long before the generalized use of travel time was introduced, tracers were being widely used in hydrology for many purposes such as discharge measurements, evaluation of flow paths, hydrograph separation, infiltration processes, or delineation of protection zones (e.g. Schudel *et al.*, 2002; Leibundgut *et al.*, 2011).

A hydrologic tracer is purposely designed to closely follow the movement of water, which poses specific constraints on its characteristics. In the literature, the term "ideal tracer" is often used to qualify suitable tracers (e.g. Flury, 2003; Kirchner *et al.*, 2010), even if in reality, such a tracer does not exist. A good water tracer should move in a manner similar to water, which limits its particle size and restricts its domain to highly soluble and non-sorptive substances. A tracer should also be conservative in behavior, i.e. not be subject to significant degradation processes during its transport time frame (e.g. Davis *et al.*, 1980; Käss, 1998). Chemical changes in the solution should not modify the tracer's transport and fate, so that the observed tracer concentration results only in dilution and mixing processes. In addition, a tracer should be analytically measurable and toxicologically harmless to the receiving environment. These criteria suggest different tracer candidates depending on site-specific characteristics. Appropriate tracers intended for unsaturated environments are for example more difficult to find than for saturated groundwater flows, as many substances may be subject to aerobic microbial degradation. In practice, the perfect tracer does not exist, and it is thus necessary to develop a good knowledge of the behavior of the tracer adopted in order to account *a posteriori* for unwanted processes affecting the observed breakthrough.

Tracers can be divided to two categories, natural (or environmental) tracers qualifying those who are inherent to the water cycle, and artificial tracers, whose injection into a hydrologic system is man-made and designed in the context of an experiment. Table 1.1 gives a (non-exhaustive) overview of the available hydrologic tracers. Environmental tracers such as chloride or water-stable isotopes have the advantage that no application is required, as tracer occurrence in the inputs is natural (taken in a broad sense) and possibly fluctuating. Hence, they can be used at large scales, for instance to evaluate the mixing between two components (see e.g. *Sklash and Farvolden*, 1979; *Kendall and Caldwell*, 1998; *Soulsby et al.*, 2003; *Leibundgut et al.*, 2011), or to estimate the reaction time in a catchment by studying how an input signal in rainfall is converted into the observed catchment output signal (*Kirchner et al.*, 2000). Reaction time can be wrongly assimilated to travel time (*van der Velde et al.*, 2010), but they differ in the sense that reaction time takes into account a continuous tracer input signal and therefore does not identify the absolute injection time the observed output (see also *Frisbee et al.*, 2013). Especially considering non-stationary TTDs, there are many combinations of continuous input and output signals implying different mixing processes, flow pathways and contributions of water of different ages stored in the hydrologic volume. Hence, it is usually only possible to use environmental tracers for the derivation of catchment travel time characteristics through model inferences requiring various assumptions including mixing and stationarity issues, often assigning well-defined mathematical forms to the TTDs (e.g. *Maloszewski et al.*, 1992; *McGuire and McDonnell*, 2006; *Rinaldo et al.*, 2006b; *Hrachowitz et al.*, 2009a,b, 2010a; *Fenicia et al.*, 2010; *van der Velde et al.*, 2010; *Birkel et al.*, 2012; *McMillan et al.*, 2012; *Benettin et al.*, 2013a; *Heidbüchel et al.*, 2013; *Hrachowitz et al.*, 2013; *van der Velde et al.*, 2014; *Harman*, 2015).

In contrast, artificial tracing can be specifically designed to fit the experiment's goals, but are limited in both time and space (*Divine and McDonnell*, 2005; *Leibundgut et al.*, 2011). This restricts the use of artificial tracers to laboratory, plot, hillslope or in some rare cases small catchment scales (see e.g. *Henderson et al.*, 1996; *Rodhe et al.*, 1996; *Feyen et al.*, 1999; *McGuire et al.*, 2007). It is also possible to choose the most suitable substance for each case study, preferably a compound that is not found naturally so that the contribution of pre-event occurrence of the tracer in the storage can be disregarded. Regarding experimental measurement of travel times, artificial tracers are particularly appropriate because the tracer input is controlled and can be limited to a single tracer pulse injection. This represents the most direct method to estimate travel times, as a sole event occurring at a known time  $t_i$  is marked, and can be followed through the monitoring of different control sections (depending on the nature of the hydrologic system in question) without any ambiguity resulting from the mixing with other components or older water containing the same tracer. Note that even in the unrealistic case of a perfect tracer as described above, the tracer signal measured in one of the output fluxes of a hydrologic system is directly proportional to the forward TTD (conditional on  $t_i$  and on the following sequence of events that have followed) until the complete release of the tracer. Under the non-stationarity assumption stated by the conditional probability on the initial time and subsequent states of the system, a single pulse injection of artificial tracer

	Environmental tracers	Artificial tracers
<b>Stable isot.</b>	Deuterium ( $^2\text{H}$ )	Naphtionate
	Oxygen-18 ( $^{18}\text{O}$ )	Pyranine
	Carbon-13 ( $^{13}\text{C}$ )	Uranine
	Nitrogen-15 ( $^{15}\text{N}$ )	Eosine
	Sulphur-34 ( $^{34}\text{S}$ )	Rhodamines
<b>Radioactive isotopes</b>	Tritium ( $^3\text{H}$ )	Duasyne
	Carbon-14 ( $^{14}\text{C}$ )	Tinopal
	Argon-39 ( $^{39}\text{Ar}$ )	Brilliant Blue
	Krypton-85 ( $^{85}\text{Kr}$ )	Sodium/potassium chloride
	Radon-222 ( $^{222}\text{Rn}$ )	Sodium/potassium bromide
	Radium-226 ( $^{226}\text{Ra}$ )	Lithium chloride
	Silicium-32 ( $^{32}\text{Si}$ )	Potassium iodide
	Chlorine-36 ( $^{36}\text{Cl}$ )	Sodium borate (borax)
	Phosphorus-32 ( $^{32}\text{P}$ )	Radionuclides
	Bromide-82 ( $^{82}\text{Br}$ )	Fluorobenzoic acids
	Noble gases	Lycopodium spores
	Chloride ( $\text{Cl}^-$ )	Bacteria
Bromide ( $\text{Br}^-$ )	Viruses	
Nitrate ( $\text{NO}_3^-$ )	Phages	
Phosphate ( $\text{PO}_4^{3-}$ )	DNA	
Sulfur hexafluoride ( $\text{SF}_6$ )	Microspheres	
Boron (B)	Phytoplankton	
Silicates		
Heavy metals		
Chlorofluorocarbons (CFCs)		
Electrical conductivity		
Temperature		

Table 1.1: List of commonly used tracers in groundwater and hydrology studies. Note that many environmental tracers can also be used as artificial tracers if the application can be clearly discerned from the background signal. Adapted from *Flury (2003); Leibundgut et al. (2011)*

is thus an incomplete — yet interesting — picture of the hydrologic behavior of a system. In order to resolve this problem, one would need to mark each input event (i.e. each  $t_i$ ) with a different, non-interacting tracer. Given the difficulty in finding suitable hydrologic tracers and the spatial and temporal limitations of artificial tracing, multiple tracer experiments are rare (e.g. *Bowman and Gibbens*, 1992; *Abdulkabir et al.*, 1996; *Stamm et al.*, 2002; *Mortensen et al.*, 2004; *Koeniger et al.*, 2010), especially in the context of TTDs. In this thesis, the use of multiple tracer pulse injections in a well-defined and monitored hydrologic system is discussed. The choice of suitable tracers is discussed in the related chapters.

### 1.5 Lysimeters as hydrologic systems

One of the major difficulties in catchment hydrology is the proper identification of the catchment boundaries and the measurement of exchanges occurring across boundaries. The fundamental governing equation for any hydrologic system is given by the law of conservation of mass, which attributes any change in the system's water storage to the difference in the input and output fluxes (see Eq. 1.1). Whereas rainfall and discharge measurements can arguably provide a reasonable estimate if the measurement sites are representative at the catchment scale and the outlet(s) are well-defined, evapotranspiration is usually much more difficult to accurately assess. As water storage cannot be directly measured, its estimation relies entirely on the accuracy of flux estimates. In this context, lysimeters (Figure 1.4) are an interesting option between laboratory and field scales and provide an extensive and detailed control on the system. They allow the reproduction of the main hydrologic driving processes of a small catchment such as infiltration through a complex soil matrix, discharge output flux through bottom drainage and the possibility to grow vegetation exposed to natural environmental conditions prompting (spatially and temporally) variable water deficits in the water storage, all at a manageable and controlled scale. Their shape (usually cylindrical) is designed to enhance vertical flow with a limited surface area, and thus provides pseudo-1D systems (though lateral exchanges and soil moisture redistribution are possible) ideal for simulating diffuse application of substance, as potential contributions of other source areas are excluded. For these reasons, lysimeters have been extensively used for many applications such as studies of pesticides leaching in soils (e.g. *Bergström*, 1990; *Winton and Weber*, 1996; *Renaud et al.*, 2004), estimation of evapotranspiration and water use for crops (e.g. *Beeson*, 2011; *Croci*, 2013; *Schrader et al.*, 2013; *Fahle and Dietrich*, 2014; *Peters et al.*, 2014) or investigations of water flow and solute transport (e.g. *Maloszewski et al.*, 1995; *Flury et al.*, 1999; *Schoen et al.*, 1999a; *Abdou and Flury*, 2004).

Weighing lysimeters allow a robust and accurate closure of the mass balance equation, as the water storage is given by the weight reading and ET can be deduced directly from the mass balance if the rainfall and the drainage fluxes are measured. Lysimeters are particularly well-suited to tracer use, as their size and well-defined boundaries provide an optimal control on the input and output mass fluxes, reducing the amount of artificial tracer needed and thereby increasing the accuracy of the analysis due to the limited dilution of the input signal.

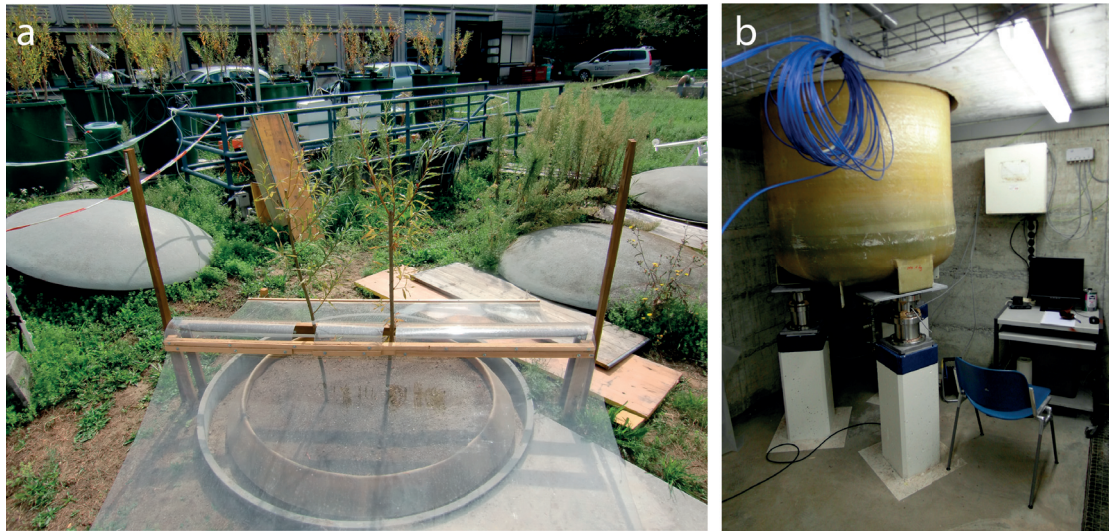


Figure 1.4: a) General overview of the outside of the lysimeter, before the start of the experiment. b) View of the interior of the lysimeter chamber, with the centralized data acquisition system.

Even though lysimeters have been used as calibrating and validating tools for models (*Flury et al.*, 1999; *Schoen et al.*, 1999b; *Herbst et al.*, 2005; *Larsbo et al.*, 2005), their size is more representative of a real soil compared to column experiments and they are therefore also appropriate to assess the bulk hydrologic response generated by complex connectivity patterns in the soil matrix (*Schoen et al.*, 1999a). Nevertheless, studies exist on the reconciliation of lysimeter data with lumped models, and those that do have been exclusively conducted using the natural isotopic composition of rainfall as tracers under the stationary assumption (e.g. *Lindström and Rodhe*, 1992; *Maloszewski et al.*, 1995; *Stumpp et al.*, 2009a,b,c). Hence, the lysimeter seems a suitable tool to investigate hydrologic and solute transport in the context of travel time studies, because it provides an experimental setup that can be well-monitored and whose scale is relevant to the main processes controlling the TTDs, e.g. mixing patterns in the internal water storage, sizable ET-induced water deficit, moisture-controlled soil connectivity and climate forcing variability.

### 1.6 Research questions and structure of the thesis

The overall objective of the present dissertation is to improve our understanding of hydrologic and solute transport for field and catchment applications, using the general approach of travel time distributions that has deservedly become popular during the last decade. More specifically, the aim is to demonstrate that the hydrologic TTDs are stationary only under unrealistic conditions, a fact which has been largely neglected for the ease of experimental data interpretations. Guidelines are also provided on the main hydrologic controls of travel times, in particular on the processes that trigger the emergence of time variability.



## 1.6. Research questions and structure of the thesis

---

To such an end, a sophisticated experimental setup has been installed, which permits extensive control and monitoring of the input and output fluxes and the volume and chemical composition of the internal storage. Its spatial scale is sufficiently large to be representative of hydrologic processes at catchment scale, which include soil moisture heterogeneity, preferential flowpaths or evapotranspiration-induced water deficit. The artificially generated rainfall sequence is also representative of the variability of natural rainfall patterns. By marking specific rainfall events with different tracers selected for their reputation of conservative hydrologic tracers, and by tracking them individually in the bottom drainage discharge and within the water storage, the necessary apparatus to directly measure forward travel times is provided. The identification of the temporal origin of the tracer measured in the discharge is the only solution to estimate a realisation of forward TTDs without any modeling aids. This can either be achieved by using multiple differentiable tracers, allowing their concurrence in the system, or by the reinjection a single tracer after the mass of its first injection has entirely exited the system, been degraded or irreversibly immobilized. Both approaches are tested and discussed (respectively called "sequenced multiple tracer injections" and "temporally displaced injections"). The processes affecting the shape of the TTDs and their transient behavior are further sought. In particular, the experimental data support theoretical speculations that under temporally variable rainfall forcing, the TTDs are inevitably non-stationary, and that time-rescaling in terms of discharge flow volume does not impart stationarity to the observed TTDs. Furthermore, the role of ET and internal mixing mechanisms of the system in shaping the TTDs is explored.

This thesis is organized as follows:

- Chapter 2 presents the experimental setup and methodology used to measure tracer travel time distributions. The results are presented and interpreted in their raw format (the breakthrough curves), without the support of models or assumptions. The data have raised unexpected and unreported tracer reactivity issues that were addressed by several *ad-hoc* and supplementary experiments in order to identify any misleading features on the tracer responses that tracer degradation or removal processes may have spawned, which would have questioned the non-stationary behavior suggested by the observations.
- A theoretical interpretation based on a recent framework accounting for non-stationary travel time distributions is presented in Chapter 3, calibrated and validated contrasting the experimental data. This modeling exercise disentangles the variability observed in the tracer responses and evaluates the respective roles of the non-stationary hydrologic forcings with regards to tracer-specific reactivity issues. It also sheds light on the ways the output fluxes sample among the different water ages in storage.
- Considering the reactivity issues raised in Chapter 2, Chapter 4 provides a reassessment of the importance of the required tracer properties and tests the suitability of water stable isotopes (the "ultimate" water tracers) in this context. The advantages and the

## Chapter 1. Introduction

---

performance of water stable isotopes tracing are discussed and compared with the results of the artificial tracers used initially.

- The last chapter presents the efforts undertaken in order to develop an experimental catchment and to initiate a long-term hydrochemical survey that could be used to apply the travel time framework at larger scale. A pesticide screening campaign clearly illustrates the influence of hydrologic dynamics on the chemical dynamics, yet the large spatial and temporal differences among the different substances highlight the complexity of the processes taking place in hydrologic transport.

Finally, the main findings of this dissertation are summarized in the conclusions along with some reflections and recommendations regarding a better understanding and description of hydrologic transport and upscaling issues.

## 2 Transport of fluorobenzoate tracers in a vegetated hydrologic control volume: Experimental results

This chapter is an adapted version of:

Queloz, P., Bertuzzo, E., Carraro, L., Botter, G., Miglietta, E., Rao, P.S.C. and Rinaldo, A. (2015), Transport of fluorobenzoate tracers in a vegetated hydrologic control volume: 1. Experimental results. *Water Resources Research*, 51(4), 2773–2792, doi:10.1002/2014WR016433.

This chapter reports about the experimental evidence collected on the transport of five fluorobenzoate tracers injected under controlled conditions in a vegetated hydrologic volume, a large lysimeter (fitted with load cells, sampling ports and an underground chamber) where two willows prompting large evapotranspiration fluxes had been grown. The relevance of the study lies in the direct and indirect measures of the ways in which hydrologic fluxes, in this case evapotranspiration from the upper surface and discharge from the bottom drainage, sample water and solutes in storage at different times under variable hydrologic forcings. Methods involve the accurate control of hydrologic inputs and outputs and a large number of suitable chemical analyses of water samples in discharge waters. Mass-extraction from biomass has also been performed *ex-post*. The results of the two-year long experiment established that initial premises on the tracers' behavior, known to be sorption-free under saturated conditions which was verified in column leaching tests, were unsuitable as large differences in mass recovery appeared. Issues on reactivity thus arose and were addressed in this thesis. Reactivity is here attributed to microbial degradation and solute plant uptake. The results suggest previously unknown features of fluorobenzoate compounds as hydrologic tracers, potentially interesting for catchment studies owing to their suitability for distinguishable multiple injections, and an outlook on direct experimental closures of mass balance in hydrologic transport volumes involving fluxes that are likely to sample differently stored water and solutes.

## **2.1 Introduction**

The intertwined dynamics of catchment water storage, connectivity of flow pathways and heterogeneous reactions are key to our understanding of basin-scale transport in the hydrologic response (e.g. *Beven, 2012*). One outstanding challenge to a general theory, subsumed by the so-called old-water paradox (*McDonnell et al., 2010*), concerns the stationarity of the response of hydrologic transport volumes to erratic and nonpoint source inputs (e.g. *McDonnell and Beven, 2014*). Stationarity, or the lack of it thereof, centers attention on how catchments store and release water and solutes (*Botter et al., 2010, 2011; Rinaldo et al., 2011; van der Velde et al., 2012; Hrachowitz et al., 2013; Benettin et al., 2013a; Bertuzzo et al., 2013; Benettin et al., 2013b; Harman, 2015*). Specifically, the mass response to a specific rainfall event is now acknowledged to be composed by water labeled by different residence times in the transport volume since injection (i.e. the 'ages'), not necessarily (and almost inevitably not) generated by the latest event (e.g. *Stewart and McDonnell, 1991; Divine and McDonnell, 2005; McGuire and McDonnell, 2006; McGuire et al., 2007*). The mixture of different ages of residence within the catchment results from transport and by differential sampling operated by outflows among water parcels in storage. When and how discharge samples within complex catchment control volumes is thus a fundamental open issue.

In soil profiles, matrix heterogeneities and lack of stationarity of the processes dominate the ephemeral triggering of preferential flow paths in unsaturated conditions, and thus the issue of determining the distributions of residence times of water in storage (e.g. *Flury et al., 1994*). Chemically variable, basin-scale storage recharge integrates instead the stochasticity of climatic forcings, the sources of water and solutes, flow path heterogeneities and fluctuating evapotranspiration from diverse assemblages of vegetation (*Stewart and McDonnell, 1991; Kirchner et al., 2010; McGuire and McDonnell, 2006; McDonnell et al., 2010*), with implications on large-scale transport. In fact, the ages in storage are a measure of the contact time between fixed and mobile phases driving mass exchange processes and biogeochemical reactions (*Rinaldo and Marani, 1987; Rinaldo et al., 1989; Stewart and McDonnell, 1991*). Age distributions are thus effective descriptors of biogeochemical function of a catchment including its export of anthropogenic inputs (*Brusseau et al., 1989; Flury, 1996; Wolock et al., 1997; McGuire and McDonnell, 2006; Hrachowitz et al., 2010a,b; Bertuzzo et al., 2013*).

Direct experimental measure of residence time distributions within a hydrologic system proves a difficult task. It would, in principle, require the tagging of every water particle to record the time elapsed from its injection to the exit from the system, measuring all outfluxes at frequencies comparable with the relevant timescale of hydrologic fluctuations and extending the measure until full delivery (typically, months to years). Natural or artificial tracers have been used to that end. One method consist of tracking water molecules by using the water natural stable isotopes oxygen-18 ( $^{18}\text{O}$ ) and deuterium ( $^2\text{H}$ ). By measuring isotopic fluctuations in both input and output water, one can infer the age structure of the water within a catchment for as long a record as the input characterization allows (e.g. *Lindstrom and Rodhe, 1986; Rodhe et al., 1996; Maloszewski et al., 1992; Kendall and Caldwell, 1998; Simic and Destouni, 1999;*

*Kirchner et al.*, 2010). Another approach consists of artificially injecting into the hydrologic system non-native soluble substances as a tool for tracking water molecules. This method has the advantage that the input can be non-continuous and controlled, and that several different tracers can be injected sequentially. When sampling outfluxes, the detection of a specific tracer would then be a direct measure of the travel time distribution (the residence times sampled at the exit) if injection into the system were unique and instantaneous. However, perfect tracers and high-frequency tagging for months or years do not exist in practice, because of the analytical burden implied and because most of the soluble compounds used as hydrologic tracers to date can undergo selective plant uptake, biogeochemical and/or microbial degradation and retardation processes (e.g. *Käss*, 1998; *Flury*, 2003; *Divine and McDonnell*, 2005). In addition, at catchment scales, spiking systematically rainfall with artificial tracers is not within reach (but see *Rodhe et al.* (1996)), and the spatial distribution of the tracer input is usually patchy. Although the linkage between hydrologic tracer breakthrough curves and travel/residence time distributions is intuitive, proper interpretation requires multiple assumptions when dealing with systems naturally in unsteady flow conditions. Note that a common misunderstanding equates non-stationarity of the system's response to unsteady state conditions for inputs and output. Rather differently, stationarity refers to time invariance of the basic mechanisms that transform inputs into outputs whether in steady or unsteady state conditions.

Here, the results of a two-year experiment centered on the transport of fluorobenzoate tracers in a vegetated hydrologic transport volume are analyzed. The specific tracers were chosen for the possibility of accurately singling out the relative concentrations of multiple injections. The experiment described here aims specifically at tracking transport and release dynamics of solutes driven by hydrologic processes. For this purpose, a controlled experiment in a large lysimeter was designed, in order to restrict heterogeneous flow pathways to sub-vertical infiltration. Lysimeters have been extensively used in hydrologic research, in particular to study solute transport and evapotranspiration dynamics (e.g. *Bergström*, 1990; *Roth et al.*, 1991; *Flury et al.*, 1994; *Schoen et al.*, 1999a; *Beeson*, 2011, and references therein) because the rates and the concentrations of inputs and outputs can be monitored and the soil water storage can be estimated by accurately weighing the system. Compared to catchment experiments, this latest feature represents a major advantage for evapotranspiration studies owing to (water) balance closure. By injecting controlled fluorobenzoate tracer pulses in the system and by retrieving their breakthrough curves in the discharge, travel and residence time distributions can be inferred for a simple and yet highly dynamical system. Soil water storage and water deficits induced by evapotranspiration are particularly in focus as key factors controlling transport, as well as losses to plant uptake, microbial degradation and residuals in soil. Evapotranspiration obviously operates preferentially at the surface and close to the roots. This could affect the transport of a tracer pulse, for example by retarding its infiltration when a dry period characterized by high ET demand immediately follows the injection. In contrast, a large input volume occurring after the application of a tracer could flush the tracer pulse deeper in the soil, which would become unavailable or less prone to be selected by ET fluxes. In addition,

## **Chapter 2. Transport of fluorobenzoate tracers in a vegetated hydrologic control volume: Experimental results**

---

the soil moisture cycles and how they propagate in the soil profile increase the complexity as they also affect water availability for ET and discharge (consider, e.g., a soil moisture below the wilting point). Adding tracer affinity for plant uptake, tracer losses can be largely driven by ET deficits and can thus be also influenced by environmental conditions. Microbial degradation is not necessarily as intimately controlled by moisture conditions and ET as plant uptake does. Microbial degradation pathways are nonetheless often different between saturated and unsaturated conditions and specific conditions in the soil can prompt microbial activity (e.g. root exudates) and thus induce preferential degradation under certain circumstances, adding another non-linear and non-stationary dimension to the hydrologic transport picture. Given the potential for a variety of loss pathways following the staggered solute injection, hypotheses on the modifications incurred in the travel and residence time distributions could then be tested by contrasting these experimental data.

This chapter is organized as follows. Section 2.2 illustrates materials and methods. They include a description of the design of the experiment, that entails multiple and replicated injections, and of the system setup and its measurement system. Properties of the specific tracers adopted, five different fluorinated benzoic acids, and analytical procedures for their measurement are also discussed, including technicalities and ex-post testing. Section 2.3 presents the results, in the form of raw data and of mass-recovery plots. Normalized and rescaled breakthrough curves are also produced to probe stationarity issues. Section 2.4 offers a discussion of the results and an outlook to catchment-scale transport experimentation. A set of conclusions closes the chapter.

## **2.2 Materials and methods**

### **2.2.1 System setup**

The hydrologic control volume was placed within a large lysimeter (Figure 2.1) situated within the EPFL campus, in a 2.5 m-deep fiberglass-polyester cylindric tank. The 1 m<sup>2</sup> open surface of the tank is at ground level and located in an open grass field equipped with meteorological stations. An underground chamber allows access to the bottom of the lysimeter where load cells record the weight.

A 50 cm layer of saturated gravel filter at the bottom of the tank is topped by a mono-horizon 2 m disturbed soil column. A geotextile mesh between the two layers prevents the soil to clog the gravel filter. The reconstituted soil is approx. 50% loamy sand obtained from a nearby construction excavation located in Denges (Switzerland) and 50% lacustrine sand with particle sizes from 0 to 4 mm (Lac Léman, Switzerland). The materials were accurately weighted and mixed with a cement mixer during the filling procedure. In order to ensure sufficient packing of soil and further compaction during the experiment, the soil was frequently soaked until saturation during the filling phase.

During the experiment, a steady water table is maintained at a constant depth of 2 m at the

interface between the soil and gravel filter. The bottom boundary condition of the lysimeter is that of free drainage, as the excess downward flux recharging the gravel filter forces water out at the outlet placed at the bottom of the system. The outlet is connected to a PVC pipe maintaining the water table level through a siphon. The pipe outlet drains into a tipping bucket (Casella Measurement, UK) equipped with a double bucket of 8 mL-resolution and a reed switch counter for discharge rate measurement. The tipping bucket is regularly calibrated by weighing the outflux in order to ensure unbiased measurements.

The lysimeter tank is supported by three concrete pillars topped with ring torsion load cells with a maximal load of 2.2 t each (HBM, Germany) on which the tank pods stand. The electrical sensibility of the cells (2.85 mV/V) allows a continuous monitoring of the weight of the system with an accuracy up to 200 g (0.005%) of the total weight. The digital transducer of the load cells has a built-in infinite response (IIR2) electronic filter to remove noise notably due to vibration and wind. A filtered reading is stored every 20 seconds.

Local soil moisture content is measured by frequency-domain reflectometry (FDR) probes (5TM from Decagon Devices Inc., USA) at four different depths in the soil column (25, 75, 125 and 175 cm). Three probes per depth were installed radially at equal distance from the center. A soil-specific calibration curve has been measured in the lab.

Two willows (*Salix viminalis*), 1.2 m and 1.4 m in height (branch cuttings of a two-year tree), were planted eight months before the experiment started, with their roots extending to at least 70 cm in the soil column (data at time of setting). This species has been chosen because of its strong climatic resistance as it can withstand long periods of droughts as well as flooding. Willows have high transpiration rates and can thus potentially create substantial water demand in the system. A translucent gable roof made of polycarbonate built under the trees canopy shields the lysimeter from natural precipitation but let the willow be exposed to the real climatic and light cycles (Figure 2.1b and c). Two openings on each side of the roof allow the crossing of an air draft and the evacuation of soil evaporation, besides allowing artificial water injection. The soil surface has been maintained bare throughout the experiment, and no organic layer could develop at the top of the column as the roof prevented accumulation of organic matter.

The evapotranspiration flux  $ET$  was derived from the mass balance, given the change in storage measured by the load cells, the input rainfall and the discharge output. Note that the term evapotranspiration encompasses the combined evaporative/transpiration fluxes measurements lumped in a single variable out flux through the upper surface.

The system is equipped for soil water and discharge sampling. Soil water can be collected at three different depths in the soil (50 cm, 100 cm and 150 cm) with three porous cups radially distributed per depth. The porous cups have a bubbling pressure of 1 bar and are connected to a vacuum circuit which is turned on at a relative pressure of -0.6 bar during 4-5 hours to draw samples of about 10 mL in each porous cup from the soil matrix. Each sample is collected by a independent tube equipped with a manifold and is connected to a controlled vacuum

## Chapter 2. Transport of fluorobenzoate tracers in a vegetated hydrologic control volume: Experimental results

---

system.

Discharge samples are collected at the tipping bucket outlet. The effluent is directed to a solenoid valve switching the flux either to the sink or to a fraction collector (Amersham Biosciences AB, Sweden) when a sample is needed. A LabVIEW™ program connected to a data acquisition system (CompactDAQ, National Instruments) is used for calculating the flow rate based on the bucket tilts read by the reed switch of the tipping bucket. It also controls the valve position and increments the fraction collector after a sample has been taken. The program interface provides user-defined parameters and allows time or flow-based sampling schemes.

A meteorological station located five meters away from the installation records air temperature, air humidity, wind direction and intensity, incoming radiation and soil temperature at 15 min-intervals.

### 2.2.2 Selection of suitable tracers

The goal of the experiment is to tag and trace selected water inputs. For this purpose, a given volume of water from a given pulse has to be independently labeled. Because the discharge flux is assumed to be, at every given time, a mixture of water originating from inputs and thus characterized by a specific age structure, it is continuously analyzed for the labeled water. The detection of the label hence suggests how water from a marked rainfall event contributes to the discharge flux.

As tracers, fluorinated benzoic acids (FBAs) were chosen, because they were reported as convenient tracers for hydrologic tracing in soils (e.g. *Jaynes*, 1994). Different species of FBAs exist, depending on the number and position of fluoride ions on the aromatic ring. Several FBA compounds have been reported as useful nonreactive water tracers, often described to have similar reactive properties as  $\text{Br}^-$  (e.g. *Bowman and Gibbens*, 1992; *Jaynes*, 1994; *Kung et al.*, 2000; *Mortensen et al.*, 2004). FBA derivatives are anionic at neutral to basic pHs and have negative-log dissociation constants ( $pK_a$ s less than 4.0), which limits sorption effects in soil (*Bowman*, 1984; *Stetzenbach et al.*, 1982; *Bowman and Gibbens*, 1992; *McCarthy et al.*, 2000). To date, few studies exist that reported chemical and microbial degradation of fluorinated compounds (*Misiak et al.*, 2011). Plant uptake of some fluorobenzoic acids has been reported (*Bulusu*, 1995; *Bowman et al.*, 1997). Analyses of soil and plant extracts reflected an uptake ranging from 0 to 50% depending on the compound and plant species and suggest possible metabolism within the plant material (*Bulusu*, 1995). Affinity for plant uptake is further assessed during this experiment via the analysis of willow twigs and leaves. Upon verification of commercial availability, reported low reactivity in saturated soils and chemical analysis capabilities, five species have been identified as suitable for the current experiment: 2-(Trifluoromethyl)benzoic acid (2-TFMBA), 3-(Trifluoromethyl)benzoic acid (3-TFMBA), 2,5-Difluorobenzoic acid (2,5-DFBA), 2,6-Difluorobenzoic acid (2,6-DFBA) and 3,4-Difluorobenzoic (3,4-DFBA). All compounds were purchased in salt powder at a minimum



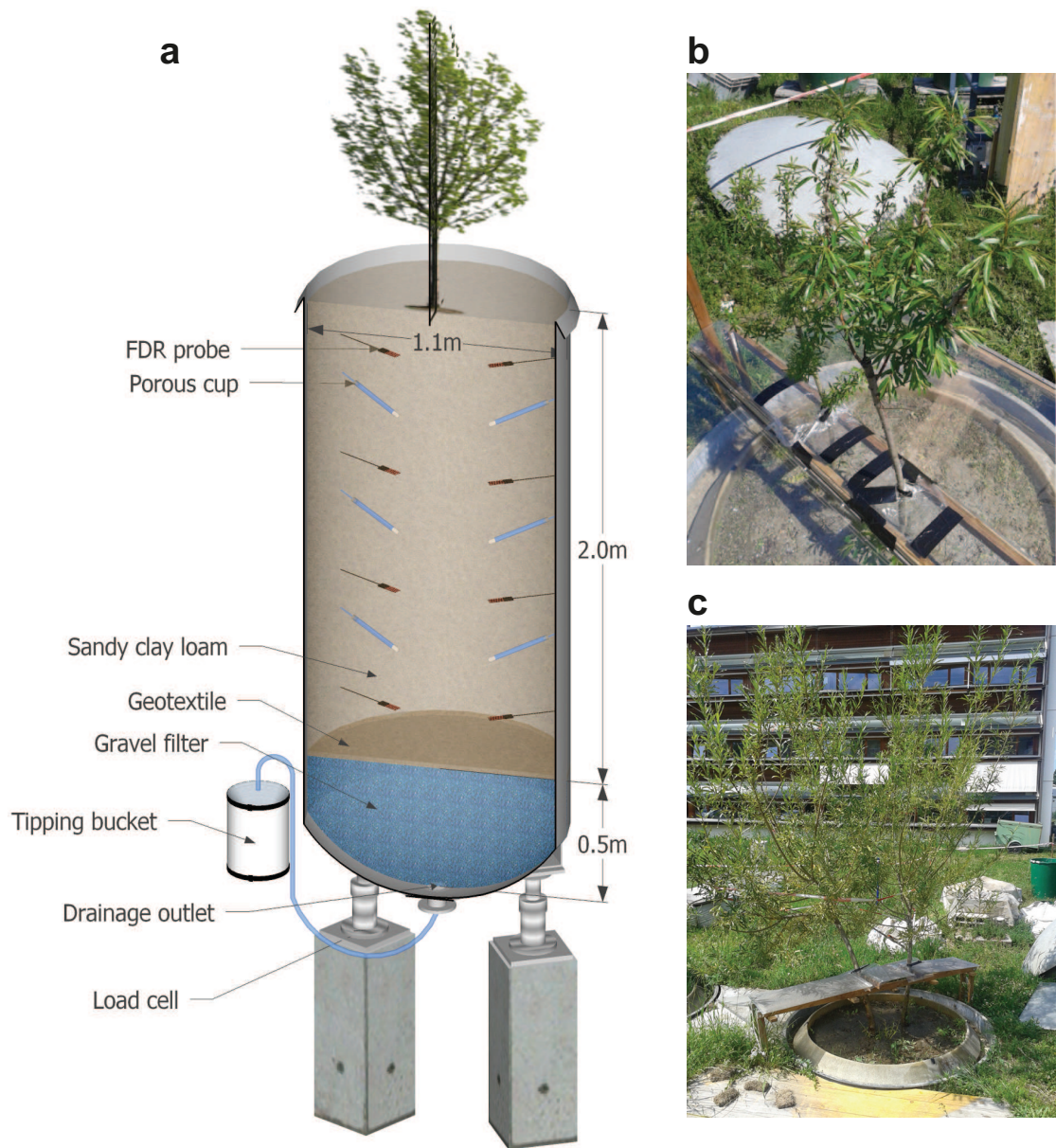
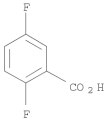
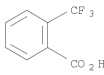
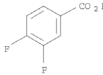
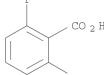
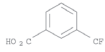


Figure 2.1: (a) General (to-scale) lysimeter scheme. An essential representation of the measurement devices is given. Note that a chamber placed underneath the lysimeter allows controls and measurement under any circumstance. Development of the willow tree (*Salix Viminalis*) in the lysimeter over the growing season. (b) April 24, 2013. (c) June 15, 2014.

## Chapter 2. Transport of fluorobenzoate tracers in a vegetated hydrologic control volume: Experimental results

Table 2.1: Properties of the fluorinated benzoic acids used as conservative tracers.

	TR1	TR2	TR3	TR4	TR5
Abbrev. name	2,5-DFBA	2-TFMBA	3,4-DFBA	2,6-DFBA	3-TFMBA
CAS No.	2991-28-8	433-97-6	455-86-7	385-00-2	454-92-2
Formula	C <sub>7</sub> H <sub>4</sub> F <sub>2</sub> O <sub>2</sub>	C <sub>8</sub> H <sub>5</sub> F <sub>3</sub> O <sub>2</sub>	C <sub>7</sub> H <sub>4</sub> F <sub>2</sub> O <sub>2</sub>	C <sub>7</sub> H <sub>4</sub> F <sub>2</sub> O <sub>2</sub>	C <sub>8</sub> H <sub>5</sub> F <sub>3</sub> O <sub>2</sub>
Structure <sup>a</sup>					
Mol. weight (g/mol) <sup>a</sup>	158.1	190.1	158.1	158.1	190.1
Solubility (g/L) <sup>a</sup>	745	1000	266	1000	802
<i>pK<sub>a</sub></i> <sup>b</sup>	2.87	3.17	3.43	2.42	3.50
LOQ (μg/L)	7.0	3.0	10.0	7.0	5.0
Intern. std.	deuterated	NA <sup>c</sup>	deuterated	deuterated	NA <sup>c</sup>

<sup>a</sup> SciFinder<sup>®</sup>, Chemical Abstracts Service: Columbus, OH. Calculated using Advanced Chemistry Development (ACD/Labs) Software V11.02 (©1994-2013 ACD/Labs)

<sup>b</sup> Serres-Piole *et al.* (2011)

<sup>c</sup> Not available at time of experiment

purity of 99% from Fluorochem (Hadfield, UK). Their chemical properties are listed in Table 2.1.

I performed a column leaching test in order to confirm the absence of significant sorption for the five selected chemicals on the same soil used in the lysimeter (Section 2.2.6). In addition, plant and soil extracts were analyzed after the experiment was terminated to examine whether FBAs had been accumulating in the biomass. Microbial degradation was probed by measuring fluoride concentration (a by-product of any FBA breakdown) in a selection of discharge and soil water samples (Section 2.2.7).

### 2.2.3 Tracer analysis

FBAs can be analyzed using different methods (Stetzenbach *et al.*, 1982; Lasa and Śliwka, 1990; Galdiga and Greibrokk, 1998). Liquid chromatography coupled with mass spectrometry appears to give the best analytical sensitivity (Dalian and Ronen, 2001; Juhler and Mortensen, 2002). The FBAs were therefore quantified by LC/MS-MS (Acquity®TQD, Waters). The limits of quantification obtained with this procedure were obtained during the calibration with standards, and varies between 3 μg L<sup>-1</sup> and 10 μg L<sup>-1</sup> according to the compound (see Table 2.1). Three of the five compounds have deuterated internal standards (2,5-Difluorobenzoic-d3 Acid, 2,6-Difluorobenzoic-d3 Acid, 3,4-Difluorobenzoic-d3 Acid) purchased at EQ Laboratories GmbH (Augsburg, Germany). 0.11 mL of a preparation containing 120 ng mL<sup>-1</sup> of deuterated standards diluted in ultrapure methanol was added in all the vials containing 1 mL of sample prior to the injection. A calibration procedure was performed to validate the analytical method

and discard potential matrix effects.

### 2.2.4 Tracer sampling

Discharge water was sampled using a flow-proportional sampling device. A 20 mL sample was taken every 1 – 3 liters of cumulative discharge flow, depending on the time during which the system is left unattended and the number of sample bottles in stock on the fraction collector tray. Soil water was also sampled every 2 – 3 days at each depth. The samples were filtered by 0.45  $\mu\text{m}$  hydrophobic syringe filters with GMF/PP membranes (BGB Analytik AG, Switzerland) as soon as possible and stored at 4 °C in prior to analysis.

### 2.2.5 Rainfall and tracer applications

The rainfall series was constructed using a marked Poisson process with inter-arrival time  $\lambda$  and mean rainfall depth  $\alpha$ , as proposed for daily rainfall in the classic approach by *Rodriguez-Iturbe et al.* (1999). The two parameters of the rainfall distribution were arbitrarily defined in order to maximize the coefficient of variation of the hydrologic travel time in the vadose zone and to minimize the ensuing mean travel time for the entire duration of the experiment. For comparison, the mean travel times were estimating using the approach of *Harman et al.* (2011), who has calculated the coefficient of variation of mean travel times as a function of two lumped parameters using a simple piston displacement model. One parameter ( $\gamma$ ) subsumes soil properties and the type of climate. Hence, given the soil properties of the lysimeter and the estimated potential evapotranspiration for a willow crop (*Persson, 1995; Schaeffer et al., 2000; Guidi et al., 2008*), the inter-arrival time and the mean rainfall depth were set to 0.67  $\text{day}^{-1}$  and 20.3 mm, respectively. Multiple rainfall sequences with selected parameters were generated.

Five rainfall events predicted to drive significantly different travel times were selected within a timespan of one month. Each rainfall event was labeled with a different FBA tracer. Two of these tracers were simultaneously re-injected 10 months later, once the outflow concentrations of all previously injected tracers were found below the detection limit. This provided two additional measurements of solute travel times which prove particularly valuable to test whether the different tracers are subject to reactivity and/or degradation processes. Replicated, compound-specific measurements of breakthrough curves for two tracers have thus been gathered. The tracers with the highest and lowest recovery ratio after the first injection (2,6-DFBA and 2,5-DFBA respectively) were selected, in order to additionally establish whether their disparity in the breakthrough is not only an artefact of different degradation extent. Discharge and soil water concentration monitoring lasted until the tracer concentration decreased below the detection limit (July 2014).

'Rainfall' events were generated manually in the lysimeter system as quasi-instantaneous pulses – poured from a watering pot directly onto the soil surface. For the labeled rainfall

## Chapter 2. Transport of fluorobenzoate tracers in a vegetated hydrologic control volume: Experimental results

---

events, a primary tracer stock solution was prepared for each FBA by dissolving the targeted mass of powder in 20 mL of ultrapure methanol. The stock solution was further diluted in the volume of water corresponding to the labeled rainfall event and immediately injected in the lysimeter. Resulting tracer concentration in the rainfall water varies in the range of 90 mg L<sup>-1</sup> to 230 mg L<sup>-1</sup>. The system was conditioned with a chosen rainfall pattern during two months before the injection of the first tracer, so that the water content profile in the soil column can be assumed to be consistent with the type of climatic forcing simulated. The five selected tracers were all injected during the first month of the experiment, starting on April 17, 2013. This relatively short period limits the overall evolution of the system between the five injections, so that all tracers would have faced roughly the same system states. This condition restricts the origins of the heterogeneity in the observed fate of the five tracers to differences in the external forcing (precipitation and evapotranspiration) during the early stages of their hydrologic journey. It is to be noted that the mass of each tracer was adjusted to obtain a concentration in the batch injection volume of the order of 0.1 g L<sup>-1</sup>, in order to avoid concentration effects between each tracer injection.

### 2.2.6 Tracer validation by leaching test

In order to assess the reactivity of the selected chemicals in the soil, a small-scale column experiment has been set-up. The column consists of a stainless-steel cylinder with a diameter of 25 cm filled with 50 cm of the same soil mixture used in the lysimeter experiment. A vertical downwards flow is induced by maintaining an 1-cm overflow above the soil surface, and can be regulated by changing the pressure head at the outlet. A mixture of the five tracers was added in the inlet zone (overflow) simulating a quasi-instantaneous pulse with a concentration of about 10 mg L<sup>-1</sup>. Samples were taken every 2 hours using a solenoid valve and a fraction collector, and a subset of the collected samples was further analysed with the same procedure as described in section 2.2.3.

After 13 days, 94, 100, 97, 100 and 102% of the mass injected was recovered for 2,5-DFBA, 2-TFMBA, 3,4-DFBA, 2,6-DFBA and 3-TFMBA respectively. The small mass excess for the last tracer is likely due to measurements error. The breakthrough curves and cumulative mass recovery are presented in Figure 2.2. The bi-modal shape of the breakthrough curves is likely induced by fluctuations of the discharge rate, which, due to the system set-up, could not be maintained perfectly constant during the experiment. These results are in accordance with the finding of *Jaynes* (1994), with a slightly retarded arrival of 3,4-DFBA and 3-TFMBA in regards to the other compounds and mass recovery within a similar range (it is to be noted that the experiment was designed with a residence time about 10 times larger than in *Jaynes* (1994)).

The negligible mass loss and low retardation of the FBAs observed in this experiment for the specific soil used, in accordance with the literature (*Bowman*, 1984; *Bowman and Gibbens*, 1992; *Jaynes*, 1994) are justified arguments for the selection of the five FBAs as individual conservative tracers for this study.

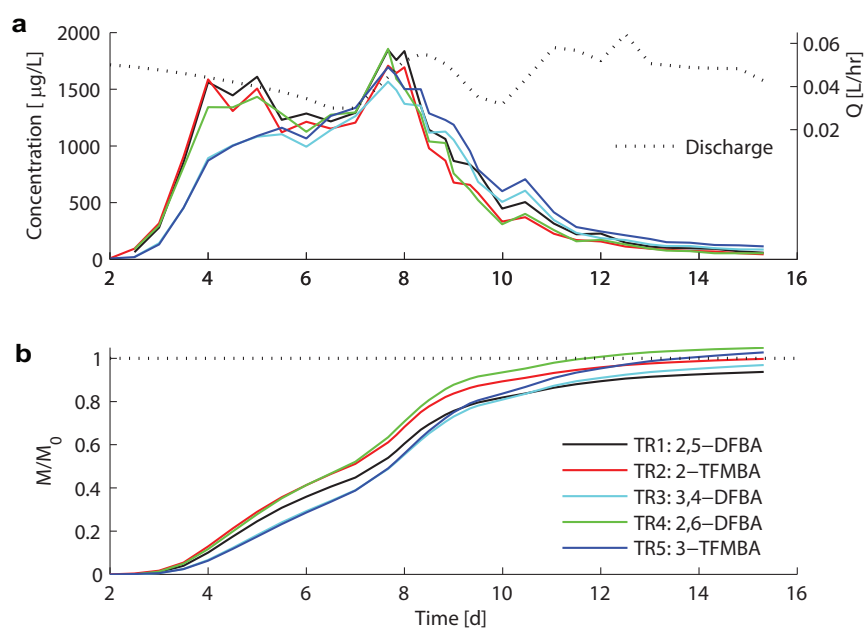


Figure 2.2: (a) Tracer breakthrough curves and (b) cumulative tracer mass recovery in the column experiment. The high recovery ratio (above 94%) indicate a good suitability of these fluorinated compounds for their use as conservative tracer in this particular soil as reported in *Jaynes (1994)*.

### 2.2.7 *Post hoc* tracer reactivity testing

At the end of the experiment, the poor overall recovery of the FBAs indicates that despite they are often considered as non-reactive tracers in the literature, we face potentially diverse processes affecting the amount of unreacted compounds found in the discharge. These processes are either 1) degrading the tracers into by-products within the system, 2) removing the tracers via non-monitored pathway (i.e. ET flux) and/or 3) accumulating the tracers within the system preventing their release in the discharge water. The possibility of these pathways *a posteriori* were investigated by measuring tracer accumulation in the plant and in the soil (destructive). Note that plant metabolism and microbial activity may also have transformed parts of the tracers applied by various degradation pathways, leading to a potentially large array of by-products (*Bowman et al., 1997; Commandeur and Parsons, 1990*). A possible microbial degradation pathway involving the release of fluoride as a by-product was also examined.

### Soil sorption

FBA extraction was performed on raw soil samples (i.e. unsorted of any organic/mineral fraction). Therefore, the levels of FBA can be difficult to interpret, as they can result from soil sorption, but also root uptake or microbial bioaccumulation. Soil cores were sampled

## Chapter 2. Transport of fluorobenzoate tracers in a vegetated hydrologic control volume: Experimental results

---

at different depths and different radial distances from the trunks after the last water flushes, and determine for each sample the content in FBAs and in organic matter (with total organic carbon measurements), so as to analyze possible correlations. A positive correlation of the FBA content with the organic matter would suggest that the FBAs are mainly bound to the organic fraction (roots or microbial mass) rather than sorbed on mineral particles. A vertical gradient of total organic carbon may be expected in this setting based on the root density distribution.

Soil cores were collected with a semi-cylindrical auger, giving a continuous sample from the surface up to the top of the gravel filter at 2 m-depth. Four vertical profiles were collected radially at 0, 15, 30 and 45 cm from the center of the lysimeter, hence at increasing distance from the trunks of the two willows. Each profile was divided into four samples with depth ranging from 0-50, 50-100, 100-150 to 150-200 cm. The samples were dried at 40 °C during 24 hours, and conditioned in airtight plastic bags. 5-10 g of each sample were used for stirred extraction with 30 mL of MilliQ water during 24 hours. The samples were filtered at 0.45  $\mu\text{m}$  with GMF filters (BGB Analytik) and concentrated on a solid phase extraction (SPE) system (Visiprep, Sigma-Aldrich) with 200 mg polymeric reversed-phase cartridges (Oasis HLB 6 cc, Waters) conditioned with 5 mL acetonitrile and 10 mL MilliQ water. After the injection of the 30 mL samples, the FBAs were recovered with 3 mL acetonitrile, concentrated at 0.1 mL and finally diluted at 1 mL with the LC/MS-MS eluent. The quantification was done with LC/MS-MS following the procedure described in section 2.2.3.

The total organic carbon (TOC) fraction of each sample was determined using the combustion catalytic oxidation method (Shimadzu TOC-V SSM).

No significant trend of carbon content was observed in the 'soil' samples, with a mean value of 0.6 and 1.4% for the total organic carbon and inorganic carbon respectively (Figure 2.3). The root network is thus considered to be homogeneously distributed in the entire volume of the lysimeter.

Tracer concentration in the soil ranges from 0 to about 10  $\text{ng g}^{-1}$ , except for TR3 which has not been detected in any sample (Figure 2.4). Higher tracer content are observed for the deepest samples with the largest distance from the center, reaching about 55  $\text{ng g}^{-1}$  for TR5 and up to 260  $\text{ng g}^{-1}$  for TR4. Generally, there is a small increase of the concentration (except for TR5) with depth, but no clear trend is observed with the radial distance from the center. The mass measured in the soil represents approximately 0.1, 0.4, 0.9 and 2.3% of the mass injected (on a total unrecovered mass of 100, 33, 99, 40 and 81% at the end of the breakthroughs) for TR1, TR2, TR4 and TR5, respectively. No correlation between the samples' tracer content and the TOC can be noticed, as the low TOC values appear homogeneous in the system, between 0.37% and 0.77%. A TOC content between 0.9% and 1% was observed for the samples corresponding to the center profile at 0-50 cm depth and to the profile at 15 cm from the center at between 100-150 cm depth.

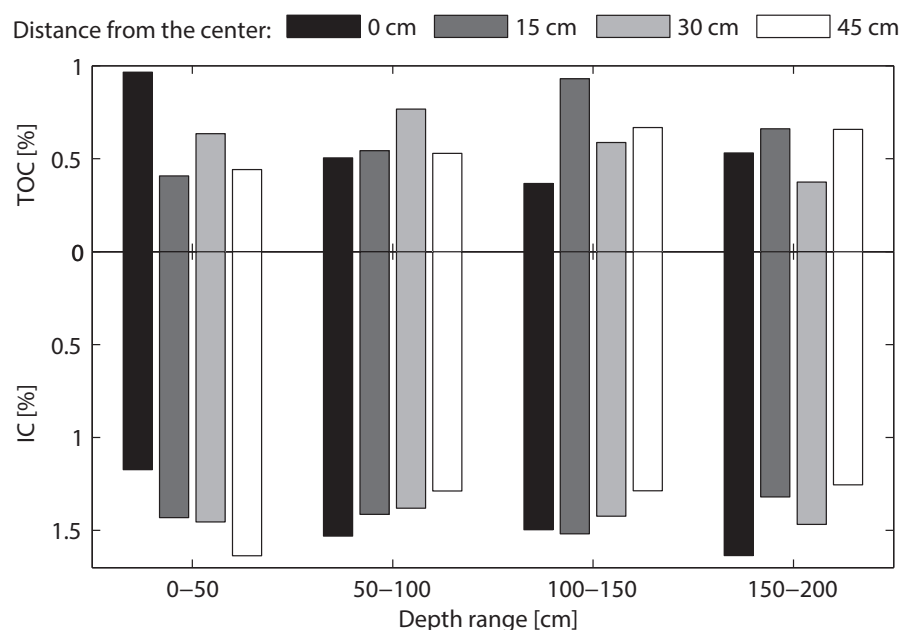


Figure 2.3: Total organic carbon (TOC) and inorganic carbon (IC) content in the soil samples. The TOC levels are low for all samples, and – except a slightly higher content in the shallower sample of the center profile – no particular trend linked to the development of the rooting can be observed.

### Plant uptake

In order to estimate the FBA content in the biomass, the two willows were cut at the soil surface, and the aerial biomass was divided and weighted as follows: upper twigs, mid twigs, lower twigs, trunk, 1st-order branches, 2nd- and 3rd-order branches. The twigs of each category were further divided into two size-classes (as the age of the twigs may change the amount of tracer that could have been metabolized before sampling). Samples in each category were randomly collected, measured and weighted. The samples were ground with a helical blade mixer (Ika M20) and a similar filtration and extraction procedure (extraction with water and SPE) as for the soil samples was used. The LC/MS-MS quantification procedure is detailed in section 2.2.3.

The detection of FBAs in the plant extracts confirms that plant uptake is a viable pathway, in particular with willows. Only TR2 and TR5 were detected, whereas the three other tracers were below the detection limit (Figure 2.5). TR2 was measured in all samples at a concentration ranging from 165 to 397 ng g<sup>-1</sup>. The TR2 concentration was significantly lower in the wood samples than in the twigs samples. TR5 concentration were two order of magnitude lower than TR2 ranging from 1.6 to 30.6 ng g<sup>-1</sup>, but also detected in all samples. The concentrations measured multiplied by the total dry biomass of each sample's category give a crude estimate of the tracer accumulated in the aerial part of the willow, which represent 3.8 mg for TR2 and 0.06 mg for TR5 (0.13% and 0.003% of the TR2/TR5 injected mass respectively).

**Chapter 2. Transport of fluorobenzoate tracers in a vegetated hydrologic control volume:  
Experimental results**

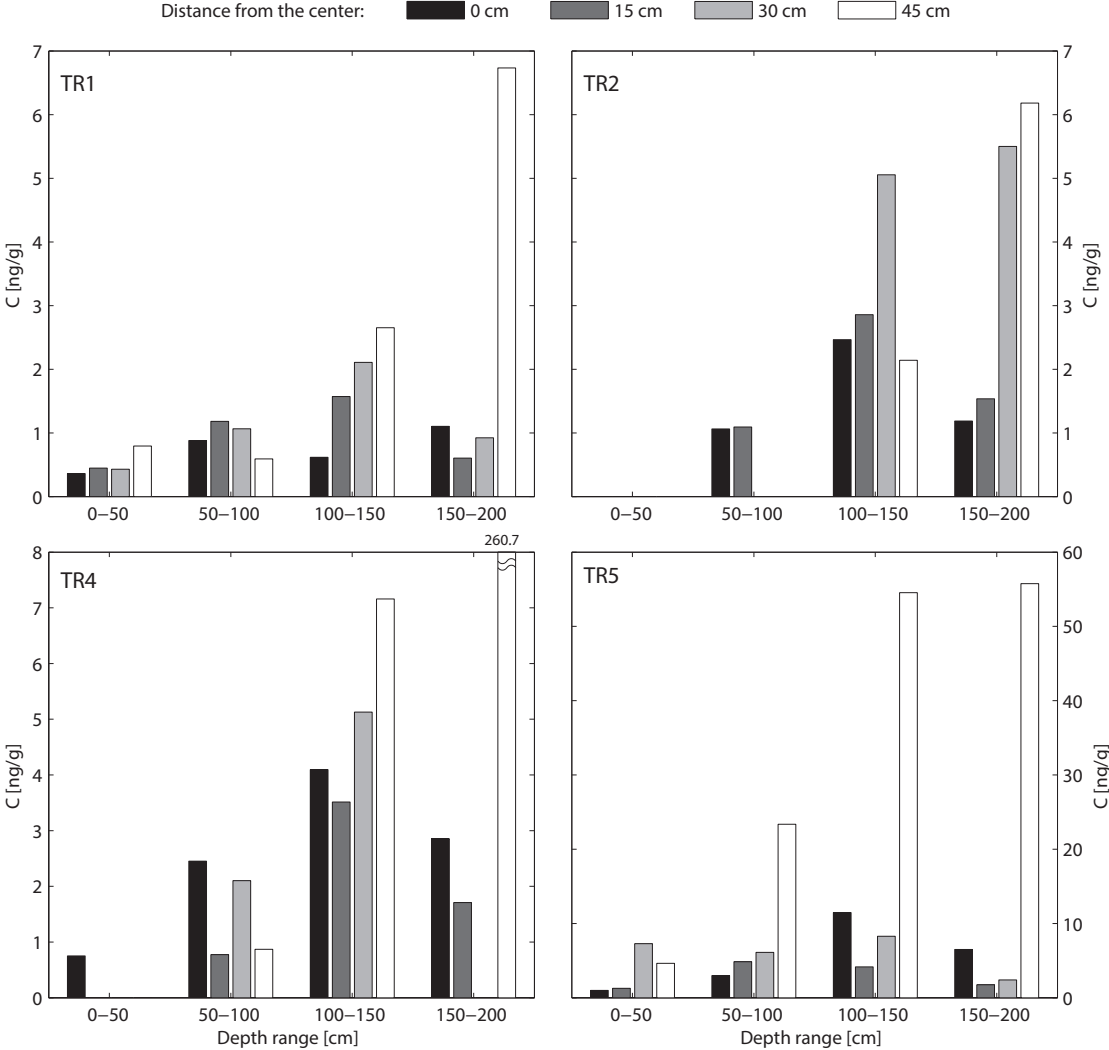


Figure 2.4: Residual tracer concentration in the soil, after extensive flushing. In general terms, an increase of tracer concentration with depth can be observed, in particular at large radial distance from the center of the lysimeter. This can be attributed to insufficient flushing in these zones, due to the convergence of the flow lines towards the centered outlet during large discharge events. No correlation with the total organic carbon content was found (Figure 2.3). Note the different concentration scales on the plots.



Note that the total aerial mass of the willows has been measured at the end of the experiment, which represents about 10 kg (1 kg with roots when the trees were planted). The biomass growth is thus not likely to affect the storage and ET measurements, as the daily growth is negligible compared to the mass changes that the system undergoes daily due to the input and output fluxes.

### Microbial degradation

Tracer microbial degradation is difficult to assess, as breakdown pathways are numerous and may differ depending on the microbial communities present in the soil. Specific literature reporting fluorobenzoic acid degradation is relatively poor and limited to mono-fluorobenzoic acids (*Commandeur and Parsons, 1990; Motosugi and Soda, 1983; Vargas et al., 2000*). In contrast, degradation of chlorofluorobenzoic acids (CBAs) has been much more investigated (they are by-products of PCBs). Numerous aerobic degradation pathways of CBAs have been described for different bacteria strains. However, similarly to FBAs, most of them usually lead to the production of catechol, which implies the release of a halide ion, or chloro/fluoro-catechol (*Commandeur and Parsons, 1990; Motosugi and Soda, 1983; Patil and Rao, 2014; Zaitsev and Karasevich, 1981*). Fluoride potentially released from microbial degradation would then be washed out, as the soil sorption can only occur by anionic exchange, unlikely in very sandy soil as here. Hence, a selection of soil water and discharge water samples were analyzed *a posteriori*, in order to identify a possible fluoride concentration increase due to microbial degradation of FBAs. fluoride concentration in aqueous samples were determined using ion chromatography (Dionex ICS-3000, USA).

The fluoride concentrations are shown in Figure 2.6. The fluoride level in the discharge water is generally low, below the analytical limit of calibration ( $0.10 \text{ mg g}^{-1}$ ). Two samples show a concentration around  $0.20 \text{ mg g}^{-1}$  early after the beginning of the first breakthrough in 2013. At the end of the first breakthrough and during the subsequent breakthrough of the 2014-injection, fluoride increases consistently up to  $0.15 \text{ mg g}^{-1}$ . The soil water samples indicate a low negative gradient with depth.

## 2.3 Results

### 2.3.1 Hydrologic fluxes

Figure 2.7 summarizes the measured in- and out-fluxes and the dynamics of soil moisture, here shown at a hourly timescale. It can be observed that soil moisture (Figure 2.7b) responds to rainfall patterns (Figure 2.7a) by producing variable inter-event moisture conditions constrained to a relatively narrow range. This is also related to the discharge response (Figure 2.7c) which is only triggered when the overall soil moisture crosses a threshold (red band on Figure 2.7b). Of the cumulative rainfall during the observed period, 39% (2243 mm) was discharged at the outlet whereas 61% (3454 mm) was either evaporated at the soil surface or transpired by

**Chapter 2. Transport of fluorobenzoate tracers in a vegetated hydrologic control volume:  
Experimental results**

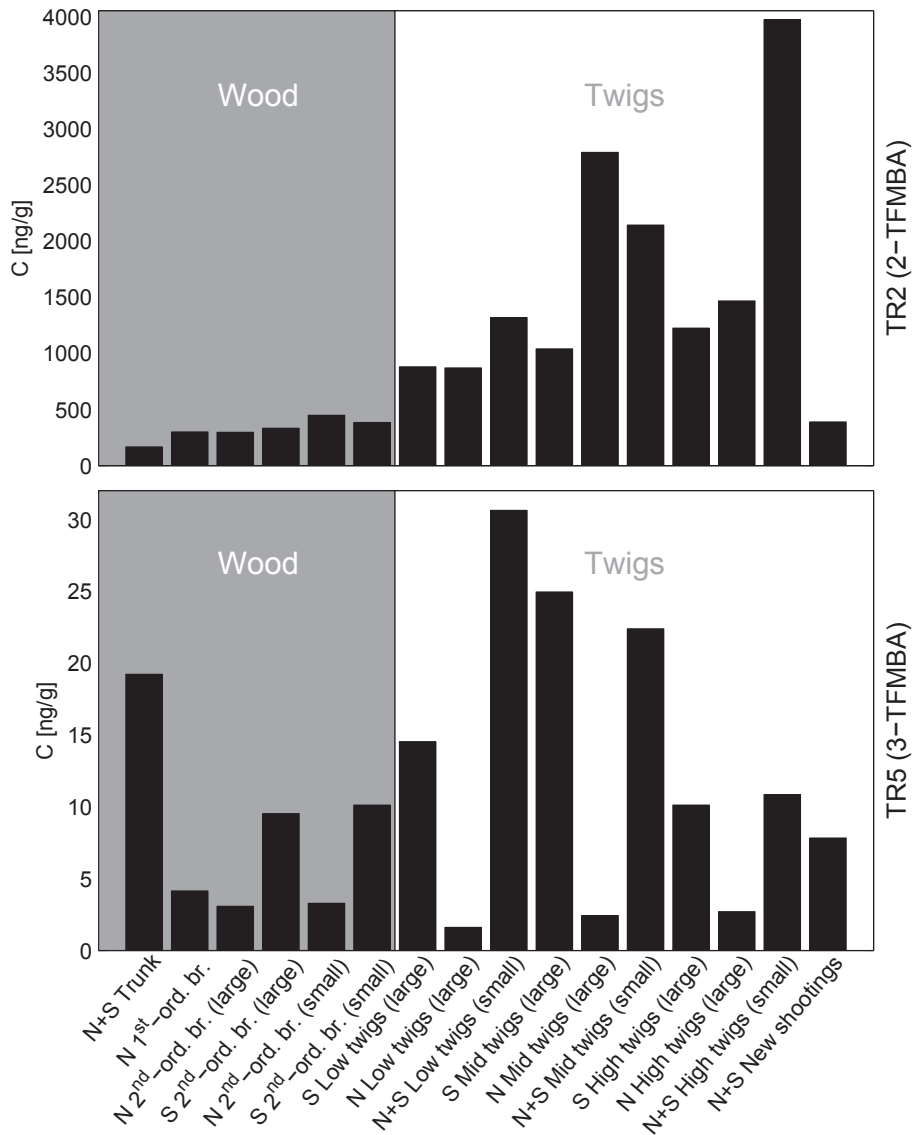


Figure 2.5: Tracer concentration in the aerial willow dry biomass. The difluoro-forms of benzoic acids were not detected, suggesting a higher susceptibility to their metabolization compared to the trifluoromethyl-forms. Wood samples were taken from the trunk, 1st- and 2nd-order branches depending on their size and tree (two trees, North and South), and the twigs samples (terminal parts of the branches with leaves) are divided depending on their size, their vertical position on the canopy and the tree. The new shootings were sampled below the translucent roof.

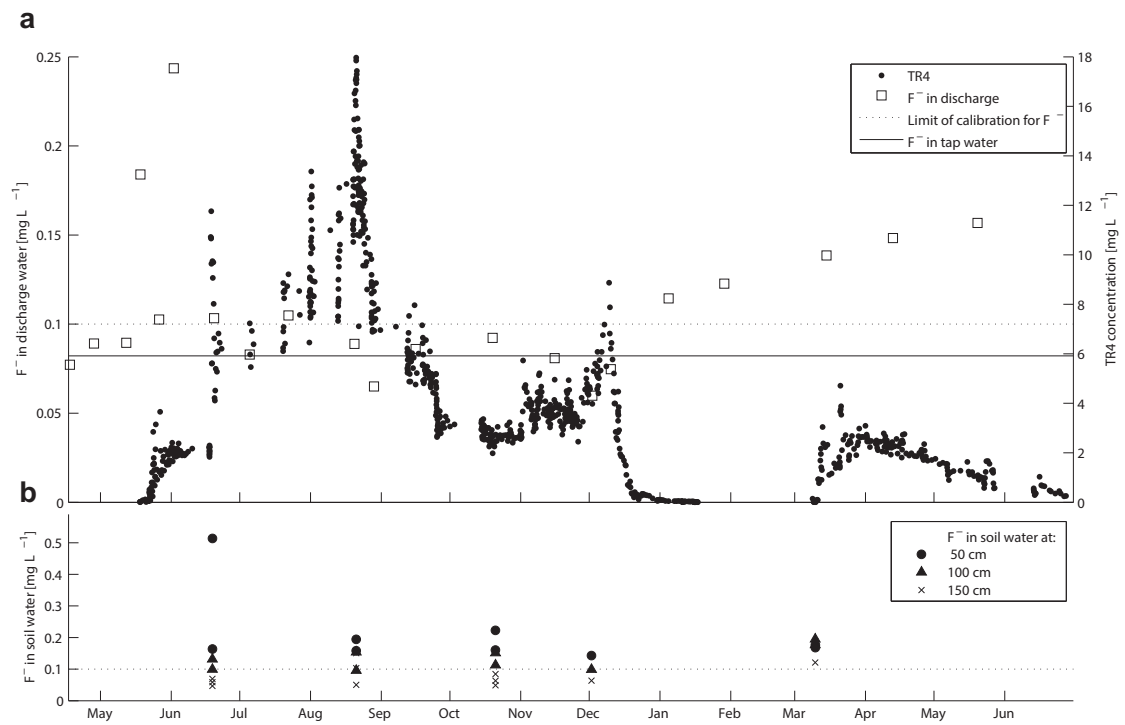


Figure 2.6: Fluoride concentration in a) discharge samples and b) soil water samples. The concentration of TR4 are also shown (black dots in a) to provide a temporal reference of the transport dynamics.

## Chapter 2. Transport of fluorobenzoate tracers in a vegetated hydrologic control volume: Experimental results

---

the willow. Values of ET rates that might appear exceedingly high are explained by the fact that willow crown and overall canopy occupy a surface much larger than the lysimeter.

A large rainfall input (83 mm) occurring at relatively wet antecedent conditions triggered the maximum observed discharge rate  $Q$  up to  $12 \text{ mm h}^{-1}$  on April 25, 2014, three hours after injection (Figure 2.7). Large discharge flow occurs more frequently in winter, when soil moisture is consistently above 0.5 due to limited ET abstractions. As shown by the event of August 26, however, a large rainfall event could drive discharge rates above  $4 \text{ mm h}^{-1}$  even in summer conditions. Antecedent rainfall are in general necessary in order to compensate the large ET demand credited by the large canopy and to increase soil moisture throughout the profile. Hence, not only the overall storage but also the spatial heterogeneity of the water content is a key factor controlling the discharge rate, a feature commonly observed in real catchments (e.g. *Hrachowitz et al.*, 2013).

The  $ET$  signal at hourly timescale mirrors daily and seasonal cycles of climate and vegetation (Figure 2.7d). Unphysical negative values were observed when  $ET$  was lower than the noise level of the load cells. It is reasonable to assume that nightly surface evaporation and plant transpiration were negligible in early spring, when the air temperature  $T$  and plant activity were low (say,  $T \leq 10^\circ\text{C}$ ). The observed signal confirms such assumption, as  $ET$  values are found close to zero between 8 pm and 9 am from the experiment start until early June and from November onwards. The daily evapotranspiration varies between  $3 - 5 \text{ mm d}^{-1}$  in spring to more than  $20 \text{ mm d}^{-1}$  in summer. Corrected for the ratio of the crown area of the actual canopy and the lysimeter surface, this represents about  $1.5 - 2.5 \text{ mm d}^{-1}$  in spring and about  $10 \text{ mm d}^{-1}$  in summer. The literature reports transpiration typically around  $5 \text{ mm/d}$  during the growing season of young willows (*Persson*, 1995; *Schaeffer et al.*, 2000). However, *Guidi et al.* (2008) measured ET values up to  $14 \text{ mm/d}$  in late summer for a fertilized willow with stem size reaching  $300 - 400 \text{ cm}$ . Moreover, as the soil surface of the lysimeter is covered by a translucent roof and well ventilated with large side openings, this installation might have acted as a greenhouse (under the willow canopy) by increasing soil surface evaporation through heating. The gradual augmentation of  $ET$  between the beginning of June till the end of July corresponds both to an air temperature increase from  $10$  to  $27^\circ\text{C}$  and to an important growth of the two willow stems of  $100 \text{ cm}$  in height (both  $250 \text{ cm}$  on July 24). The sudden decreases of the  $ET$  flux visible in Figure 2.7d on a few occasions (e.g. June 29, July 29 and August 7) corresponds to important rapid temperature drops of  $5-10^\circ\text{C}$ . The simultaneous noise increase in the signal can be explained by the weather degradation often characterized by strong precipitation that generate unexpected water inputs in the system by flowing through the roof chinks. The data were averaged and corrected to produce a positive definite time series of abstractions as shown in Figure 2.7.

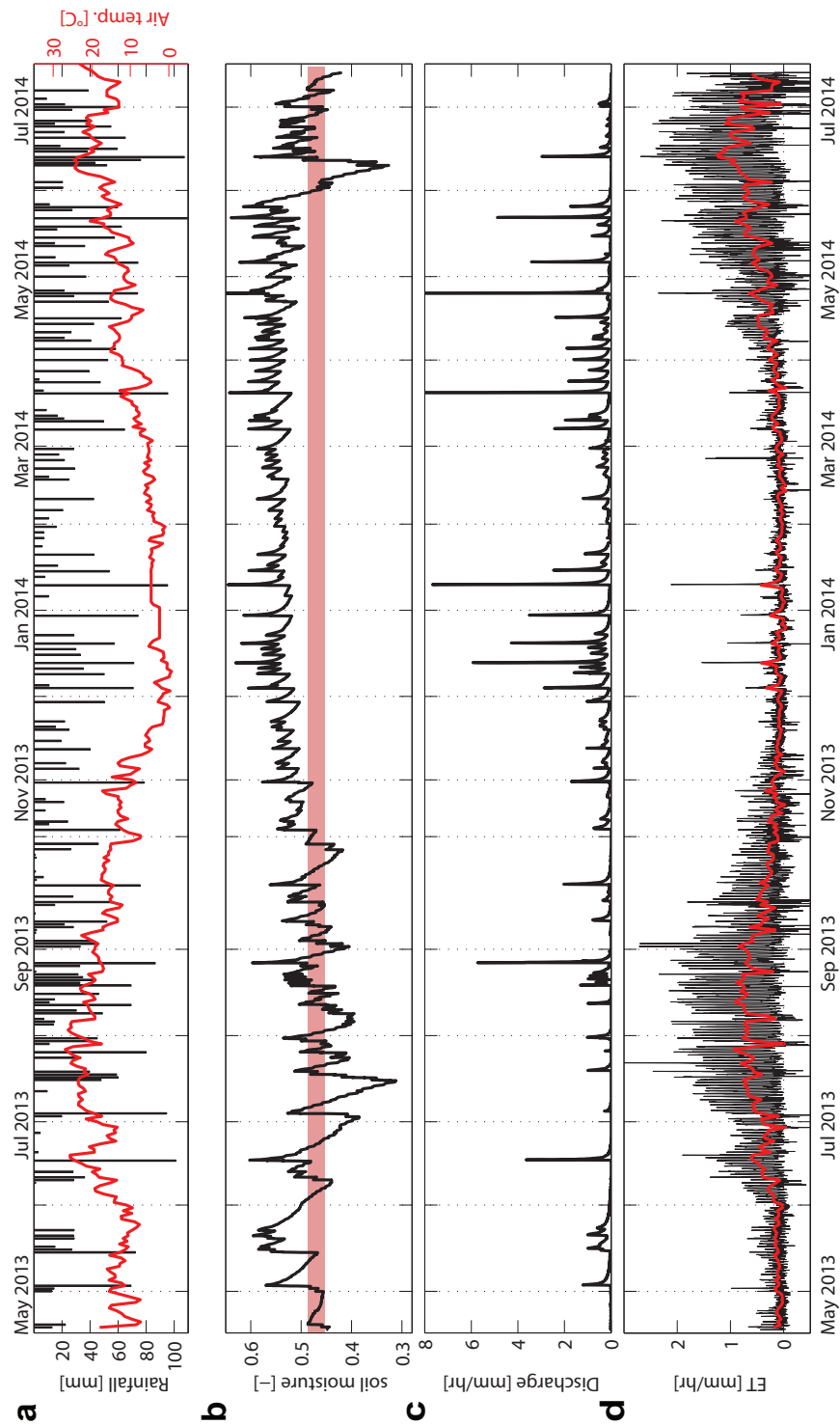


Figure 2.7: Input and output fluxes of the system during the selected experiment period. (a) Daily rainfall events and mean daily temperature (red). (b) Soil moisture i.e. relative fraction of saturated soil porosity  $\epsilon \in (0, 1)$ . The red band shows the lower and upper quartiles of soil storage that triggers discharge flux. (c) Discharge rate at the outlet. (d) Hourly (black) and mean daily (red) evapotranspiration flux.

## Chapter 2. Transport of fluorobenzoate tracers in a vegetated hydrologic control volume: Experimental results

---

### 2.3.2 Tracer dynamics and fluxes

Figure 2.8a shows the precipitation sequence. It emphasizes the events that were marked with a specific tracer. For the ease of reference throughout the chapter, 2,5-DFBA is referred to as TR1, 2-TFMBA as TR2, 3,4-DFBA as TR3, 2,6-DFBA as TR4 and 3-TFMBA as TR5. The tracer breakthrough curves (Figure 2.8b) display the measured concentrations in the discharge samples normalized to the initial concentration of the injection batch volumes for each tracer. The maximum peak relative concentration was recorded for TR4 at 0.18 on August 21, 98 days after its injection. The relative peak concentration for TR2 and TR5 were also measured on the same date (112 and 96 days after their injection), but at a much lower concentration (0.024 and 0.012 respectively). In contrast TR3 peaked only 46 days after injection where the maximum relative concentration was only 0.001. TR1 was never detected in the discharge, but only in soil water samples, as described below. At the end of the first injection period (January 2014), the concentration of all five tracers in the outflow was below the analytical limit for quantification.

The total mass recovered in the outflow with time is shown in Figure 2.9b by the shaded area. Considering that TR4 was injected 15 days after TR2, and that the initial mass of TR4 in rainfall was more than 2.5 times the initial mass of TR2, the export patterns of TR2 and TR4 are synchronized, and the amount of tracer mass exported during each discharge event is similar for the two compounds. In contrast, TR5, injected only 2 days after TR4 (and with a similar initial mass as TR2) shows a more attenuated export dynamics, with only about 18% of its initial mass recovered in the discharge, whereas TR2 and TR4 were recovered at 67% and 60% respectively. Less than 0.2% of the mass of TR3 was recovered in the discharge.

Owing to the sampling of soil water at the control ports placed at three different depths, a concentration profile in time inside the soil column can be estimated for each tracer (Figure 2.9a). Even if the data available are spatially discrete, they show interesting features. For instance, even if TR1 has not been detected in the discharge (see Figure 2.9b), it was measured in the soil water samples during three months at detectable concentrations (in the order of 0.1% of the initial concentration of the input) at all depths. In contrast, TR3 was measured in the discharge samples (0.1% of total recovery), but it was only detected in soil water samples at 50 cm at a maximal concentration about one order of magnitude lower than TR1.

The behavior of the water pulses labelled with TR2 and TR4 proves very different from TR1 and TR3, in that the total mass recovered is much higher for the first two (60-70% against less than 0.2% respectively). The total tracer mass in the system (black dots in Figure 2.9b) has been calculated by assessing the mean concentration for each control plane (then averaging on all planes) and multiplying it by the current water storage. We observe that initially, this estimation captures the entire input tracer mass for TR2 and TR4, whereas only 50% of the input mass of TR5 is measured and less than 1% for TR1 and TR3 (note that the y-axis varies by orders of magnitude between the plots). This method may actually underestimate the mass in storage due to the low-depth resolution of concentration measurements and the assumption of homogeneously distributed soil moisture, especially if the tracer pulse volume is small (e.g.

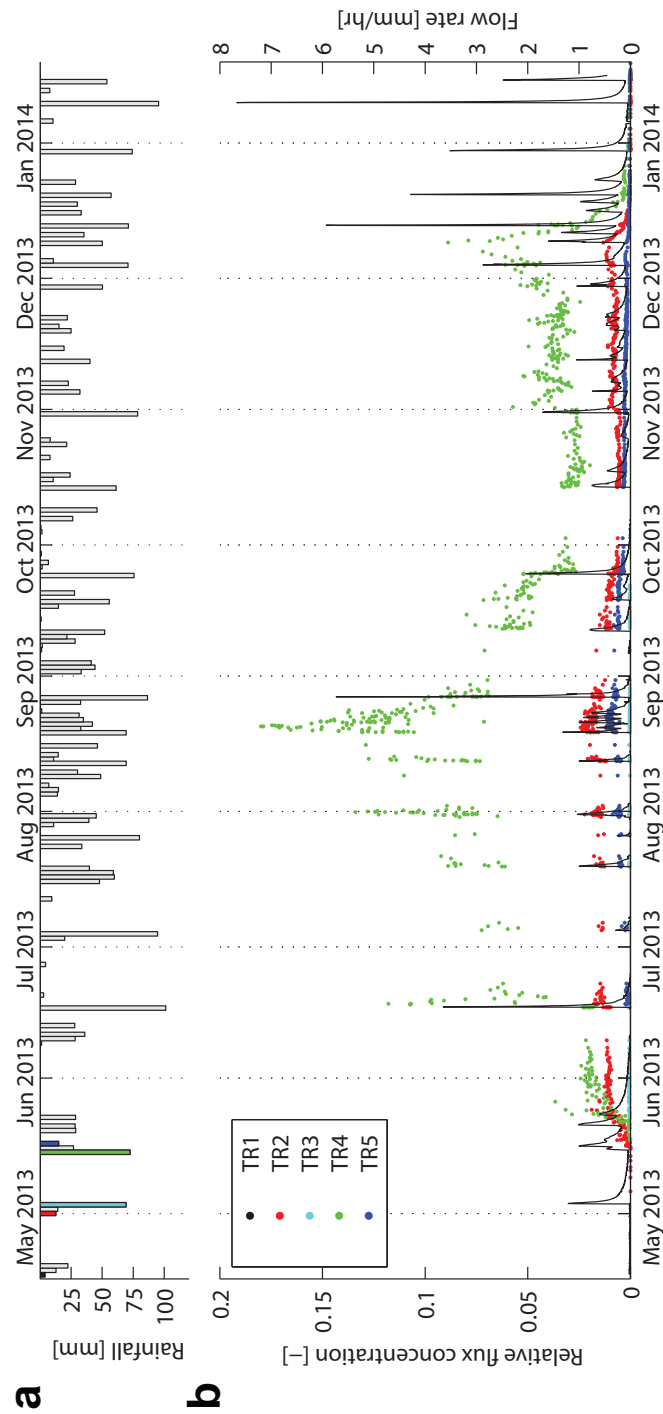


Figure 2.8: Results of the tracer experiment, for the sequenced injection of 2013. (a) Sequence of applied precipitation with tracer-marked events (colored). (b) Tracer breakthrough curves in the discharge expressed in relative concentration to their respective input (colored dots) and flow rate (black line).

## Chapter 2. Transport of fluorobenzoate tracers in a vegetated hydrologic control volume: Experimental results

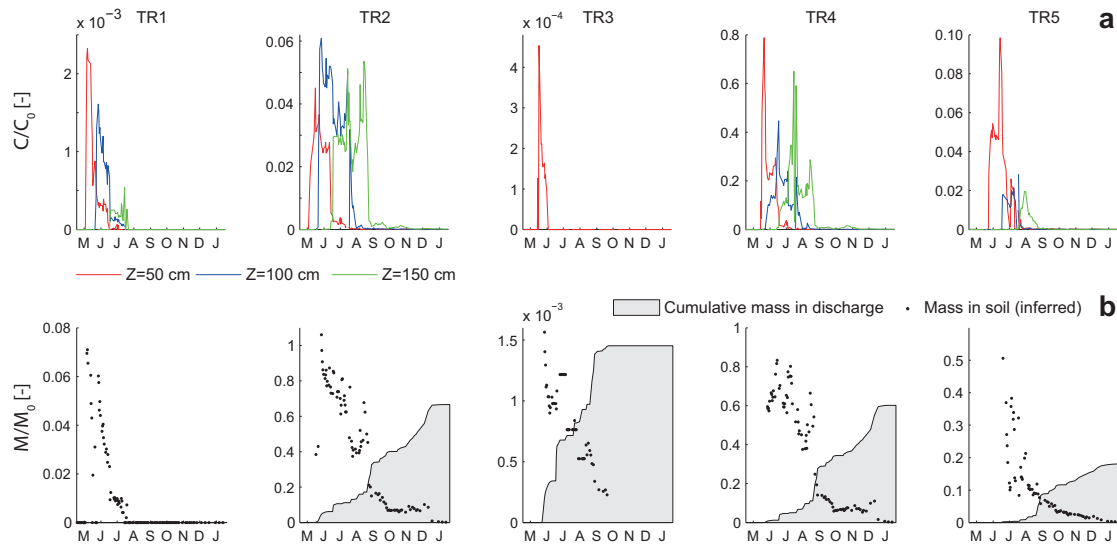


Figure 2.9: Tracer data in the soil water for the sequenced injection of 2013. (a) Temporal evolution of the relative concentration of each tracer in the soil water at three control planes distributed in depth (concentration average of all soil water samples available per depth). (b) Estimation of the relative total mass of each tracer in the soil column and gravel filter (points) with cumulative tracer mass having exited the system through discharge (grey area).

if the pulse is temporarily be located outside the probes' volume of influence, as in the case for the TR1 data in May). However, one notes that the input volume of TR3 was very large (77 l), and yet the maximal relative concentration observed at the upper depth is 0.04, the lowest value measured for all tracers. The estimated TR3 mass at this depth is later recovered in the discharge, which suggests that most of the mass loss occurred in the early phase of the breakthrough and at shallow depths. In contrast, TR1 is detected at all depths and in higher concentration, even though the input volume was much smaller (5 l) and therefore more prone to bypass the localized sampling points. As for TR1, only a fraction of the input mass of TR5 is detected early in the soil water (about 40%, less than 10% for TR1). The overall concentration decreases considerably with depth for the two tracers, suggesting a degradation or uptake of the tracer. In comparison, the overall concentration per depth for TR2 and TR4 does not seem affected by such a reduction. Finally, the TR5 pulse shows intermediate infiltration and export patterns between TR1/TR3 and TR2/TR4. About 20% of the initial mass has been retrieved in the discharge and the estimated mass in the soil column has never exceeded 50%.

When injected simultaneously (like in the second validation injection from February 2014), TR1 and TR4 (least and most recovered tracers during the first test, respectively) demonstrate identical release dynamics even if the signal of TR1 is mitigated compared to TR4 (black lines in Figure 2.10a). The mass recovery of TR1 was 45% at the end of the sampling period, and 69% for TR4. In contrast, the recovered TR4 mass during the first injection after the same cumulative discharge volume was 60% (Figure 2.10, insets).



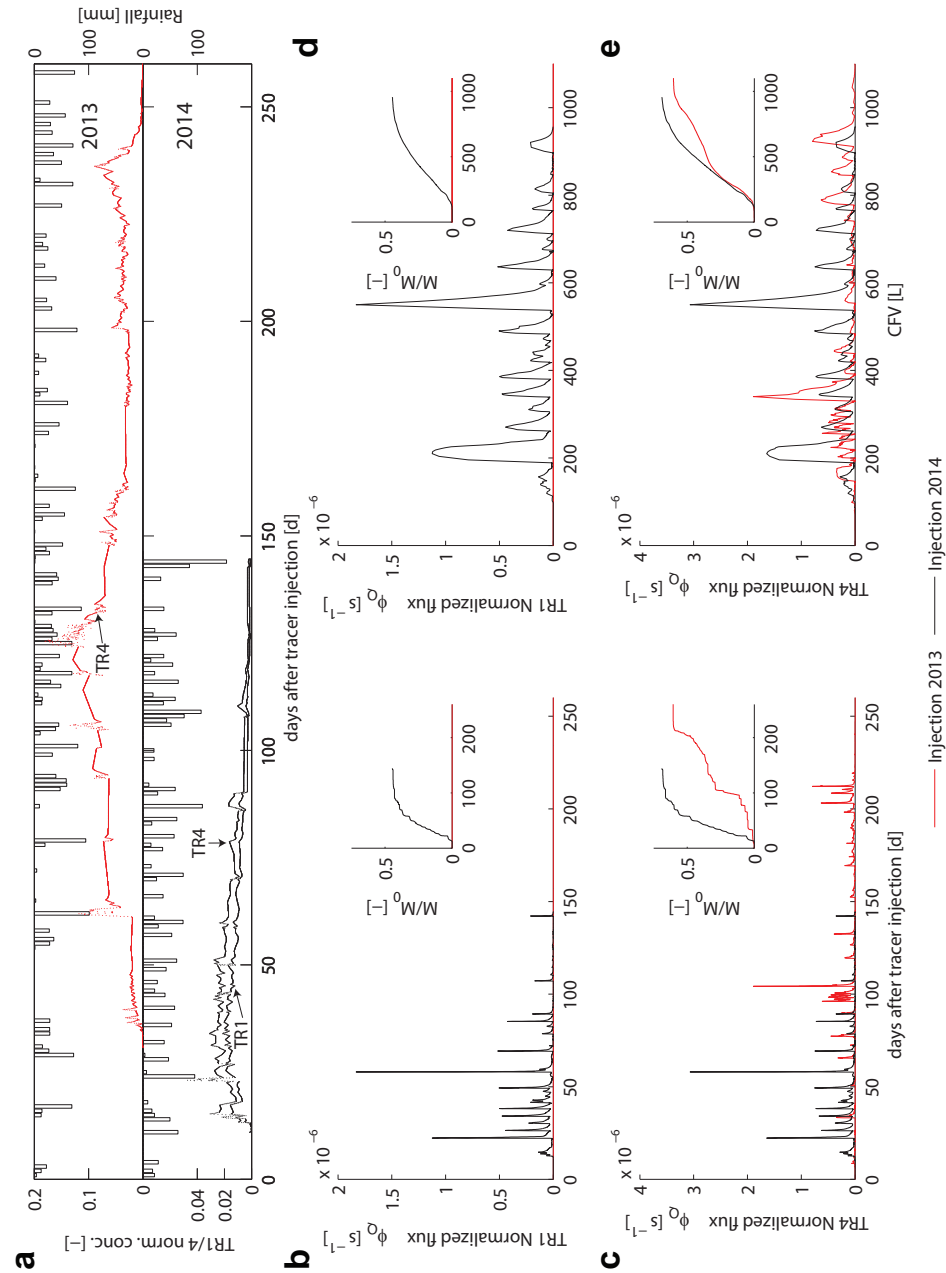


Figure 2.10: Comparison of the discharge concentration and mass fluxes between the validation tracer test conducted in 2014 (with simultaneous injection of TR1 and TR4, represented in red) and the sequenced injection in 2013 (only TR1 and TR4 are shown, represented in black). a) Concentration breakthrough of the 2013 injection (top panel) and 2014 injection (bottom panel), with their respective rainfall sequence (bars). b) and c) show the mass flux and cumulated mass recovery (inset) for TR1 and TR4 respectively, plotted versus the elapsed time since injection. Note that TR1 was not detected at all during the 2013 injection. d) and e) also represent the mass flux of TR1 and TR4, but plotted versus the rescaled time since injection, proportional to the volume discharged *CFV*.

## Chapter 2. Transport of fluorobenzoate tracers in a vegetated hydrologic control volume: Experimental results

---

Further interpretations of the mass recovery are contained in Section 2.2.7 following *ex post* analyses of biomass and samples.

The various degrees of mass recovery of the tracers indicate that they are all subject to degradation or removal processes, possibly at various extents specific to each tracer. This restricts the analysis to hydrologic transport of the three tracers that were significantly retrieved (TR2, 4 and 5). Because two FBAs did not appear in discharge samples after the first injection, interpretation of the results in terms of reactive hydrologic transport emerged as necessary to explain the observed discrepancies. The comparison of the breakthroughs of the same tracer injected twice at different times (TR1 and TR4) dismisses instead the specific reactivity issue, and is therefore presented first in the discussion (Time displaced injections). This sheds light on the interpretation of the multiple tracer injection. Finally, inferences on the reaction processes affecting the FBAs in this experiment are discussed in the last section, based on the tracing results and complementary testing presented in Section 2.2.6 and 2.2.7.

## 2.4 Discussion

### 2.4.1 Temporally displaced injections

The re-injection of TR1 and TR4 provides a demonstration on the effects of the hydrologic forcing on the solute transport features. In contrast to the short-time injection sequence of multiple tracers of 2013 (discussed below), we can compare here (Figure 2.10a) two breakthroughs of the same tracer injected at different times and dismiss potentially distinct reactive behaviors among the tracer species. Therefore, disparities in terms of concentration and load dynamics for a specific tracer only result from the different hydrologic forcing and the sequence of conditions experienced by the system. Figure 2.10a shows the precipitation sequence and the concentration breakthrough of TR1 and TR4 in 2013 (top panel) and 2014 (bottom panel). For TR4, the concentration dynamics prove substantially different between 2013 and 2014, both in terms magnitude (note the y-axis scale) and shape. The duration of the breakthrough is about 1.5 times longer in 2013 than in 2014, and reach a maximal relative concentration almost four times larger than in 2014.

Figure 2.10c shows the normalized mass fluxes of TR4 for each injection. In this case, the magnitude of the tracer load is comparable between the two injections, meaning that the water discharge was generally greater in 2014 to compensate lower concentrations in producing similar mass exports. This is especially true for the early phases of the 2014 injection, because it took place in late February (mid-April in 2013) when temperature and plant activity were low and ET losses relatively small leading to increased discharge responses for a specific rainfall volume. In the case of TR4, we clearly observe non-stationarity of the system's ability to transfer inputs into outputs both in terms of concentrations and mass fluxes. The different precipitation pattern between 2013 and 2014 would of course induce a different timing of the tracer export events. However, in the case of an invariant transfer input-output function, the

tracer responses would appear much more alike, and the cumulative recovery curves (Figure 2.10c, inset) would evolve similarly. Instead, we observe that the major part of the tracer injected in 2013 is recovered after more than 100 days, whereas the 2014 pulse is recovered much earlier.

ET plays a central role on the hydrologic and solute response. Part of the rainfall inputs never reach the bottom drainage of the system to produce discharge, but is rather withdrawn by the vegetation and transpired or is evaporated at the soil surface. The consequences of ET on solute transport is evident as it obviously affects the water balance (and therefore the discharge response for a rainfall event). However, ET also conveys more intricate aftermaths on internal mixing, because it operates on different pools of water (and consequently water characterized by different ages) than discharge does. Note that this represents an important issue on reactive transport as the exposure time to various degradation/removal processes is altered (discussed in section 2.4.3).

In an effort to investigate the non-stationarity solely induced by the variability of the water balance (i.e. the effects of the variable precipitation influx and variable ET water outfluxes), the tracer fluxes were rescaled using the cumulative flow volume (CFV)  $t \rightarrow \int_{-\infty}^t Q(x) dx$  as independent variable (Figure 2.10e). With this approach, the differences in the rainfall structure and ET deficits between the 2013- and 2014-injection are implicitly integrated in the dynamics of the tracer mass outflux curve, as the metrics used is the effective hydrologic outcome of the system exposed to the specific environmental forcing of each injection year. It had been argued, in fact, that this choice yields stationary travel time distributions even under unsteady flow conditions provided that changes in the storage  $S(t)$  are not major (Niemi, 1977). The result is plotted in Figure 2.10e. It is not surprising that the mass load exported per drainage volume unit discharged evolves, but one might have expected a unimodal shape, picturing the progressive arrival of the tracer front (i.e. the tracer concentration in the discharge water increases gradually) until the mass pulse's centroid is reached followed by a decrease until all tracer is discharged. Instead, we observe here multiple peaks corresponding, in terms of chronological time, to large discharge events. This implies that the composition of the discharge constantly evolves sampling water from different pools. The latter point suggests that when precipitation occurs, soil moisture increases and is redistributed, connecting water parcels that were previously hydrologically isolated as customary in macropore flow in unsaturated soils. ET also plays a key role, as it samples water from pools that can be different than those accessible to the discharge, especially in a lysimeter installation. This is particularly evident for evaporation, which arguably samples water mostly at shallow depths, thereby changing both the availability of water and the hydrologic connectivity in the system. It is showed in Figure 2.10c that almost no tracer outflux occurs between 100 and 200 days after the 2013 injection, which corresponds to the summer months (July-September) when ET was maximum. Although the ET deficit was notable, the multiple rainfall events generated during this period have prompted a non-negligible discharge (about 300 l corresponding to CFV values between 400 and 700 l in Figure 2.10e). Whether or not the tracers may undergo plant uptake, the fact is that TR4 was still in the volume during this period as TR4 export increased

## Chapter 2. Transport of fluorobenzoate tracers in a vegetated hydrologic control volume: Experimental results

---

again significantly later on, but was not readily accessible for discharge because of the specific conditions in the system.

The re-injection of TR1 is less explanatory than TR4 in deciphering the key features of bulk transport, as no breakthrough was observed for this tracer in 2013. Nevertheless, this experiment illustrates an important implication of non-stationary transport when a reactive solute is at stake. The first injection of TR1 objectively dismissed any premise of non-reactivity, as the entire tracer input mass disappeared in the system and was never observed in the discharge samples. In contrast, the reinjection of the tracer in 2014 resulted in a total mass recovery of 45% (Figure 2.10b, inset), only slightly lower than TR4 which was injected simultaneously. This discrepancy emerges because the exposure time of the tracer to the potential degradation/removal processes changes significantly between 2013 and 2014 as a consequence of non-stationary transport and mixing. As the processes that are involved in the tracer removal (discussed in section 2.4.3) may entail complex dynamics like e.g. selective plant uptake or microbial degradation controlled by environmental conditions, it proves difficult to relate the mass loss with the hydrological and environmental conditions encountered by the system. This issue is further analyzed and discussed in the framework of a modeling exercise presented in Chapter 3 (Queloz *et al.*, 2015a).

### 2.4.2 Sequenced multiple tracer injections

In 2013, five tracers have been injected sequentially within a one month period. The initial conditions were thus variable and a different forcing occurred for each tracer shortly after their injection. Nevertheless, as the mean travel time until the tracers exited the system through discharge was much longer than for the one-month injection period, the tracers experienced mostly the same system's states during most of their transport in the soil. Despite similar overall forcing, we observe very different tracer responses (Figure 2.8). The total mass recovery ranging between 0 and 67% suggests that removal/degradation processes have occurred and affected the tracers to various extents. However, the simultaneous reinjection in 2014 of TR1 and TR4 – *a priori* two dissimilar tracer in terms of reactivity given the results of the 2013 injection – shows fully synchronized discharge concentrations, with the relative concentration of TR4 about 1.5 times larger than TR1 during almost the entire breakthrough (Figure 2.10a). Hence, TR1 seems more prone to degradation or uptake. In the absence of hydrologic differentiation, however, the effects of each specific tracer dynamics is mainly limited to the magnitude of the signal rather than to its timing.

All things considered, hydrologic processes exhibit a key role in explaining the radically different behaviors of the five tracer injected in 2013. In Figure 2.11a, the fluxes are normalized and the time axis is adjusted to the injection time of each tracer, respectively. Whereas the signals of TR2 and TR4 (separated now with a 14-days lag equal to the time that separates their injection) are similar most of the time, we note that they only diverge between 0 and 56 days. This is even clearer in Figure 2.11c where time is rescaled in terms of CFV (see Section

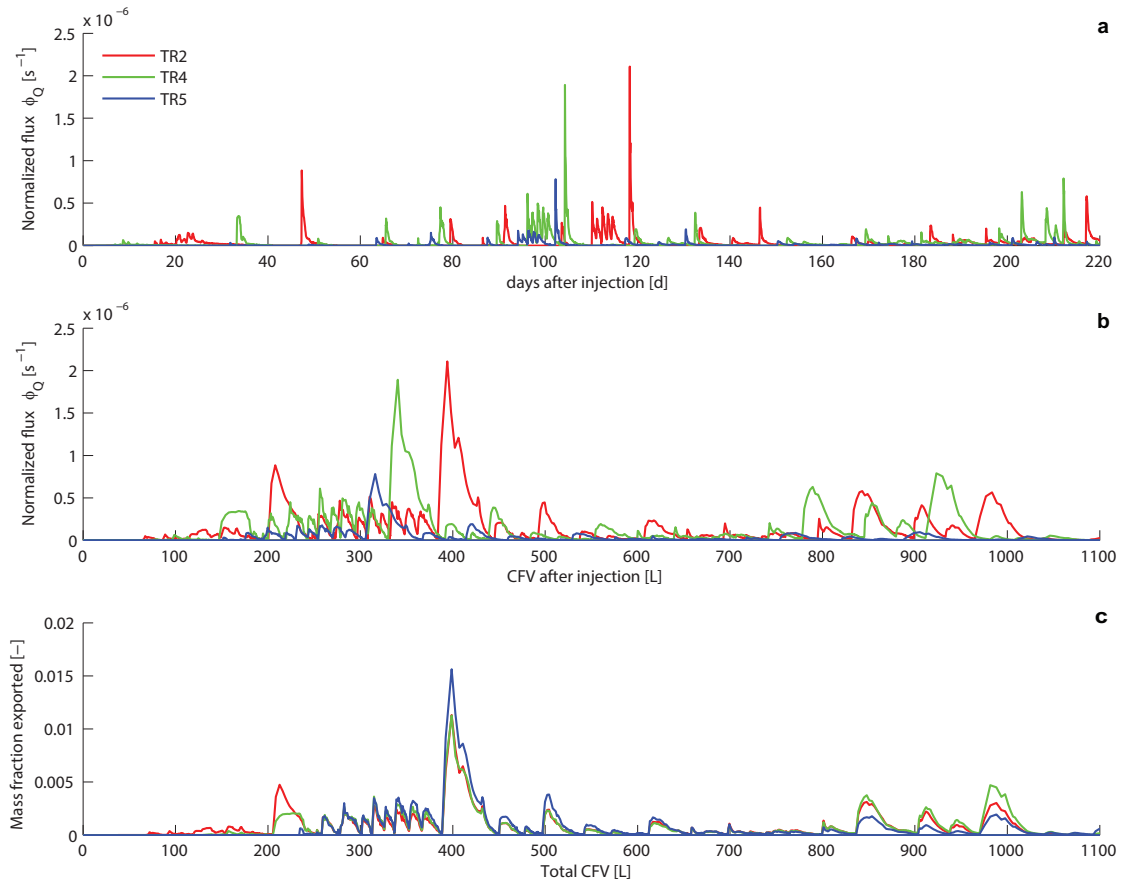


Figure 2.11: Summary of results of the transport experiment. (a) Tracer normalized flux  $\phi_Q$  plotted versus chronological time  $t$ ; (b) Tracer normalized fluxes plotted versus the rescaled elapsed time since injection, proportional to the volume discharged  $CFV = \int_{t_i}^t Q(x) dx$ . (c) Fraction of the total mass recovered exported per cumulative flow volume (CFV) discharged since the injection of TR1.

2.4.1), as the signals become similar only after 220 and 300 liters for TR4 and TR2 respectively. Therefore, the comparison of TR2 and TR4 reveals that their availability for discharge is distinct in an early phase after their injection, but becomes equivalent after some time (for example, the discharge event occurring 33 days after the injection of TR4 and 47 days after the injection of TR2 mobilizes proportionally more TR2 than TR4, whereas the following discharge events mobilize TR2 and TR4 equally).

TR5 was recovered at a much lower ratio than TR4 and TR2 (18% against more than 60%), yet the normalized flux in Figure 2.11b,c exhibits common features of TR5 with the other tracers. The early discharge events that generate mass export for TR2 and TR4 do not affect TR5, whose breakthrough begins only after 170 liters CFV. As soon as TR5 is detected in the discharge, the mass flux shows the same shape as for the other two tracers. Its magnitude is about half those of TR2 and TR4, but if the signals of each tracer are normalized by their maximum value, we observe that the relative magnitude of the TR5 signal is identical with the others until about

## Chapter 2. Transport of fluorobenzoate tracers in a vegetated hydrologic control volume: Experimental results

---

600 liters CFV, and decreases afterwards. Hence, the weaker outflux of TR5 is due to mass loss that occurred early in the system's transport, i.e. before the beginning of its breakthrough. These data are not sufficient to identify whether TR5 is degraded or removed by plant uptake from the system, but the similarities of the relative signals suggest that if it is the case, all tracers (TR2, TR4 and TR5) are affected in a similar manner. The final decrease of TR5 outflux relative to the TR2/TR4 arises because TR5 is almost completely removed from the system.

Two main outcomes of the measurements of TR2, TR4 and TR5 are worth discussing further. When solute pulse injections are operated sequentially under different environmental conditions, we observe similar breakthrough dynamics until the entire solute mass has exited the system. This is because each single discharge event mobilizes the different solutes equally and thus the relative quantity of solute exported during one event is the same for all compounds. However, this only occurs after a suitable period following the solute injection, while the solute spreads in the system. It appears that most of the differentiation between the various injections (and various tracers) in terms of mass loss occurs during this period. Unequal reactivity of the tracers cannot be ruled out, but Figure 2.11c suggests that the accountable degradation processes arise soon after injection. Consequently, as the hydrologic conditions during early transport phases are different for each tracer, they may also influence the degradation processes and induce the variability observed among the tracers. This issue is further discussed in the next section and Chapter 3 where the ways in which the outfluxes sample the storage are investigated in details.

### 2.4.3 On reactivity

During this experiment, the largest mass recovery observed was 69%. All tracers thus prove to be reactive in the system, despite the fact that FBAs are often considered conservative tracers and have been used in several hydrological studies specifically for this asset (e.g. *Bowman*, 1984; *Kung et al.*, 2000; *Juhler and Mortensen*, 2002). This experiment was initially not designed for quantifying the tracer mass loss that can be attributed to a specific degradation or removal pathway, nor it aims at identifying the nature of these sinks. Hence, considering the results, the data at hand were used and interpreted and *ad-hoc* testing was conducted in order to diagnose the implications of the interactions between hydrologic transport and solute reactivity (Section 2.2.7).

Potential passive processes, in particular soil sorption, were regarded using the results of the leaching test (Section 2.2.6) and soil extracts analysis carried out after the end of the experiment. The high FBA recovery of the column leaching tests using the same materials indicates that no sorption occurs in this soil, at least under saturated conditions. In addition, the large number of samples collected at different depths do not contain significant amount of tracer. Note that the method used actually overestimates the concentration of the tracer sorbed, as the soil samples contained residual water at time of collection. These findings are in agreement with previous findings of *Jaynes* (1994), and suggest that active processes – that

are simplified here in two categories: ET uptake and microbial degradation – are responsible for the observed mass loss.

Whereas plant uptake was demonstrated for two of the five tracers (as they have been found in the plant's wood and leaves), the measured concentration found would only account for a negligible fraction of the initial mass injected (Section 2.2.7). It has been shown that these compounds are prone to plant uptake and can be used as a carbon source for plant metabolism (Bulusu, 1995; Bowman *et al.*, 1997). The two tracers found in the plant tissues (also in 2014 leaves) are interestingly 2-TFMBA (TR2) and 3-TFMBA (TR5), two trifluoromethylbenzoic acids that were injected only in 2013. This might be explained by a very slow transport of FBAs within the plant tissues. As roots were not sampled, they might thus contain larger amount of the tracers. TR1, TR3 and TR4 were in contrast to TR2 and TR5 all difluorobenzoic acids, and despite a much larger mass of some of them was applied (e.g. TR4, which was additionally reinjected in 2014), there were not observed in the plant extracts. Either the difluorobenzoic acids are not prone to plant uptake, or they are metabolized more readily than trifluoromethylbenzoic acids. However, Bowman *et al.* (1997) reported significant uptake for 2,6-DFBA (TR4) and 3,4-DFBA (TR3). Note that *Salix spp.* are used in phytoremediation to remove chlorobenzoic acids, a by-product of polychlorinated biphenyl (Susarla *et al.*, 2002), which also advocates for the ability of willows to uptake these compounds.

As already mentioned (Section 2.2.7), microbial degradation of FBAs has not been specifically studied, but the similarity between fluoro- and chlorobenzoic acids argues for the consideration of microbial degradation as a potential process affecting the tracers in this system. The possible degradation pathway involving dehalogenation in the first place has been assessed by measuring fluoride concentration in the soil water and discharge water. The concentrations are too low to be accountable for a sizable fraction of the FBAs that would have been metabolized by microorganisms, but the negative concentration gradient of fluoride with depth and the brief peak in the discharge observed when the FBAs breakthrough starts speak for a preferential degradation at shallow depth and during a limited period after the tracer injection (i.e. when the tracers is mostly at the top of the column). This is, however, insufficient to understand the global picture of microbial degradation, as a major degradation pathway appears to involve fluorocatechol (not analysed) as the first breakdown product.

FBAs tracers are thus likely to be affected by ET uptake and microbial activity rather than by soil sorption processes. In this light, the tracer breakthroughs and the temporal distribution of the tracers in the column can be investigated and provide additional information on how the removal mechanisms operate in combination with hydrologic transport. As mentioned in section 2.4.2, the similarity of the tracer outflux dynamics (for the tracer that were significantly recovered) during most of the breakthrough, but a short period following their injection, demonstrates that the differentiation in terms of degradation/removal operates during this limited time at least for TR2, TR4 and TR5. This does not imply that no further mass removal occurs afterward, but in this case these tracers would be equally affected.

## Chapter 2. Transport of fluorobenzoate tracers in a vegetated hydrologic control volume: Experimental results

---

TR1 and TR3 do not allow to support the above observations as they have not been detected in the discharge, but looking at their behaviours within the system (Figure 2.9a) gives some clue about their transport. The pulse of TR1 seems slowly forced downwards, and remains detectable at every control plane for an extended period (over two months). In contrast, TR3 is only detected at 50 cm depth during two weeks (May 14 - June 3) and is measured in the discharge flow only eight days after it initially reached the depth of 50 cm. A possible explanation for this discrepancy can be proposed based on the input sequence: the input mass of TR1 was relatively small, and shortly after its injection subsequent rainfall events occurred, allowing a progressive infiltration and dilution of the pulse in the system. However, the rainfall following injection of TR1 were not sufficient to trigger discharge flow until early May, when the large pulse of TR3 was applied. Therefore, microbial degradation and/or plant uptake may have easily removed the small mass of TR1 during this period. Instead, the mass of TR3 injected in the pulse was much larger and followed by a long dry period in the course of which ET could not have uptake all the mass of tracer in the soil. The observed patterns, plus the fact that TR3 could not be found in the soil analyses, suggest that degradation in the system likely occurred, at least for this tracer.

Having shown experimentally that plant uptake is a possible removal pathway for FBAs, ET fluxes thus provide a major source of non-stationarity for solute transport, not only in terms of timing, as it has already been demonstrated, but also in terms of mass export. As an example, let us assume similar *ET* uptake for all tracers and preferential water withdrawal at shallow depth by the willow. The sequence of rainfall that follows an injection would have a great influence on the mass loss and export as it changes solute concentration distribution in the soil profile, thus affecting availability for uptake. It can be noticed in the 2013-injection that the tracers with the highest recovery ratio (TR2 and TR4) were both closely followed by significant rainfall events (Figure 2.8). These rainfall events were large enough to induce transport of the tracer through the entire profile, as they begin to be detected in the discharge at this occasion. In contrast, TR1 and TR3 inputs were not followed by rainfall, and were thus exposed to an extended dry period shortly after their injection. This tracer pulse represents the most accessible water for ET flux, as ET preferentially withdraws shallow water.

TR5 presents an intermediate situation between TR2/4 and TR1/3. The rainfall events that followed the TR5 pulse after three days were sufficient to force the tracer pulse down to 50 cm, but it has not been detected deeper in the profile before a large water input occurred on June 17, also triggering TR5 outflux in the discharge. As it is discussed in the previous section and demonstrated in Figure 2.11c, the similarity between the breakthroughs of TR5 and TR2/4 suggests that the difference in terms of total recovery of the tracers should originate from the period preceding TR5 breakthrough in the discharge. ET uptake and/or preferential biodegradation at shallow depth could induce this mass removal. Note that microbial degradation can be enhanced by rhizodeposition (*Deavers et al.*, 2010; *Vrchatová et al.*, 2013) and therefore induced by environmental conditions prompted by the vegetation.

Examining the evolution of soil water tracer concentration during selected dry periods (with



no discharge flow and no precipitation) could have informed on where, and at what stage of the tracer transport, degradation processes occur, but the soil water concentrations are subject to important heterogeneity effects preventing interpretation at a fine time scale. In addition, these measurements appear to reflect only part of the picture: all tracers are found in the deepest soil water samples (Figure 2.9a) much later than their occurrence in the discharge (Figure 2.8). This could be a consequence of the strong negative pressure applied by the porous cups, which are also able to extract residual pore water tightly bound to the soil matrix. Instead, discharge occurs in high soil moisture conditions and when strong connectivity is prompted. This allows different and more "remote" water pools to contribute to discharge that are able to by-pass the volumes sampled the porous cups. The higher soil water concentrations observed for TR2 at 100 cm compared to those at 50 cm support these statements, showing either that the pulse has by-passed the sampling at shallow depth, or that the representability of the samples at either depths due to heterogeneity.

## 2.5 Conclusions

The controlled injection of five fluorobenzoate tracers within a vegetated hydrologic control volume subject to erratic rainfall patterns was intended to highlight non-stationarity of the bulk transport processes attributable to variable hydrologic conditions. The results of the two-year experiment established that the premises on the tracers behavior, known to be conservative and therefore suitable for hydrological studies, were disproved as large differences in mass recovery appeared. This provided nonetheless a valuable dataset from these experiments, available as an attachment to this manuscript, as issues on reactivity arose and were addressed in this chapter.

The dataset serves well the original research question, that is to evaluate how hydrologic fluxes store and sample water and solute within controlled transport volumes, whose interpretation by travel and residence time distributions is the subject of Chapter 3. The experimental results presented are interesting in their own right in that they highlight selective transport properties of a particular class of fluorobenzoate tracers previously thought to be nearly non-reactive but in reality highly sensitive to microbial degradation and plant uptake under the type of unsaturated conditions faced by hydrologic transport.

The experiment shows that the discharge response of tracers pulses is largely non-stationary, not only due to the variation of the climatic forcing, but also due to the prevailing soil moisture and ET deficits during hydrologic transport. The results also suggest that moisture conditions are particularly influential during a short period after the pulse injection, as most of the differences in terms of mass loss among the tracers occur during such time. This emphasized the fact that ET uptake and/or microbial degradation potentially operates on specific pools of the water stored that can be different than those used by discharge.

This study suggests previously unknown features of potentially interesting hydrologic tracers suited to distinguishable multiple injections; and provides an analysis on the issues to

## **Chapter 2. Transport of fluorobenzoate tracers in a vegetated hydrologic control volume: Experimental results**

---

be resolved towards a direct experimental closure of mass balance in hydrologic transport volumes involving significant output fluxes (like in this case ET from a diverse assemblages of vegetation and discharge from a different compliance surface) that are likely to sample stored water and solutes in different ways.

### **3 Transport of fluorobenzoate tracers in a vegetated hydrologic control volume: Theoretical inferences and modeling**

This chapter is an adapted version of:

Queloz, P., Carraro, L., Benettin, P., Botter, G., Rinaldo, A. and Bertuzzo, E. (2015), Transport of fluorobenzoate tracers in a vegetated hydrologic control volume: 2. Theoretical inferences and modeling. *Water Resources Research*, 51(4), 2793–2806, doi:10.1002/2014WR016508.

A theoretical analysis of transport in a controlled hydrologic volume, inclusive of two willow trees and forced by erratic water inputs, is carried out by contrasting the experimental data described in Chapter 2. The data refer to the hydrologic transport in a large lysimeter of different fluorobenzoic acids seen as tracers. Export of solute is modeled through a recently developed framework which accounts for non-stationary travel time distributions where the way output fluxes (namely, discharge and evapotranspiration) sample the available water ages in storage is parametrized. The relevance of this work lies in the study of hydrologic drivers of the non-stationary character of residence and travel time distributions, whose definition and computation shape this theoretical transport study. The results show that a large fraction of the different behaviors exhibited by the tracers may be charged to the variability of the hydrologic forcings experienced after the injection. Moreover, the results highlight the crucial, and often overlooked, role of evapotranspiration and plant uptake in determining the transport of water and solutes. This application also suggests that the ways in which evapotranspiration selects water with different ages in storage can be inferred through model calibration contrasting only tracer concentrations in the discharge. A view on upscaled transport volumes like hillslopes or catchments is maintained throughout the paper.

### **3.1 Introduction**

The concept of travel time has often been used in hydrology to characterize and model solute transport processes within hillslopes, aquifers or catchments (e.g. *Kreft and Zuber*, 1978; *Jury et al.*, 1986; *Maloszewski et al.*, 1992; *Haggerty et al.*, 2002). However, only recently the travel-time literature evolved so as to include a detailed and realistic representation of the processes that drive solute circulation through the hydrologic response. Traditional approaches such as the lumped convolution approach (e.g. *Rodhe et al.*, 1996; *Kirchner et al.*, 2000; *Broxton et al.*, 2009; *McGuire and McDonnell*, 2006; *Seeger and Weiler*, 2014) were progressively made more general to account for the inherent time variability of fluxes and storages (*Botter et al.*, 2010; *Hrachowitz et al.*, 2009a, 2010a; *Heidbüchel et al.*, 2013; *Ali et al.*, 2014), which underlies the key differences between backward and forward distributions in hydrologically meaningful control volumes (*Niemi*, 1977; *Rinaldo et al.*, 2011; *Cvetkovic et al.*, 2012; *Harman*, 2015). Similarly, the formalization of the differences and relationships between travel and residence times distributions (*Botter et al.*, 2011; *van der Velde et al.*, 2012) opened the way to a spatially-integrated representation of the age selection processes operated by bulk hydrologic fluxes like discharge and evapotranspiration. The approach complemented newly available high frequency datasets (e.g. *Kirchner and Neal*, 2013), which offered the opportunity to develop new methods and test novel modeling approaches to real-world transport problems (*van der Velde et al.*, 2010; *Heidbüchel et al.*, 2012; *Birkel et al.*, 2012; *McMillan et al.*, 2012; *Hrachowitz et al.*, 2013; *Davies et al.*, 2013; *Harman and Kim*, 2014; *van der Velde et al.*, 2014; *Harman*, 2015).

In this chapter a general transport model (*Botter et al.*, 2010, 2011; *Rinaldo et al.*, 2011; *Bertuzzo et al.*, 2013; *Benettin et al.*, 2013a) is used to gain insight on data gathered during a controlled experiment which is described in Chapter 2. The experiment provides direct observational evidence of the non-stationary character of transport processes in a controlled hydrologic transport volume, and highlights the key role of plant uptake and degradation processes for solute circulation dynamics.

The significance of the present work lies in the comparative assessment of the current needs for practical modeling tools that reconcile recent theoretical advances with field experiments - which is one of the main goals of this chapter.

Despite the small spatial scale used in the experiment, this modeling task may be considered equally significant and challenging as larger catchment studies. Indeed, transport processes are herein modeled using bulk measurements (output and input fluxes and storage mass at any time) of the same type of those that can possibly be measured or inferred at catchment scale (e.g. *Brutsaert and Nieber*, 1977; *Kirchner*, 2009; *Botter et al.*, 2009). Moreover, at catchment scale the overall effect of heterogeneous attributes may be smoothed when integrated fluxes are dealt with, thereby easing a robust description of any flowpath heterogeneity within the travel time formulation of transport (*Dagan*, 1988; *Botter et al.*, 2005; *Cvetkovic et al.*, 2012). Significantly, the experiment retains key features of field studies like the random nature of

rainfall (which was added as a sequence of quasi-instantaneous inputs) and the structural difference between the sampling of stored water particles operated by plant roots and drainage structures. On the other hand, transport features that can possibly emerge at hillslope and catchment scales, e.g. those induced by dynamically changing hydrological connectivity, cannot be investigated in this experiment. Despite these limitations, modeling the outcome of a lysimeter experiment of the type handled here is deemed a challenging test for this theoretical framework.

## 3.2 Methods

### 3.2.1 Experimental data

Hydrological time series and tracer breakthrough curves were recorded during a large lysimeter experiment running from April 2013 to July 2014. A detailed description of the set-up and discussion of the experimental data are reported in Chapter 2. A 2 m-deep, 1 m<sup>2</sup>-surface area lysimeter was filled with a sandy clay loam soil and planted with two willow stems (*Salix viminalis*). A 50 cm saturated gravel filter drains infiltration water to the outlet equipped with discharge flow measurement and flow-rated sampling system. A translucent roof located beneath the canopy protects the lysimeter surface from natural precipitation; instead, random rainfall following a marked Poisson process (Rodriguez-Iturbe *et al.*, 1999) was manually injected. Load cells provide an accurate reading of the weight of the system and therefore allow the indirect estimate of evapotranspiration fluxes. Five selected rainfall events in the beginning of the experiment were each marked with a different tracer (various fluorobenzoic acids) that can be easily quantified in water samples using mass spectrometry techniques. Extensive discharge flow sampling was performed to precisely record the tracer breakthrough curves and calculate the outgoing tracer mass flux. A conceptual scheme of the lysimeter is reported in Figure 3.1a. The data-set used here is summarized in Figure 3.1b.

### 3.2.2 Travel-time formulation of transport and age-selection schemes

Let us consider a hydrologic control volume with a single input flux  $J$  (e.g. precipitation) and two output fluxes: discharge  $Q$  and evapotranspiration  $ET$ . The proposed framework could be readily generalized to model more complex schemes involving multiple control volumes (in series or in parallel, see e.g. Bertuzzo *et al.* (2013); Benettin *et al.* (2013a)) or multiple input/output fluxes (e.g. irrigation, pumping, etc). The theoretical approach for the simple case of a single control volume is first illustrated. The residence time  $T$  (also termed age) of a tagged water particle in storage within the control volume is defined as the time elapsed since its entrance in the control volume. Therefore, the residence time distribution (RTD)  $p_S(T, t)$  - the probability density function of the residence time of the water particles contained in the control volume at time  $t$  (Botter *et al.*, 2011) - characterizes at any time the age composition of the storage. The residence time of a particle that leaves the system as  $Q$  or  $ET$

**Chapter 3. Transport of fluorobenzoate tracers in a vegetated hydrologic control volume: Theoretical inferences and modeling**

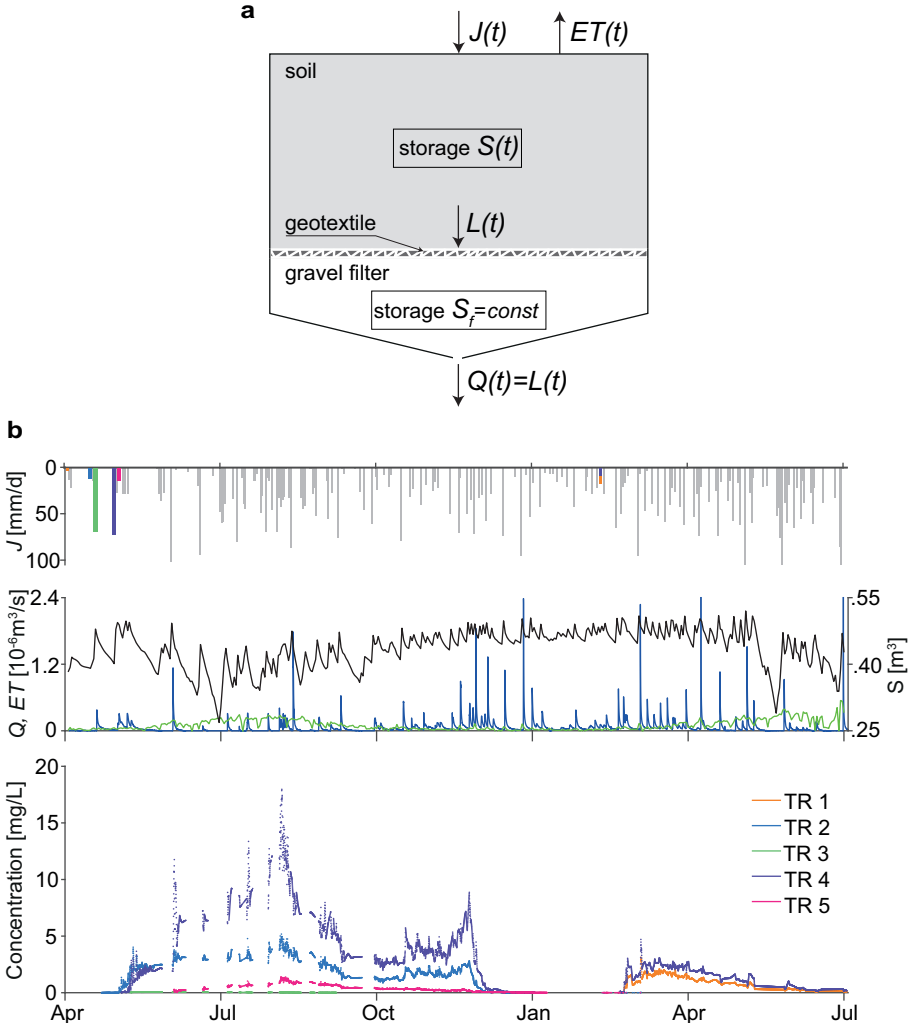


Figure 3.1: a) Conceptual scheme of the lysimeter. From a modeling viewpoint, the system is divided into two control volumes: a 2 m-deep, 1 m<sup>2</sup>-surface-area soil layer and a 50 cm-deep gravel filter. Precipitation input is termed as  $J(t)$ , evapotranspiration as  $ET(t)$ , flow at the interface between soil and filter as  $L(t)$  and bottom outflow as  $Q(t)$ . The system set-up does not allow changes in water storage of the filter, therefore  $Q(t) = L(t)$ . b) Time series of hydrological and chemical variables. The rainfall pulses marked with the 5 different tracers are displayed with different colors in the top panel. Their breakthrough curves are displayed with the corresponding color in the bottom panel. Middle panel shows the time series of water storage  $S$  (black), outflow  $Q$  (blue) and  $ET$  (green).

is termed travel time (also known as transit time). The corresponding travel time distributions (TTDs) can be seen either as forward ( $\vec{p}_Q(T, t_i)$ ,  $\vec{p}_{ET}(T, t_i)$ ) or backward ( $\vec{p}_Q(T, t)$ ,  $\vec{p}_{ET}(T, t)$ ) distributions (Niemi, 1977; Rinaldo et al., 2011; Cvetkovic et al., 2012). In the former case the age distribution refers to the set of particles that simultaneously entered the system at a time  $t_i$ , while in the latter case the age distribution pertains to the set of particles that are simultaneously leaving the system at time  $t$ . The forward TTD can be thought as the flux in the outflow corresponding to an instantaneous marked injection of a unit volume at time  $t_i$ . The backward TTD represents instead the age distribution of the water sampled in the outflow at time  $t$ . If  $\theta(t_i)$  is defined as the fraction of the precipitation influx  $J(t_i)$  that ends up exiting as outflow  $Q$ , continuity and Niemi (1977) yield (Botter et al., 2011):

$$\vec{p}_Q(t - t_i, t)Q(t) = \theta(t_i)J(t_i)\vec{p}_Q(t - t_i, t_i), \quad (3.1)$$

whose physical meaning consists of equating the fraction of particles that exits as  $Q$  at time  $t$  with age  $t - t_i$  (at left hand side) to the fraction of rainfall entered at  $t_i$  that exits as  $Q$  at time  $t$  (at right hand side). An analogous relation can be written for evapotranspiration TTDs.

Tracking the temporal evolution of the ages of the water particles stored within the control volume requires the specification of how outgoing fluxes sample the available ages in the storage. This is usually done by specifying the relationship between residence and backward TTDs through suitable selection functions (Botter et al., 2011; Botter, 2012; Benettin et al., 2013b). Recently, van der Velde et al. (2012) proposed to characterize age-selection processes by expressing the relevant distributions not as a function of age  $T$  but rather using a ranked age  $P_S$ , that expresses the relationship between a certain age and all the other ages actually in storage. Specifically, the new variable  $0 \leq P_S(T, t) \leq 1$  represents the fraction of storage younger than  $T$  at a given time  $t$ , and it is defined by the following equation:

$$P_S(T, t) = \int_0^T p_S(\tau, t) d\tau. \quad (3.2)$$

Therefore, at every time there exists a unique relation between  $T$  and  $P_S$  which allows backward TTDs to be expressed in the domain of the new variable  $P_S$ :  $\vec{p}_Q(T, t) \mapsto \vec{w}_Q(P_S, t)$  and  $\vec{p}_{ET}(T, t) \mapsto \vec{w}_{ET}(P_S, t)$ .  $\vec{w}(P_S(T, t), t)$  are derived distributions (i.e. distributions of a function of the random variable  $T$ ) and are termed ‘‘StorAge Selection’’ (SAS) functions because they determine how the resident ages are selected by the outflows. Once SAS functions are specified, the related time-variant RTDs and TTDs can be derived accordingly (see below).

The advantages of modeling age-selection through the transformed variable  $P_S$  are manifold.  $P_S$  can assume values between 0 and 1, corresponding to the youngest and the oldest storage in the system, respectively. Therefore the support of the distribution  $\vec{w}_Q(P_S, t)$  is also fixed and equal to the interval  $[0, 1]$ .  $\vec{w}_Q(P_S, t)$  is a probability distribution function and can be parameterized. In forward modeling, it is therefore possible to specify directly the SAS functions to characterize how the output fluxes ( $Q$  and  $ET$ ) select the different ages available within the control volume and derive the corresponding backward TTDs. Moreover, the ranked age

### Chapter 3. Transport of fluorobenzoate tracers in a vegetated hydrologic control volume: Theoretical inferences and modeling

---

$P_S$  arguably embodies a better proxy of the position of a particle within the system (*van der Velde et al.*, 2012) - where the position should not depend on the actual value of the particle age but rather on the fraction of older particles stored within the system. In turn, the particle position in soil columns and hillslopes may strongly control the probability of being routed to the outflow or uptaken by plants.

As highlighted by the notation, the distributions  $\overleftarrow{w}(P_S, t)$  can be time-variant to mirror the variability in time of age-selection processes ruled by the outflows, e.g. depending on the external forcings and on the state of the system. However, even if a constant SAS function is assumed ( $\overleftarrow{w}(P_S, t) = \overleftarrow{w}(P_S)$ ), the framework would consistently produce time-variant TTDs, because the RTD (and thus the relation between  $T$  and  $P_S$ , see equation 3.2) is also time-variant.

A graphical representation of the modeling framework is presented in Figure 3.2. White bars in Figure 3.2a sketch a RTD as a function of the residence time  $T$  at a certain time  $t$ . A histogram is used to illustrate the actual numerical implementation of the framework where the age domain is discretized with finite time-steps. Defining  $S(t)$  as the total storage at time  $t$ , it is to be noted that  $S(t)p_S(T, t)dT$  represents the volume of water injected in the system around  $t - T$  which is still inside the control volume at time  $t$ . Notice that if at  $t - T$  no input occurred,  $p_S(T, t) = 0$ . Figure 3.2b shows the residence time cumulative distribution  $P_S(T, t)$  which allows the transformation of variable  $T \mapsto P_S$ . The distribution  $\overleftarrow{w}_Q(P_S, t)$  (Figure 3.2d) prescribes the age-selection processes occurring in discharge formation. The function  $\overleftarrow{w}_Q(P_S, t)$  can hardly be directly measured, because this would imply labeling with different tracers all the different ages contained in the control volume. Therefore, the shape of this distribution needs to be assumed and possibly calibrated. In this example,  $Q$  preferentially selects high values of  $P_S$ , i.e. the older water in storage. As  $\overleftarrow{w}_Q(P_S(T, t), t)$  is a derived distribution, the following relation holds:  $\overleftarrow{w}_Q(P_S, t)dP_S = \overleftarrow{p}_Q(T, t)dT$ . Therefore the solid blue area in Figure 3.2d and 3.2c represents the probability that a water particle with age around  $T_1$  is sampled for contributing to the outflow  $Q(t)$  at time  $t$ . Repeating this procedure for all the age intervals in storage allows a proper computation of the backward TTD in the age domain ( $\overleftarrow{p}_Q(T, t)$ , Figure 3.2c). Notice that even if  $\overleftarrow{w}_Q(P_S, t)$  is smooth and regular, the corresponding backward TTD  $\overleftarrow{p}_Q(T, t)$  is highly irregular due to the irregular shape of the RTD, which mirrors the time variability of input and output fluxes. Finally, the quantity  $Q(t)\overleftarrow{p}_Q(T, t)/S(t)$  (blue shaded bars in Figure 3.2a) represents the fraction of storage with a certain age that is routed to the discharge flow per unit time. An analogous procedure (Figure 3.2e and 3.2f) can be implemented to compute the age distribution of particles that are evapotranspired. In the displayed example evapotranspiration preferentially selects young water. The difference between how the two output fluxes select different ages is evident in Figure 3.2a where it can be seen that  $Q$  is mainly composed by old water while  $ET$  by new one. Different choices of  $\overleftarrow{w}_Q(P_S, t)$  and  $\overleftarrow{w}_{ET}(P_S, t)$  allow modeling different age-selection schemes flexibly.



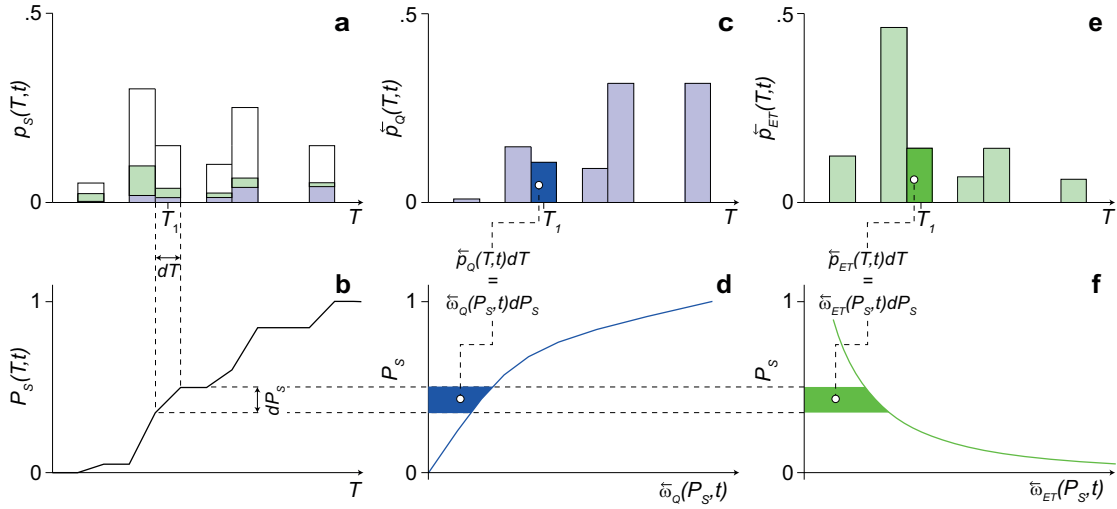


Figure 3.2: Graphical representation of the modeling scheme. For this representation it is assumed that  $dt = 1$ . See detailed description on the main text.

### 3.2.3 Solute transport

The framework described in section 3.2.2 deals with transport and mixing processes of water particles within a hydrologic control volume and can be readily generalized to describe transport of solutes. If the tracer in focus is ideal (i.e. it undergoes the same transport processes as the water carrier without degradation, chemical, physical or biological reactions or evapoconcentration), the concentration  $C_J$  of a parcel of water injected in the system would travel unaltered and the concentration  $C_Q$  in the discharge would be straightforwardly derived as:

$$C_Q(t) = \int_0^{\infty} C_J(t-\tau) \bar{p}_Q(\tau, t) d\tau. \quad (3.3)$$

In equation 3.3,  $C_Q$  is expressed as a weighted average of the concentrations of the water parcels within the system where the weight is the relative fraction of outflow that is sampled from each parcel – the backward TTD. However, ideal tracers do not exist. In fact, even passive tracers can exhibit a resistance to being selected by transpiration (e.g. in case they are toxic to plants). This different resistance can cause an enrichment of solute concentration (evapoconcentration) as a parcel travels through the system (Bertuzzo *et al.*, 2013; Hrachowitz *et al.*, 2013). As the framework presented in section 3.2.2 tracks the fate of every particle of water traveling through the system, evapoconcentration can be directly accounted for. Moreover many tracers can undergo decay/degradation under field conditions. A general approach is achieved by defining  $C(T, t)$  as the solute concentration at time  $t$  of the water input injected at time  $t - T$  and by assuming that the concentration of water evapotranspired from such water input is  $\alpha C(T, t)$ , with  $\alpha \in [0, 1]$  (Bertuzzo *et al.*, 2013). The two extreme cases are  $\alpha \equiv 0$ , where no solute is selected and  $\alpha \equiv 1$ , where the solute has the same affinity of the water to be transpired. Whenever  $\alpha < 1$ , solute concentration changes with time. In addition to this physical process, a linear degradation at a rate  $k$  is also accounted for, which fairly

### Chapter 3. Transport of fluorobenzoate tracers in a vegetated hydrologic control volume: Theoretical inferences and modeling

---

well describes the behavior of mass loss rates in the soil of many solutes of practical interest. By coupling mass balances of water and solute of single water pulses, the evolution of the concentration becomes (see section 3.2.5):

$$C(T, t) = C_J(t - T) \exp \left[ (1 - \alpha) \int_0^T \frac{ET(t - T + \tau) \overline{p}_{ET}(\tau, t - T + \tau)}{S(t - T + \tau) p_S(\tau, t - T + \tau)} d\tau - kT \right], \quad (3.4)$$

which allows generalizing equation 3.3 to the case of solutes that undergo evapoconcentration:

$$C_Q(t) = \int_0^\infty C(\tau, t) \overline{p}_Q(\tau, t) d\tau. \quad (3.5)$$

The algorithm used for the numerical implementation of equations 3.4 and 3.5 is described in section 3.2.5.

#### 3.2.4 Application to fluorobenzoate transport

The extensive analyses carried out in Chapter 2 suggest that, besides bottom outflow, there are two other possible export pathways for tracer mass: plant uptake and microbial degradation. All these processes can be modeled using the framework developed in section 3.2.3.

Because of the marked differences between the relevant physical properties of the lysimeter components, the system is conceptualized as a series of two control volumes, the soil and the gravel filter (Figure 3.1). As the geotextile placed between the soil and the filter (Figure 3.1) prevents willow roots to penetrate into the filter,  $ET$  from the filter can be assumed to be null. Moreover the lysimeter set-up does not allow changes in water storage of the filter (unless resorting to unreasonable storativity changes), so it can be assumed that filter recharge, here termed  $L$ , is equal to bottom outflow, termed  $Q$ , at every time (Figure 3.1). Under such assumption, all water storages, input and output fluxes of the two control volumes i.e.  $S(t)$ ,  $J(t)$ ,  $ET(t)$ ,  $L(t)$  and  $Q(t)$ , Figure 3.1b) are known from the measurements carried out. The model described in sections 3.2.2 and 3.2.3 is first applied to the soil control volume forced by the precipitation input  $J(t)$  with tracer concentration  $C_J(t)$  to compute the concentration  $C_L(t)$  of tracer in the filter recharge  $L(t)$ . Transport processes are then modeled in the gravel filter assuming as input the flux  $L(t)$  with concentration  $C_L(t)$  and compute the concentration  $C_Q(t)$  in the bottom outflow.

To apply the model, SAS functions  $\overline{w}(P_S, t)$  must be specified, and are selected them among a suite of (time-invariant) power-law functions:  $\overline{w}_Q(P_S) = \beta P_S^{\beta-1}$ . For  $\beta > 1$  ( $\beta < 1$ ), the outgoing flux has a preference for older (younger) ages, see e.g. Figure 3.2d (3.2f);  $\beta = 1$  corresponds to the random sampling scheme where ages are sampled according to their relative abundance in the control volume. This formulation is parsimonious yet flexible and is able to model a wide range of age-selection behaviors.

The breakthrough curve of a single tracer is hence completely determined by five parameters:  $\beta_{ET}$ ,  $\beta_L$ ,  $\beta_Q$  (the exponents of the SAS functions corresponding to the outgoing fluxes  $ET$  and  $L$  from the soil volume and of the outflux  $Q$  from the filter, respectively), the affinity to be evapotranspired  $\alpha$  and the degradation rate  $k$ . To ease the interpretation of the results, the half-life of the solute  $DT_{50} = (\ln 2)/k$  is used. When multiple tracers are modeled simultaneously, each solute  $i$  is possibly characterized by different parameters  $\alpha_i$  and  $DT_{50,i}$ , leading to a total number of 13 parameters in this study.

I use a Monte Carlo approach to calibrate the parameters contrasting measured and modeled time series of mean daily concentrations of the five tracers in the discharge. A criterion based on the Residual Sum of Squares (RSS) is used to select the behavioral simulations (*sensu Beven*, 2012) which are used to plot the results. Further details are provided in section 3.2.6. The model is validated using data pertaining a subsequent injection of two out of five tracers (Figure 3.1b).

### 3.2.5 Details on analytical and numerical methods

Let us term  $s(T, t)dT = S(t)p_S(T, t)dT$  the volume of water of residence time around  $T$  present in the system at time  $t$ .  $s(T, t)$  is the solution of the following partial differential equation (*Botter et al.*, 2011; *van der Velde et al.*, 2012; *Benettin et al.*, 2013a):

$$\frac{\partial s(T, t)}{\partial t} + \frac{\partial s(T, t)}{\partial T} = -Q(t)\overleftarrow{p}_Q(T, t) - ET(t)\overleftarrow{p}_{ET}(T, t), \quad (3.6)$$

with boundary conditions  $s(0, t) = J(t)$ . In equation 3.6, the variation in time of  $s(T, t)$  is expressed in terms of aging (second term of the left-hand side) and removal by  $Q$  and  $ET$  (right-hand side). The partial differential equation 3.6 can be reduced to a family of ordinary differential equations by looking at the solution along characteristic curves of the type  $(T(z), t(z))$ . Curves of the type  $T(z) = z$  and  $t(z) = z + t_i$  are characteristics, as revealed by the following equation:

$$\frac{ds(z, z + t_i)}{dz} = \frac{\partial s(T, t)}{\partial T} \frac{dT}{dz} + \frac{\partial s(T, t)}{\partial t} \frac{dt}{dz} = \frac{\partial s(T, t)}{\partial t} + \frac{\partial s(T, t)}{\partial T}. \quad (3.7)$$

Combining equations 3.6 and 3.7 and using the relations  $T = z$  and  $t = z + t_i = T + t_i$ , we finally obtain

$$\frac{ds(T, T + t_i)}{dT} = -Q(T + t_i)\overleftarrow{p}_Q(T, T + t_i) - ET(T + t_i)\overleftarrow{p}_{ET}(T, T + t_i), \quad (3.8)$$

with initial condition  $s(0, t_i) = J(t_i)$ . Equation 3.8 describes how the volume of a pulse of water injected in the system at time  $t_i$  evolves while aging. The difference between the approaches of equations 3.6 and 3.8 is similar to the difference between Eulerian and Lagrangian approaches, the focus being the residence time rather than the spatial position. Equation 3.6 focuses on a particular residence time  $T$  and follows different water pulses aging through that residence time. On the contrary, equation 3.8 follows the fate of a single water pulse aging inside the

### Chapter 3. Transport of fluorobenzoate tracers in a vegetated hydrologic control volume: Theoretical inferences and modeling

---

system.

Analogously, the time evolution of the mass of solute  $m(T, t = T + t_i)dT$  carried by the water pulse entered around  $t_i$  can be derived as:

$$\begin{aligned} \frac{dm(T, T + t_i)}{dT} &= \frac{d(s(T, T + t_i)C(T, T + t_i))}{dT} = \\ &= -C(T, T + t_i)[Q(T + t_i)\overline{p}_Q(T, T + t_i) + \alpha ET(T + t_i)\overline{p}_{ET}(T, T + t_i)] - km(T, T + t_i), \end{aligned} \quad (3.9)$$

with initial condition  $m(0, t_i) = J(t_i)C_J(t_i)$ . In equation 3.9,  $C(T, T + t_i)$  represents the solute concentration of the water pulse while  $\alpha C(T, T + t_i)$  is the concentration in the evapotranspiration flux. The term  $-km(T, T + t_i)$  at the RHS accounts for degradation. Coupling equations 3.8 and 3.9 and solving for  $C(T, T + t_i)$ , the solution 3.4 reported in section 3.2.3 is straightforwardly derived.

From a numerical viewpoint, first the sequence of injections is discretized at hourly time step, then the evolution of the volume and of the solute mass of every single pulse of water are computed by integrating equations 3.8 and 3.9. At any time the backward TTDs  $\overline{p}_{ET}(T, t)$  and  $\overline{p}_Q(T, t)$  are computed as explained in section 3.2.2 based on the current RTD  $p_S(T, t) = s(T, t)/S(t)$ .

Water stored in the two control volumes at the beginning of the experiment ( $t = 0$ , the injection of the first tracer) needs to be accounted for in the simulation. This is done by considering that, at any time  $t$ , the initial storage is older than  $t$ , and therefore contributes to the output fluxes as prescribed by the corresponding backward TTDs (i.e. with probability  $\int_{P_S(t,t)}^1 \overline{w}(x, t)dx$ ).

#### 3.2.6 Model calibration

Parameters are calibrated by contrasting measured and modeled time series of mean daily concentrations of the five tracers at the lysimeter outlet. A MonteCarlo approach is used, which randomly selects  $10^4$  sets of parameters controlling TTDs ( $\beta_{ET}, \beta_L, \beta_Q$ ) from uniform distributions with ranges illustrated in Figure 3.3a. For each parameter set and for each tracer  $i$ , 400 pairs of parameters  $\alpha_i$  and  $\log_{10}(DT_{50,i})$  are randomly selected in the intervals  $[0, 1]$  and  $[0, 4.5]$ , respectively, and tested. As the breakthrough curves exhibit very different behaviors, each time series of concentration is first normalized dividing it by its maximum value for all tracers but 1 and 3, which show null or negligible export. The performance of each simulation is evaluated through the residual sum of squares ( $RSS_i$ ).

For each tracer  $i$ , a set of parameters ( $\beta_{ET}, \beta_L, \beta_Q, \alpha_i, DT_{50,i}$ ) is considered behavioral (*sensu Beven, 2012*) if  $RSS_i < A$ , where  $A$  is a suitable threshold, and the subset of parameters controlling the TTDs ( $\beta_{ET}, \beta_L, \beta_Q$ ) is able to achieve a good performance also for all other tracers ( $RSS_j < C \forall j \neq i$ ). The latter constraint is imposed because, while tracers can have specific properties (i.e.,  $\alpha_i, DT_{50,i}$ ), water carrying them is obviously subject to the same

transport processes. The threshold  $A$  is arbitrarily fixed to 5, a value which corresponds to an error that is deemed acceptable.

### 3.3 Results

Frequency distributions of behavioral parameter sets are reported in Figure 3.3. The corresponding modeled breakthrough curves and fractions of exported mass for the five tracers are compared to measured data in Figure 3.4. The very different patterns of transport exhibited by the five marked injections are quite well captured by the model.

Parameter distributions (Figure 3.3) reveal that the exponents of the backward TTD related to the soil control volume ( $\beta_L$  and  $\beta_{ET}$ ) are clearly identified, while model results are less sensitive to variations of age-selection processes in the gravel filter ( $\beta_Q$ ). Inferred backward TTDs indicate that  $ET$  has a clear preference for young water ( $\beta_{ET} < 1$ ), while discharge for old water ( $\beta_L > 1$ ). The distribution of  $\beta_Q$  is wider, such that no clear age-selection patterns emerge. The mean value of  $\beta_Q$  is 1.51, relatively close to a random sampling scheme ( $\beta = 1$ ). Parameters describing the affinity to be transpired and degradation processes (i.e.  $\alpha_i$  and  $DT_{50,i}$ ) could not be clearly identified because different combinations of the two processes, both representing possible sinks of tracer mass, can lead to similar export dynamics. The breakthrough curves of tracer 2, 4 and 5 can be explained by an almost conservative behavior (i.e. negligible degradation, high  $DT_{50,i}$ ) and high affinities (i.e.  $\alpha_i$  close to 1), but also by progressively shorter half-lives (of the order of a hundred days) and lower affinities (Figure 3.3b). Long half-lives could not be clearly identified because, given the time scale of the experiment, any  $DT_{50,i}$  longer than a thousand days leads to indistinguishable outcomes. Tracer 1 never broke through the bottom outflow. This null export can be explained either by fast degradation or by a combination of conservative behavior and plant uptake. On the contrary, the almost null export of tracer 3 can be reproduced only by assuming a short half-life. As opposed to all other tracers, its behavior cannot be explained only by assuming plant uptake and no degradation.

Even though the peaks of the observed breakthrough curves (Figure 3.4, top panels) are not perfectly reproduced in some cases (e.g. tracer 4), their timing is well captured by the model. Similarly, the timing of the first sharp increase of fluorobenzoic acid concentration is well reproduced. The temporal evolution of the fraction of mass recovered in the discharge (bottom panels of Figure 3.4) is also well reproduced for all tracers. For comparison, Figure 3.4 reports also the hypothetical export dynamics of an ideal tracer (i.e.  $\alpha = 1$  and  $DT_{50} = \infty$ ) and of a conservative tracer which is not subject to plant uptake (i.e.  $\alpha = 0$  and  $DT_{50} = \infty$ ). The mass flux of an ideal tracer in the outflow is proportional to the forward TTD and, as such, it depends on the time of injection. Indeed, the total mass exported at the end of the experiment is rather different for the 5 injections considered (red-dashed lines in Figure 3.4b). The behavior of an ideal tracer, which perfectly tracks the transport of water, is compatible with that of all tracers but tracer 3. No plant uptake ( $\alpha = 0$ ) causes evapoconcentration of the tracer and leads to

**Chapter 3. Transport of fluorobenzoate tracers in a vegetated hydrologic control volume:  
Theoretical inferences and modeling**

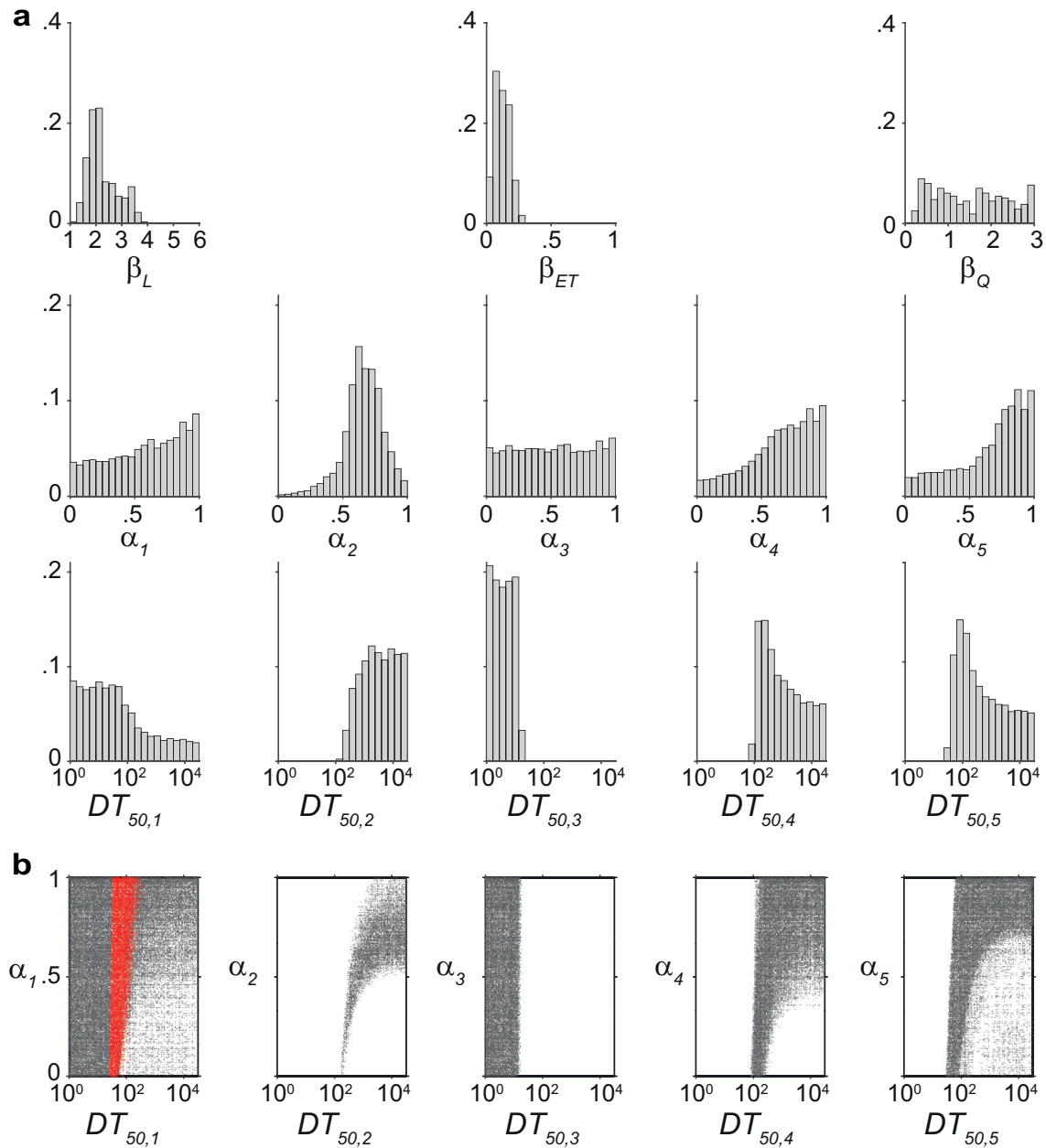


Figure 3.3: a) Frequency distributions of behavioral parameter sets. b) Scatter plot of behavioral pairs of parameters  $\alpha_i$  and  $DT_{50,i}$ . Red dots in the first sub-panel indicate behavioral pairs  $(\alpha_1, DT_{50,1})$  obtained using also the information collected in the second injection of tracer 1.  $DT_{50,i}$  is expressed in days.

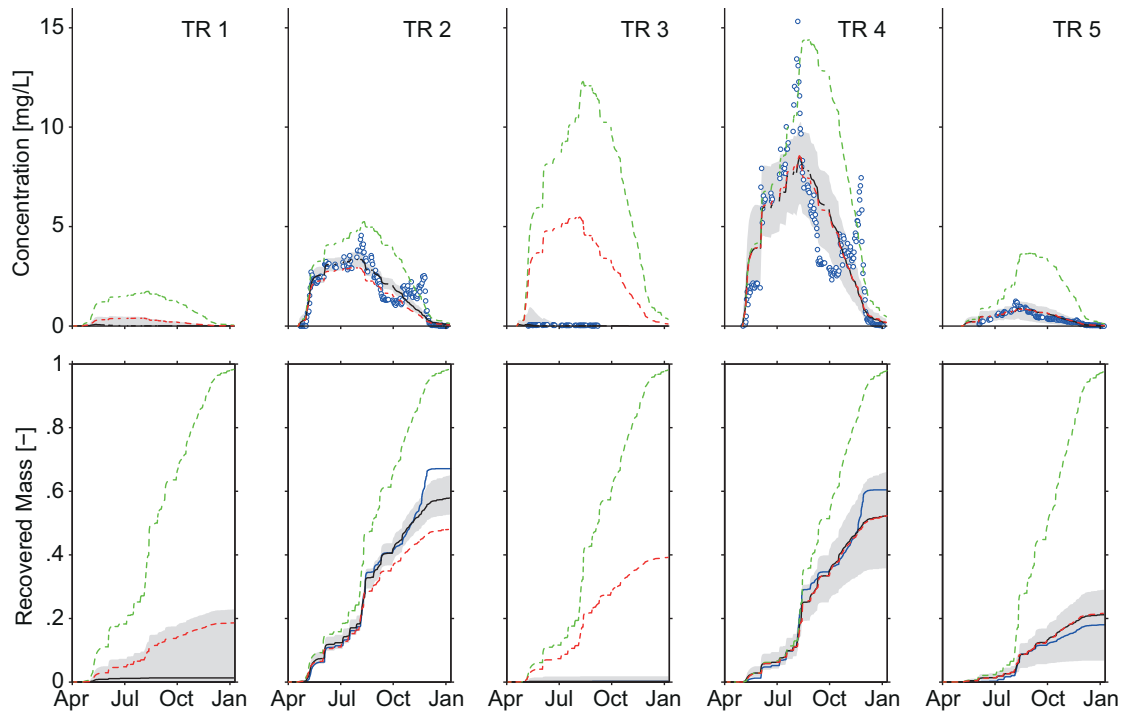


Figure 3.4: Comparison between simulated and measured breakthrough curves (top panels) and fractions of injected mass retrieved in the bottom outflow (bottom panels) for the five tracers (columns). Blue circles and blue lines represent measured data. Black lines and gray shaded areas show the medians and the 5–95 percentile ranges of the behavioral simulations, respectively. Red and green dashed lines show the median behavior of an ideal tracer (i.e.  $\alpha = 1$  and  $DT_{50} = \infty$ ) and of a conservative tracer which is not subject to plant uptake (i.e.  $\alpha = 0$  and  $DT_{50} = \infty$ ), respectively

higher breakthrough curves and fractions of recovered mass close to unity by the end of the experiment (green-dashed lines in Figure 3.4).

The selected behavioral parameter sets are used to model the simultaneous re-injection of tracer 1 and 4 (occurred when previously injected tracers were no longer detectable in the system, Figure 3.1b) without further calibration. Results of this validation analysis are reported in Figure 3.5. These two tracers exhibited very different dynamics during the first injection: tracer 1 was never recovered at the outlet while tracer 4 had the highest fraction of exported mass (Figure 3.4). When injected simultaneously, the two tracers show similar patterns (Figure 3.5). These very different behaviors, which depend on the different hydrologic forcings occurred during the experiments, can be reproduced by the model. However, the wide distributions of behavioral parameters  $\alpha_1$  and  $DT_{50,1}$  lead to a wide spectrum of possible outcomes for the modeled export of tracer 1. Using also the information gathered in the re-injection of tracer 1 in the calibration phase, it is possible to better identify the parameters  $\alpha_1$  and  $DT_{50,1}$  (red dots in Figure 3.3b).

While experimental data allows us to estimate transport dynamics only for the marked injec-

### Chapter 3. Transport of fluorobenzoate tracers in a vegetated hydrologic control volume: Theoretical inferences and modeling

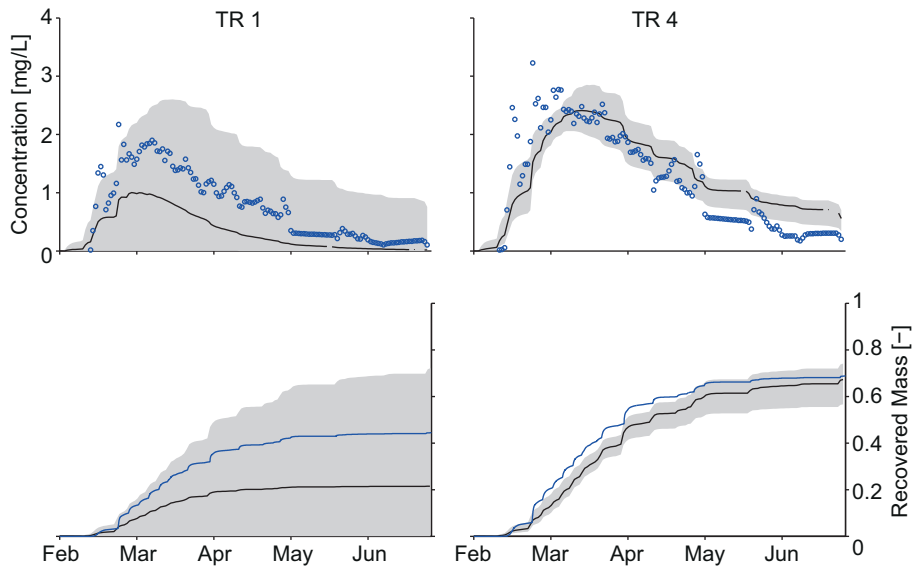


Figure 3.5: Validation of model results. Comparison between simulated and measured breakthrough curves (top panels) and fractions of injected mass retrieved in the bottom outflow (bottom panels) for the re-injection of tracer 1 and 4. Symbols as in Figure 3.3. Model results are obtained using the behavioral parameter sets obtained in the first experiment (Figure 3.3) without further calibration.

tions, a model calibrated on measured data allows inferring the hydrologic history of every component of the storage. Figure 3.6 presents an overview of the time evolution of hydrological variables and of the RTD and forward and backward TTDs. For the sake of simplicity, a single control volume is referred to: the soil component of the lysimeter (Figure 3.1a). Oblique lines in Figure 3.6c show pairs of  $t$  and  $T$  such that at  $t - T$  an injection occurred and thus RTDs and backward TTDs are greater than 0. Following these oblique lines one can see the evolution of the relative contribution of a water input (injected at the intersection with the  $x$ -axis) to the storage ( $p_S(T, t)$ ), the outflow flux ( $\bar{p}_L(T, t)$ ) and the evapotranspiration flux ( $\bar{p}_{ET}(T, t)$ ). Forward TTDs (Figure 3.6d) are instead defined for all ages but only for times when an injection took place. The different age-selection processes occurring in the formation of  $Q$  and  $ET$  result in very different mean travel times: around 70 days for  $Q$  and 10 for  $ET$  (Figure 3.6f). Note how the means of forward and backward TTDs differ. When outflow is null, e.g. between September 24 and October 12,  $\bar{p}_L(T, t)$  and the corresponding mean are not defined.

The time window displayed in Figure 3.6 spans from August to December to highlight the different transport dynamics induced by the different magnitude of  $ET$  (Figure 3.6b). During winter (low  $ET$ ) the fraction of precipitation that will leave the system through outflow ( $\theta(t_i)J(t_i)$ , blue bars in Figure 3.6a) dominates, while it is reduced during summer. In such period a water particle is more likely to exit through the outflow. As a consequence, the mean forward travel time (the mean travel time of all particles injected at a certain time) is lower (Figure 3.6f). It can be noticed how large rainfall events reduce mean residence time by bring-



ing young water (with age equal to zero) into the system. The time evolution of the outflow mean backward travel time (the mean travel time of all particles exiting as  $L$  at a certain time) follows closely that of the mean residence time ( $r = 0.95$ ), indicating that, although outflow samples preferentially old water, the average age is controlled by the availability of ages in storage.

### 3.4 Discussion

The results presented suggest that the large variance exhibited by the transport dynamics of tracer 1, 2, 4 and 5 can be explained by the behavior of an ideal tracer which tracks water transport features, including transpiration, without degrading. Under these conditions the fate of the water inputs marked with different tracers are determined by the hydrologic signal faced by the water parcels while traveling through the system. This is also supported by the results of the model validation. When the tracers are injected simultaneously, they exhibit similar transport behaviors. This provides strong experimental evidence, supported by a robust theoretical framework, of the non-stationary character of travel time distributions.

While the initial five injections of tracer occurred within one month, release in the outflow lasted for almost 9 months. Therefore a large fraction of the hydrologic conditions experienced by the marked injections were identical. This result suggests that in the actual system the conditions faced immediately after injection are crucial to determine the overall fraction of water that will leave the system through discharge outflow. In particular, the role of plant uptake for hydro-chemical balance cannot be underestimated when analyzing TTDs at any scales. Plants are able to transpire a large fraction of soil water. The amount of water withdrawn, the presence of possible fractionation processes or the age distribution of water particles incorporated by plants may bear profound effects on catchment scale transport features. In this modeling exercise, the fitted parameters indicate that  $ET$  samples preferentially new water, while  $Q$  samples older water. This result was somewhat expected given the predominantly vertical nature of the flow in the lysimeter. At catchment scales, different results could be expected. Surface and subsurface sub-horizontal flows or macropores can rapidly convey a large amount of event water to the outlet, possibly increasing the relative importance of new water in the catchment-scale backward TTD, particularly during high flows (*van der Velde et al.*, 2012; *Benettin et al.*, 2013a). Moreover, significant geomorphological complexity, say epitomized by catchment width functions (the relative proportion of injection sites equally distant from the outlet), are known to impact mixing and sampling patterns, possibly resulting in higher degrees of mixing between different ages in stream waters.

The results presented in Figure 3.6 show that even time-invariant SAS functions produce time-variant transport features (e.g. mean travel times) depending on the state of the system (i.e. the storage) and on the external forcings (i.e. the evapotranspiration rate). More complex, time-variant age selection schemes obtained assuming that the exponents  $\beta$  vary linearly with water storage, similarly to *Harman* (2015) were also tested. No significant improvement was

### Chapter 3. Transport of fluorobenzoate tracers in a vegetated hydrologic control volume: Theoretical inferences and modeling

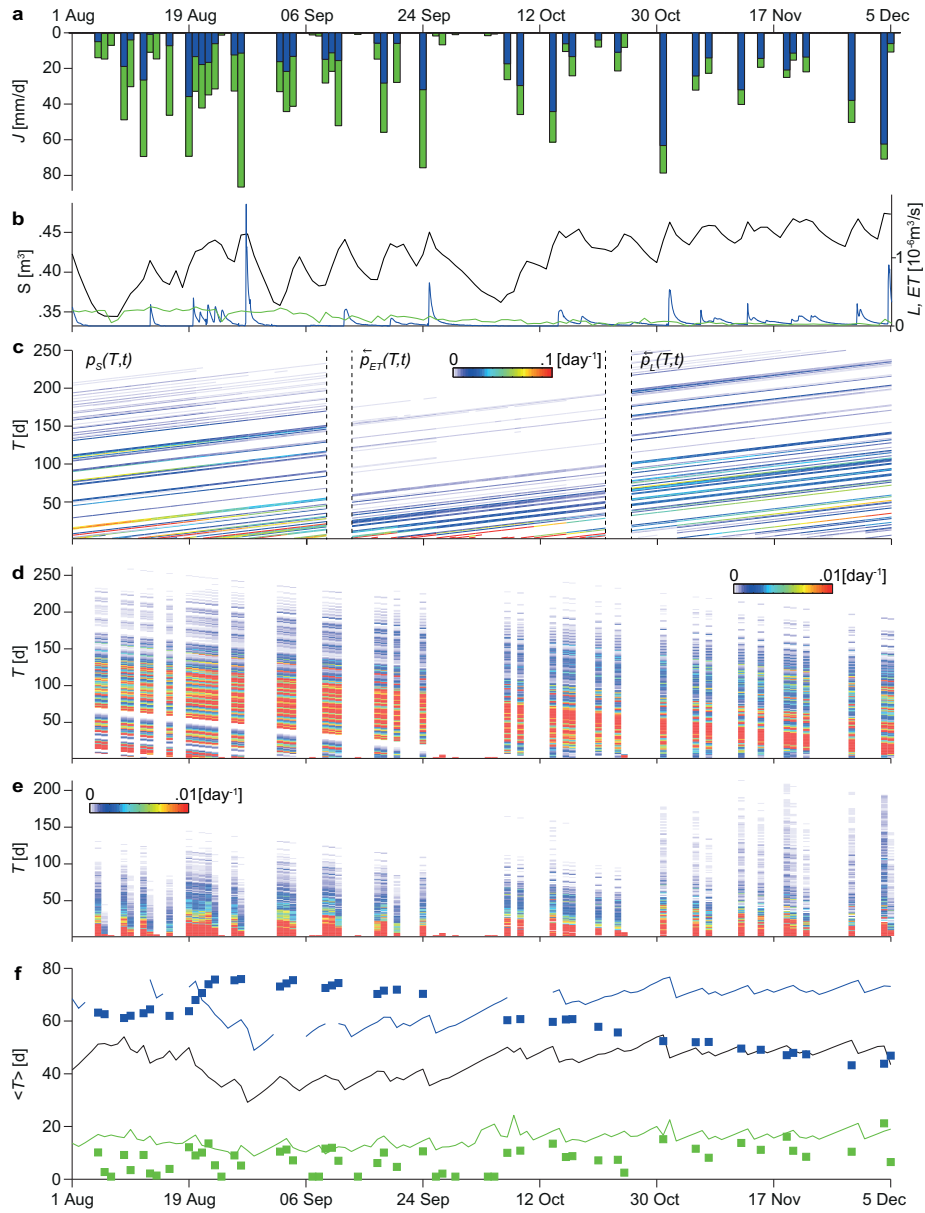


Figure 3.6: Summary of relevant distributions in the soil control volume. a) Time series of rainfall, fraction of rainfall inputs that will leave the system through outflow  $L$  ( $\theta(t)J(t)$ , blue bars) and  $ET$  ( $(1 - \theta(t))J(t)$ , green bars). b) Time series of water storage  $S$  (black), outflow  $L$  (blue) and  $ET$  (green). Panels c) show RTD  $p_S(T, t)$ , backward TTDs  $\bar{p}_{ET}(T, t)$  and  $\bar{p}_L(T, t)$  as a function of age ( $y$ -axis) and time ( $x$ -axis). Analogously, the forward TTDs  $\bar{p}_L(T, t)$  and  $\bar{p}_{ET}(T, t)$  are displayed in panel d) and e), respectively. f) Time series of mean residence time (black line), mean outflow (blue) and  $ET$  (green) travel times for forward (squares) and the backward (lines) distributions. Distributions are calculated with  $\beta_L = 2$  and  $\beta_{ET} = 0.2$ . To achieve precise estimates of the variables displayed, the duration of the data-set available have been synthetically extended up to three years repeating three times the observed time series of hydrological variables (May 2013-May 2014), one before and one after the actual experimental period.

found for the lysimeter experiment. Nonetheless, it will be interesting to test this hypothesis in more complex settings.

### **3.5 Conclusions**

There exists a growing consensus within the hydrologic community on the fact that collection of hydrologic data should be complemented with measurements of tracers to properly understand how water moves through catchments (*McDonnell and Beven, 2014*). This calls for simple, flexible and commonly accepted tools to interpret tracer data in terms of residence and travel time distributions. I believe that the framework presented herein fulfills such requirements.

Overall the results presented show that a framework for hydrologic transport based on time-variant travel time distributions is able to explain the non-stationary behavior exhibited by experimental data of tracer transport in a large lysimeter. Although the scale of the experiment is small compared to that of hillslopes and catchments, this approach relies solely on input and output fluxes and thus general guidelines for the application at larger scales can be drawn. The precise knowledge of the lysimeter structure allowed us to identify two separate control volumes (the soil and the gravel filter). At larger scales, however, clear structures and boundaries can hardly be identified, let alone measured. At first instance one could resort to a single control volume to assess residence and travel time distributions from tracer data. In this case heterogeneity of flowpaths, source areas and mixing in catchment storage are charged to the storage selection functions. The application of the method needs the further specification of the time series of all hydrological fluxes and of the storage. While the experimental set-up allows the perfect knowledge of all fluxes, in real-life applications they would need to be measured (precipitation and discharge) or estimated through suitable models (evapotranspiration). Once all fluxes are reasonably estimated, the storage inside the control volume can be inferred via mass balance up to an additive constant: the initial storage, which represents a crucial model parameter controlling the volume of water potentially available for mixing. If simple power-law SAS functions of the type introduced in section 3.2.4 are to be employed, the model requires the calibration of three additional parameters: namely  $\beta_{ET}$ ,  $\beta_Q$  and the coefficient  $\alpha$  for the tracer in focus. For the latter, the type of tracer (e.g. chloride, water isotopes) and information about land use and vegetation cover can be used to constrain the *prior* distribution of this parameter. If the tracer is expected to undergo non-negligible degradation at time scales comparable with the mean travel time, such process can be accounted for at the cost of an additional parameter. However, as highlighted also by the results presented herein, degradation may hamper parameter identification. Therefore, the analysis of conservative tracers is suggested to be more informative for characterizing transport processes. As displayed in Figure 3.6, the calibrated model allows estimating in retrospect the time evolution of mean residence time and mean forward and backward travel time for both discharge and evapotranspiration in a framework that consistently accounts for non-stationary behaviors.

### **Chapter 3. Transport of fluorobenzoate tracers in a vegetated hydrologic control volume: Theoretical inferences and modeling**

---

The procedure outlined assumes that the hydrologic forcings (precipitation, discharge and evapotranspiration) are either measured or estimated and that they are directly used as inputs for the transport model. This allows a quick interpretation of tracer data in terms of residence and travel time distributions. However, more complex schemes can be envisioned where the hydrologic and the transport models (possibly with multiple control volumes) are coupled. It has been shown that the simultaneous calibration of such models against flow and tracer data allows reducing the uncertainties on the underlying hydrologic processes (see e.g. *Fenicia et al.*, 2010; *McMillan et al.*, 2012; *Bertuzzo et al.*, 2013; *Hrachowitz et al.*, 2013).

When *Botter et al.* (2010) first introduced the framework adopted herein for time-variant travel time distributions, one critical point that immediately emerged was that a proper characterization of the distribution of the age of water in the discharge cannot be decoupled from the characterization of the age distribution in the evapotranspiration flux. However, directly measuring proxies of evapotranspiration age experimentally can prove hard even at plot scale. This modeling exercise shows that, as evapotranspiration modifies the availability of ages in storage possibly sampled by discharge, it is possible to infer how evapotranspiration samples the storage from measurements of discharge age composition. This has been suggested at the lysimeter scale; however, the same approach can arguably be applied to any upscaled control volume.

## 4 Water stable isotopes: a transport experiment

This chapter compares the information provided by water stable isotopes tracer transport in a large, vegetated lysimeter contrasting the transport of two organic tracers selected among the group of fluorobenzoic acids (FBAs), whose properties are described in Chapter 2. The experiment was set up in order to provide control on the variable hydrologic input and output fluxes and study how the bottom drainage samples water pools of different ages within the storage. A water pulse marked by the two FBAs and with a contrasting isotopic composition of the source water which compounds the simulated rainfall was injected in the beginning of the growing season. Samples of discharge flow were analysed for organic tracers and oxygen-/hydrogen- isotopic ratios. Water stable isotopes, acknowledged as convenient water tracers for their conservative behavior (i.e. absence of retardation) show a biased response signal in the discharge due to evaporation enrichment. They are therefore no better than moderately reactive organic tracers for a direct interpretation in terms of hydrologic travel times. By modeling (the stationary and) kinetic fractionation due to evaporation at the soil surface, the overall evaporation flux (3% of the total evapotranspiration flux) accountable for the significant drift of the discharge's isotopic composition is estimated. The specific  $\delta^2\text{H}/\delta^{18}\text{O}$  signature operated by evaporation is then used in order to correct the isotopic content of the discharge and expressed the response in terms of pulse fraction, an equivalent metrics to the relative concentration (used for the FBAs). The signal provided by the isotopic composition after correction proves in agreement with the two FBAs' signals. However, the performance of the former is hardly better due to a high sensitivity of the correction method to the natural fluctuations of the respective  $\delta^2\text{H}$  and  $\delta^{18}\text{O}$  isotopes. Hence, water stable isotopes are ideal tracers only for hydrologic systems that are not subject to evaporation (say, owing to rapid infiltration or dense vegetation cover). They can also be used to efficiently estimate evaporation if  $\delta^2\text{H}$  and  $\delta^{18}\text{O}$  are jointly measured.

### 4.1 Introduction

Water stable isotopes ( $^{18}\text{O}$  and  $^2\text{H}$ ) have been extensively used as water tracers in hydrologic studies, from lysimeter-scale to world-wide characterization of global water exchanges (e.g. *Maloszewski et al.*, 1995; *Kendall and Coplen*, 2001; *Jasechko et al.*, 2013). Their natural ubiquitous occurrence makes them good candidates for large scale applications, because it discards the need to artificially label water parcels as the natural fluctuations can be used as a continuous input signal. For this reason, water stable isotopes have been largely used in catchment studies to measure the contribution of different pools (e.g. precipitation, soil water, groundwater) in a water flux (e.g. stream discharge), examine how waters are stored and mixed within hydrologic volumes and determine water flowpaths (e.g. *Martinec et al.*; *McDonnell et al.*, 1990; *Neal et al.*, 1992; *Clay et al.*, 2004; *Fette et al.*, 2005).

Since a few decades, the description of a catchment's hydrologic response in terms of travel time has become more and more common (e.g. *Jury et al.*, 1986; *Rinaldo and Marani*, 1987; *Maloszewski et al.*, 1992; *Haggerty et al.*, 2002). Travel time is defined as the time spent by a water parcel within a hydrologic control volume from its injection until it exits the system via an output flux. Due to the non-stationarity of the climatic forcing and the heterogeneity of the flow pathways, the hydrologic response of a system is constituted by a full spectrum of travel times that can be described through a probability distribution. The advantage of the use of travel time as a catchment descriptor is that it blends all kind of processes affecting water transport (storage, connectivity of flowpathways, evapotranspiration, etc.) into a single state variable. However, the measurement of travel time proves a difficult task, as one requires to record each water particle's input and output time, in hydrologic systems often characterized by long mean travel times. For that matter, using water stable isotopes as water tracers appears as a suitable method, because the natural input signature made by the fluctuations of the isotopic composition of precipitation is tracked in the outlet of the control volume (e.g. *Maloszewski et al.*, 1992; *Rodhe et al.*, 1996; *Simic and Destouni*, 1999; *Hrachowitz et al.*, 2010b). Nevertheless, the deconvolution of the output signal, given a continuous variable input signal is required to infer the travel time distribution, and this can only be done assuming it to be stationary in time. The lack of stationarity of such transfer function has now been recognized by a number of papers (e.g. *Botter et al.*, 2010; *Hrachowitz et al.*, 2009a, 2010a; *Birkel et al.*, 2012; *van der Velde et al.*, 2012; *Heidbüchel et al.*, 2013). Experimentally, this makes the interpretation of natural isotopic signals much more difficult as the travel time distributions of water parcels may be different depending on their time of entry in the system and the specific conditions encountered. A non-ambiguous solution involves the use of multiple tracers independently injected instead of a continuous single-tracer signal, so that the injection time is unequivocally known (*Queloz et al.*, 2015b). Such experiments are rare (*Kirchner et al.*, 2010; *Birkel et al.*, 2011) because artificial injections are needed, and this is usually difficult to achieve at the catchment scale. Moreover, appropriate water tracers are lacking. In Chapter 2, the performance of five fluorobenzoic acids as multiple tracers is evaluated in a large lysimeter experiment. It has been observed that the interpretation of tracer breakthrough curves in terms of travel time is

challenging because the tracers demonstrated reactivity within the transport volume. Thereby, it becomes difficult to determine whether differences observed in the breakthroughs are due to compound-specific reactivity or to different hydrologic conditions encountered during the transport of each tracer resulting in the variability of the travel time.

Here, I compare and interpret the breakthrough curves of two FBAs with oxygen- and hydrogen-isotopes, for a 20-liter pulse of desalinated sea water (i.e. distinctively labeled isotopically) marked with the the two organic tracers injected in a large vegetated lysimeter (Chapter 2). Isotopes are not affected by soil sorption effects, microbial degradation or discrimination via plant uptake in contrast to FBAs. Isotopes are however subject to evaporation-induced fractionation that may affect the resulting observed isotopic signals (e.g. *Gonfiantini*, 1986). Notwithstanding the advantage of using FBAs over water stable isotopes to have multiple compounds analytically differentiable (hydrogen and oxygen isotopes cannot usually be used as two independent tracers because their natural occurrence is highly correlated), the benefits of isotopes over the FBAs for their use as conservative water tracers are assessed.

The terminology used for isotopes in hydrology is given first, followed by a description of the fractionation process affecting the isotopic composition during evaporation. This is later used to (1) evaluate the overall evaporation flux during the duration of the experiment and (2) correct the observed isotopic content of the discharge water to account for evaporation enrichment. This allows to calculate the contribution of the pulse in the discharge water at any time, which is equivalent to the pulse travel time.

## 4.2 Theory

### 4.2.1 Basic definitions

By water isotopes, we refer to the most common stable isotopes of hydrogen ( $^1\text{H}$  and  $^2\text{H}$ ) and oxygen ( $^{16}\text{O}$  and  $^{18}\text{O}$ ), which are the constituents of the water molecule. Hence, the isotopologues of water are any combination of the O- and H- isotopes constituting a water molecule. The lighter isotopes are usually found in higher concentrations on the Earth's surface, which brings the commonly used " $\delta$ " label, describing the fraction of heavy isotopes (in ‰) relative to a standard of known composition:

$$\delta \text{ (in ‰)} = (R_X / R_S - 1) \cdot 1000, \quad (4.1)$$

with  $R_X$  and  $R_S$  denoting the ratio of the heavy to the light isotope (e.g.  $^{18}\text{O}/^{16}\text{O}$ ) of sample and standard, respectively. Note that to simplify the notation, only the heavy isotope species is noted after the  $\delta$  term even if this refers to the ratio between the heavy and light isotope (i.e.  $\delta^{18}\text{O}$  for  $\delta^{18}\text{O}/^{16}\text{O}$ ). The standard values used here are those from the Vienna Standard Mean Ocean Water (VSMOW) reported in Table 4.1. Oxygen and hydrogen isotopes naturally fractionate on the Earth's surface due to evaporation and condensation processes (see 4.2.2). The use of water stable isotopes as a tool for classifying catchment in term of hydroclimatic

## Chapter 4. Water stable isotopes: a transport experiment

---

Table 4.1: Reference standards for water stable isotopes according to the Vienna-SMOW.

Isotope	Ratio	Ratio abundance
$^2\text{H}$	$^2\text{H}/^1\text{H}$	$1.5575 \cdot 10^{-4}$
$^{18}\text{O}$	$^{18}\text{O}/^{16}\text{O}$	$2.0052 \cdot 10^{-3}$

environments has been an active field of research for many decades (e.g. *Craig*, 1961; *Dincer*, 1968; *Kendall and Coplen*, 2001; *Jasechko et al.*, 2013). The fractionation processes and the hydrologic behavior of oxygen and hydrogen are similar, and therefore their isotopic concentrations are linearly covariant. The mean relationship between deuterium and oxygen-18 in natural meteoric water of different parts of the world is termed global meteoric water line (GMWL) and has been described by *Craig* (1961):

$$\delta^2\text{H} = 8 \cdot \delta^{18}\text{O} + 10. \quad (4.2)$$

The GMWL results from fractionation occurring during the evaporation of ocean water (water vapor is depleted in heavy isotopes) and subsequent condensation during the formation of rain drops, close to the chemical equilibrium (*Horita and Wesolowski*, 1994). Local meteoric water lines (LMWL) describing the stable isotopic ratios in a specific region may have slopes of less than eight due to kinetics effects induced by evaporation processes in disequilibrium. A measure of this disequilibrium is given by the deuterium excess, described as the intercept value of a linear function of slope 8 fitted on the sample values (*Dansgaard*, 1964):

$$d = \delta^2\text{H} - 8\delta^{18}\text{O}. \quad (4.3)$$

The deuterium excess is especially sensitive to evaporative processes (notably ocean surface temperature and the humidity of the air during evaporation (*Merlivat and Jouzel*, 1979), providing a useful tool for evaluating the extent of evaporation of local samples compared with the GMWL (for which  $d = 10\text{‰}$ ).

Solutions with different isotopic compositions mix conservatively (*Kendall and Caldwell*, 1998), and the resulting isotopic concentration of a mixture of two or more endmembers can be calculated in  $\delta$  notation just as with regular concentration. Hence, on a graphic representing the isotopic compositions of water ( $\delta^2\text{H}$  plotted versus  $\delta^{18}\text{O}$ , as in Figure 4.2), the mixing between two endmembers plots along straight lines between their original isotopic contents (note that this is not the case for isotopologue other than water present at different concentrations of their original solutions).

### 4.2.2 Isotopic fractionation

The heavy isotopic species of water (i.e.  $^1\text{H}^2\text{H}^{16}\text{O}$  and  $^1\text{H}_2^{18}\text{O}$ ) are less volatile and therefore less easily evaporated than the lighter counterpart. The difference between the isotopic content of the vapour and the liquid phase at thermodynamic equilibrium is defined by the



fractionation factor  $\alpha$ :

$$\alpha_e = R_l / R_v, \quad (4.4)$$

with  $\alpha_e$  the fractionation factor at equilibrium,  $R_l$  and  $R_v$  the isotope ratios of the liquid phase and vapour phase at equilibrium, respectively. The equilibrium fractionation factors of oxygen and hydrogen isotopes decrease slightly with temperature, each species at a different rate (*Gonfiantini*, 1986). *Horita and Wesolowski* (1994) have experimentally determined their values for a large temperature range and derived the following regressions:

$$\begin{aligned} 10^3 \ln[\alpha_e(^2\text{H})] &= 1158.8(T^3/10^9) - 1620.1(T^2/10^6) + 794.84(T/10^3) \\ &\quad - 161.04 + 2.9992(10^9/T^3), \\ 10^3 \ln[\alpha_e(^{18}\text{O})] &= -7.685 + 6.7123(10^3/T - 1.6664(10^6/T^2) + 0.3504(10^9/T^3), \end{aligned} \quad (4.5)$$

with  $T$  the temperature in degrees Kelvin. Such thermodynamic equilibrium is not always achieved during isotopic exchange processes, in particular in case of an unsaturated atmosphere (relative humidity  $h < 100\%$ ) or if the air above the evaporative surface is subject to mixing or is blown away (*Araguás-Araguás et al.*, 2000). Under these circumstances, a kinetic effect controlled by isotope-specific molecular diffusion in the air adds up to the fractionation at equilibrium.

A model describing the isotopic composition of the evaporation flux including both fractionation effect at equilibrium and kinetic fractionation has been proposed by *Craig and Gordon* (1965), and reads:

$$\delta_E = \frac{(\delta_L - \epsilon_e)/\alpha_e - h \cdot \delta_A - \epsilon_k}{1 - h + \epsilon_k}, \quad (4.6)$$

with  $\delta_L$  and  $\delta_A$  the isotopic concentration (relative to a standard, see Eq. 4.1) of the evaporative surface and the atmosphere respectively,  $h$  the relative humidity,  $\epsilon_e = \alpha_e - 1$  the equilibrium fractionation factor and  $\epsilon_k$  the kinetic fractionation factor. The kinetic fractionation factor depends on the ratio of the molecular diffusion coefficients of the light and heavy isotope, and is proportional to the moisture deficit  $(1 - h)$  (*Craig and Gordon*, 1965). Diffusion coefficients ratios for oxygen and hydrogen were experimentally determined by *Merlivat* (1978), who has found:

$$\begin{aligned} \epsilon_k(^{18}\text{O}) &= 0.0142(1 - h), \\ \epsilon_k(^2\text{H}) &= 0.0125(1 - h). \end{aligned} \quad (4.7)$$

### 4.3 Material and methods

#### 4.3.1 General experimental set-up

The hydrological time series and water stable isotope data were collected between February and July 2014 in a large lysimeter, located on the EPFL campus in Lausanne, Switzerland (Chapter 2). The lysimeter consists in a large soil column (2 m-deep, 1 m<sup>2</sup>-surface area) resting on three load cells providing an accurate reading of the weight of the system and hereby an indirect continuous measurement of the water storage. The open top of the lysimeter is at ground-level (an underground chamber allows the access from below) and is planted with two willow stems (*Salix viminalis*) prompting sizable transpiration fluxes. A translucent gable roof placed under the canopy prevents natural rainfall from penetrating in the lysimeter, but leaves the trees exposed to natural ambient conditions. Openings at the two extremities of the gable roof allow air exchange and limit the temperature increase underneath. Rainfall was simulated by manually injecting tap water on the soil surface according to a marked Poisson process (Rodhe *et al.*, 1996). A water table is maintained in a 50-cm gravel filter at the bottom of the lysimeter. Excess draining water is discharged by a outlet pipe and measured using a tilting bucket. As the water input flux is controlled and bottom discharge is measured, the overall evapotranspiration flux can be derived from the mass balance, as water storage changes are monitored by the load cells. A detailed description of the experimental set-up is provided in Chapter 2. A meteorological station located five meters away from the installation records air temperature, air humidity, wind direction and intensity, incoming radiation and soil temperature at 15 min-intervals.

#### 4.3.2 Preparation and application of the isotopically labelled pulse

The rainfall pulses injected in the system are all composed of fresh local tap water (LTW). All the antecedent water injections since the initial filling (Autumn 2012) of the lysimeter were also done by the same water source. The tap water distributed at EPFL essentially originates from Lake Geneva (EauService, Lausanne). This large pool provides water with stable properties in time, due to the deep collection point (157 m under lake surface) and important mixing in the lake and in the intermediate reservoirs (*Fontes and Gonfiantini*, 1970). Isotopic content statistics of the LTW are reported in Table 4.2.

On February 26, a rainfall marked with a different isotopic content than LTW was applied. The 19.7 L-pulse was composed of distilled sea water (SW), collected from the "Acqua Alta" offshore platform (courtesy of Roberto Zonta, National Research Council, Italy) in the Gulf of Venice (Northern Adriatic, Italy). This water has a much higher content in heavier isotopes (Table 4.2), and can thus be tracked as a conventional human-applied tracer (e.g. such as inorganic anions, dyes, etc.). This isotopically-labeled water pulse was also marked with two difluorobenzoic acids (2,5-DFBA and 2,6-DFBA) in order to provide a comparison between two different types of tracers. These tracers are studied in detail in Chapter 2, where their

Table 4.2: Isotopic composition of source and pulse water.

	$\delta^{18}\text{O}$ (‰)	$\delta^2\text{H}$ (‰)
Local tap water (LTW)	-12.28(±0.03)	-89.76(±0.21)
Sea water pulse (SW)	0.96(±0.02)	6.33(±0.42)

properties and their application are described.

### 4.3.3 Sampling, conditioning and isotope analysis

Samples were collected within the soil column at different depths and in the discharge flow. Discharge was sampled proportionally to the flow rate every 1-3 l using a switch valve and a fraction collector (see section 2.2). Soil water was extracted using twelve ceramic suction probes (1-bar bubbling pressure) distributed at three different depths (50, 100 and 150 cm). Porous cups water extraction has been successfully used in other studies and were not reported to cause isotopic fractionation (*Hunt et al.*, 1996; *Clay et al.*, 2004). The samples were collected as early as possible (mostly less than a day), filtered by 0.45  $\mu\text{m}$  hydrophobic syringe filters with GMF/PP membranes (BGB Analytik AG, Switzerland), conditioned in 3 ml glass vials filled to the top with septum screw caps and stored at 4 °C.  $\delta^2\text{H}$  and  $\delta^{18}\text{O}$  were carried out using a Cavity Ring Down Spectrometer (CRDS) L2130-*i* (Picarro, USA), a High-Precision Isotopic Water Analyzer with a specific calibration procedure.

### 4.3.4 Evaporation model

The steady-state water balance for the lysimeter can be written by considering all input and output fluxes to/from the system:

$$I = E + T + Q, \quad (4.8)$$

with  $I$  the water inputs,  $E$  and  $T$  the soil evaporation and plant transpiration respectively and  $Q$  the bottom discharge. Note that the setup described in section 4.3.1 allows the closing of the water balance for the combination of  $E$  and  $T$ , but does not allow to differentiate between the two different processes. As evaporation affects the isotopic composition of the evaporation flux and residual water in contrast to transpiration — which does not operate significant fractionation at the soil level (this is however not the case at the shoot level) — the water stable isotopes can be used to isolate the two processes. The stable isotope mass balance can thus be written similarly:

$$\delta_I I = \delta_E E + \delta_T T + \delta_Q Q, \quad (4.9)$$

where  $\delta_{I,E,T,Q}$  are the fractions of heavy isotopes in the water inputs, the evaporation flux, the transpiration flux and the discharge flux, respectively. Combining Eq. 4.8 and 4.9, the

## Chapter 4. Water stable isotopes: a transport experiment

---

evaporation flux reads:

$$E = \frac{I(\delta_T - \delta_I) + Q(\delta_Q - \delta_T)}{\delta_T - \delta_E} \quad (4.10)$$

The system is assumed to be in steady state during the period of experiment (the storage at the end of the experiment is equal to the initial storage, so that Eq. 4.8 applies). As evaporation only affects soil water at shallow depths, it is considered that the soil water subject to evaporation has an isotopic composition equal to that of input water. The latter was only composed of tap water except for a single sea water pulse. The overall composition of the input water is therefore approximated by:

$$\delta_I = (I - V_{SW})\delta_{LTW} + V_{SW}\delta_{SW}, \quad (4.11)$$

with  $\delta_{LTW}$  and  $\delta_{SW}$  the isotopic composition of local tap water and sea water pulse respectively, reported in Table 4.2.  $V_{SW}$  is the volume of the sea water pulse volume and  $I$  is the total input volume injected during the whole experiment period. As the plant root system expands through the entire depth of the soil column, the transpired water is assumed to have the same isotopic composition as the water being discharged:

$$\delta_T = \delta_Q = \frac{\sum_{i=1}^n \delta_{s_i}}{n}, \quad (4.12)$$

i.e. the isotopic content of both discharge and transpiration flux is the mean value of the measured discharge samples  $\delta_{s_i}$ . Therefore, Eq. 4.10 simplifies as:

$$E = I \frac{\delta_Q - \delta_I}{\delta_Q - \delta_E}. \quad (4.13)$$

To calculate  $\delta_E$ , the evaporation model developed by *Craig and Gordon* (1965) described in Eq. 4.6 is used. The isotopic composition of atmospheric moisture  $\delta_A$  has been experimentally measured for the Lake Geneva region (*Fontes and Gonfiantini*, 1970). The parameters (for hydrogen and oxygen isotopes) used in the model are summarized in Table 4.3.

## 4.4 Results

### 4.4.1 Isotopes and difluorobenzoic acids breakthrough

The results concerning the hydrological behavior of the experiment are described in detail in Chapter 2. The DFBA and heavy isotopes breakthrough of the marked pulse are presented in Figure 4.1. Both organic tracers and both isotopes display a synchronized concentration breakthrough, even though 2,5-DFBA is systematically measured at a lower concentration resulting in a final recovery at the end of the experiment of 45% and 70% for 2,5-DFBA and 2,6-DFBA respectively. However, the two isotopic signals appear quite different from the DFBA signals

Table 4.3: Summary of the parameters used for the evaporation model.

Parameter	Value	Unit	Reference
$Temp$	12	[°C]	meas.
$h$	76	[%]	meas.
$I$	2766.1	[L]	meas.
$Q$	968.0	[L]	meas.
$V_{SW}$	19.7	[L]	meas.
$\delta_I(^2H)$	-89.07	[‰]	meas., Eq. 4.11
$\delta_I(^{18}O)$	-12.18	[‰]	meas., Eq. 4.11
$\delta_Q(^2H)$	-85.76	[‰]	meas., Eq. 4.12
$\delta_Q(^{18}O)$	-11.38	[‰]	meas., Eq. 4.12
$\delta_A(^2H)$	-147.55	[‰]	<i>Fontes and Gonfiantini (1970)</i>
$\delta_A(^{18}O)$	-17.20	[‰]	<i>Fontes and Gonfiantini (1970)</i>
$\alpha(^2H)$	1.0930	[-]	<i>Horita and Wesolowski (1994), Eq. 4.5</i>
$\alpha(^{18}O)$	1.0104	[-]	<i>Horita and Wesolowski (1994), Eq. 4.5</i>
$\epsilon_k(^2H)$	$0.0125(1 - h)$	[-]	<i>Merlivat (1978), Eq. 4.7</i>
$\epsilon_k(^{18}O)$	$0.0142(1 - h)$	[-]	<i>Merlivat (1978), Eq. 4.7</i>

and fluctuate to a much greater extent. Yet a main carrier signal can be perceived between mid-March and June which roughly corresponds to the DFBA signals. The background oxygen- and hydrogen- isotopic content (i.e. before the beginning of the breakthrough observed for the DFBA) also fluctuates notably, and is significantly larger than the isotopic content of the source water (Table 4.2) which suggests an enrichment in heavy isotopes occurring during the transport of water through the column. This is also confirmed by the estimation of the final recovery rate of the pulse at the end of the experiment which largely exceed 100% both for  $\delta^{18}O$  and  $\delta^2H$  (even when considering the mean observed background concentration observed during the first days of measurements instead of the source water initial isotopic composition). Overall, evaporation seems to consistently bias the isotopic composition of the discharge.

#### 4.4.2 Evaporation estimation

Figure 4.2 represents the ratio between  $\delta^{18}O$  and  $\delta^2H$ . The discharge samples spread well along a local water line of slope 3.8 (gray line). However, if only mixing between the source water and the pulse water controls the observed isotopic content of the discharge water, all samples would fall along the mixing line (black line) connecting the source and pulse water composition (see 4.2.1). This supports the ansatz that another process affects the resulting isotopic composition observed in the discharge water. As the system includes only one influx (precipitation  $I$ ) of known isotopic composition and three outputs (discharge  $Q$ , plant transpiration  $T$  and ground surface evaporation  $E$ ) of which only  $Q$  is actually measured,  $E$  and/or  $T$  are thus likely to operate selectively regarding the isotopic composition. Water plant uptake

## Chapter 4. Water stable isotopes: a transport experiment

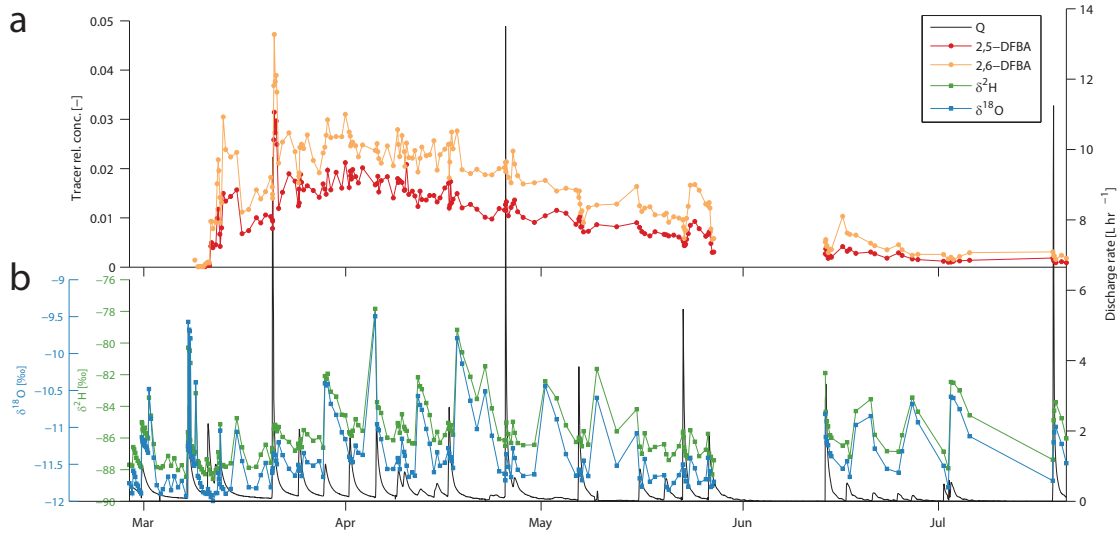


Figure 4.1: Tracer and isotopes discharge breakthrough curves: (a) relative concentration of 2,5-DFBA and 2,6-DFBA and (b) oxygen and hydrogen isotopic composition expressed in  $\delta$ -values. The markers represent the samples analyzed. Measured discharge rate is plotted in black and expands other both panels (right y-axis).

is, however, known to be non-selective at the root level (e.g. *Bariac et al.*, 1991). In contrast, evaporation and condensation at equilibrium alter oxygen- and hydrogen- isotope linearly with a ratio of about 8 (explaining the slope of the GMWL). However, kinetic evaporation may result in lower slopes because  $^{18}\text{O}$  and  $^2\text{H}$  are not evaporated at the same rate depending on the environmental conditions. Their different atomic masses involve different molecular diffusivities when equilibrium is not reached (see 4.2.2). Using the model proposed by Craig and Gordon (1965) (Eq. 4.6) for estimating the isotopic content of the evaporation flux and the evaporation model described in section 4.3.4, an estimation of the evaporation over the entire experiment period is provided here. The evaporation induces an enrichment of the residual soil water, which is then flushed down by subsequent rain inputs and consequently imparts its evaporative isotopic signature onto the discharge water sampled.

Evaporation over the 5-months experiment totals 54 liters when oxygen isotope data are used, and 61 liters with hydrogen data. This represents between 3 to 3.4% of the total ET flux (1798 liters) and 2 to 2.2% of the total input flux (2766 liters). The small evaporation fraction difference provided by oxygen- and hydrogen- data suggests that their respective model and estimated parameters ( $\delta_A$ ,  $\alpha$  and  $\epsilon_k$ ) are appropriate and that evaporation fractionation is able to accurately explain the observed drift in both isotope species of the discharge.

A sensibility analysis was performed to identify whether evaporation proves particularly responsive to specific parameters. A Monte-Carlo method was adopted and 10000 sets of parameters were generated, selected randomly among the parameter distributions derived from measurements or available data (Table 4.4). The results are presented in Figures 4.3 and 4.4 for oxygen and hydrogen isotopes respectively, where each gray point corresponds to a re-

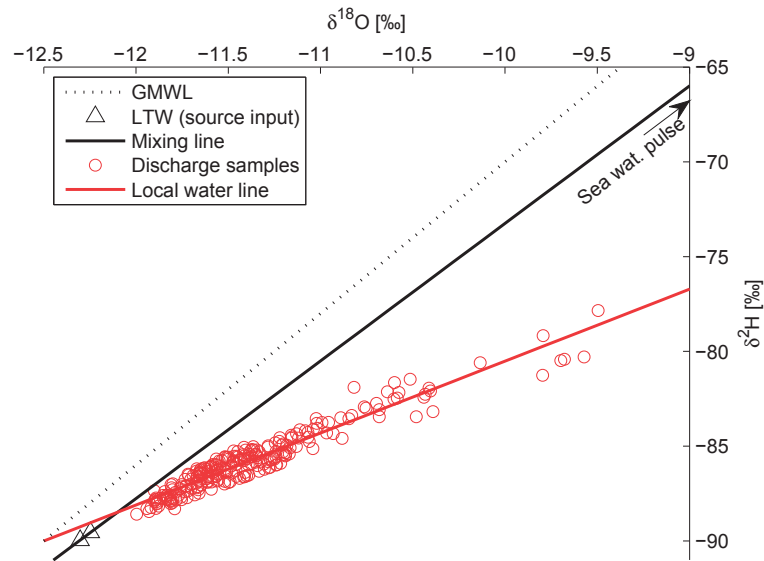


Figure 4.2:  $\delta^2\text{H}/\delta^{18}\text{O}$  relationship of the discharge samples (local water line - LWL) and mixing line representing the theoretical isotopic composition of the mixture between source water (LTW) and pulse water (which falls out of the graph, as the composition is close to 0 for hydrogen and oxygen). The global meteoric water line (GMWL) is plotted here for reference.

alization of one set of parameters, the red line shows the sensibility of the model when all other other parameters are fixed according to Table 4.3. The mean evaporation of all realizations with oxygen data is 3.76%, close to the deterministic result reported above. Environmental conditions (temperature and relative humidity) are not very sensitive parameters within the range of their measurements (the vertical dashed lines are the minimum and maximum values recorded). In contrast, the isotopic content of input water affects more the estimation of total evaporation as the more pronounced slope of the single contribution of this parameter shows. The atmospheric isotopic composition, estimated from literature data, becomes particularly sensitive when the atmosphere is depleted in heavy isotopes compared to the input water, therefore fostering kinetic fractionation. We observe that evaporation roughly stays below 10% with the discharge and transpiration isotope distributions considered. Both distributions are the same, i.e. a Gaussian distribution with mean and standard deviation values equal to the discharge samples' first and second moments. This implies that the contribution of the imperfect mixing between source and pulse water (also increasing the heavy isotope fraction in regards to source water only) is imbedded in the description of such parameters. Despite the broad parameter distributions considered in this analysis, we observe that evaporation is mostly restricted below 10%. Mean temperature and relative humidity over the entire period is not likely to be limiting, as evaporation is relatively insensitive to such parameters. It is to be noted that oxygen data provide a much more consistent estimation of evaporation than hydrogen ( $\sigma_E(\delta^{18}\text{O}) = 0.33$  and  $\sigma_E(\delta^2\text{H}) = 23.18$ ), because evaporation tends to draw the samples' isotopic content towards lower  $\delta^2\text{H}/\delta^{18}\text{O}$  slope than the mixing line of slope 8 (see

## Chapter 4. Water stable isotopes: a transport experiment

Table 4.4: Stochastic distributions parameters used for the Monte-Carlo sensitivity analysis.

Distrib.	Parameter	Mean value	Std. error	Unit
Normal	Temp	12	5	[°C]
	$h$	76	15	[%]
	$\delta_I(^2\text{H})$	-89.07	0.48	[‰]
	$\delta_I(^{18}\text{O})$	-12.18	0.07	[‰]
	$\delta_Q(^2\text{H})$	-85.76	1.76	[‰]
	$\delta_Q(^{18}\text{O})$	-11.38	0.45	[‰]
	$\delta_T(^2\text{H})$	-85.76	1.76	[‰]
	$\delta_T(^{18}\text{O})$	-11.38	0.45	[‰]
Distrib.	Parameter	Min	Max	Unit
Uniform	$\delta_A(^2\text{H})$	-193	-100	[‰]
	$\delta_A(^{18}\text{O})$	-25	-14	[‰]

Figure 4.2), thus favoring  $\delta^{18}\text{O}$  to differentiate evaporation effect from mixing.

### 4.4.3 Pulse contribution in the discharge by accounting for evaporation enrichment

Evaporation is relatively modest compared to discharge and transpiration fluxes, it has however a significant effect on the isotopic content of the residual soil water eventually flushed down and sampled as discharge water. Figure 4.2 shows that the observed isotopic composition of the discharge is skewed compared to the mixing line along which the samples would fall if no fractionation had occurred during the time a water parcel spends in the system. Assuming that oxygen- and hydrogen- isotopes mix similarly in the system, such that the sample volume contains an isotopic content representative of the mixing both in terms of  $\delta^{18}\text{O}$  and  $\delta^2\text{H}$ , the position of each sample can be graphically described starting from the isotopic composition of source water (triangles in Figure 4.2) plus the combination of mixing with a fraction of pulse water (i.e. displacement along the mixing line) and an evaporation effect (responsible for the samples drifting away from the mixing line). Knowing how evaporation affects the oxygen and hydrogen isotopic contents in respect to each other would allow us to backtrack the isotopic evolution of the samples, and therefore to project the samples' composition on the mixing line. The position on the mixing line thus provides a direct equivalent to the relative concentration, that is the fraction of pulse water relative to source water. Using the Craig and Gordon (1965) model (see Eq. 4.6), the evolution of the isotopic composition of a water volume of initial isotopic content equal to the source water being progressively evaporated under the same conditions has been calculated as presented in section 4.4.2. The relative enrichment of  $\delta^2\text{H}$  in respect to  $\delta^{18}\text{O}$  is linear, with a slope of 3.65 (calculated with the relevant parameters presentable in Table 4.3). Temperature and humidity variability within the observed range does not affect this relationship perceptibly. Note that this evaporation line is, however, highly



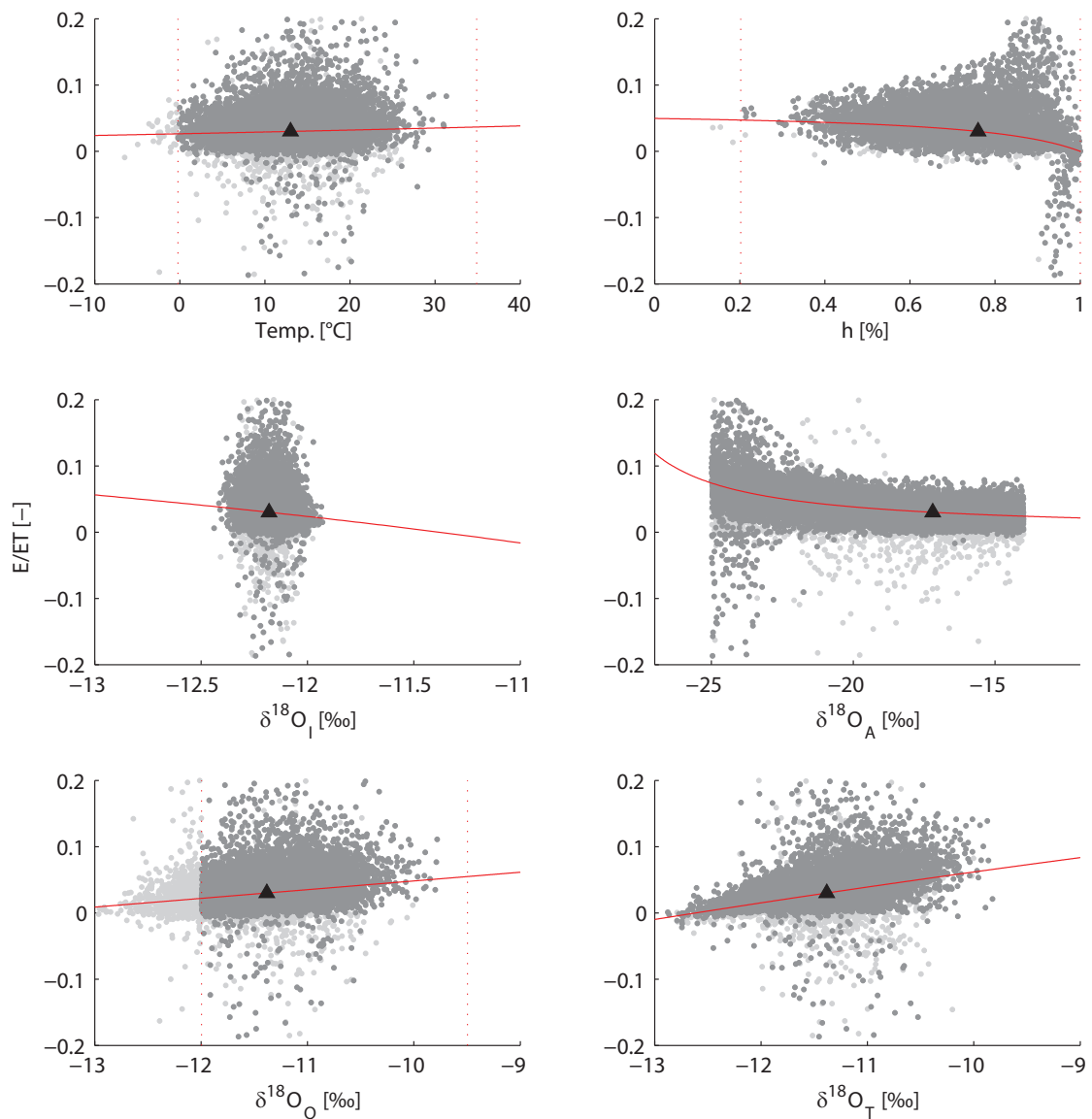


Figure 4.3: Monte-Carlo sensitivity analysis for the evaporation fraction  $E/ET$  based on the oxygen data. The grey dots represent a realization of one parameter set. Light grey is used when at least one parameter in the set falls outside of the observed range for this parameter (measured ranges are constrained within the vertical dashed red lines). The solid red line show the sensitivity of evaporation to a single parameter. A similar analysis is available based on deuterium data in Figure 4.4.

sensitive to the isotopic composition of the atmosphere, which controls the extent of the kinetic fractionation effect. The mean and standard deviation of this evaporation line's slope are respectively 3.27 and 1.44 when uniform distributions of  $\delta_A(^2\text{H})$  and  $\delta_A(^{18}\text{O})$  as in Table 4.4 are considered. The corrected isotopic content for each sample was obtained by calculating the intersection coordinates between the mixing line and the local evaporation line with a supposed slope of 3.65 which intercepts the measured composition. The fraction of pulse

## Chapter 4. Water stable isotopes: a transport experiment

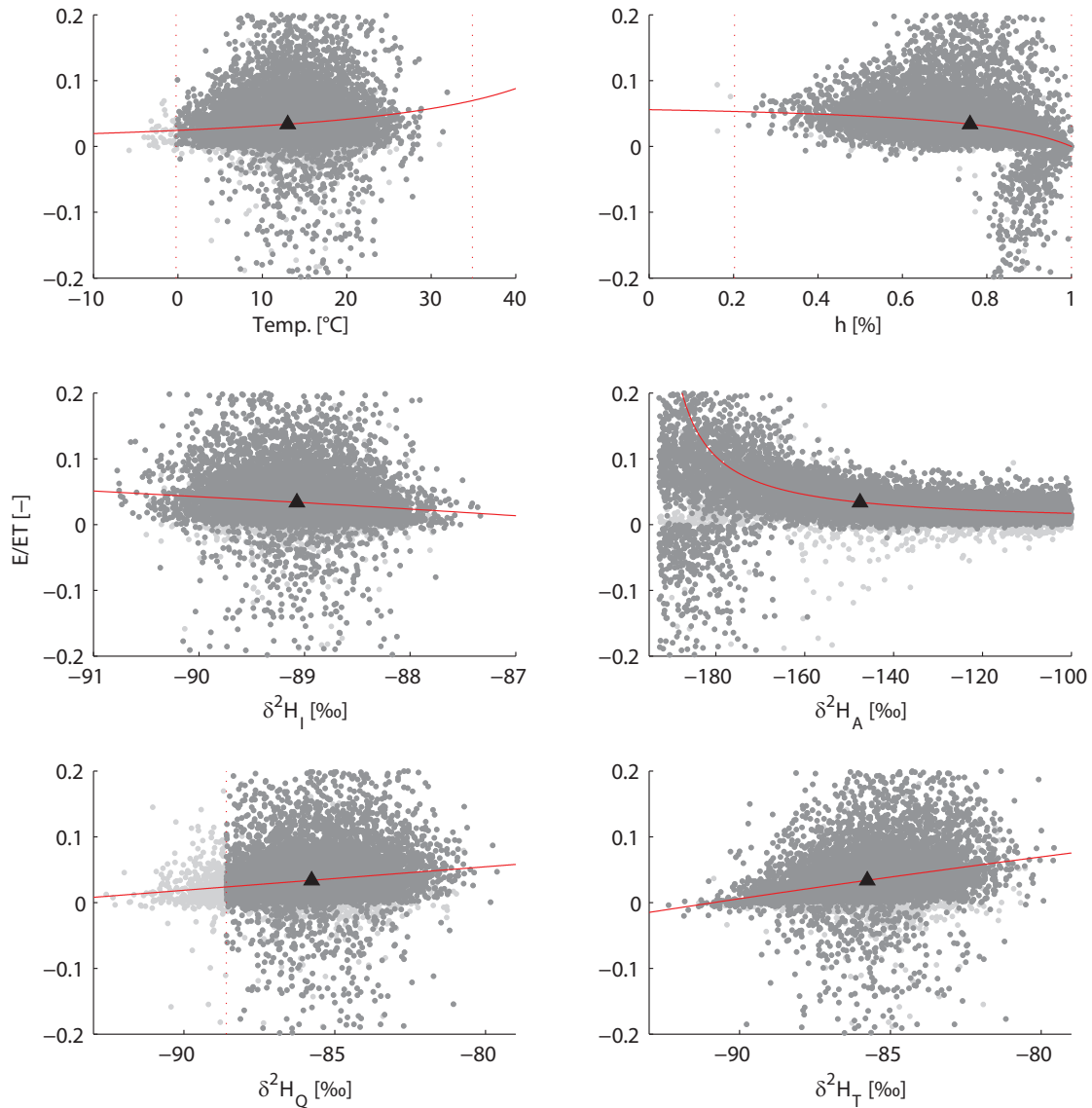


Figure 4.4: Monte-Carlo sensitivity analysis for the evaporation fraction  $E/ET$  based on the deuterium data. The grey dots represent a realization of one parameter set. Light grey is used when at least one parameter in the set falls outside of the observed range for this parameter (measured ranges are constrained within the vertical dashed red lines). The solid red line show the sensitivity of evaporation to a single parameter. A similar analysis can be seen for oxygen data in Figure 4.3

water in the discharge sample is further calculated by normalizing the distance separating the projected corrected values with the source water coordinates over the distance between the pulse and source water coordinates.

The result is plotted in Figure 4.5a, together with the relative concentration of 2,5-DFBA and 2,6-DFBA. Note that only one line is drawn for both isotopes, as the method described above

is solely based on the ratio of enrichment between the oxygen and hydrogen isotopes and thus the corrected evaporation-corrected isotopic content provides the same contribution for both species. Compared to Figure 4.1 which contrasts the raw signals, the high-frequency fluctuations of the isotopes are more dampened, and the relative contribution of the pulse in discharge water is of a similar intensity for the DFBA and the isotopes. The correction of the isotopic content is a sensitive method, particularly because the slope of the mixing line and evaporation line are not radically different (7.25 and 3.65 respectively, i.e. 1.43 and 1.30 in degrees) and the observed relative isotopic composition of  $\delta^{18}\text{O}$  and  $\delta^2\text{H}$  naturally varies to a certain degree. Hence, all small variations are necessarily reported to the corrected isotopic composition, which is restricted to only a few percents of the total range between the source and pulse water. This probably explains the first isotope peaks observed before the DFBA start to breakthrough. However, a lot of common features are identified between the DFBA and isotopes signals, like the flat peaks observed around May 15 or the following large peaks on May 22. It is interesting to note that the May 15 peaks occur after the discharge peaks, showing that pulse water only gets mobilized for discharge during the recession, whereas on May 22, an increased fraction of pulse water is observed simultaneously with the discharge peak. The effect picturing the mobilization of "new" water for discharge has an opposite effect later in the experiment, where the discharge peaks are immediately followed by slight signal decrease due to dilution with new water issued from the last input of source water.

The cumulative pulse recovery (Figure 4.5b) shows the fraction of the pulse that has been recovered since injection. Issues regarding the highest recovery of 2,6-DFBA than 2,5-DFBA are discussed in detail in Chapter 2, but microbial degradation and/or plant uptake in the early phase of the breakthrough affecting at different extents the two tracers are suggested. As water stable isotopes are conservative (except for evaporation fractionation already accounted), the lower recovery of isotopes compared to 2,6-DFBA during the early phase of the experiment is difficult to explain. Besides the high sensitivity of the method discussed above that may lead to a skewed estimation of the pulse fraction, water isotopes in soil water may mix more thoroughly than the DFBA tracers. This could translate into different mobilities within the soil column, and a propensity for isotopes to mix and penetrate more efficiently into the smaller pores than the DFBA, reducing their availability to be flushed down by subsequent water inputs. However, the isotope recovery increases progressively and eventually exceeds this of 2,6-DFBA in the middle of the experiment. The estimated final recovery of the isotopes (87%) is higher than the recovery of 2,5-DFBA and 2,6-DFBA (respectively 46% and 21%) as the latter are likely to undergo degradation and/or removal processes. Note also the acquisition and sampling system failure that has occurred between May 27 and June 13 which may have led to the underestimation of the isotopes and DFBA output fluxes jointly with the recovered pulse fraction.

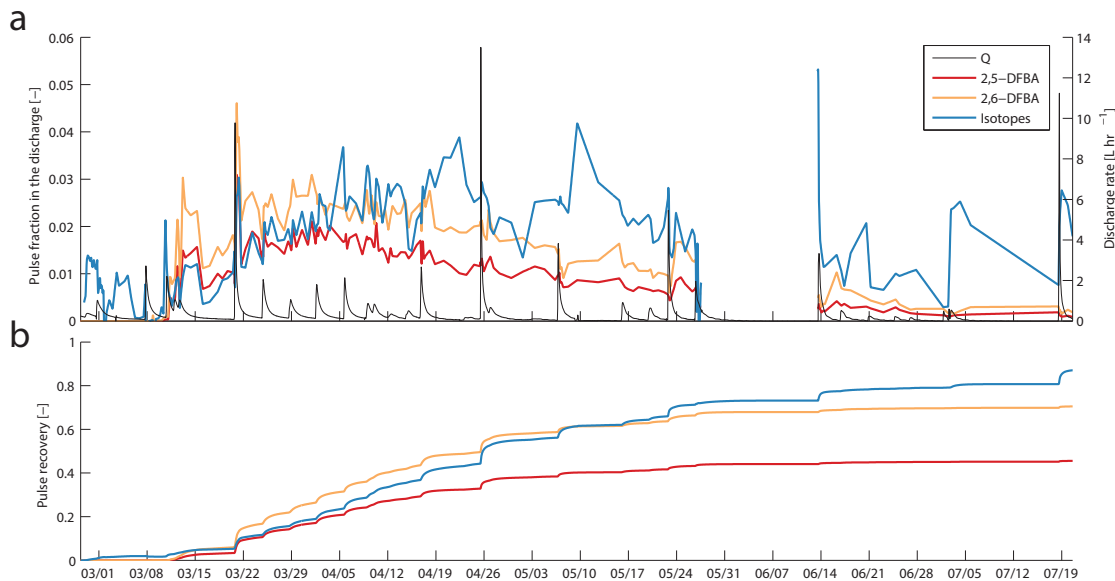


Figure 4.5: (a) Fraction of the pulse water and (b) cumulative pulse recovery in discharge based on DFBA and isotopes data. Note that the y-axis unit in (a) is equivalent to the relative concentration for the DFBA tracers, as the concentration in tap water is null.

## 4.5 Discussion

The observed isotopic signature of the output signal aimed at reflecting the transport of a tagged water parcel proves considerably biased by heavy isotope enrichment due to a limited evaporation compared to the total ET flux. This result somehow challenges the usual conservative behavior that is assumed to qualify water isotopes especially for studies involving the isotopic content of precipitation water as endmember, because evaporation fractionation may have a significant effect on the isotopic content of the residual water. This could be particularly critical when only oxygen- or hydrogen- isotopes are measured, as evaporation cannot be distinguished from the mixing of different endmembers. In this case, it is not possible to identify the signatures of each individual process by analyzing the  $\delta^2\text{H}$ - $\delta^{18}\text{O}$  relationships as it has been done here. Evaporation fractionation issues can, however, be limited by different factors as soil texture (a coarser texture allows rapid infiltration and reduces the amount of water available for evaporation at shallow depth) and soil cover. Under such specific conditions, *Stumpp et al.* (2009a,b) found that evaporation had no effect on the isotopic content of the discharge of a similar lysimeter setup. Nevertheless, the quantification of both oxygen- and hydrogen- isotopes - which has become more convenient with recent analytical methods - is strongly recommended before dismissing evaporation as a noteworthy process.

Note that in a small-scale experiment like the one at hand and when evaporation may significantly significantly enriched the residual water, the ability to define the isotopic content of the tracked pulse is a valuable asset. In fact, one would try to maximize the difference between the isotopic composition of the source water and that of the pulse, in order to increase the

sensitivity of the mixing's estimation. In addition, a careful selection of the ratio between the hydrogen- and oxygen- heavy isotopes of the marked pulse would in addition allow the distinction between the respective mixing and evaporative isotopic signatures.

The assumption that vegetation does not differentiate heavy and light isotopes upon root water uptake is a justified assumption still holding in the relevant literature (e.g. *Treydte et al.*, 2014) since the work of *Dawson and Ehleringer* (1991, 1993). As the root network of the willow is believed to expand along the entire depth of the lysimeter, it was assumed that the isotopic composition of the transpiration flux (only seen as the water uptake at the root level, as isotopic fractionation may occur later in the plants) is the same as the isotopic composition of the discharge (Eq. 4.12). This simplification arguably holds when considering the mean isotopic content of cumulative fluxes over long timescales (e.g. of the order of the entire experiment), but may not be proven at shorter timescales, because evaporation variably affects the isotopic content of the shallow residual water, depending on meteorological conditions. This residual water of varying isotopic composition later mixes within the hydrological volume, resulting in a heterogenous isotopic content of the storage. Now, as it was highlighted in Chapter 3, discharge and evapotranspiration (therefore also transpiration) do not select identically the stored water, which means that the isotopic composition of the discharge and of the transpiration flux may not be the same at a given time. This could also explain the differences remaining between the FBAs tracer responses and this of the corrected isotopic response (Figure 4.5). Regarding such issues, lysimeter studies using water stable isotopes can be particularly useful, as isotopes are easily sampled in soil and discharge water, but are also among the few tracers that can be measured in plants and in the transpiration flux using suitable methods (*Zhang et al.*, 1999; *Koeniger et al.*, 2010; *Treydte et al.*, 2014).

## 4.6 Conclusions

Understanding the internal mechanisms governing the hydrologic response of a system often involves the use of tracers, especially at catchment scale where most of the processes are concealed below the ground surface and are hardly monitored. In an ideal world, only the availability of unlimited amounts of perfect tracers and their continuous measurements in all exit fluxes would allow a direct estimation of the hydrologic travel time distributions. However, every tracer is specifically affected by different processes (e.g. sorption/desorption effects, microbial degradation, plant uptake, evaporation, etc.), which perturb its transport (and recovery) with respect to that of water. In addition, artificial applications of tracer is usually not conceivable at catchment-scales, and the natural fluctuation of a compound (water isotopic composition, chloride, etc.) is preferred as continuous input signal rather than the application of artificial pulses. The interpretation of a tracer response to describe the hydrologic transport of a system is therefore only possible via thorough understanding of the effects of such processes, in order to remove all artifacts affecting the tracer.

To this aim, lysimeters present major advantages because they allow control on the system

#### **Chapter 4. Water stable isotopes: a transport experiment**

---

while reproducing similar processes as in a real catchment. The different predispositions to specific processes between hydrological tracers can even be beneficial — when well understood — in order to identify and quantify these processes. In this sense, water stable isotopes have allowed here to quantify evaporation on the system, while they have not provided much information about the hydrologic response in regard to the two organic tracers jointly introduced.

The need for suitable water tracers will increase in the future, in particular given the growing recognition of the non-stationarity of travel time distributions which discredits the direct derivation of travel time from the measurement of a continuous input and output tracer signal. Valuable information can be obtained from multiple tracers regarding (1) time-variant input and output fluxes (namely evaporation and transpiration) and (2) the moisture-dependant internal mixing processes controlling the hydrologic response. However, this is only possible when the respective reactive behavior of each tracer is well understood, in order to reconcile the signals of tracers differently affected. Notwithstanding this fact, the amount of tracers available — particularly those found naturally in the environment — will remain limited, and insufficient to provide a comprehensive picture of a non-stationary hydrologic response; in this sense, experimentally-constrained models are the only tool that will provide the ability to fully describe the hydrologic behavior of a transient system.

## 5 Catchment-scale experimental site and pesticides dynamics screening

This chapter presents the work undertaken in the Chamberonne catchment close to Lausanne (Switzerland), which aims at initiating a long-term hydrochemical survey of a characteristic small-size agricultural catchment of the Swiss Plateau. An existing network of hydrologic stations equipped for water sampling was extended and upgraded in order to generate continuous high-resolution hydrologic datasets. A pesticides screening campaign was undertaken in Spring 2013, during which the storm discharge generated by three heavy precipitation events were simultaneously sampled at all monitoring stations. Among the 19 substances screened (mostly agricultural herbicides, fungicides and insecticides), 14 were detected in the samples. The measured concentrations are usually in the order of the  $ng L^{-1}$ , but some substances show large spatial and temporal concentration differences. Applications of plant protection products during the campaign were indicated by important (up to 100-fold) concentrations increase of some substances between two sampled events. All substances measured present concentration dynamics clearly related to discharge dynamics. However, the timing of the peak concentration with respect to discharge peak varies among the compounds (atrazin concentration is even inversely correlated to discharge) displaying different mobilization times among the substances. Even if restricted to three 1-day time-windows, these results suggest the complexity of the underlying transport and reactive processes controlling solute transport at catchment scales.

### 5.1 Introduction

The Chamberonne catchment is situated in the vicinity of Lausanne city. This catchment is well representative of those encountered in the Swiss Plateau with a predominant agricultural component upstream dominated by cropland and forests and more urbanized areas downstream characterized by a large percentage of sealed surfaces. The total area approaches 40 km<sup>2</sup> of which about 37% of the surface is impervious. A map of the watershed with a simplified land cover repartition can be seen in Figure 5.1. Two major tributaries – Sorge draining the west part of the catchment and Mèbre draining the east part – are both flowing southwards, and converge to form the Chamberonne at about 1 km of the outlet in Lemane Lake (374 m.s.l.). Each tributary carries about half of the overall discharge measured at the outlet. About 6.6 km above the convergence of the two streams, Sorge further divides into tributaries named Chamberonne (West) and Petite Chamberonne (East) near Villars-Ste-Croix. The highest altitude of the catchment is reached close to Cugy and slightly exceeds 800 m.s.l. The average slope is 4%. The watershed is mainly covered by moraines (generally ground moraines) on top of a molassic substrate (*Bersier, 1952; Weidmann, 1988*). During the last century, many communes in Switzerland have undergone land consolidation, a process that aims to restructure the repartition of land parcels in the cadaster by merging, exchanging or reorganizing in order to avoid dispersion of land under the same properties and therefore reduce labor and costs. Land consolidation often comes with other incentives like streams regulation, renovation and straightening of access roads and drainage of wetlands (to gain arable surface) or agricultural fields (to improve water infiltration and avoid ponding). In the Chamberonne catchment, where almost all communes have been subject to land consolidation, it can be considered that virtually every crop field in this region is tile-drained. This is less marked for pastures, which are not inevitably drained. The drainage system can be however different from place to place, as land consolidation have been undertaken at different time, and no drainage cadaster is available. Tile drains usually discharge without buffer or treatment in a nearby stream or in the wastewater drainage system. The mean annual discharge of the Chamberonne network at the outlet is 1010 L/s (2000-2008), and the mean baseflow ( $Q_{347}$ ) from 1993 to 2008 is 226 Ls<sup>-1</sup> (DEGE, Canton de Vaud).

### 5.2 Agricultural practices

Since the early 1990s, the sale of plant protection products has decreased by more than 30% in Switzerland according to Science Industries Switzerland (Business Association Chemistry Pharma Biotech), and tends to stabilize recently. The increased specificity of the active ingredients and the resulting better plant protection efficiency of the new plant protection products developed have allowed a sizable diminution of the applied loads. However, plant protection products remain extensively used in the country and are found at increasing concentration in surface waters (*Klein et al., 2007*). Apart from sales data, no statistics related to the actual use of plant protection products exist in Switzerland. Farmers are required to maintain a record of applications, in particular for inspection instances, but these are not indexed nor made



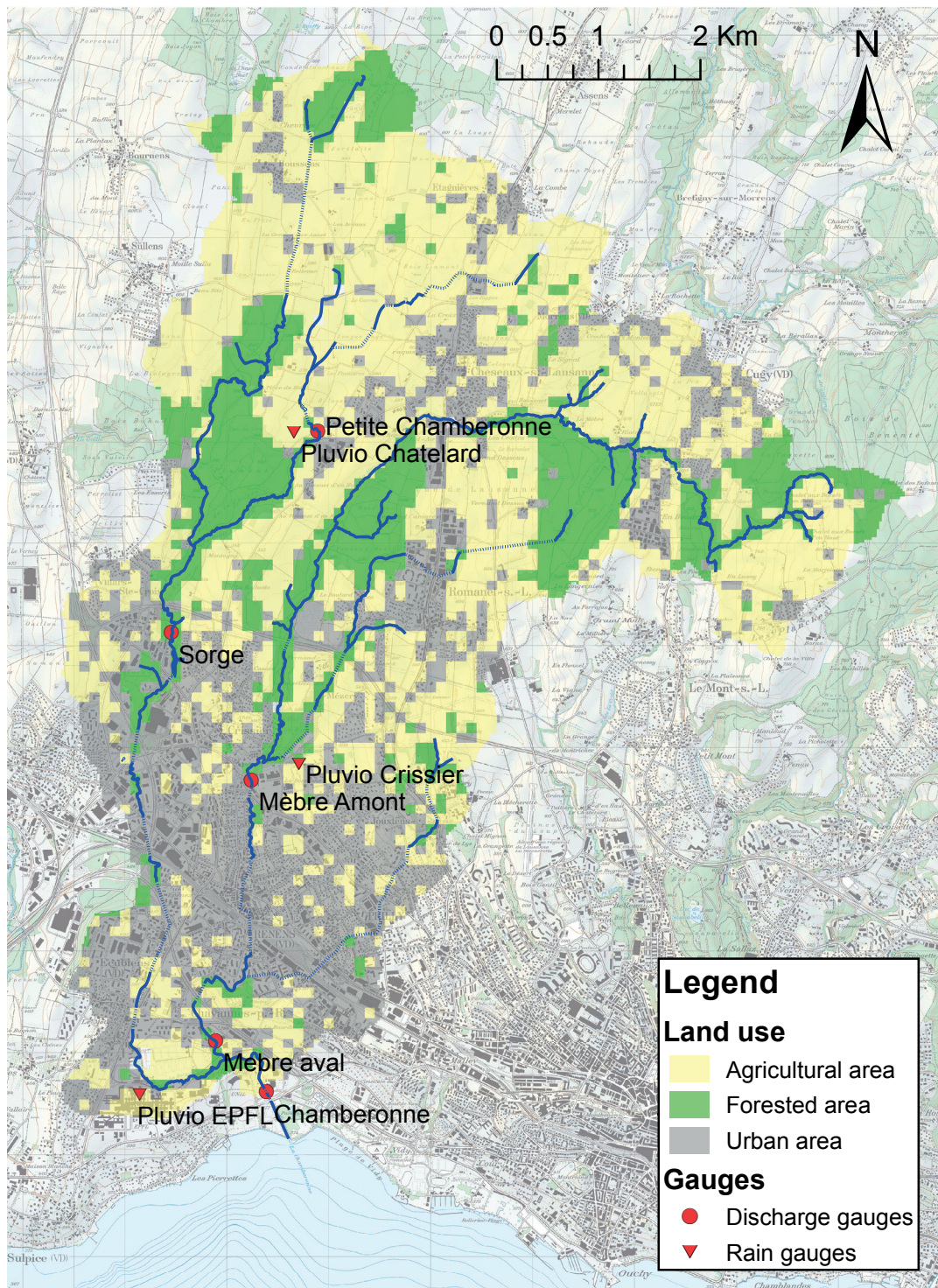


Figure 5.1: Topographic map of the Chamberonne catchment with simplified land cover and monitoring equipment. Background map from Swisstopo<sup>©</sup>.

## Chapter 5. Catchment-scale experimental site and pesticides dynamics screening

---

available without the consent of the farmer. In order to follow the evolution of the use of plant protection products, the AGRIDEA (Swiss association for developing agriculture and rural areas) has conducted a survey of the agricultural practices in terms of plant treatments for a pilot network of swiss farmers (*Fabre et al.*, 2010). The resulting statistics were further used by the CIPEL (Swiss-french commission for the water protection of Lake Léman) in order to notably assess pesticides use on a local basis depending on the agricultural land use statistics (*Klein et al.*, 2007). These two reports are the only sources available from which the following agricultural practices and pesticides use for the Chamberonne catchment are taken, together with data collected during a survey conducted in 2012 on the catchment. A full description is given in *Stalder* (2012).

Based on a representative commune of the Chamberonne catchment in terms of land use in the agricultural area, croplands occupies 90% of the surface, 10% is covered by meadows and pastures and less than 1% is used for arboriculture. The treatment practices being largely different depending on these categories, cropland are responsible for 93% of the pesticides mass applied, arboriculture for 6.5% and meadows and pasture less than 0.5%. The presence of a tree nursery in the catchment can thus significantly affect the quantities and the types of products that may be found in receiving waters, as protection treatments are more intense and diverse than for croplands. The distribution of cropland types in 2012 and 2013 revealed by this survey shows a strong similarity with the data from AGRIDEA at the country scale, mainly composed by autumn wheat, colza, corn, sugar beet and autumn barley (sorted by decreasing fraction of surface). Wheat and barley are either treated or cultivated *in extenso*, the latter preventing the use of growth regulators, insecticides and chemical stimulator of natural defence. The fraction of crops cultivated *in extenso* increases due to policy incentives, but remain less than 45% overall.

Multiple pesticides are usually applied for a specific crop, they may be combined as active ingredients in a commercial product, but there are also sometimes applied separately. Therefore, the amount of applications (of a specific active ingredient at a given date) is generally higher than the amount of interventions, defined as a treatment applied at a given date. Table 5.1 summarizes the applications and interventions statistics (1992-2004) for the different crops observed in the Chamberonne catchment (*Fabre et al.*, 2010). One observes that in general, two active substances are applied per intervention. Two periods of intervention can be emphasized: spring treatment, occurring during the growth period between January 15 and September 15 (mainly around mid-April), and autumn treatment which is applied during a crop rotation or before a new seeding, between July 15 and November 15.

The substances potentially used are numerous and are subject to change every year, notably depending of the market retail price of the commercial products. The substances mostly used between 1992 and 2004 for the crops found in the Chamberonne catchment are enumerated below (*Fabre et al.*, 2010):

Table 5.1: Mean number of annual applications and interventions per parcel and amount of plant protection products (respectively herbicides, fungicides and insecticides) used per hectare. Adapted from (Fabre *et al.*, 2010)

	Interv. <sup>a</sup>	Appl. <sup>a</sup>	Herb.	Fung.	Insect.
Autumn wheat (treated)	3.45	6.66	0.74	0.29	<0.01
Autumn wheat ( <i>in extenso</i> )	1.39	3.41	0.81	-	-
Autumn barley (treated)	2.96	5.77	1.10	0.25	<0.01
Autumn barley ( <i>in extenso</i> )	1.46	3.29	1.03	-	-
Corn	1.23	2.58	1.03	-	0.01
Colza	2.89	3.94	0.92	0.06	0.02
Sugar beet	4.66	10.63	2.32	0.13	0.05

<sup>a</sup> in  $kg\ ha^{-1}$

**Autumn wheat (treated):** Isoproturon (H), Diflufenican (H), Ioxynil (H), MCP-P (H), Chlorothalonil (F), Epoxiconazole (F), Teflubenzuron (I);

**Autumn wheat (*in extenso*):** Isoproturon (H), Ioxynil (H), Diflufenican (H);

**Autumn barley (treated):** Isoproturon (H), Diflufenican (H), Glyphosate (H), Prochloraz (F), Epoxiconazole (F), Cyproconazole (F), Ethephone (R), Trinexapac-ethyl (R);

**Autumn barley (*in extenso*):** Isoproturon (H), Diflufenican (H), 2,4-D (H), Flufenacete (H);

**Corn:** Atrazine (H; forbidden since 2011), Metholachlor (H), Sulcotrione (H);

**Colza:** Tebutam (H), Napropamide (H), Clomazone (H), Carbendazime (F), Bifenthrine (I), Cypermethrin (I), Lambda-Cyhalothrine (I);

**Sugar beet:** Phenmedipham (H), Metamitron (H), Metholachlor (H).

H: Herbicides F: Fungicides I: Insecticides R: Regulators

This enumeration is only to give an overview of the wide range of substances potentially used for plant protection, and is subject to annual changes in terms of substances, amount applied, and dates of applications. Pesticides measurements should thus not be focused on a single substance, but the analytical method should include as many compounds as possible, especially if the local agricultural practices are not known in details and if pesticides are sampled without a prior knowledge of antecedent applications.

### 5.3 Catchment gauging

#### 5.3.1 Water-level gages

In order to calibrate the hydrologic model, long-term stream discharge data are required. Multiple discharge gages have been updated or installed in the Chamberonne network and are recording the water level at different sites in the catchment. The positions of the gages are indicated on Figure 5.1. The existing water level gages at the sites *Mèbre aval* and *Sorge* have been replaced with 3-parameters (water level, temperature, electrical conductivity) HyMADD gages (MADD Technologies, Switzerland) in the winter 2011. The monitoring station *Mèbre amont* has been moved slightly uphill of the former location; the former site was situated in a tunnel with an important slope and a stone-paved concrete floor. The water velocity is important in the tunnel even at low stage, and the stones of the floor are creating a lot of turbulences, making a precise measurement of the water level difficult at low-flow stages. In addition, the water depth was often too low to allow the measurement of electrical conductivity. A sufficient water depth can be ensured even for dry-weather flow at the new site. A new station *Petite Chamberonne* has been installed in the upper part of the Sorge sub-catchment specifically for the monitoring of pesticides, as the drainage area is essentially composed of agricultural areas. The gage is installed at the outlet of a short gallery (Figure 5.2) where a sufficient water depth and limited high-frequency level variations can be ensured. A small concrete platform has been constructed to receive a sampler case.

An extended monitoring station for the Chamberonne outlet has been installed in summer 2010 and is from that time monitored by the Ecological Engineering Laboratory (ECOL) in EPFL. The station is equipped with independent conductivity, turbidity, temperature, dissolved-oxygen and water level gages. A small hut contains the logging equipment and a refrigerated ISCO sampler (ISCO 4700, Teledyne Isco Inc., USA). The roof of the gallery at this site is equipped with the flow measurement system HYDROPIX (*Jeanbourquin et al.*, 2011; *Nguyen et al.*, 2009).

#### 5.3.2 Flow gauging and rating curves

In order to calculate the flow rate corresponding to a given water level, one has to determine the site rating curve  $Q = f(H)$ . For this purpose two different methods are used: chemical gaging and estimation of the velocity field at a river cross section. Both methods are punctual, and as the rating curves are non-linear and sometimes non-monotonous (they largely depend on the river cross-section), multiple measurements are required at various water stages. Chemical gaging involves the use of a sodium salt solution injected instantaneously and measured downstream with an electrical conductivity probe. Knowing the exact mass injected, the observation of the concentration measured in the plume allows the estimation of the flow rate



Figure 5.2: Installation of the gaging station *Petite Chamberonne*.

by the mean of mass conservation principle:

$$M = Q \int_{t_i}^{t \gg t_i} C_{mes} dt, \quad (5.1)$$

with  $M$  the mass injected,  $Q$  the flow rate,  $t_i$  the injection time and  $C_{mes}$  the measured concentration in the plume. Note in Eq. 5.1 that this method assumes a constant flow rate between  $t_i$  and until the plume has completely passed the control section ( $t \gg t_i$ ). Chemical gaging can only be used when the former statement can be assumed, and if no significant water input is present between the injection site and measurement location. The distance covered by the plume should be sufficiently long to assume a cross-sectional complete mixing (more efficient in turbulent flow). The estimation of velocity field involves the use of an impeller or electromagnetic current meter. The flow velocity is measured along the cross section at different depths and abacuses are used to derive a mean velocity. Flow velocity gaging is time consuming and the flow rate has also to remain constant during the measurement transect, which can be of concern at high flow stage since the discharge can vary rapidly during storm conditions. When possible, chemical gaging is preferred for its simplicity and rapidity. Chemical and flow velocity gaging have been conducted on all ECHO stations from 2011 onwards.

A continuous stage-discharge rating function for each station is then established based on the gaging measurements. Two widely used methods are fitted on the data:

### Power law

$$Q_{pow} = a \cdot H^b; \quad (5.2)$$

### Parabolic law

$$Q_{par} = c_1 H^2 + c_2 H + c_3. \quad (5.3)$$

Both functions were fitted on the available gaging measurements (both chemical and flow velocity if specified) for each station using the least square method.

### 5.3.3 Rain gauges

Antecedent and current rainfall data are collected by the ECHO rain gage located on the EPFL campus and by the cantonal rain gage (DGE, Canton de Vaud) located in Crissier (see Figure 5.1). A new rain gage has been installed in the upstream part of the catchment in 2012, close to the monitoring station *Petite Chamberonne*. This rain gage is considered to be representative of the rainfall patterns observed in the upper agricultural part of the catchment.

## 5.4 Pesticide sampling campaigns

During spring 2013, automatic samplers (Teledyne ISCO 6712, USA) equipped with 24-bottles (Polyethylene, 1 L) rack were deployed at all ECHO gaging stations. The goal of the campaign was to identify some of the substances that can be found in the receiving surface water (screening), and also to study the concentration dynamics of those substances during a rain event (i.e. until peak flow and during the recession). Hence, a sampling procedure was manually activated on the four sampling sites after strong rainfall, and lasted for 24-36 hours after activation. No prior information about plant protection products applications were available. Sampling procedure details and the dates of the event sampled are shown in Table 5.2.

The sampling bottles were collected on the same day, stored at 4 °C before filtration at 0.45  $\mu m$  with mixed cellulose ester filters (Whatman, GE Healthcare, UK) and then frozen at -20 °C. An analytical method developed by the ECOL laboratory at EPFL was used, allowing to detect and quantify 19 substances (Table 5.3) using an Ultra Performance Liquid Chromatograph (UPLC) coupled to tandem quadrupole mass spectrometers (MS-MS) (Acquity TQD, Waters®) with online solid phase extraction (SPE).

## 5.4. Pesticide sampling campaigns

Table 5.2: Details of the sampling procedure at each site and for each rain event. PteC, SOR, MAM and MAV refers to the sampling stations *Petite Chamberonne*, *Sorge*, *Mèbre amont* and *Mèbre aval* respectively.

	Event 1 11-12 April				Event 2 27-28 April			Event 3 27-28 May
	PteC	SOR	MAM	MAV	PteC	MAM	MAV	PteC
Time / Flow pacing	T	T	T	T	T	T	F	T
N spl./bottle	4	4	4	4	6	6	4	6
Spl. volume (mL)	200	200	200	200	120	120	200	120
Spl. freq. (min/m <sup>3</sup> )	15	15	15	15	15	15	702 <sup>a</sup>	15
Start time	3PM	3PM	3PM	3PM	1PM	1PM	1PM	1PM

<sup>a</sup> Equivalent to 13–23 min depending on the discharge rate.

Table 5.3: List of the pesticides screened with the analytical method and their type. The EQS (Environmental Quality Standard) is defined as the limit concentration in waters in order to protect human health and the environment (INERIS, France). The limit of quantification (LOQ) of the analytical method is also given for each compound.

	Type <sup>a</sup>	EQS <sup>b</sup> ( $\mu\text{g L}^{-1}$ )	LOQ ( $\text{ng L}^{-1}$ )
Benzotriazole	O	246	50.0
Methylbenzotriazole	O <sup>d</sup>	200	10.0
Atrazin	H	0.6	1.0
Terbutryn	H	0.17	1.0
Isoproturon	H	0.3	1.0
Diuron	H	0.2	2.0
Irgarol	B	0.004	2.0
Mecoprop	H	4.4	1.5
Triclosan	O	0.05	200.0
Carbendazim	F	0.1	5.0
Chloridazon	H	0.1	1.0
Diazinon	I	0.003	1.0
Propiconazol	F	5.8	1.0
Pymetrozin	I	NA <sup>c</sup>	5.0
Tebufenozid	I	NA <sup>c</sup>	3.0
Metamitron	H	10	2.0
Chlortoluron	H	0.1	1.0
Terbuthylazine	H	0.06	1.0
Ethofumesate	H	32	50.0

<sup>a</sup> H: Herbicide F: Fongicide I: Insecticide B: Biocide (urban) O: Other <sup>d</sup>: Degradation product.

<sup>b</sup> Sources: Directive 2013/39/EU (European Union), Ecotox centre (EAWAG-EPFL, Switzerland), *Chèvre et al.* (2007, 2008).

<sup>c</sup> Not Available.

### 5.5 Results and discussion

#### 5.5.1 Rating curves

The stage-discharge point measurements using velocity field and chemical gaging methods are displayed in Figure 5.3. Usually both methods are in good agreement, except for the station *Sorge* where chemical gaging did not provide satisfactory results. Stage-discharge measurements with NaCl have thus been discarded, because the analysis of the salt breakthrough curves (see Eq. 5.1) has revealed some issues likely due to unidentified varying NaCl inputs upstream, which affect the discharge calculation (e.g. background NaCl concentration is not recaptured at the end of the breakthrough). Both the power law and parabolic law approximate well the stage-discharge relationship for all stations in the water levels range observed, with coefficients of determination above 0.9. For the calculation of discharge presented in the following section, the power law was preferred, because it usually performs slightly better (when not equivalent) to the parabolic law, and it has the advantage to be monotonously increasing, which is not the case for the parabolic law at low values. For the *Petite Chamberonne*, the gaging measurements cover well the range of observed stages (rarely above 0.5 m). At *Sorge*, *Mèbre amont* and *Mèbre aval*, water level frequently reach 0.8, 0.7 and 1.2 m respectively, thus exceeding the range covered by the gaging measurements. The rating curves for these stations have thus a sizable uncertainty for high water levels and may misestimate the discharge during storm events. Additional gaging measurements at high flow would be necessary to restrain this concern.

#### 5.5.2 Discharge and rainfall

Discharge rates are calculated from the water level measurements and the rating curves described above. A hyetograph and the simultaneous hydrographs for each station are shown in Figure 5.4 for April and May 2013, the period during which pesticide sampling was performed. Peak flow is observed simultaneously at all stations about 3 hours after the maximal rainfall rate has occurred, which dismisses significant delays caused by in-stream hydrologic routing. For a better lisibility of the overall discharge dynamics, the maximum discharge rates observed on the rainfall event of April 12 (sampled for pesticides) exceed the y-axis limit. Discharge reaches 0.8, 4.5, 7.5 and  $44 \text{ m}^3 \text{ s}^{-1}$  at *Petite Chamberonne*, *Sorge*, *Mèbre amont* and *Mèbre aval* respectively. Whereas these values are realistic for the three first stations (this storm event is among the five largest of 2013),  $44 \text{ m}^3 \text{ s}^{-1}$  seems irrational considering the setting of *Mèbre aval* station. This downstream station receives sizable discharge contributions from separated sewers and storm overflows of the dense urban area around during heavy rain, yet the cross section could hardly handle such a discharge. Stage-discharge measurements are thus particularly needed at this station in order to better define the rating curve at high flow rate.



## 5.5. Results and discussion

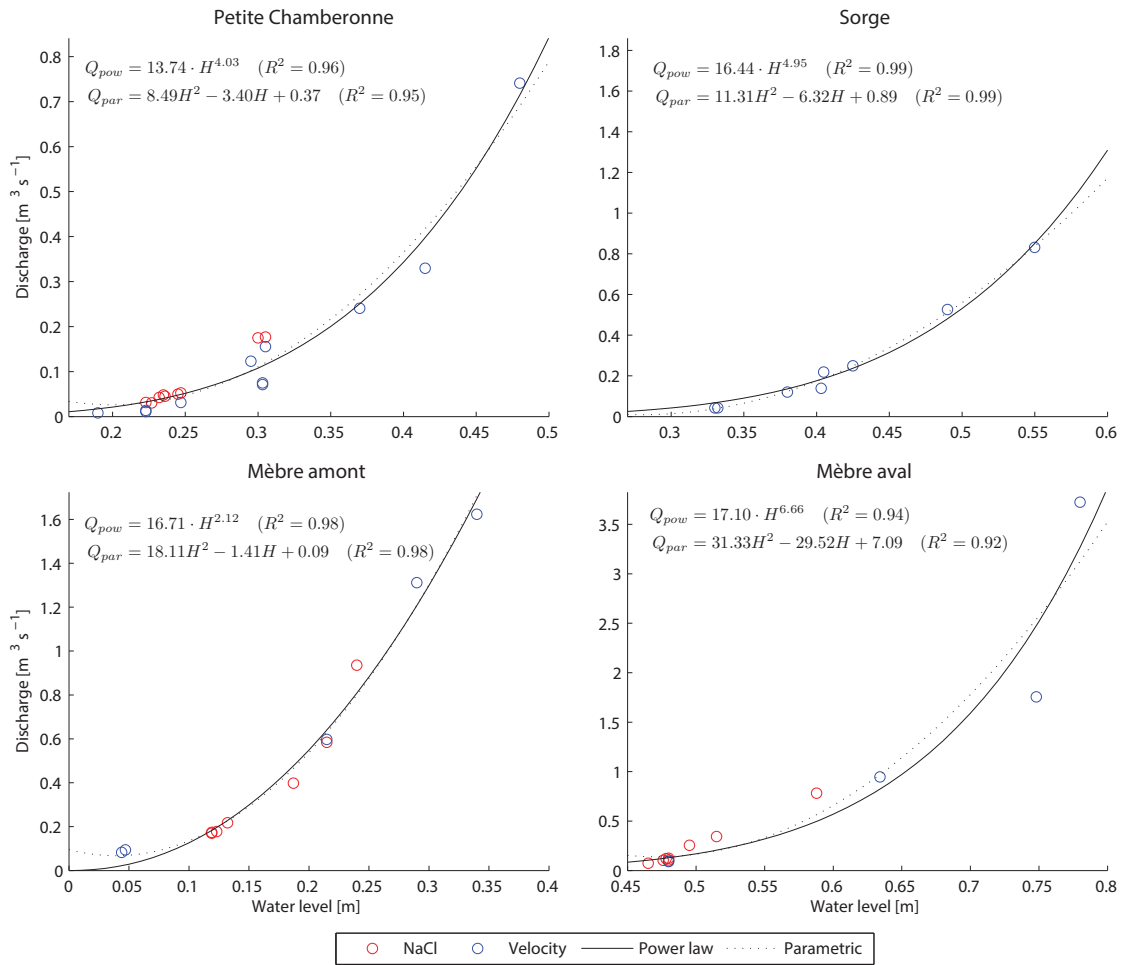


Figure 5.3: Rating curves for the ECHO gaging stations fitted with power laws and parametric functions on gaging measurements (NaCl and flow velocity field).

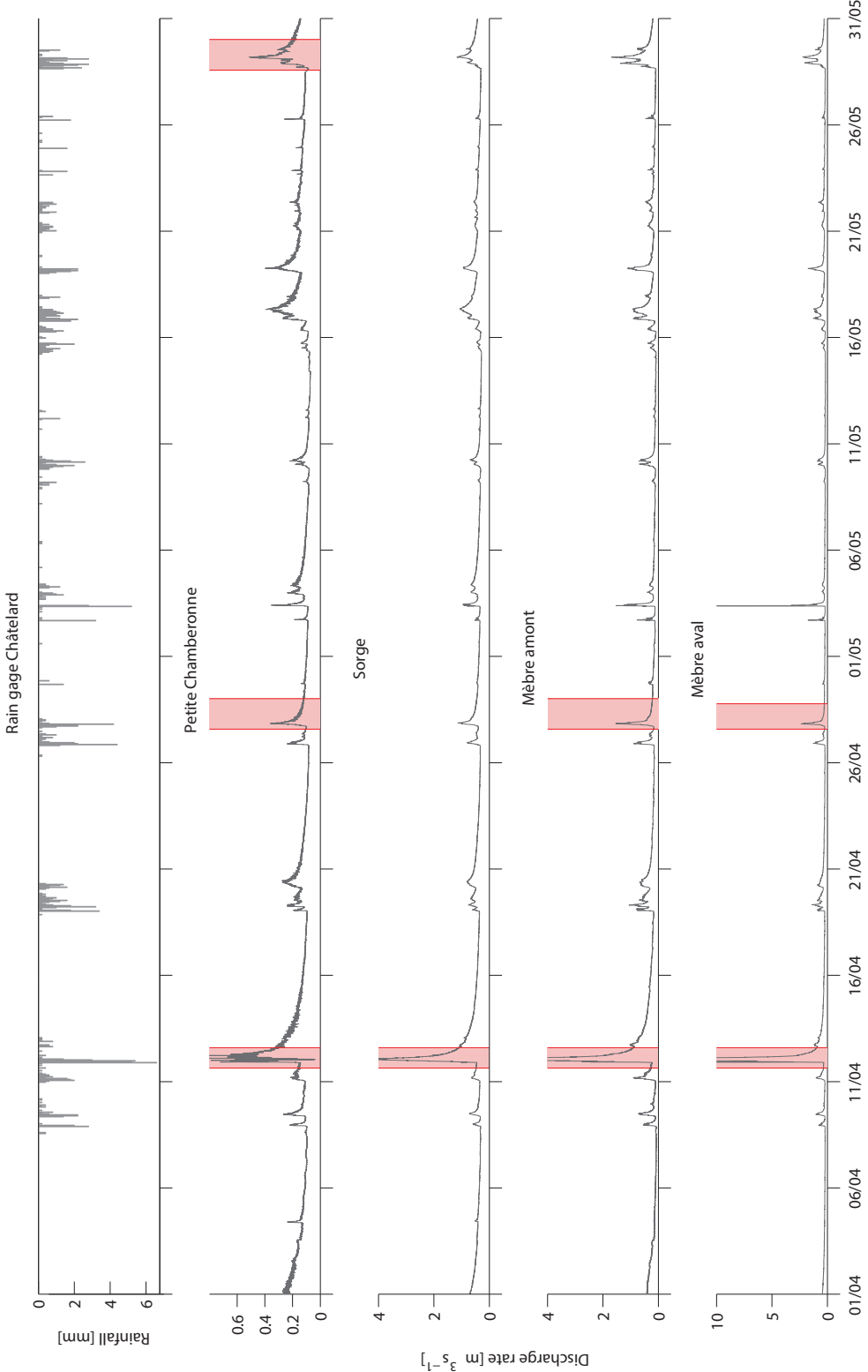


Figure 5.4: Rainfall observed at the Châtelard rain gage and discharge rate at all ECHO stations during April–May 2013. The red bands shows the periods that where show the rainfall event sampled for pesticides

### 5.5.3 Pesticide concentrations

The analysis of pesticides during the three rainfall events sampled reveals in-stream concentration ranging from a few  $ng L^{-1}$  to more than  $1500 ng L^{-1}$  (for mecoprop). Whereas ethofumesate, irgarol, propiconazol, pymetrozin and tebufenozid were never found in the samples, eleven other substances were frequently detected at varying concentrations. Table 5.4 summarizes the mean concentration for each compound during a sampling period (usually 24 samples). It can be noticed that some substances have been measured at similar concentrations at the different stations and during the different rainfall events (e.g. atrazin, terbutryn, isproturon). In contrast, benzotriazole, mecoprop and met amitron present significant changes in concentration, likely originating from agricultural applications that have occurred between the sampling periods. Note that the environmental quality standard EQS (see Table 5.3) is never exceeded (neither for the mean nor for the maximum concentration, not reported here), except for diazinon (very low EQS).

Table 5.4: Overview of the screened substances and their mean concentration (in  $ng L^{-1}$ ) of all samples collected during an entire rain event for each sampling station. A color code is provided for clarity, reporting the following concentration classes: 0 – 5, 5 – 10, 10 – 50, 50 – 100 and  $> 100 ng L^{-1}$ . PteC, SOR, MAM and MAV refers to the sampling stations *Petite Chamberonne*, *Sorge*, *Mèbre amont* and *Mèbre aval* respectively.

	Event 1				Event 2			Event 3
	PteC	SOR	MAM	MAV	PteC	MAM	MAV	PteC
Benzotriazole	75.54	187.58	88.26	94.59	ND <sup>a</sup>	85.97	95.41	143.34
Methylbenzotr.	36.94	59.55	57.71	49.15	21.58	43.25	46.79	59.46
Atrazin <sup>b</sup>	6.25	3.66	3.67	3.10	6.92	5.37	5.00	6.33
Terbutryn	2.00	1.80	1.52	2.18	2.58	ND	1.27	1.19
Isoproturon	1.73	ND	2.38	1.43	1.31	1.25	1.16	ND
Diuron	20.12	11.18	14.87	11.90	7.83	13.9	12.3	6.34
Irgarol	ND	ND	ND	ND	ND	ND	ND	ND
Mecoprop	4.91	8.25	19.00	21.32	558.86	181.52	212.46	65.48
Triclosan	ND	ND	ND	ND	ND	ND	5.45	ND
Carbendazim	10.75	7.53	8.00	8.76	ND	6.27	5.70	5.90
Chloridazon	ND	ND	ND	ND	ND	1.29	ND	ND
Diazinon	ND	ND	4.48	2.74	ND	1.41	2.30	1.80
Propiconazol	ND	ND	ND	ND	ND	ND	ND	ND
Pymetrozin	ND	ND	ND	ND	ND	ND	ND	ND
Tebufenozid	ND	ND	ND	ND	ND	ND	ND	ND
Metamitron	ND	ND	4.50	5.58	ND	ND	3.43	194.85
Chlortoluron	38.00	24.45	19.68	17.01	9.55	2.02	2.63	6.58
Terbutylazine	8.92	9.21	4.03	5.14	8.10	4.14	12.46	11.19
Ethofumesate	ND	ND	ND	ND	ND	ND	ND	ND

<sup>a</sup> ND: Not detected

<sup>b</sup> Forbidden in Switzerland since 2011

We observe that the concentrations of pesticides usually follow similar dynamics as the dis-

## Chapter 5. Catchment-scale experimental site and pesticides dynamics screening

---

charge rate, as shown for a selection of substances in Figure 5.5. However, the peaks of some compounds can appear a couple of hours before or after the peak discharge. The dynamics of mecoprop (Figure 5.12) is particularly interesting regarding this matter: during the first storm event, the concentration peak is systematically observed about 2-4 hours before the discharge peak occurs, which is verified at all four sampling stations. During the second event about two weeks later, the concentration are about 100-fold those during event 1, indicating an application of this substance between the two campaigns. The larger concentrations measured at *Petite Chamberonne* – the most upstream station – suggest that mecoprop has likely been used in large quantities in particular in the agricultural fields around this station (smaller applications elsewhere on the catchment are also presumed, as the stations *Mèbre amont* and *aval* are on a different tributary and also show high concentrations). In contrast to event 1, the concentration peaks during event 2 occurs simultaneously with the discharge peak at *Petite Chamberonne*, and about 10 hours later for the two stations on the *Mèbre* tributary. As the mecoprop observed during the first sampled event is likely issued from old applications (possibly from the year before), it can have been progressively transported through the hydrologic system by antecedent rainfall, and therefore be readily mobilized during another large precipitation event. During the second event, the substance takes a longer time to reach the stream, because it has to be transported all the way for the application site to the sampling site in the stream, resulting in a retarded concentration peak. This lag is shorter at *Petite Chamberonne*, probably because of the proximity of the sampling station to the application site.

The similarity between discharge and substance dynamics (with a varying lag time) is typical for solute transport, because the hydrology is the main driver of substance transport, and it is largely controlled by the climatic forcing which triggers different hydrologic processes such as overland flow, infiltration, tile drains discharge, etc. As it has been shown, solute transport is however considerably affected by the sources (timing and location) and the whole history of hydrologic events that have occurred between the application and the time when a substance is observed at a control section (i.e. sampling site), because they control the distribution of the solute within the hydrologic system and consequently their propensity to be transported and pass through the control section during a subsequent event. During the time a substance spends within the hydrologic system, the compounds' reactivity also modifies its availability for further transport events. The data collected during these campaigns show a nice example of the impact of the persistence of the herbicide atrazin. This substance is forbidden in Switzerland since 2011, but as it is shown in Figure 5.8, atrazin is still systematically measured at concentrations around 5-10  $ng L^{-1}$ . It is worth noting that its concentration dynamics is the inverse of what is usually seen, i.e. the concentration decrease during peak flow. Figure 5.5 emphasizes the differences of the concentration dynamics of benzotriazol, diuron, atrazin and chlortoluron during a selected storm event (the concentration are normalized by the maximum concentration of each compound). As atrazin is not used any more, it originates from legacy storages in the hydrologic system, e.g. in groundwater or under recalcitrant forms (sorbed) that are not readily available. Hence, the normally constant background atrazin concentration in

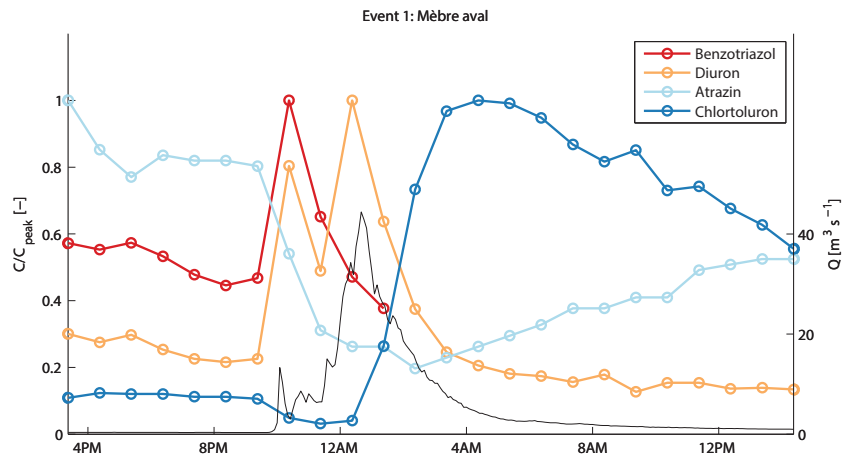


Figure 5.5: Comparison of benzotriazole, diuron, atrazin and chlortoluron normalized concentration dynamics during a storm event (11-12 April at *Mèbre aval*).

streamflow (due to the slow release of atrazin in labile forms and contribution of groundwater) is diluted by storm water exempt of atrazin during rain events, which explains the sudden concentration drop as soon as the discharge increases. Note also that the other substances are markedly different, with the earlier peak observed for benzotriazol. As this substance is not a pesticide, but a corrosion inhibitor, it most likely originates from urban zone and may be discharged by separated sewer systems, therefore shortening the transport pathway to the stream in regards to natural hydrologic pathways. Chlortoluron instead shows a concentration increase much later, and a slower recession. This herbicide used for cereal protection is mostly used in autumn. This suggests that the chlortoluron is rather located deeper in the soil rather than at the surface, and therefore cannot be rapidly washed out by storm water (e.g. via surface runoff) but may be mobilized by infiltration water which contributes only later to the storm discharge.

All chemographs of this pesticide campaigns are detailed in Figure 5.6–5.18.

## 5.6 Detailed chemographs

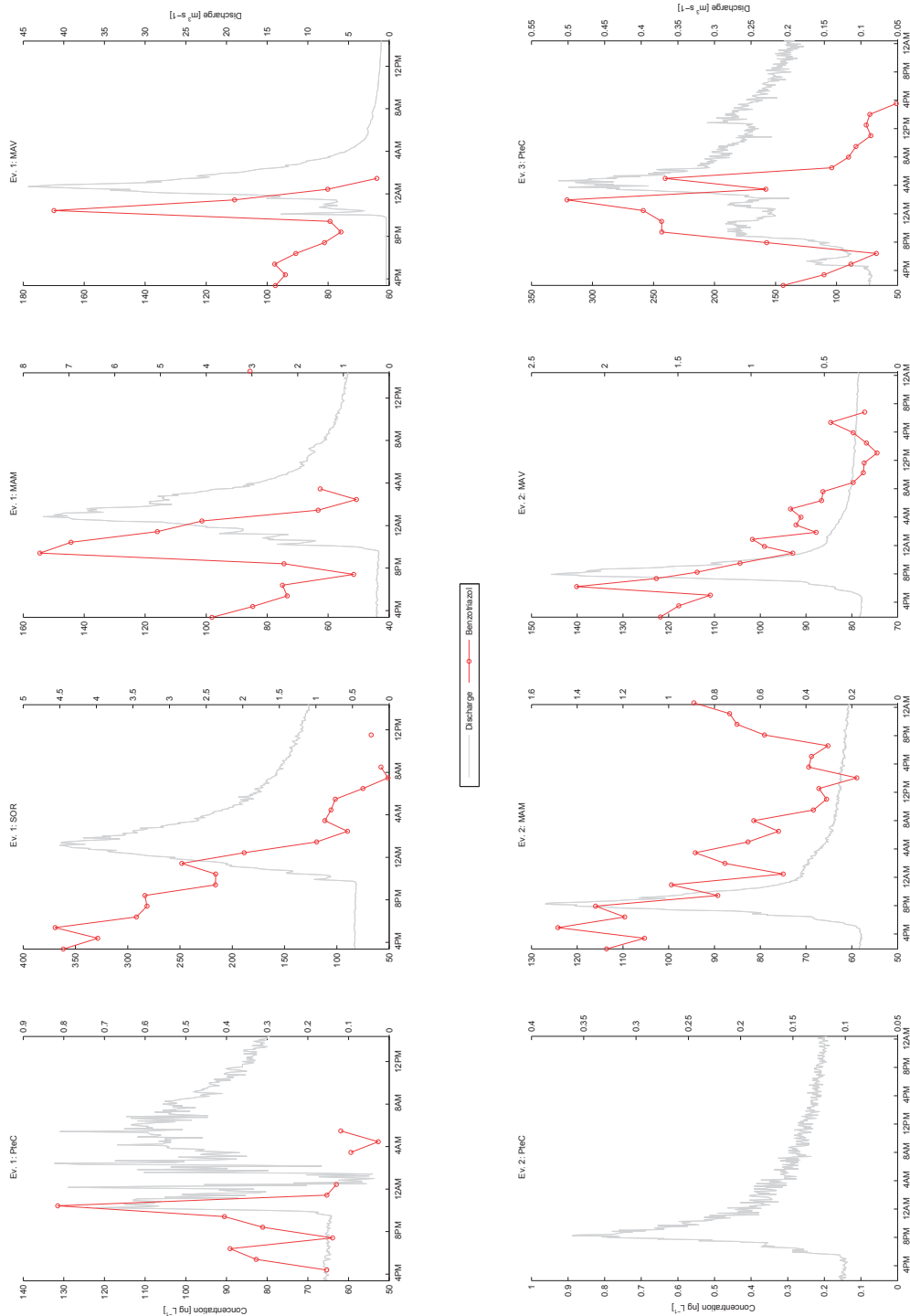


Figure 5.6: Benzotriazole concentration dynamics observed during Event 1, 2 and 3 at each sampling station (red line). Measured discharge at the same site is shown (grey line).

## 5.6. Detailed chemographs

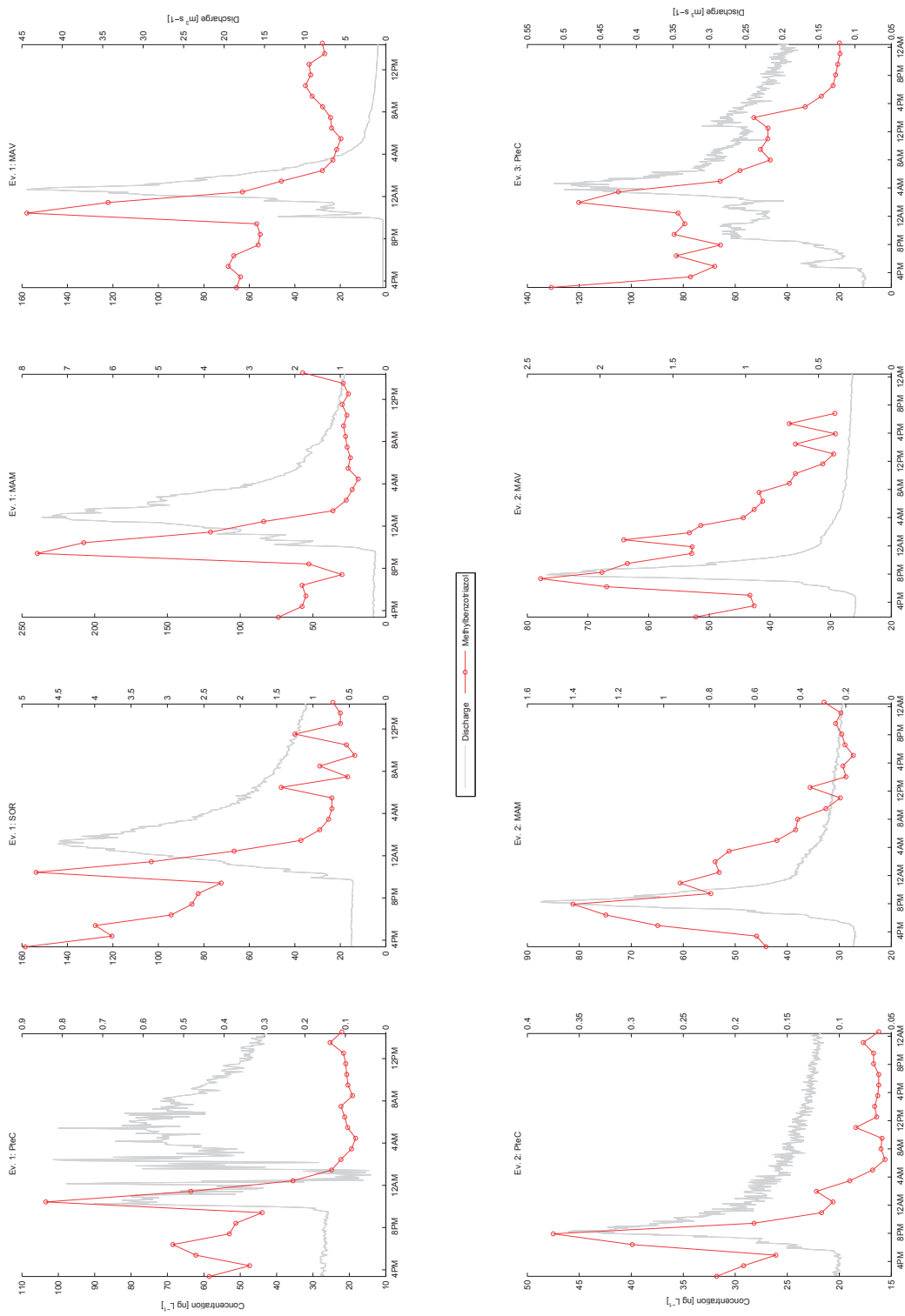


Figure 5.7: Methylbenzotriazole concentration dynamics observed during Event 1, 2 and 3 at each sampling station (red line). Measured discharge at the same site is shown (grey line).

## Chapter 5. Catchment-scale experimental site and pesticides dynamics screening

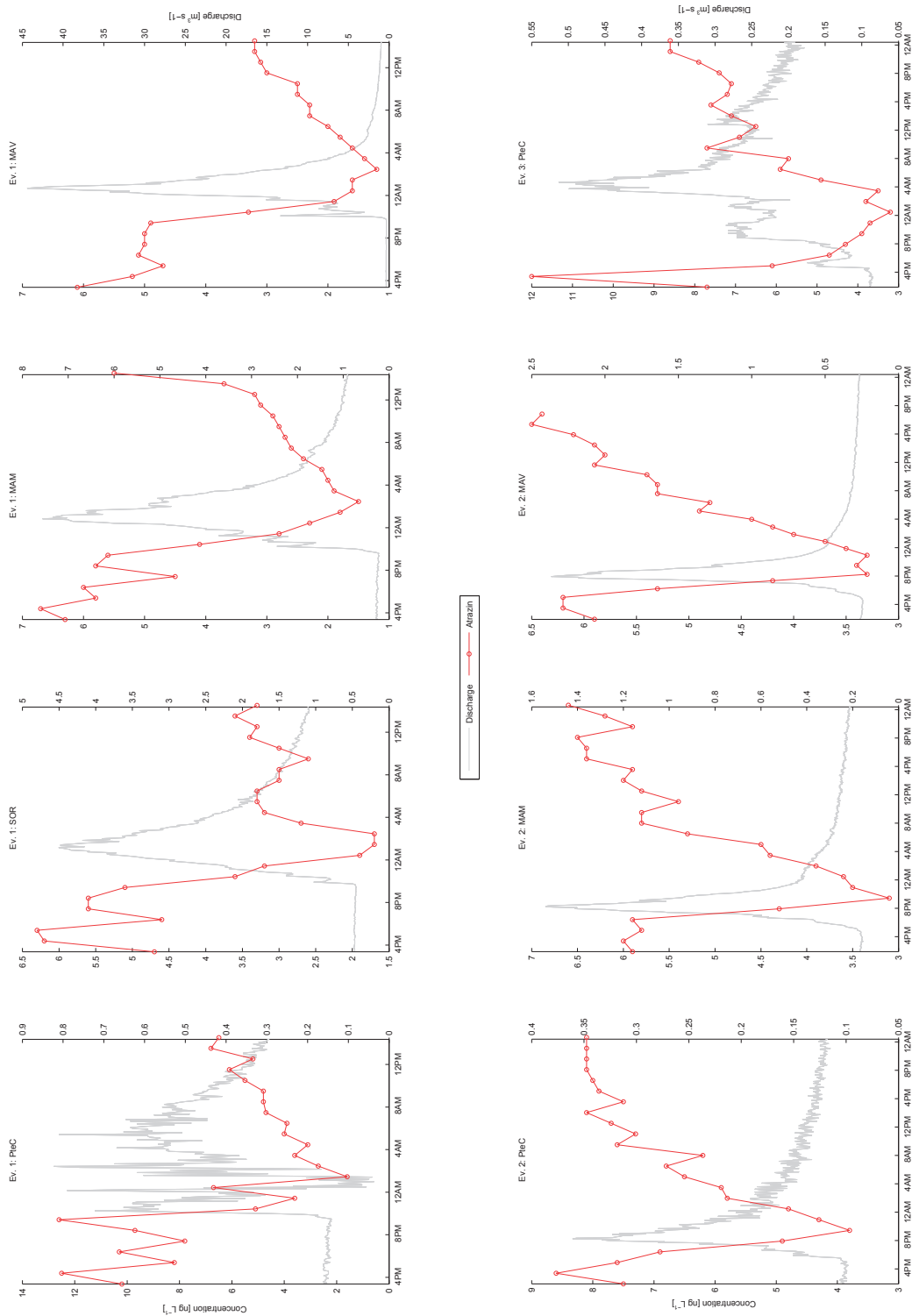


Figure 5.8: Atrazine concentration dynamics observed during Event 1, 2 and 3 at each sampling station (red line). Measured discharge at the same site is shown (grey line).



## 5.6. Detailed chemographs

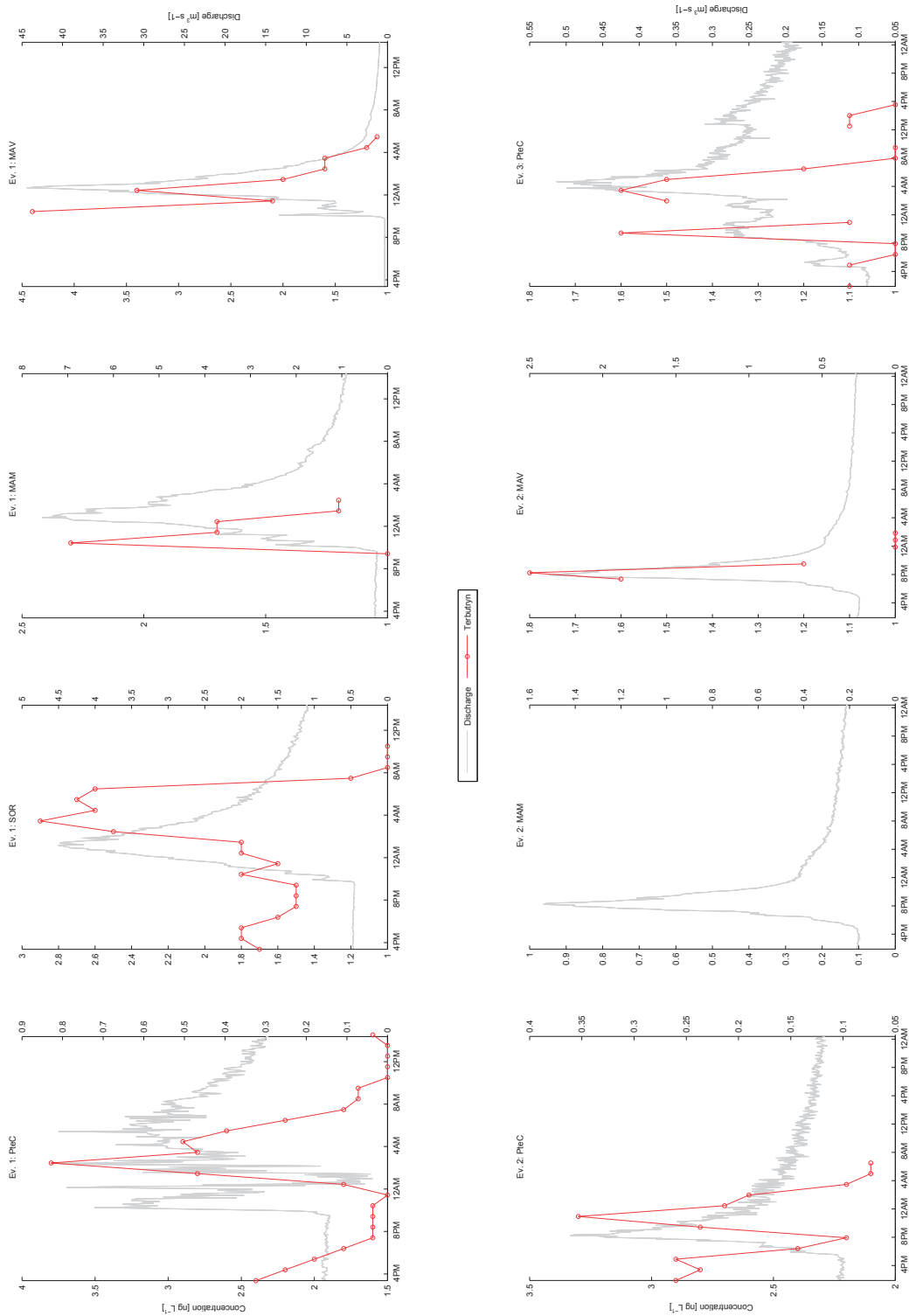


Figure 5.9: Terbutryn concentration dynamics observed during Event 1, 2 and 3 at each sampling station (red line). Measured discharge at the same site is shown (grey line).

## Chapter 5. Catchment-scale experimental site and pesticides dynamics screening

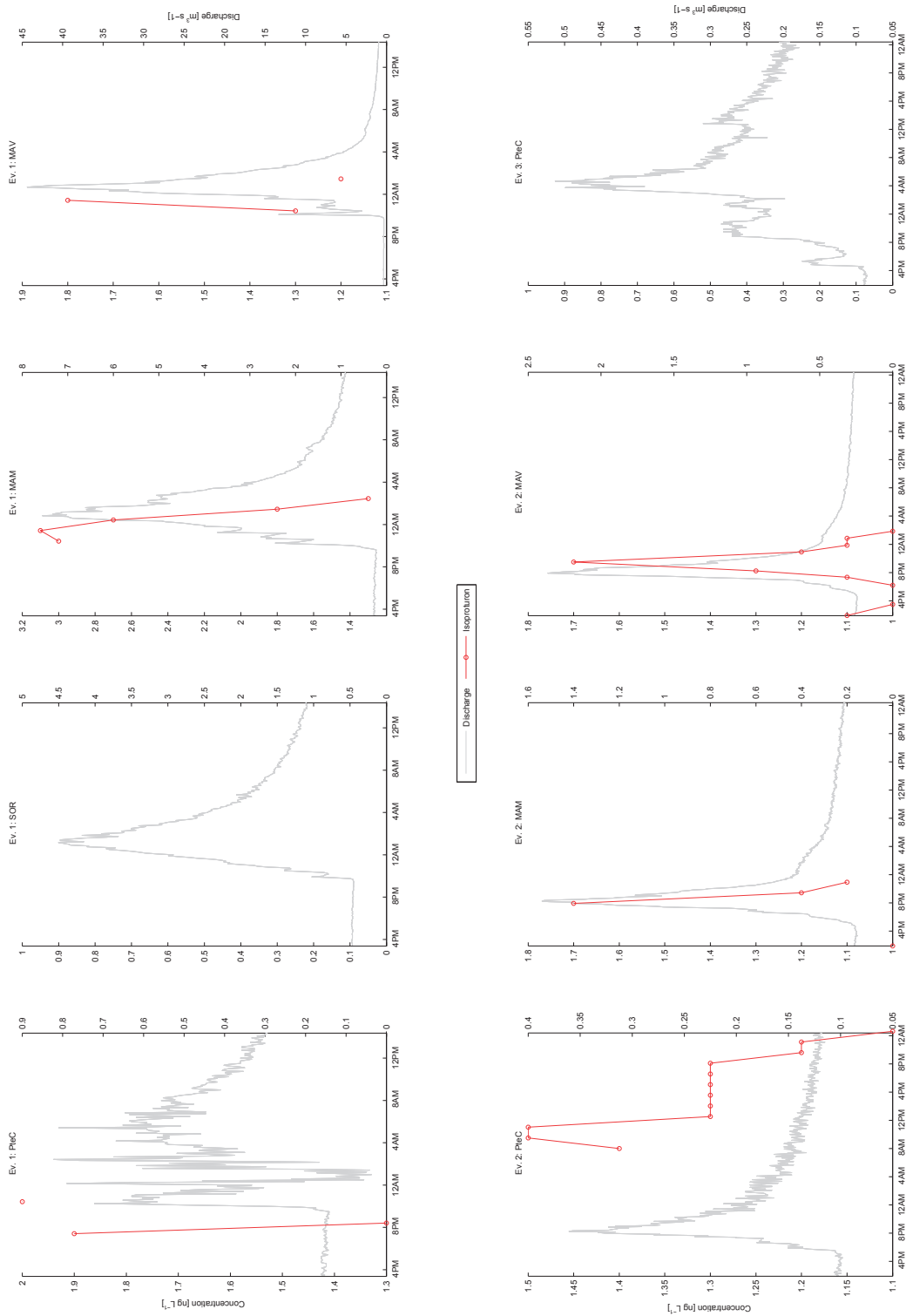


Figure 5.10: Isoproturon concentration dynamics observed during Event 1, 2 and 3 at each sampling station (red line). Measured discharge at the same site is shown (grey line).

## 5.6. Detailed chemographs

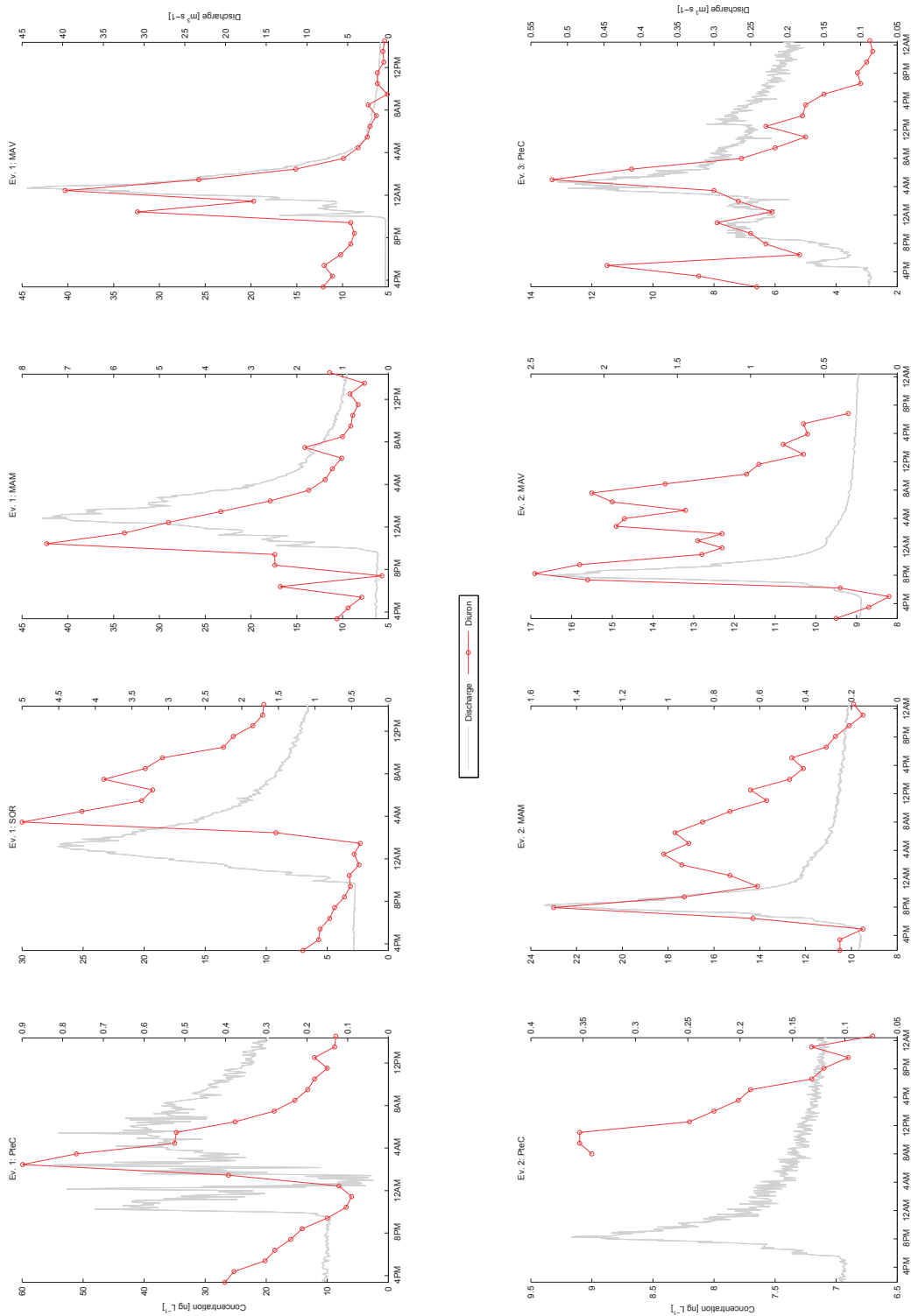


Figure 5.11: Diuron concentration dynamics observed during Event 1, 2 and 3 at each sampling station (red line). Measured discharge at the same site is shown (grey line).

## Chapter 5. Catchment-scale experimental site and pesticides dynamics screening

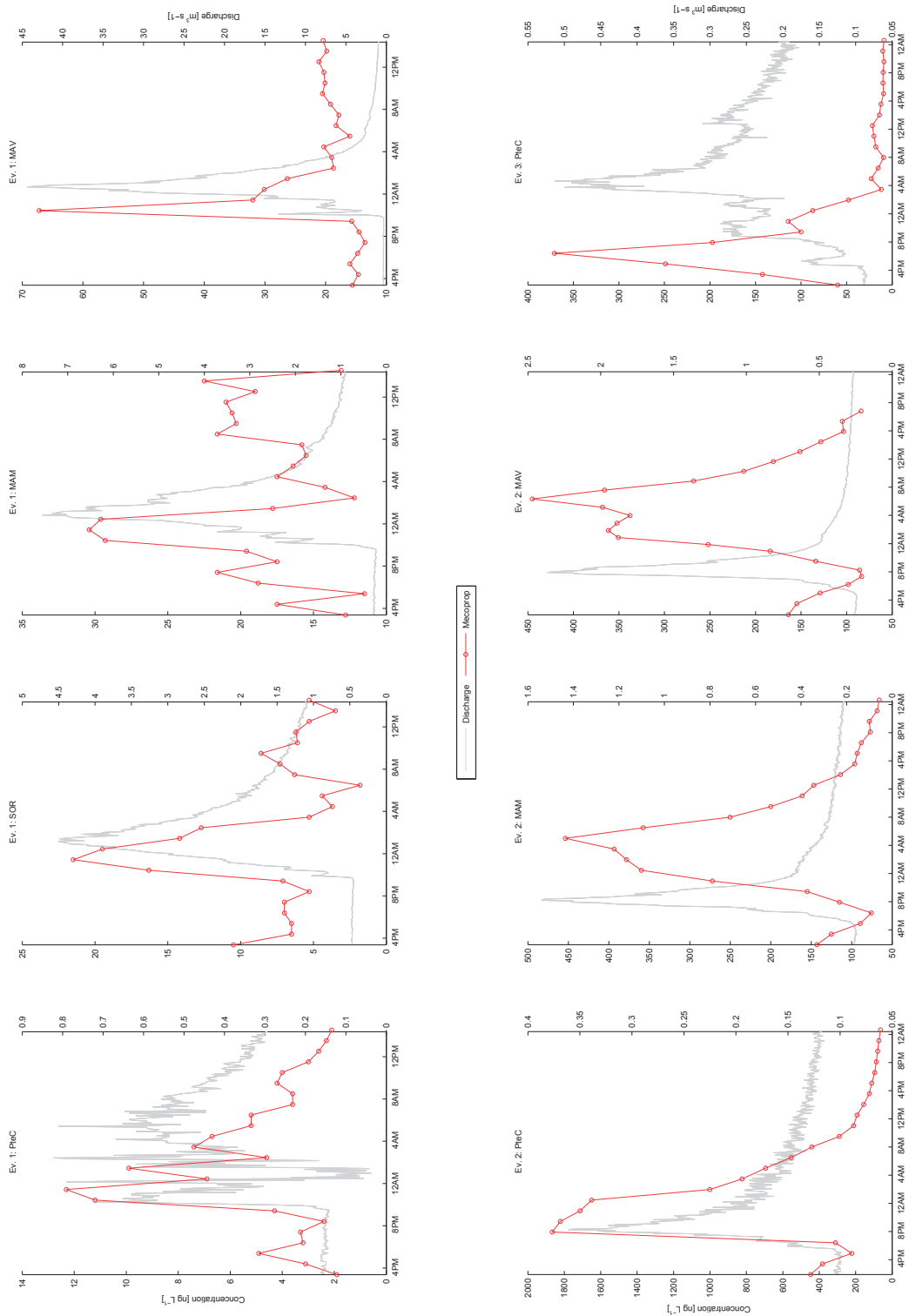


Figure 5.12: Mecoprop concentration dynamics observed during Event 1, 2 and 3 at each sampling station (red line). Measured discharge at the same site is shown (grey line).

## 5.6. Detailed chemographs

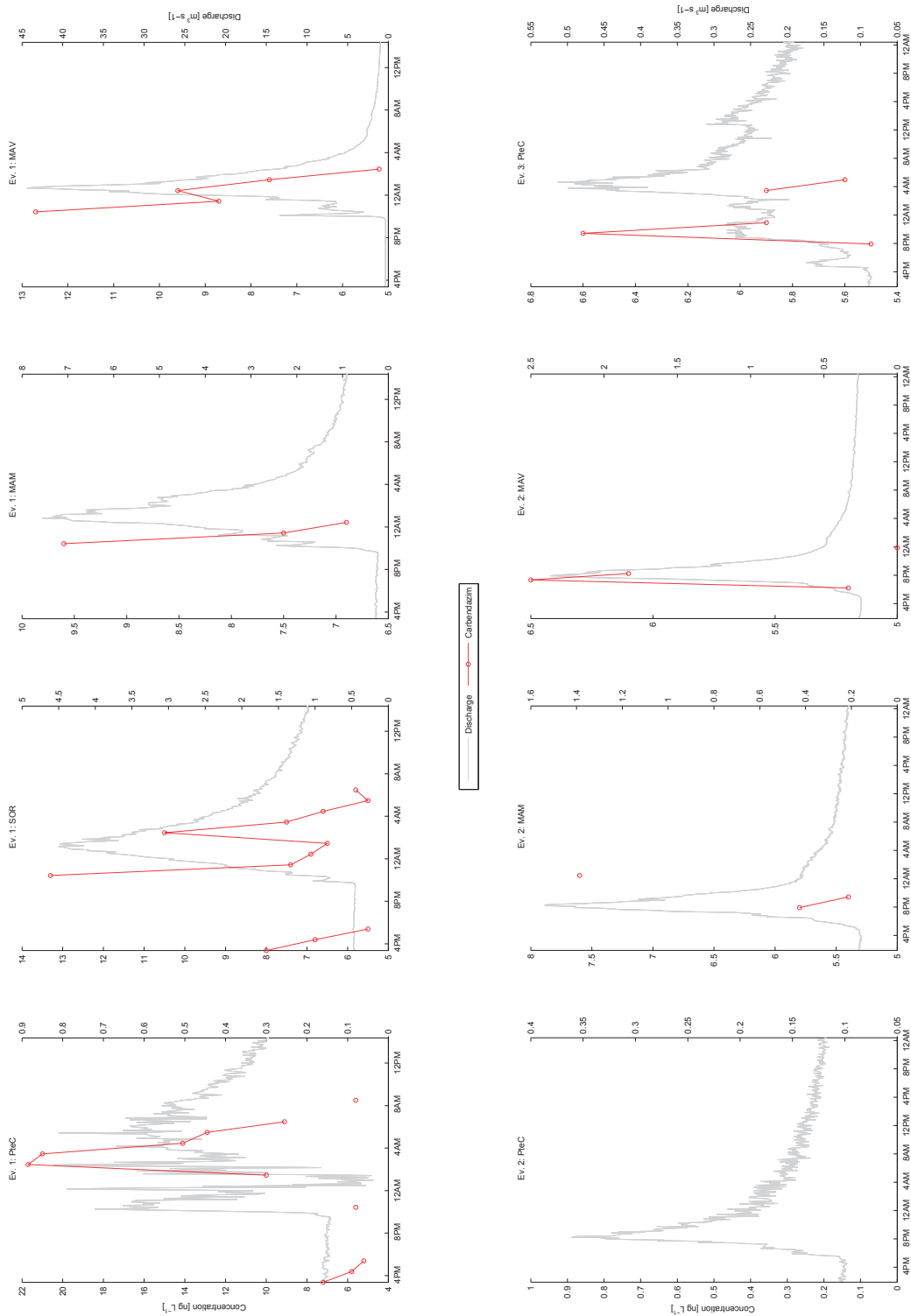


Figure 5.13: Carbendazim concentration dynamics observed during Event 1, 2 and 3 at each sampling station (red line). Measured discharge at the same site is shown (grey line).

## Chapter 5. Catchment-scale experimental site and pesticides dynamics screening

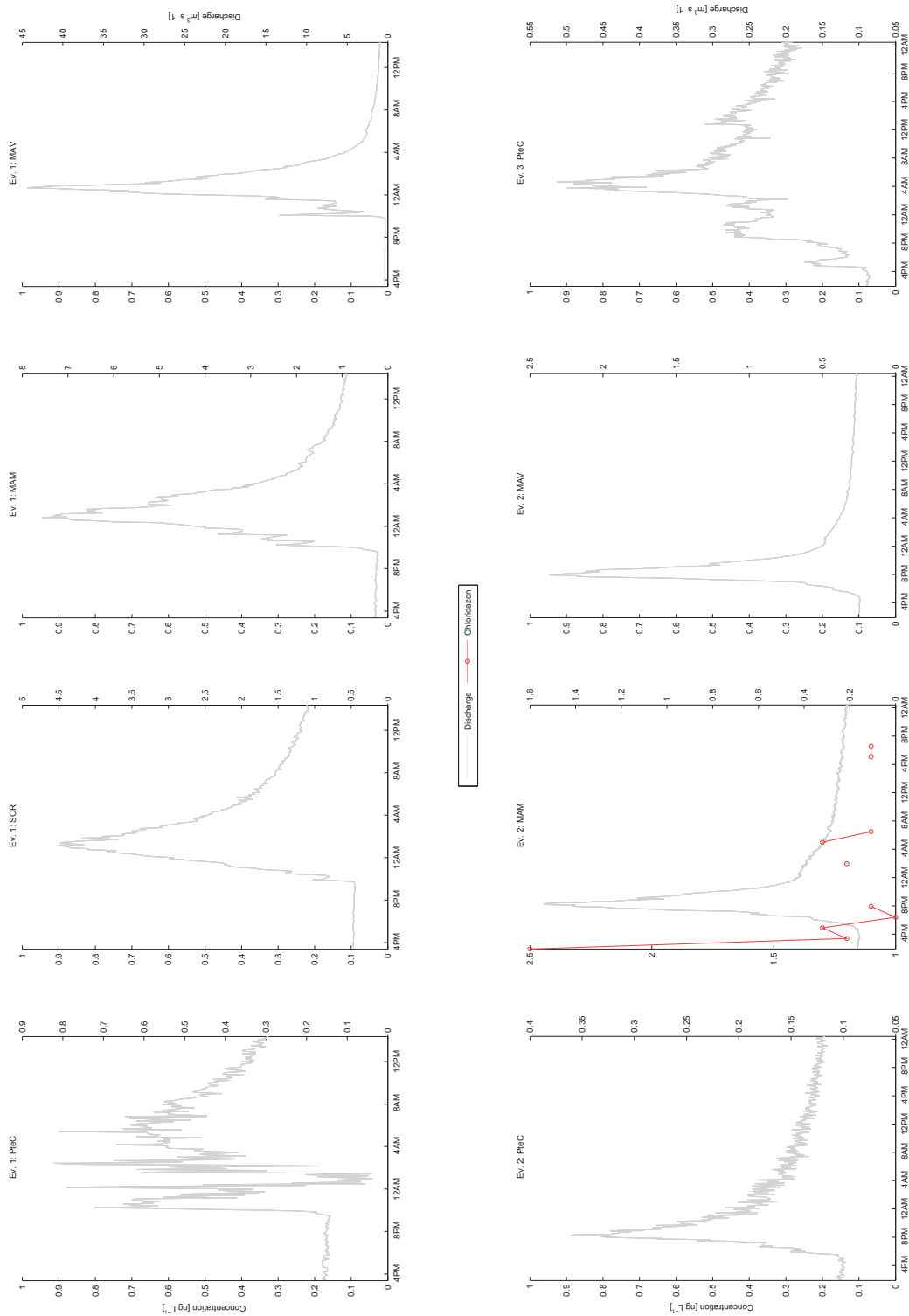


Figure 5.14: Chloridazon concentration dynamics observed during Event 1, 2 and 3 at each sampling station (red line). Measured discharge at the same site is shown (grey line).

## 5.6. Detailed chemographs

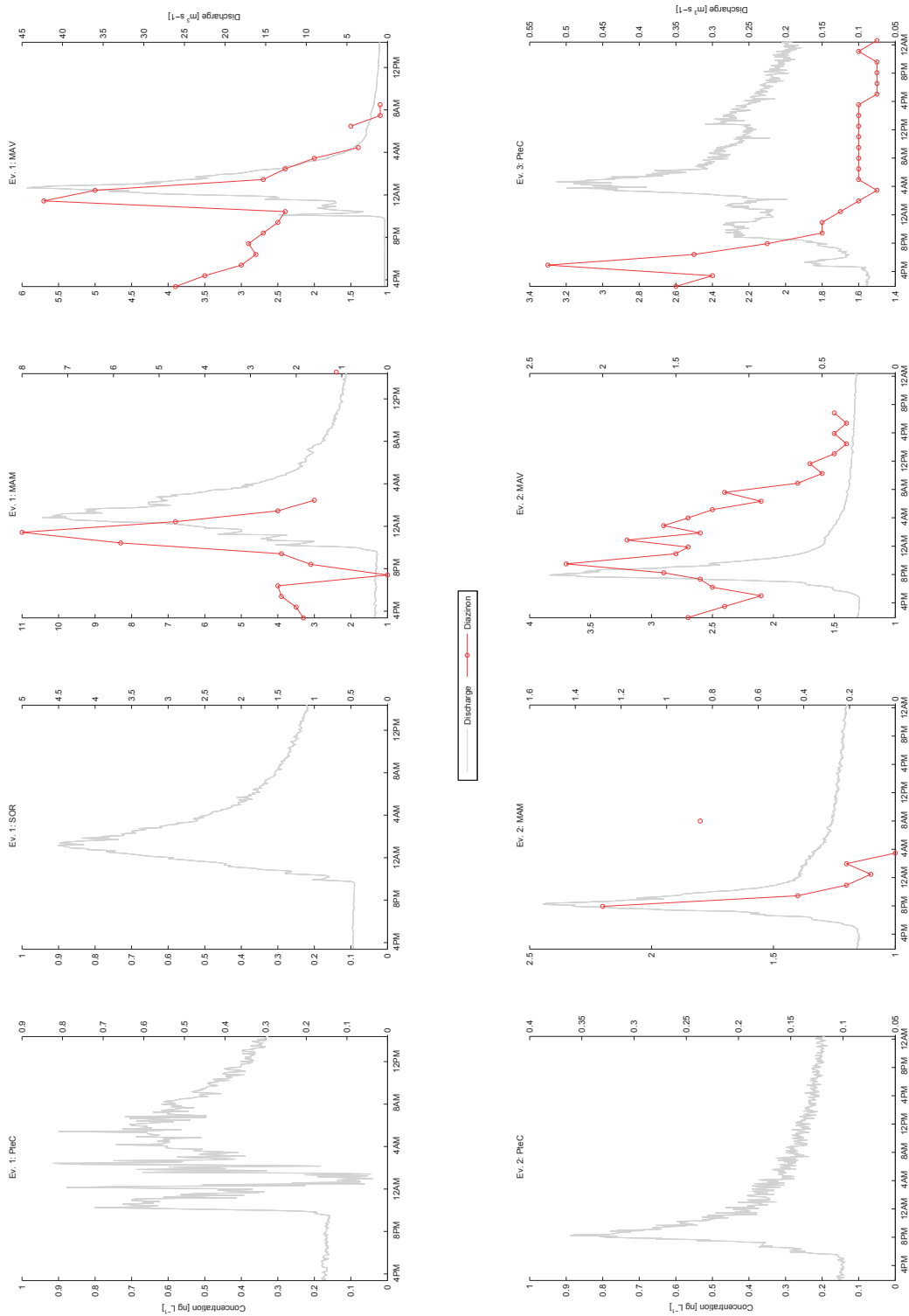


Figure 5.15: Diiazinon concentration dynamics observed during Event 1, 2 and 3 at each sampling station (red line). Measured discharge at the same site is shown (grey line).

## Chapter 5. Catchment-scale experimental site and pesticides dynamics screening

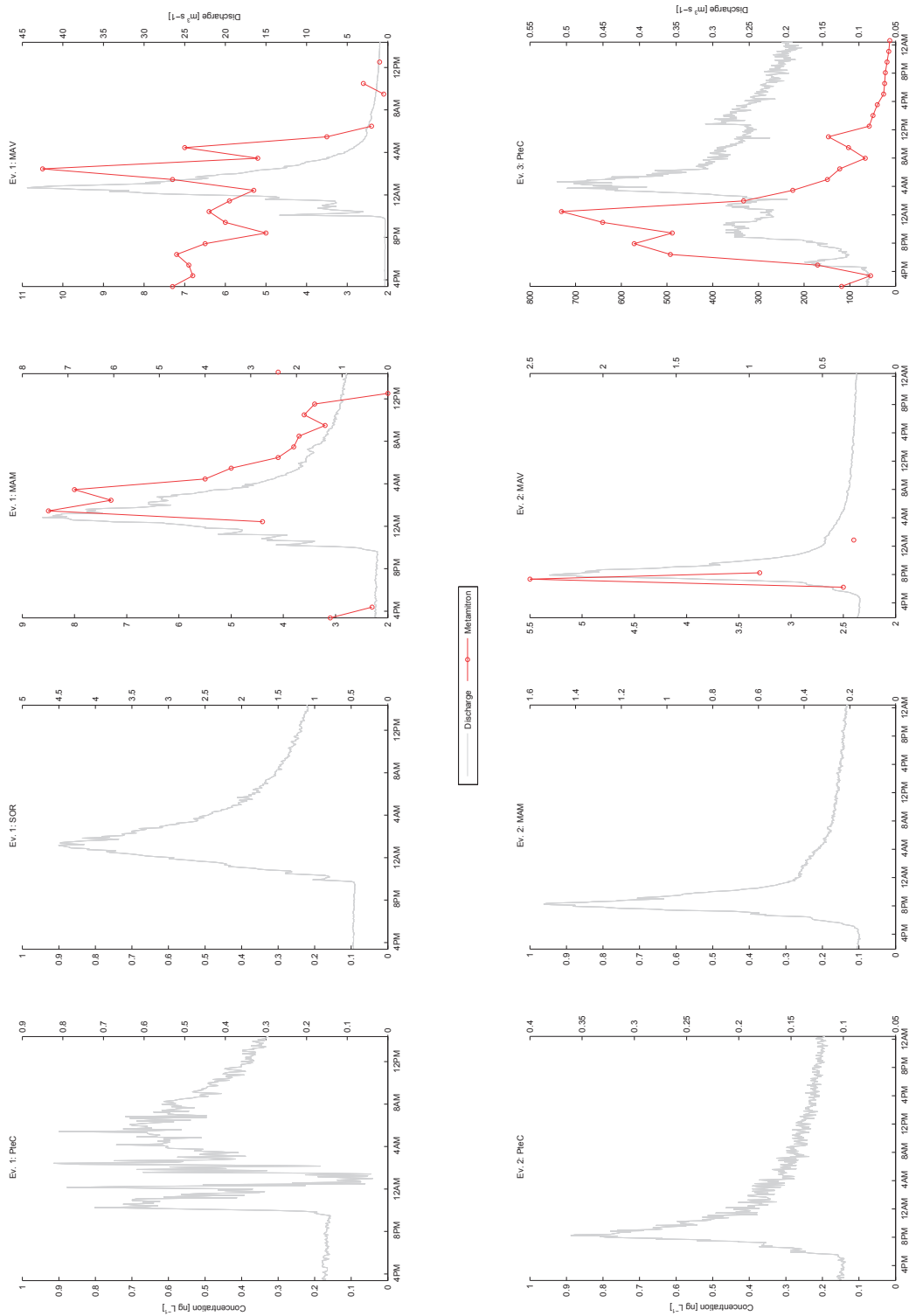


Figure 5.16: Metamitron concentration dynamics observed during Event 1, 2 and 3 at each sampling station (red line). Measured discharge at the same site is shown (grey line).



## 5.6. Detailed chemographs

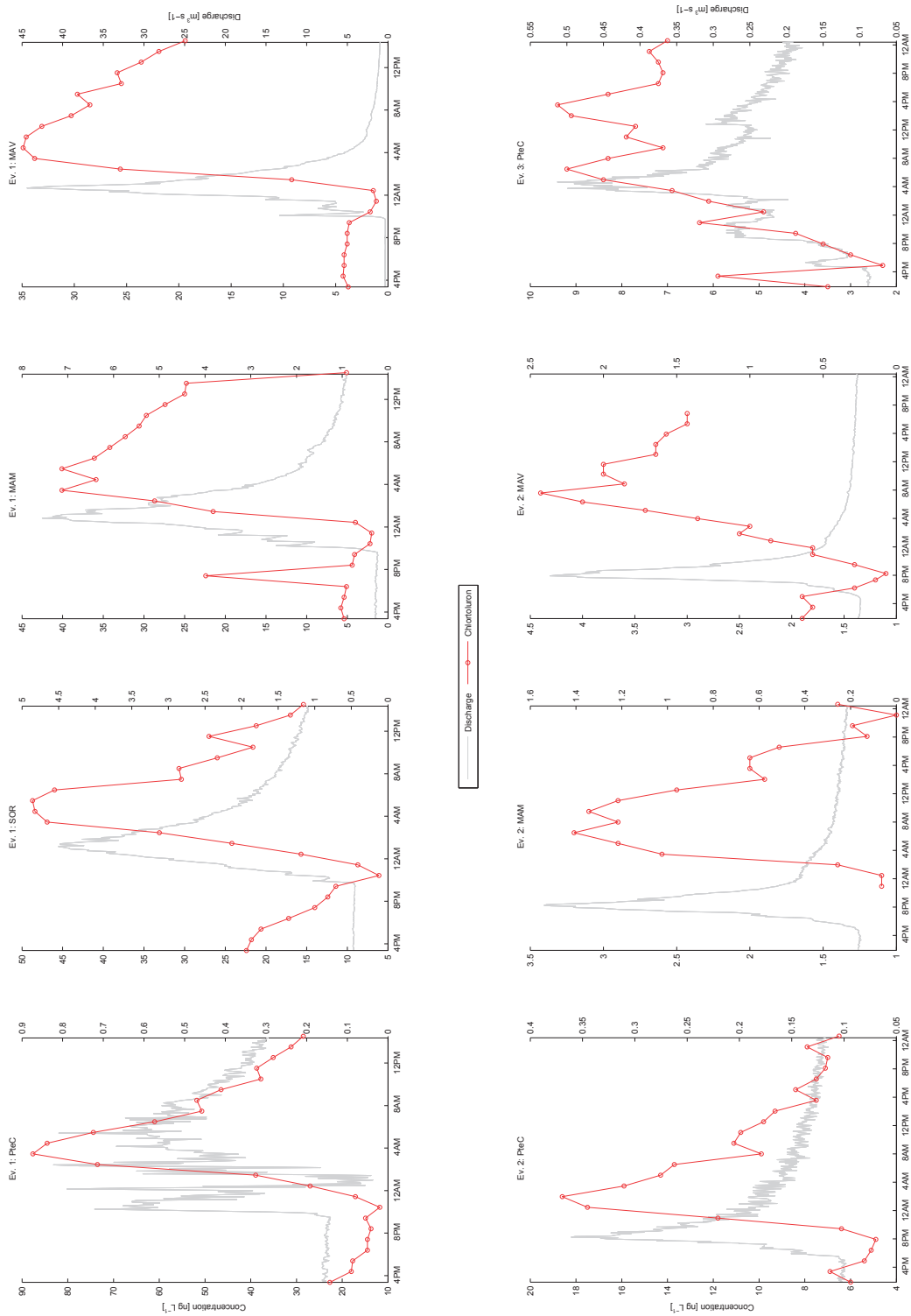


Figure 5.17: Chlorotoluron concentration dynamics observed during Event 1, 2 and 3 at each sampling station (red line). Measured discharge at the same site is shown (grey line).

## Chapter 5. Catchment-scale experimental site and pesticides dynamics screening

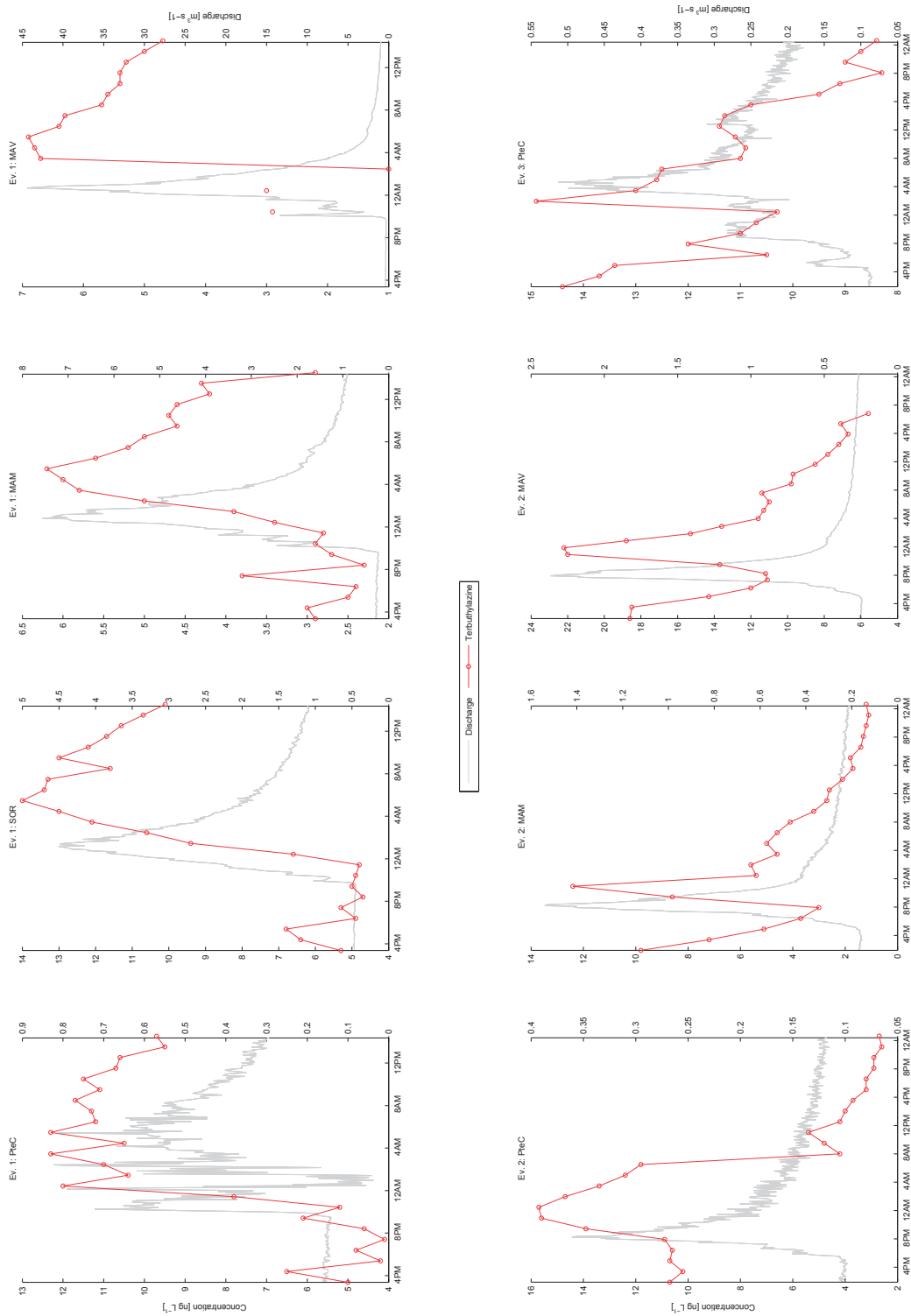


Figure 5.18: Terbutylazine concentration dynamics observed during Event 1, 2 and 3 at each sampling station (red line). Measured discharge at the same site is shown (grey line).

## **5.7 Conclusions**

The recent advances in analytical methods allow to detect an increasing number of substances at trace concentration. Beside the high costs of these analyses, characterizing pesticides losses to surface waters remains an challenging task, because the high temporal and spatial variability of pesticides occurrence illustrated here requires a very demanding sampling effort in order to catch relevant dynamics. In this light, modeling can be critical to evaluate and predict the leaching of non-point source substances in receiving environments and to assess the ecotoxicological risk for aquatic ecosystems. The development of an appropriate model should move from the description of hydrologic fluxes, which are the common transport drivers for all substances, and further accounting for compound specific biogeochemical reactions affecting the persistence in the hydrologic system. The selection of relevant experimental sites and the collection of long-term high-resolution tracer and pesticides datasets, together with a close collaboration with the local users in order to characterize substance applications would set the prerequisites for a better understanding of solute transport at catchment scales.



## 6 Conclusions and perspectives

In this thesis, experiments on reactive solute transport across various hydrologic transport volumes have been complemented by field work and theoretical analyses to develop a general framework suited to large-scale reactive processes under a unified approach embodied by the travel time formulation of hydrologic transport. Such framework is especially useful and efficient at scales where spatial heterogeneity and time variability of the forcing are important, because it integrates many processes affecting hydrologic transport into a single lumped attribute. As it has been demonstrated, this provides a significant advantage, because of the parsimonious requirement for parameters which avoids the estimation or measurement of numerous physical attributes often subject to significant uncertainty at the catchment scale.

The estimation of travel times through tracer data, however, presents a number of challenges that were experimentally addressed in this thesis. For an artificial tracer spiking a single pulse injection, the breakthrough curve measured at the discharge outlet theoretically provides a direct measurement of the forward travel time distributions (TTDs), but only in the case of a perfect tracer whose mobility is identical to that of water and which is not subject to discrimination by plant uptake nor degradation or sorption of any kind. It is difficult to find a tracer which fulfils all these conditions, as it was specifically demonstrated in this thesis for fluorobenzoic acids (FBAs) and water stable isotopes. Despite the purported conservative behavior of FBAs reported by many studies and their suitability for hydrologic tracing in soils, the total tracer mass recovery in the discharge was partial at best (and null in some cases), suggesting mass removal processes attributable to selective plant uptake and/or microbial degradation. The isotopic content of discharge outflows was instead shown to be significantly affected by surface evaporation, and as such an evaporation model should be used in order to correctly evaluate the contribution of the tracer-labeled pulse. Reactivity along the transport pathways or partial affinity of evapotranspiration (ET) for a specific tracer (i.e. evapoconcentration) are particularly problematic if these processes are not well known for the substance in question. Their respective magnitudes cannot be determined and their impact on the TTDs (markedly different for each process) remains obscure. Overall, this thesis' experimental work suggests that perfect tracers hardly exist when considering hydrologic transport through real

## Chapter 6. Conclusions and perspectives

---

and entire systems.

The pronounced differences between the observed breakthrough curves and the mass recovery of the five FBA isomers injected sequentially under distinct conditions question whether the apparent variability of the tracer discharge response is a rather a demonstration of non-stationary TTDs, or mainly an artefact emerging from selective chemical/biological behaviors among the tracers. In addition to *ad hoc* reactivity testing, which supports limited degradation of these compounds and rather suggests plant uptake, the reinjection of two tracers (thereby dismissing the claim of compound-specific reactivity) conclusively confirms that the discharge responses of a given tracer vary widely depending on the prevailing conditions. Temporally displaced pulse injections of a single tracer instead of sequenced multiple tracers injections eliminate all issues related to the uncertainty of tracer-specific reactivity, but require that the entire previously injected tracer mass had exited the system (or be irreversibly immobilized or degraded). The latter is time-demanding and impractical at large scales. As it has been shown here, such an approach demonstrates that TTDs are inevitably non-stationary, because the variability of the climatic forcing prompts soil moisture and evapotranspiration constantly changing dynamics, and modifies the conditions for mixing and transport processes. However, as long as the behavior of the tracer used differs from that of water through reactivity of any kind or incomplete plant uptake of the tracer, the tracer response observed in the discharge cannot be reckoned as the direct equivalent of a TTD.

Even if tracer experiments are crucial to evaluate and describe hydrologic and solute transport in terms of TTDs in real settings, they are not sufficient for the following reasons:

1. It proves extremely difficult to measure TTDs directly as perfect tracers do not exist in practice and reactivity issues usually affect the tracer responses;
2. Even with extensive prior knowledge of the tracer properties, the tracer responses blend all kinds of reactive and transport processes and prevent the assessment of their respective contribution;
3. Hydrologic transport is inherently non-stationary, even at limited scales such as the one reported here. One tracer pulse injection only illustrates the system's response in a specific combination of conditions, but may not provide a representative picture under different circumstances. Sequenced multiple tracer injections or temporally displaced injections are found to be appropriate methods to disentangle the variability of the tracer responses, but both are experimentally challenging and not conceivable at large scales.

Modeling proves a necessary tool in order to reconcile observed tracer responses with their TTDs, to explain possible degradation or removal pathways of the tracer and predict the TTDs for different sets of conditions that cannot be tested experimentally or empirically. Here, it was shown that a simple model based on time-variant TTDs is able to adequately explain

---

the non-stationary behavior of the discharge tracer signals of particular classes of FBAs in a large vegetated lysimeter. Interestingly, the knowledge of input and output fluxes alone may allow the estimation of discharge and evapotranspiration storage selection functions, which define how an output flux samples the water among the available ages in storage. Note that the age distribution in the evapotranspiration flux is difficult to assess directly through tracer measurements of a the ET flux. However, as ET changes the resulting structure of ages available in storage, discharge age composition measurements allow the deduction of the ET counterpart. Uncertainties regarding the tracer's reactive behavior remain an issue, as it may hamper the assessment of evapotranspiration tracer fluxes and age selection functions.

A modeling framework tested at the lysimeter scale has the potential for promising upscaling to catchment scales, in particular because of its flexibility and of the low parameters' requirement. Considering a single control volume (e.g. a whole catchment), thereby encompassing flow pathway heterogeneity, source areas and internal mixing patterns, hydrologic transport is entirely described through two storage selections functions, one for the discharge and one for ET. Depending on the type of probability density functions assumed, this restricts the necessary calibration parameters to a minimum. Reaction kinetics can be easily accounted for in this framework, as they are decoupled from the general hydrologic transport component described by the TTDs. Yet, the contact time between the transported solute and the immobile medium holding the chemical and biological reaction drivers controlling the mass exchanges (characterized by appropriate reactive parameters) is precisely the travel time. First-order degradation occurring homogeneously within the hydrologic volume was considered in this thesis, however this reactive scheme can be easily relaxed to incorporate more complex reactions of various orders. As the model continuously keeps track of the complete age structure in the storage, it can also conceivably account for reaction kinetics affecting specific age ranges (ranked or absolute ages), which could be relevant to describe specific degradation processes that can be recognized to be temporally restricted (e.g. enhanced microbial degradation at shallow depth, thus affecting younger ages).

The theoretical and modeling framework describing hydrologic and solute transport presented in this thesis is shown to be particularly useful and practical due to its simple and flexible structure. The absence of any pre-requisite in terms of physical parameters and the minimal calibration requirements imply the necessity of appropriate and demanding tracer data. It has been shown that neither tracer experiments — even in a small, simplified and well controlled hydrologic control volume — nor modeling alone can decouple the complex and evolving interactions between the processes controlling hydrologic transport. In this light, some perspectives are provided below concerning related research areas where progress is deemed most necessary and on which further research is already underway.

- The integration of information from different tracers represents a major challenge. In this thesis, it has been shown that spiking rainfall with artificial tracers is a current challenge even at small spatial scales. The use of natural tracers thus constitutes a viable choice for catchment-scale hydro-chemical transport studies. Existing methods

of theoretical interpretation need to be corrected, however, as they are typically biased either to recent or old water. Currently, studies are ongoing to establish a formal estimation of the partitioning of isotopic content during evaporation and uptake for many natural tracers. However, there are still unresolved challenges to isotope hydrology that might be impacted by the use of the formulation of transport by TTDs (e.g. by the specification of suitable storage sampling functions). In particular, transport models need to include tools that enable a spatially explicit characterization of inputs and an improved understanding of the isotopic composition of soil/vegetation water. In this general context, model-guided field validation represents a sensible step for interpreting laboratory evidence and scaled-up, catchment-scale transport experiments;

- The description of transport using TTDs, and in particular the related problem of choosing suitable storage sampling functions, proposes a paradigm shift away from a variety of approaches that require significant assumptions (e.g. to fit parameters of stationary transit time distributions to observed data) towards a coherent mathematical framework which explicitly takes into account flow and transport under variable hydrologic drivers. Applications to diverse hydrologic settings, already underway in a number of research groups worldwide, are needed to build a general case from an archive of case studies based on reliable field data. More work is needed on accurate large-scale numerical studies embedding significant geomorphological complexity;
- The meaning (and possibly the existence) of ideal tracers that follow the same velocity field as water parcels should be revisited in light of the experimental and theoretical findings shown in this thesis. In fact, the experiments using FBAs and water stable isotopes suggest that even if a tracer does not undergo chemical or biological changes in soils and is mobilized identically to water, it may still show limited (or enhanced) affinity to vegetation uptake or specific partitioning during evaporation. This being the case, the process of evapotranspiration would directly impact the chemical or isotopic composition of the storage and consequently the water quality of the discharge. This also inevitably affects the residence times of water parcels, regardless of the ideal — seen from a mere soil-water mass exchange perspective — nature of the tracer. Hence, a deeper understanding of vegetation uptake and evaporation affinity for different ages is critical to increase our understanding of catchment-scale transport phenomena. Among the repercussions of the results presented here, the development of suitable technologies allowing the direct measurement of solute uptake from large-scale assemblages of diverse vegetation cover would be key to mass balance closures without making critical assumptions;
- Another challenge highlighted by these results pertains to the study of catchment-scale reactive transport (i.e. a catchment-equivalent of reaction kinetics) within the general transport framework presented here. In fact, the residence time distribution inherently defines the contact times between fixed and mobile components, which drive mass exchange phenomena. Regardless of the physical, chemical or biological reaction



---

undergone by the solute mass within stored water parcels, the mobile mass sampled by the outflows is inevitably controlled by the evolving residence time distribution and by age-selection. A critical issue therefore concerns the combination of complex geochemistry processes with the large-scale, integrative characterization of catchment transport processes. A distinct advantage of the transport framework championed in this thesis is its parameters may be decoupled from the ones characterizing reaction kinetics, thereby allowing a direct use of multiple tracers experimental data and effective parameter calibrations;

- Approaches that consider an entire catchment as a unique control volume, without storage partitions of any kind, are appropriate given our enhanced ability to measure and estimate directly in- and out-fluxes, which avoids introducing internal subdivisions with their own state variables. Modern technology for remote acquisition and manipulation of meteorological and hydrological data serves such purposes well. In treating whole catchment transport volumes, however, the behavior of sampling functions transforming residence into TTDs proves far more complex than a simple random sampling scheme, for which exact solutions are available. To that end, future studies will demonstrate how travel-time based transport theories can be used to parameterize entire heterogeneous catchment with time-varying attributes;

Finally, the results of this thesis suggest that the availability of high-quality hydro-chemical datasets, suitably arranged to represent diverse catchment configurations, remains necessary for our understanding of solute transport and persistence at catchment scales and for a reasoned interpretation of hydro-biogeochemical processes in general. High-frequency measurements should be undertaken for the relevant input and output fluxes, and maintained for long enough that one obtains the tailing of residence time distributions (typically ranging from months to several years). This places significant constraints on field data collection, analysis and interpretation. Though seen from a relatively narrow perspective, these results suggest the need to re-evaluate the traditional interpretation of field experiments especially concerning concentration breakthrough curves of instantaneous pulses (the forward picture) in light of long-term station-wise gauging of exiting ages in streamflow (the backward picture). The theoretical apparatus connecting these interpretations challenges the uniqueness and usefulness of observed forward breakthrough curves for the now-recognized need to predict and understand their backward duals. This holds whenever the system under investigation is considered to host non-stationary transport phenomena, which is most often the case for the hydrologic response of natural watersheds. It is therefore argued that the core of the present thesis treats a important new problem for current hydrologic research that will provide, it is believed, food for thought for many years to come.



## **A Details of the lysimeter experiment**

## A.1 Lysimeter filling



Figure A.1: Replacement of the lysimeter tank in the compartment (left). Previous holes drilled in the wall were filled with polyester resin and reinforced with fiberglass mat (right).



Figure A.2: Filling and instrumentation of the lysimeter. The FDR probes and porous cups monitored depths can be seen on the right. Filling state and top-depth FDR probes before the planting of the willow (top left). The porous cups were sealed with epoxy resin (bottom left).

## A.2 Load cells

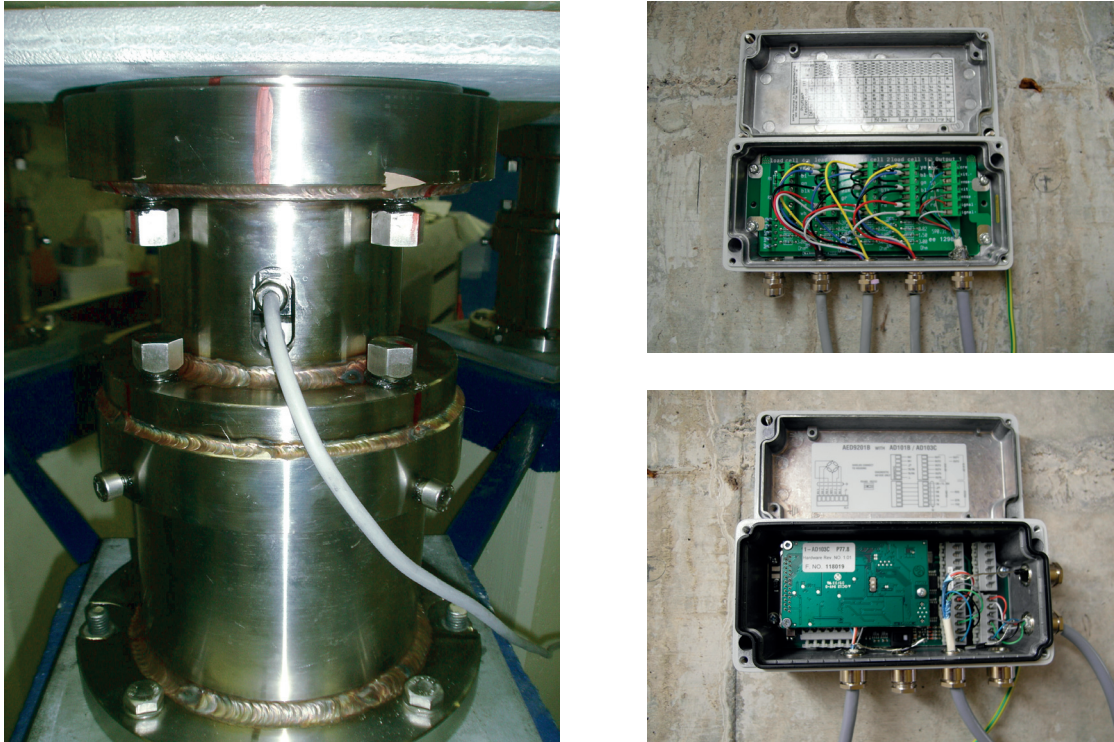


Figure A.3: The casing containing the load cell (left) allows to unload the cell during intervention inside the lysimeter and to finely adjust the position of the tank on the pillars. A junction box (VKK1-4, HBM, Germany) and a digital transducer (AED9201B, HBM Germany) are shown on the top and bottom right respectively.

The weighing system of the lysimeter plant (6 lysimeter tanks) is centralized on a single data acquisition system. Each lysimeter has three pods equipped with a one ring torsion load cell (RTNC3/2.2T, HBM, Germany) with a nominal value of 2.2 metric tons each (6.6 tons total). The load is measured by the change in tension induced by a deformation of a resistive membrane (wheatstone bridge principle). The electric signals of the three load cells of one unit are summed up in the junction box (VKK1-4, HBM). The junction box transmits the additive signal to an analogic-digital transducer (AED9201B, HBM). The A/D transducers of each lysimeter are connected in series, such as the first A/D transducer transmits its digital signal (a data bus containing the measurement reading and all setting parameters of this unit) to the next A/D transducer, which adds its own signal to the bus, and so on for the six units. Note that power supply can also be distributed among the transducer similarly, however one power supply plug (18...30V) cannot supply more than 3 units. The bus containing the data of the six lysimeters is transmitted to a computer by an interface convertor to RS-232 (SC232/422B, HBM) and can be read either by the dedicated software (AED\_Panel32) from HBM or by any custom program decoding the bus (the structure of the bus is provided by the manufacturer).

## Appendix A. Details of the lysimeter experiment

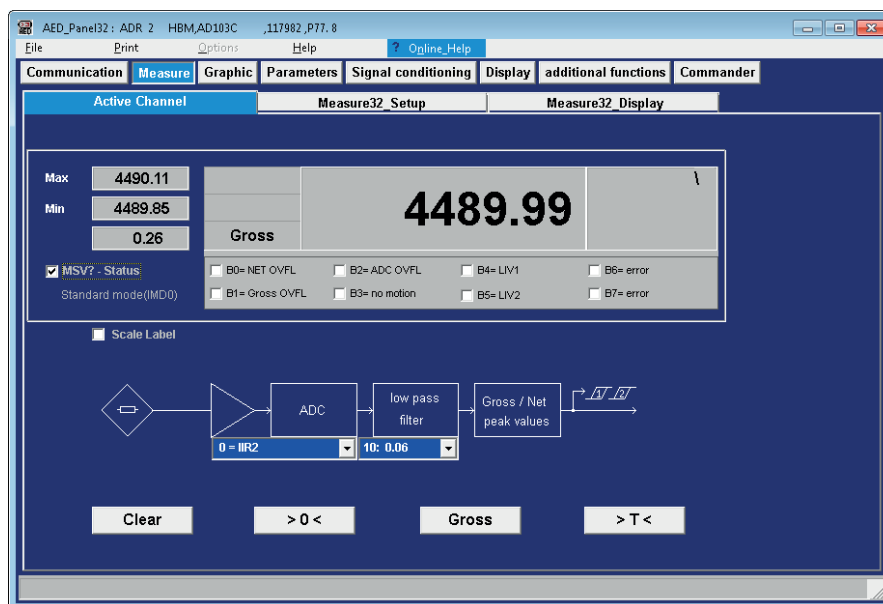


Figure A.4: Overview of AED\_Panel32 software (HBM, Germany) for the programming, monitoring and data acquisition of the load cells.

Table A.1: Relevant parameters for the lysimeter load cells. The parameters not detailed here are deactivated or are set to 0-value. For a detailed description of the parameters, refer the the AED manual from HBM.

<b>Communication</b>		
Address	ADR	2
Baudrate	BDR	28400
Output Format	COF	8
Terminator Execution	TEX	172
<b>Filtering and measurement rate</b>		
High Speed Mode	HSM	0
Filter Mode	FMD	0
Digital Low Pass Filter	ASF	10
Internal Conversion Rate	ICR	7
<b>Calibration and A/E conversion</b>		
Gross/Net	TAS	1
Tare Value	TAV	0
Nominal Output Value	NOV	542977
Resolution	RSN	1
Decimal Point	DCM	2
Multirange Switch Point	MRA	0
Calibration Weight	CWT	1000000
Dead Load Weight	LDW	46801
Nominal Load Weight	LWT	1215522
Internal Zero Adjust	SZA	33
Internal Fullscale Adjust	SFA	820165

### Important remark regarding load cells calibration

The system has a resolution of 1'000'000 digits. Theoretically, an unloaded array of load cells (in this case, an array of three 2.2T-load cells) outputs a 0-value, and a 1'000'000'000-value when loaded at the nominal value (6.6 metric tons). A factory calibration is performed by the manufacturer and given in the SZA and SFA parameters (see Table A.1). These parameters represent the output value (in "digits" unit) unloaded and at the nominal value respectively. However, as most of the HBM products have an output range of 0...2mV/V, **the SFA value provided corresponds to the digital output at 2mV/V, even if the load cells used here have an maximal output range of 2.85mV/V**. Therefore, when a physical calibration cannot be performed (required a loading up to the nominal value, or at least 80% provide an accurate calibration curve), an electronic calibration (based on the factory parameters) is required, but one has to account for the difference in the voltage range. Calibration can be performed in different ways, the procedure used here is detailed below:

SZA	33
SFA <sub>2mV/V</sub>	820'165
SFA <sub>2.85mV/V</sub>	$(820'165 - 33) / (2 - 0) \cdot 2.85 = 1'168'721$
LDW	46'801 (reading before calibration of the dead load)
LWT	$1'168'721 + 46'801 = 1'215'522$
NOV	$(1'000'000 / 1'215'522) \cdot 660000 = 542977$

One should refer to the documentation provided by HBM for further details.

### A.3 Willow development



(a) 24 April 2013



(b) 09 September 2013



(c) 26 April 2014



(d) 15 June 2014

Figure A.5: Pictures of the development stages of the willow between 2013 and 2014.



# B FDR installation and soil specific calibration

## B.1 Description of the equipment

An array of FDR (Frequency Domain Reflectometry) probes (5TM, Decagon Devices Inc., USA) was installed in the lysimeter in order to provide information about the distribution of water within the column, as the overall water content is measured by the weighing system. Four depths (25, 75, 125 and 175 cm) were equipped with three FDR probes each, equally distributed radially at about 30 cm from the center. As the volume of influence of the 5TM is rather small (0.3 L), having multiple probes per depth allows to average the reading of all probes and increase the representativeness. It also serves as a backup if a probe fails, as no intervention is possible.

The 5TM supplies a 70 MHz oscillating wave to the prongs that charges accordingly to the dielectric permittivity of the surrounding medium, which is proportional to the soil volumetric water content. The Topp equation (*Topp et al.*, 1980) has been widely used a generic equation to convert the measured dielectric constant into a volumetric water content. It usually provides appropriate results for a wide range of mineral soil, but as the reconstituted soil used to fill the lysimeter is homogeneous, it has been preferred to calculate a specific calibration curve to increase the accuracy of the measurements.

Each probe encompasses a microprocessor that measures the charge and the temperature and output digital values, either according to the Serial (TTL) or SDI-12 protocol. The latter has been chosen, as it allows the combination of the signals of multiple probes into a one data bus, which can be read by a single digital port on most of the datalogger (here a CR800, Campbell Scientific, USA). A junction bus with jack connectors has been designed to facilitate the connection of the 12 probes and allow a rapid identification of a potential probe failure (which can shut down the entire array).

## Appendix B. FDR installation and soil specific calibration

---



Figure B.1: Installation of the FDR probes in the lysimeter, upper depth (25 cm).

### B.2 Calibration procedure

The same soil as in the lysimeter was used for the calibration procedure, together with eight 5TM probes connected to a CR800 datalogger (Campbell Scientific, USA) with RS232 communication protocol to a laptop.

The experiment consists in filling a certain amount of soil with a known water content, then measure the dielectric permittivity with each of the 8 probes, add water and measure again, and repeat the procedure until soil saturation. The 8 probes provide a fair amount of measurement replicates, and the entire calibration procedure was reproduced 4 times.

The procedure applied is described below:

1. Take the soil and let it dry in an oven, according to the standard procedures: 105°C for 24-36 hours.
2. Take a can, big enough to allow complete immersion of the probe, the one I used is 12 cm of diameter and 20 cm high, and weigh it.
3. Fix a certain height in the can, and measure the corresponding volume ( $V_{tot}$ ).
4. Fill the can with the soil, until it reaches the fixed height. During this procedure is important to pack the soil, make it as similar as possible to the soil in the lysimeter (soil density may influence the dielectric permittivity), then weigh the soil.
5. Take the soil moisture probes, and measure one by one the dielectric permittivity of dry soil.

## B.2. Calibration procedure

---

6. Given an approximation of the volume of void of 40%, the goal is to fill the void with water in different steps. For example the steps could be  $PWC = 0 - 5 - 10 - 15 - 20 - 25 - 30 - 35 - 40\%$  of water. This corresponds to a water weight (WW) of:

$$WW = \frac{PWC}{100} V_{tot}.$$

Now we can calculate the real volumetric water content (RVWC):

$$RVWC = \frac{WW}{\rho_w} \cdot \frac{1}{V_{tot}}.$$

7. Take a cylinder and fill it with the correct first-step weight of distilled water.
8. Mix the weighted water with the soil, with the help of a small shovel, then pack again the soil.
9. Measure the dielectric permittivity with each probe one by one, for a sufficient time.
10. Now add water until reaching the second step and repeat steps from 7 to 9.
11. When the first sample is completely saturated, repeat the whole procedure from 1 to 10 until the defined amount of replicated samples is reached.
12. All the data are now collected, the calibration function can be obtained by a simple third order interpolation of the data acquired.

A third-order polynomial has been fitted on the calibration data using the least square approach, and gives:

$$RVWC = 4.6 \cdot 10^{-6} \epsilon_a^3 - 4.8 \cdot 10^{-4} \epsilon_a^2 + 3.4 \cdot 10^{-2} \epsilon_a - 0.11,$$

with a coefficient of determination  $R^2 = 0.973$ . This calibration curve was used to estimate the local water content of the lysimeter.

## Appendix B. FDR installation and soil specific calibration

---

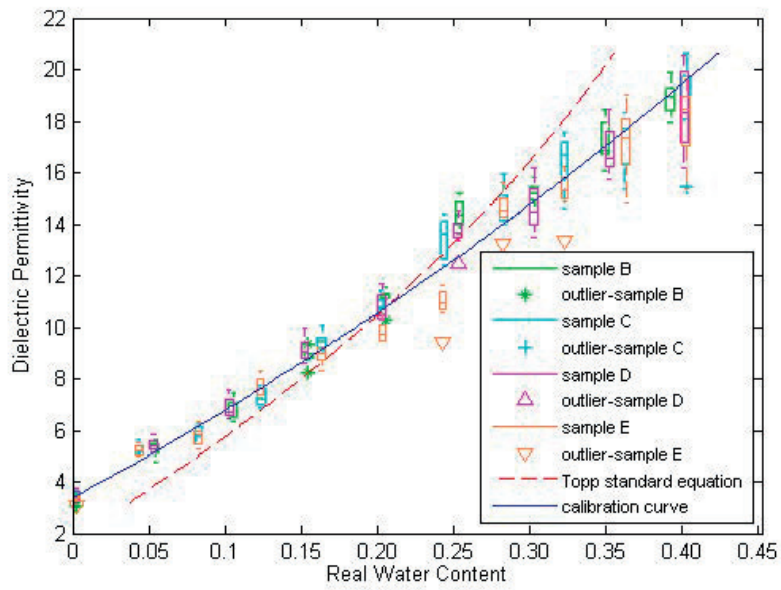


Figure B.2: Soil-specific calibration curve obtained with 8 independent measurements (8 probes) and 4 soil samples (B-E). The Topp equation is given for reference.

# C Lysimeter discharge flow measurement and sampling details

## C.1 Description of the discharge device

The lysimeter discharge is collected in a tipping bucket (Casella Measurement, UK). The reed switch sends a signal to a acquisition system (see below) at every tipping (~8 mL) in order to calculate the flow rate. The water of the runnel flows to a solenoid electro-valve (SMC VX3344M, Switzerland) which guides the water either to the sink or to a fraction collector (FRAC-100, Amersham Biosciences AB, Sweden). The position of the valve is also controlled by the acquisition system. When a tension of 24V is maintained, the valve switches to the fraction collector. A bottle change of the fraction collector is operated after a TTL impulse of 50ms-width is received by the acquisition system.

The acquisition system is based on a CompactDAQ chassis (cDAQ-9174) from National Instruments™ with USB connection. Three modules are fitted in the chassis: a TTL digital Input/Output Module (NI 9401) for reading the impulses of the tipping bucket's reed switch, a Universal Sink/Source Digital Input module (NI 9435) which controls the fraction collector with 2 signals (operable and feed) and a 30VDC relay module (NI 9481) which supplies the electro-valve.

The acquisition system is controlled by a custom-made program created with LabView (National Instruments™). Two log files are written by the program, one containing each the start and end time of each sample taken, the other recording the time and volume of each tipping. The interface allows the user to set the characteristics of the tipping bucket (tipping volume) and of the fraction collector (number of samples and sample volume). Flow-paced and constant time-paced sampling can be chosen. A mode only logging the discharge rate (no sampling) is also available. The interface window provides the controls and useful reading of the current measurements, as shown in Figure C.1.

## Appendix C. Lysimeter discharge flow measurement and sampling details

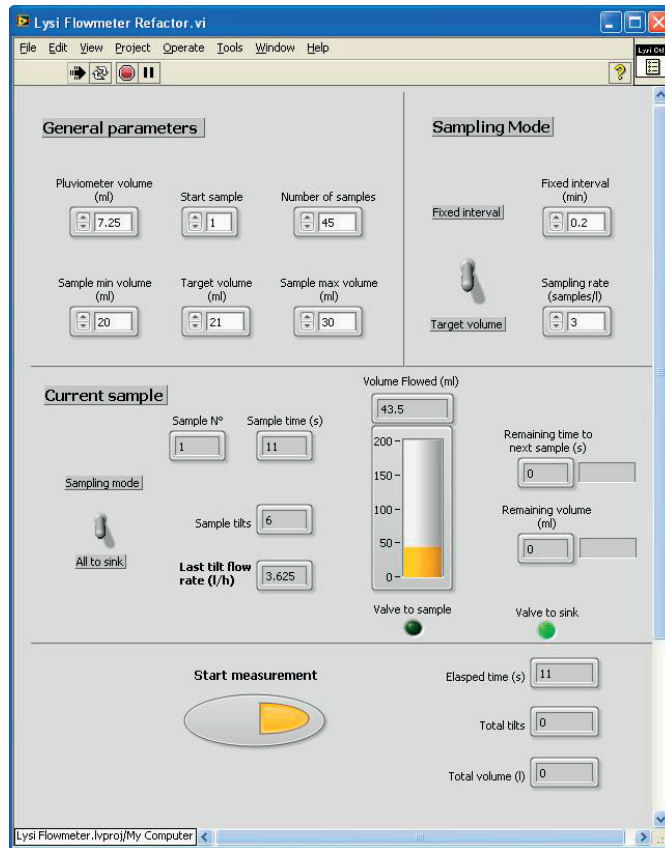


Figure C.1: Programming interface of the discharge measurement and sampling.

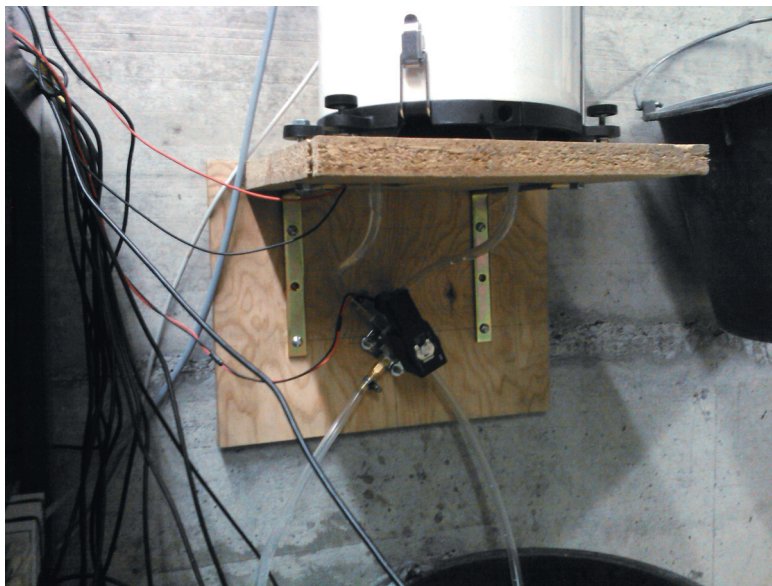


Figure C.2: Discharge measurement and sampling system. The tipping bucket on top discharges the water to a electro-valve, distributing it either to the sink or to a fraction collector.

## C.2 Soil water sampling

Samples of soil water are collected by an array of 9 ceramic porous cups placed inside the lysimeter during the filling (3 porous cups per depth, 3 depths monitored at 50, 100 and 150cm). A vacuum of about -0.6 bar is applied during about 4-5 hours (depending on the soil moisture) to draw a sufficient volume of water retained in the soil pores. The sampling setup is described in Figure C.3. Each porous cup is connected to the air tubing network and water tubing network. The polyamide tubes enter in the porous cup through the rubber cap of the cup, which ensure an air tight connection. The tube of the water network goes to the bottom of the porous cup (which is installed in the ground with a 30°-tilt), and the tube of the air network stops a few millimeters below the cap, in order to avoid aspiration of water. The sampling procedure described below allows an efficient simultaneous samples collection under controlled vacuum:

1. The valves W1,...,9 and A2 are closed. The valve A1 is open, the vacuum pump is switched on the pressure controller is set to maintain a vacuum of -0.6 bar ( $\pm 5\%$ ) by the commutation of a valve that cut the connection to the vacuum pump when the instruction is fulfilled. The vacuum is therefore applied in all porous cups and eventual leaks are compensated automatically. The safety vask ensures that if a porous cups is filled by water before passing to step 2, the water that would be sucked up in the air tubing does not penetrate in the sampling controller and in the vacuum pump;
2. After 4-5 hours, the valve A1 is closed, and the valve A3 is slowly opened to reestablish atmospheric pressure in the porous cups. The valve A2 is open to apply a vacuum in the sampling bottles. By the successive opening of the valves W1 to W9, the water that has been drawn through the ceramic during step 1 and which stays at the bottom of the porous cups is collected in the respective sampling bottles without any cross-contamination. The valves are left open sufficiently long to ensure a complete emptying of the porous cups and of the water tubes.
3. All valves are closed, the vacuum pump and the pressure controller are switched off. The samples are collected, filtered and conditioned.

### Appendix C. Lysimeter discharge flow measurement and sampling details

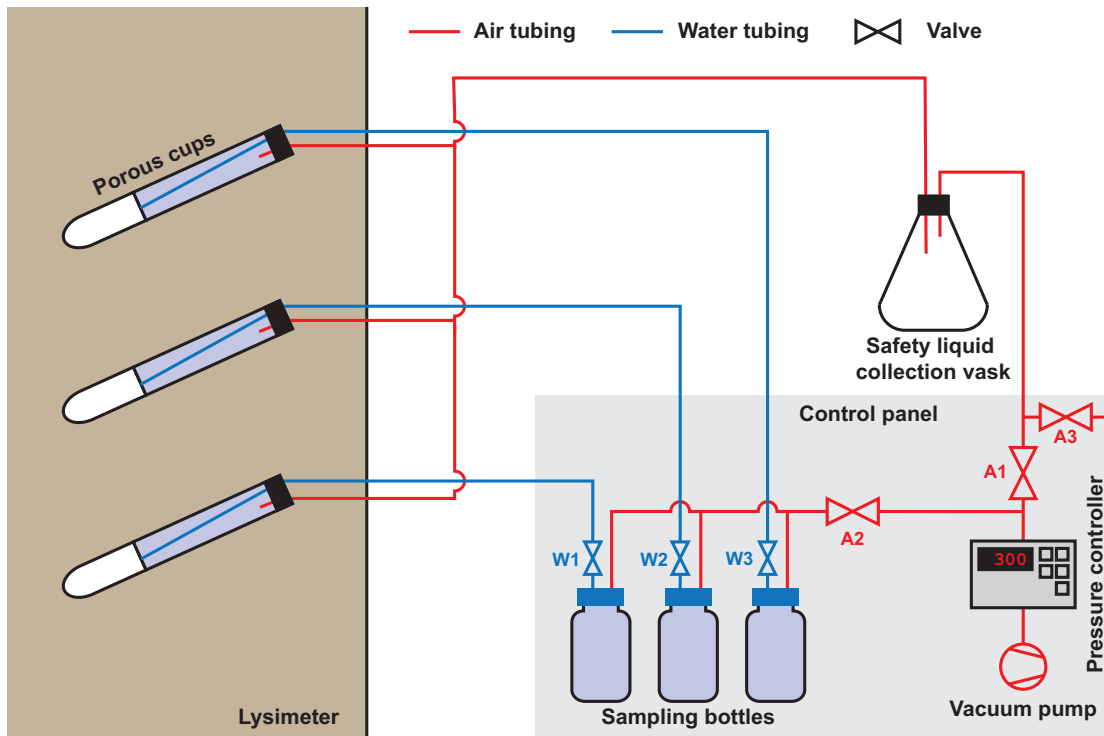


Figure C.3: Schematic illustration of the soil water sampling system. Note that for clarity, only three porous cups are represented.



## D Experimental details on the leaching test

A leaching test using the fluorobenzoic acids (FBAs) has been performed in a 50cm-long stainless steel column containing the same soil mixture as in the lysimeter. This experiment is described in section 2.2.6. Further details regarding the experimental design are given here.

At the bottom, the column is fitted with a perforated stainless steel plate topped by a mesh (openings width of 0.5 mm) which retains the medium in place. The cylindrical bottom part of the column is terminated with a port. A tube connects the bottom port to a flow-control jar that acts like a siphon and allows to regulate the flow as its height can be adjusted along a retort stand. The outlet of the flow-control jar flows by gravity to a solenoid electro-valve (VX3224, SMC, Switzerland) which guides the flow either to a fraction collector (FRAC-100, Amersham Biosciences, Sweden) fitted with a 45-bottles tourniquet or the a discharge container. The container is placed on an logging integrative balance (Ohaus Navigator XL, USA) which allows an approximate measurement of the flow rate. A custom-made microcontroller system controls the sampling, which is set to generate one 20 mL composite sample every 2 hours (resulting from 2x10 mL samples every hour). An Arduino Uno board (Italy) with embedded timer switches the valve to the fraction collector during the desired time by the actuation of a PCB relay and sends a TTL-pulse to the fraction collector to prompt an incremental tube change. Samples conditioning and analyses are identical to the lysimeter samples (see sections 2.2.3 and 2.2.4). A webcam was installed in order to allow a remote control of the proper operation of the sampling system.

The water input flux is induced by a constant 1 cm (500 mL) overflow on top of the sand column. The overflow is maintained by a compensation system: an metallic rod whose extremity is adjusted at 1 cm above the sand surface is connected to a inverse timed relay and a power supply. As the relay is also connected to the metallic casing of the column, electrical current can flow when water touches the metallic rod, thereby closing the circuit. When the water level decreases, the electrical circuit is opened because the rod is not any more connected to the column. This activates the relay and opens an electrovalve during a designed time, allowing a water tank placed above the column to discharge water and reestablish the overflow volume.

## Appendix D. Experimental details on the leaching test

---

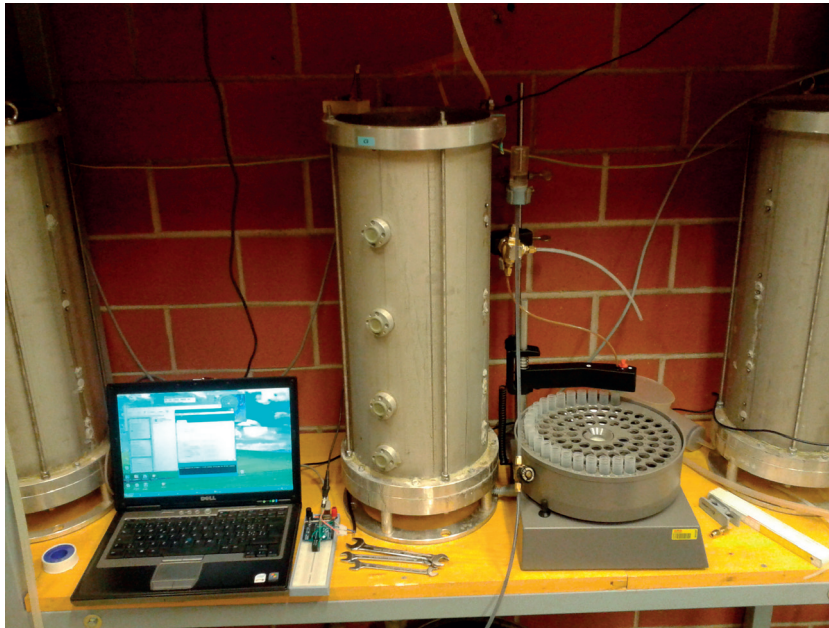


Figure D.1: Overview of the column experiment set-up.

The tracers were injected in sequential pulses of a solution containing about  $10 \text{ mg L}^{-1}$  of each of the five tracers. In order to avoid disrupting the constant flow rate, the overflow regulation system was disconnected during the tracer injection, and the overflow deficit was manually compensated by the injection of the tracer solution. Eight injections of 25-80 mL of solution were done during a period of less than 5 hours, totalizing a solution volume of 526 mL.

# **E Development of a wireless controller for flexible sampling strategies based on real-time flow monitoring**

## **E.1 Context**

- Assessing stream water quality involves point sampling, as most substances cannot be measured on-line;
- Diffuse applications of pesticides are flushed by rainfall and enter the hydrological cycle;
- The transport of substances in a hydrological system is episodic, controlled by the climatic forcing; this results in highly variable concentration in receiving surface waters;
- Substance concentrations dynamics in surface waters is usually correlated with discharge dynamics;
- As most of the substance loads occurs during storm event, constant time-paced sampling may misestimate the total loads;
- Flow-paced sampling schemes proposed by water samplers require the coupling with expensive external sensors from the same manufacturer;
- Usual flow-paced sampling schemes proposed by water samplers does not predict storm flow duration and may miss the end of large storm's recession if no more empty bottle is available.

## **E.2 Prototype concept**

- Develop a controller for flexible user-defined and site-specific sampling schemes compatible with common automatic samplers (TTL, SDI-12, etc.);
- Minimize total cost in order to favor the increase of sampling sites instead of high precision flow measurements with expensive sensors;

## Appendix E. Development of a wireless controller for flexible sampling strategies based on real-time flow monitoring

- Implementation of an energy-saving "stand-by" state during dry period and wireless warning system to inform the user of a new sampling event upon flow-triggered wake-up;
- Hydrograph-specific sampling scheme, auto-adaptive in case of multiple discharge peaks;
- Real-time server upload of the data and easy access from a remote computer or mobile device;
- Low-cost, light weight and easy set-up, manipulation, deployment and maintenance.

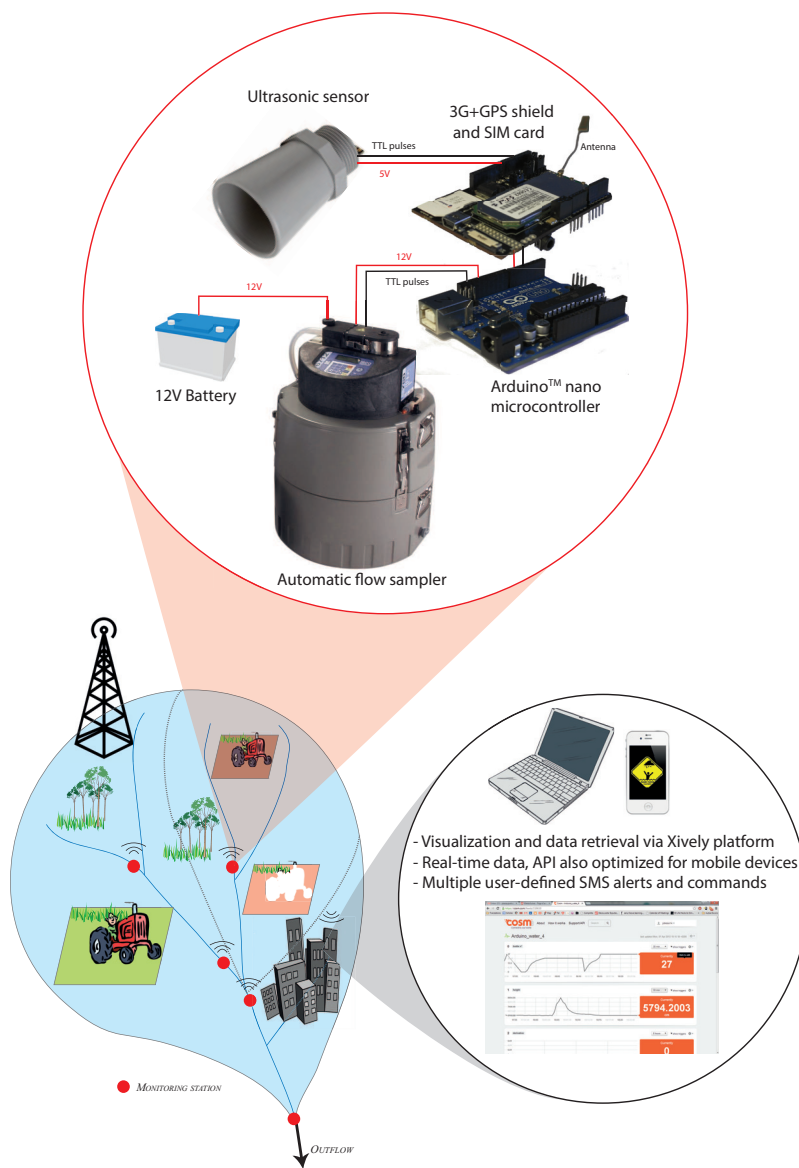


Figure E.1: Scheme of the sampling system.

### E.3 Sampling model

The sampling scheme is based on four different states, depending on the hydrologic conditions measured by any kind of discharge or water level gage. In case of a water level gage (e.g. ultrasonic or pressure sensor), the site-specific rating curve has to be defined in the program. The analogical signal of the gage is read and interpreted by the microcontroller. Recent discharge history is kept in the memory in order to define the actual state and predict the sampling time of the next sample. A log of the discharge rates can be kept on a storage entity (e.g. sd card) or transmit to a remote data server at regular intervals (allowing online remote data visualization).

**Stand-by** This case is active when discharge flow is low (e.g. baseflow), i.e. before a storm event. All sampling bottles are empty. The sampler is in waiting mode, and the sampling controller is in a low-energy mode, only monitoring and recording the discharge rate (data transmission to the server can be activated upon request). The switch to the next state `rising limb` is triggered when the discharge exceeds of a user-defined discharge threshold or discharge derivative threshold (Figure E.2). Note that sampling can also be started manually or by sending a SMS-command.

**Rising limb** This state is active during the early period of a storm event, during which the discharge rate increased rapidly. The controller sends a sampling command (e.g. TTL on the ISCO samplers) at regular, user-defined intervals. This triggers the taking of a sample, which detailed procedure (rinsing, purge, etc.) has to be set on the sampler. The controller switches to the next state (`recession`) once the peak flow has been observed. A small lag is observed between the actual time when the peak flow occurred and the time when it is determined, because the system waits that the discharge has consistently decreased (e.g. when the discharge has decreased by 5% compared to the maximal recorded value). This retroactively ensures that the peak flow has been reached at  $t_p$ . The controller then switches to `recession` mode.

**Recession** As the peak flow  $Q_p$  has been reached at time  $t_p$ , a recession model is applied in order to predict the shape and the duration of the recession. The model used is based on the non-linear equation of *Brutsaert and Nieber* (1977):

$$Q(t) = Q_p(1 + c \cdot t)^n, \quad (\text{E.1})$$

with  $Q_0$  the peak flow,  $c$  and  $n$  the model parameters. The parameters  $c$  and  $n$  have to be determined *a priori* based on discharge records for each control section and specify in the program. The end of the recession is reached when the discharge falls below a lower threshold, e.g.:

$$Q = 0.05 \cdot Q_0. \quad (\text{E.2})$$

From Eqs. E.1 and E.2, the duration of the recession can be estimated. The available

## Appendix E. Development of a wireless controller for flexible sampling strategies based on real-time flow monitoring

empty bottles (those left after the sampling during the rising limb) are then distributed over the entire recession duration (at regular flow-volume or time intervals) in order to be able to sample the whole recession. The user can decide to keep "emergency" empty bottles in case of wrong estimation of the recession time or the arrival of another storm before the end of the recession.

During the recession, the controller constantly recalculates the current state of the recession and adapt the forecasted sampling times. If a consistent discharge increase is observed, the system switches back to rising limb mode. The number of available bottles is always updated.

Once the end of the recession has been reached, the system switches to the next mode end of program, and sends an SMS-alert to inform that a sampling procedure has been completed. Note that SMS-alerts can also be configured to inform whenever a sample has been taken, when a change of state is observed or if multiple flow peaks have been measured.

End of program The system goes back a dormant state similar to stand-by except that the system cannot be waken up by arriving storm events.

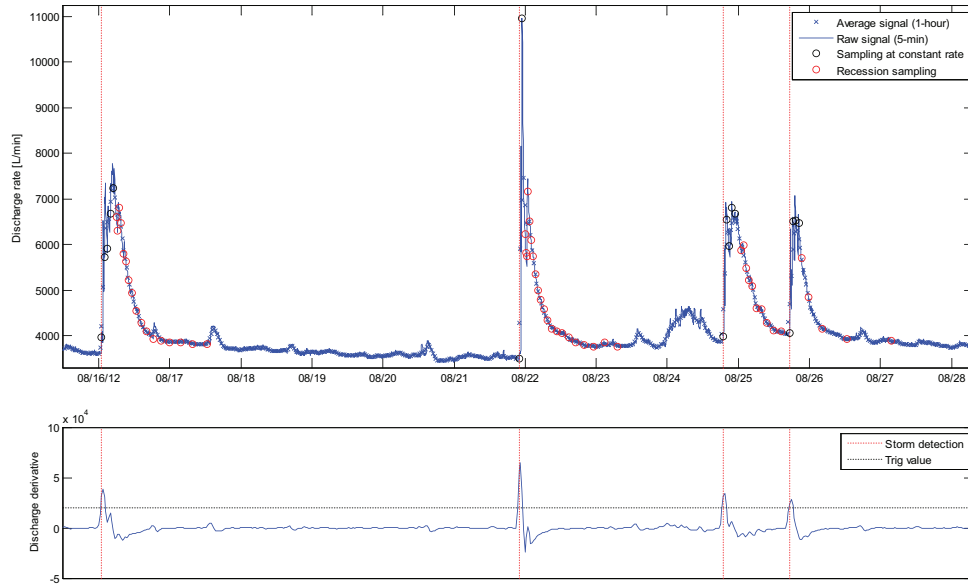


Figure E.2: Example of a sampling procedure. A storm event is detected when a trigger value of the discharge derivative is reached (bottom panel). Sampling at constant rate follows during the rising limb, and switches to recession-specific mode once the discharge peak has been observed. Note the larger sampling intervals during the last storm. The two last storms are considered as a multiple peaks event, i.e. the operator does not have the time to replace empty bottles in the sampler.

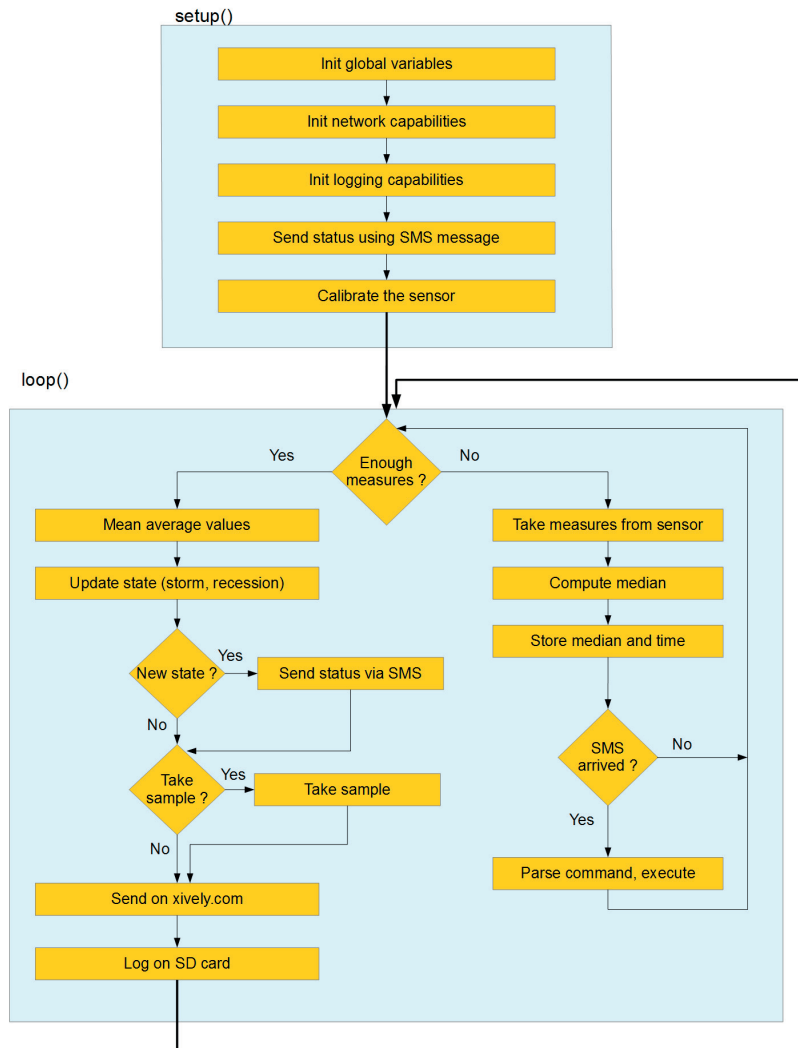


Figure E.3: Workflow of the microcontroller program.

## E.4 Technical equipment

- Microcontroller: Arduino Uno or Arduino Due
- Data logging: Assembled data logging shield from Adafruit
- Communication: 3G/GPRS shield for Arduino and GPRS/GSM antenna
- Water level gage: MaxBotix Ultrasonic Precision Rangefinder (MB7389 HRXL – MaxSonar-WRMT)

**Appendix E. Development of a wireless controller for flexible sampling strategies based on real-time flow monitoring**

---

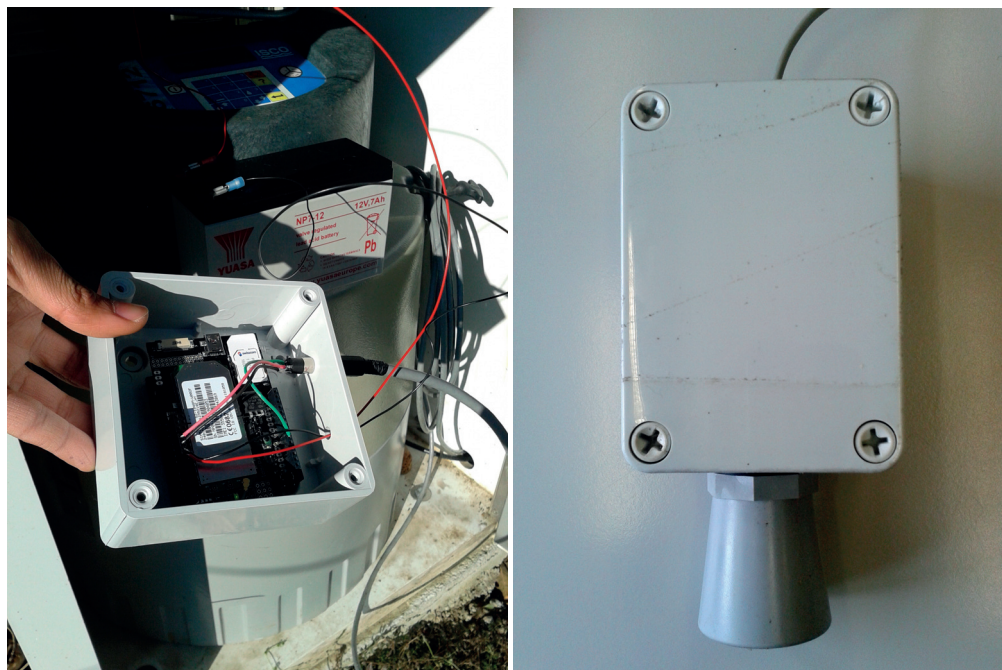


Figure E.4: Assembled sampling controller and ISCO sampler in the background (left) and mounted ultrasonic sensor (right).



## Bibliography

- Abdou, H. M., and M. Flury (2004), Simulation of water flow and solute transport in free-drainage lysimeters and field soils with heterogeneous structures, *European Journal of Soil Science*, 55(2), 229–241.
- Abdulkabir, M. O., K. J. Beven, and A. D. Reeves (1996), Flow separation in undisturbed soil using multiple anionic tracer. part 3: unsteady core-scale infiltration experiments, *Hydrological Processes*, 10(11), 1467–1482.
- Ali, M., A. Fiori, and D. Russo (2014), A comparison of travel-time based catchment transport models, with application to numerical experiments, *Journal of Hydrology*, 511, 605–618.
- Araguás-Araguás, L., K. Froehlich, and K. Rozanski (2000), Deuterium and oxygen-18 isotope composition of precipitation and atmospheric moisture, *Hydrological Processes*, 14(8), 1341–1355.
- Arnold, J. G., P. M. Allen, and G. Bernhardt (1993), A comprehensive surface-groundwater flow model, *Journal of Hydrology*, 142(1–4), 47–69.
- Bariac, T., E. Deleens, A. Gerbaud, M. Andre, and A. Mariotti (1991), La composition isotopique (18O,2H) de la vapeur d'eau transpirée: Etude en conditions asservies, *Geochimica et Cosmochimica Acta*, 55(11), 3391–3402.
- Beeson, R. C. (2011), Weighing lysimeter systems for quantifying water use and studies of controlled water stress for crops grown in low bulk density substrates, *Agricultural Water Management*, 98(6), 967–976.
- Benettin, P., Y. van der Velde, S. E. A. T. M. van der Zee, A. Rinaldo, and G. Botter (2013a), Chloride circulation in a lowland catchment and the formulation of transport by travel time distributions, *Water Resources Research*, 49(8), 4619–4632.
- Benettin, P., A. Rinaldo, and G. Botter (2013b), Kinematics of age mixing in advection-dispersion models, *Water Resources Research*, 49(12), 8539–8551.
- Bergström, L. (1990), Use of lysimeters to estimate leaching of pesticides in agricultural soils, *Environmental Pollution*, 67, 325–347.

## Bibliography

---

- Bersier, A. (1952), Carte géologique de la Suisse 1:25'000: 27 Jorat (CN 1223).
- Bertuzzo, E., M. Thomet, G. Botter, and A. Rinaldo (2013), Catchment-scale herbicides transport: Theory and application, *Advances in Water Resources*, 52, 232–242.
- Beven, K. (1981), Kinematic subsurface stormflow, *Water Resources Research*, 17(5), 1419–1424.
- Beven, K. (2012), *Rainfall-runoff modelling: the primer (second edition)*, 457 pp., John Wiley & Sons, Ltd, Chichester, West Sussex.
- Beven, K., and P. Germann (1982), Macropores and water flow in soils, *Water Resources Research*, 18(5), 1311–1325.
- Birkel, C., D. Tetzlaff, S. M. Dunn, and C. Soulsby (2011), Using time domain and geographic source tracers to conceptualize streamflow generation processes in lumped rainfall-runoff models, *Water Resources Research*, 47.
- Birkel, C., C. Soulsby, D. Tetzlaff, S. Dunn, and L. Spezia (2012), High-frequency storm event isotope sampling reveals time-variant transit time distributions and influence of diurnal cycles, *Hydrological Processes*, 26(2), 308–316.
- Botter, G. (2012), Catchment mixing processes and travel time distributions, *Water Resources Research*, 48.
- Botter, G., E. Bertuzzo, A. Bellin, and A. Rinaldo (2005), On the Lagrangian formulations of reactive solute transport in the hydrologic response, *Water Resources Research*, 41(4).
- Botter, G., T. Settin, M. Marani, and A. Rinaldo (2006), A stochastic model of nitrate transport and cycling at basin scale, *Water Resources Research*, 42(4).
- Botter, G., E. Milan, E. Bertuzzo, S. Zanardo, M. Marani, and A. Rinaldo (2009), Inferences from catchment-scale tracer circulation experiments, *Journal of Hydrology*, 369(3–4), 368–380.
- Botter, G., E. Bertuzzo, and A. Rinaldo (2010), Transport in the hydrologic response: Travel time distributions, soil moisture dynamics, and the old water paradox, *Water Resources Research*, 46(3), W03,514.
- Botter, G., E. Bertuzzo, and A. Rinaldo (2011), Catchment residence and travel time distributions: The master equation, *Geophys. Res. Lett.*, 38(11), L11,403.
- Bowman, R. S. (1984), Evaluation of some new tracers for soil water studies, *Soil Sci. Soc. Am. J.*, 48(5), 987–993.
- Bowman, R. S., and J. F. Gibbens (1992), Difluorobenzoates as nonreactive tracers in soil and ground water, *Ground Water*, 30(1), 8–14.
- Bowman, R. S., J. Schroeder, R. Bulusu, M. Remmenga, and R. Heightman (1997), Plant toxicity and plant uptake of fluorobenzoate and bromide water tracers, *J. Environ. Qual.*, 26(5), 1292–1299.

- Broxton, P. D., P. A. Troch, and S. W. Lyon (2009), On the role of aspect to quantify water transit times in small mountainous catchments, *Water Resources Research*, 45.
- Brusseau, M. L., P. S. C. Rao, and R. W. Gillham (1989), Sorption nonideality during organic contaminant transport in porous media, *Critical Reviews in Environmental Control*, 19(1), 33–99.
- Brutsaert, W., and J. L. Nieber (1977), Regionalized drought flow hydrographs from a mature glaciated plateau, *Water Resources Research*, 13(3), 637–643.
- Bulusu, R. (1995), *Plant Uptake of Fluorobenzoates Used as Soil and Groundwater Tracers*, New Mexico Institute of Mining and Technology.
- Carraro, L. (2014), Inferring age mixing processes and travel time distributions from a lysimeter experiment, Master thesis, Università Degli Studi Di Padova, Padova, Italy.
- Chèvre, N., C. Loeppe, H. Singer, C. Stamm, K. Fenner, and B. I. Escher (2006), Including mixtures in the determination of water quality criteria for herbicides in surface water, *Environmental Science & Technology*, 40(2), 426–435.
- Chèvre, N., C. Loepfe, K. Fenner, H. Singer, B. Escher, and C. Stamm (2007), Pesticides dans les eaux superficielles de suisse. critères de qualité basés sur les effets des substances., *Gas Wasser und Gewässer*, 7, 529–539.
- Chèvre, N., E. Maillard, C. Loepfe, and K. Becker-van Slooten (2008), Determination of water quality standards for chemical mixtures: Extension of a methodology developed for herbicides to a group of insecticides and a group of pharmaceuticals, *Ecotoxicology and Environmental Safety*, 71(3), 740–748.
- Christiansen, J. S., M. Thorsen, T. Clausen, S. Hansen, and J. C. Refsgaard (2004), Modelling of macropore flow and transport processes at catchment scale, *Journal of Hydrology*, 299(1–2), 136–158.
- Clay, A., C. Bradley, A. J. Gerrard, and M. J. Leng (2004), Using stable isotopes of water to infer wetland hydrological dynamics, *Hydrology and Earth System Sciences*, 8(6), 1164–1173.
- Commandeur, L. C. M., and J. R. Parsons (1990), Degradation of halogenated aromatic compounds, *Biodegradation*, 1(2-3), 207–220.
- Craig, H. (1961), Isotopic variations in meteoric waters, *Science*, 133(3465), 1702–1703.
- Craig, H., and L. Gordon (1965), Stable isotopes in oceanographic studies and paleotemperatures, *Tongiorgi, (V. Lischi e Figli, Pisa, 1965)*, pp. 9–130.
- Croci, F. (2013), Biophysical controls on evapotranspiration: numerical models and experimental observations, Master thesis, Università Degli Studi Di Padova, Padova, Italy.

## Bibliography

---

- Cvetkovic, V., C. Carstens, J.-O. Selroos, and G. Destouni (2012), Water and solute transport along hydrological pathways, *Water Resources Research*, 48(6), W06,537.
- Dagan, G. (1988), *Flow and Transport in Porous Formations*, 257 pp., Springer-Verlag, New York.
- Dalian, O., and Z. Ronen (2001), Analytical procedure for simultaneous use of seven fluorobenzoates in multitracer tests, *Ground Water*, 39(3), 366–370.
- Dansgaard, W. (1964), Stable isotopes in precipitation, *Tellus*, 16(4), 436–468.
- Darracq, A., G. Destouni, K. Persson, C. Prieto, and J. Jarsjö (2010), Quantification of advective solute travel times and mass transport through hydrological catchments, *Environmental Fluid Mechanics*, 10(1-2), 103–120.
- Davies, J., K. Beven, A. Rodhe, L. Nyberg, and K. Bishop (2013), Integrated modeling of flow and residence times at the catchment scale with multiple interacting pathways, *Water Resources Research*, 49(8), 4738–4750.
- Davis, S. N., G. M. Thompson, H. W. Bentley, and G. Stiles (1980), Ground-water tracers — a short review, *Ground Water*, 18(1), 14–23.
- Dawson, T. E., and J. R. Ehleringer (1991), Streamside trees that do not use stream water, *Nature*, 350(6316), 335–337.
- Dawson, T. E., and J. R. Ehleringer (1993), Isotopic enrichment of water in the “woody” tissues of plants: implications for plant water source, water uptake, and other studies which use the stable isotopic composition of cellulose, *Geochimica et Cosmochimica Acta*, 57(14), 3487–3492.
- Deavers, K., T. Macek, U. Karlson, and S. Trapp (2010), Removal of 4-chlorobenzoic acid from spiked hydroponic solution by willow trees (*Salix viminalis*), *Environmental Science and Pollution Research*, 17(7), 1355–1361.
- Dincer, T. (1968), Use of oxygen 18 and deuterium concentrations in water balance of lakes, *Water Resources Research*, 4(6), 1289–1306.
- Divine, C. E., and J. J. McDonnell (2005), The future of applied tracers in hydrogeology, *Hydrogeology Journal*, 13(1), 255–258.
- El-Sheekh, M. M., H. M. Kotkat, and O. H. E. Hammouda (1994), Effect of atrazine herbicide on growth, photosynthesis, protein synthesis, and fatty acid composition in the unicellular green alga *Chlorella kessleri*, *Ecotoxicology and Environmental Safety*, 29(3), 349–358.
- Fabre, G., J. Dugon, and R. Charles (2010), Pratiques phytosanitaires en grandes cultures de 1992 à 2004, *Tech. rep.*, AGRIDEA.

- Fahle, M., and O. Dietrich (2014), Estimation of evapotranspiration using diurnal groundwater level fluctuations: Comparison of different approaches with groundwater lysimeter data, *Water Resources Research*, pp. n/a–n/a.
- Fenicia, F., S. Wrede, D. Kavetski, L. Pfister, L. Hoffmann, H. H. G. Savenije, and J. J. McDonnell (2010), Assessing the impact of mixing assumptions on the estimation of streamwater mean residence time, *Hydrological Processes*, 24(12), 1730–1741.
- Fette, M., R. Kipfer, C. J. Schubert, E. Hoehn, and B. Wehrli (2005), Assessing river-groundwater exchange in the regulated Rhone River (Switzerland) using stable isotopes and geochemical tracers, *Applied Geochemistry*, 20(4), 701–712.
- Feyen, H., H. Wunderli, H. Wydler, and A. Papritz (1999), A tracer experiment to study flow paths of water in a forest soil, *Journal of Hydrology*, 225(3-4), 155–167.
- Fiori, A., and D. Russo (2008), Travel time distribution in a hillslope: Insight from numerical simulations, *Water Resources Research*, 44(12), W12,426.
- Flury, M. (1995), Transport of anions and herbicides in a loamy and a sandy field soil, *Water Resources Research*, 31(4), 823.
- Flury, M. (1996), Experimental evidence of transport of pesticides through field soils — a review, *J. Environ. Qual.*, 25(1), 25–45.
- Flury, M. (2003), Dyes as tracers for vadose zone hydrology, *Reviews of Geophysics*, 41(1), 1002.
- Flury, M., H. Flühler, W. A. Jury, and J. Leuenberger (1994), Susceptibility of soils to preferential flow of water: A field study, *Water Resources Research*, 30(7), 1945–1954.
- Flury, M., M. V. Yates, and W. A. Jury (1999), Numerical analysis of the effect of the lower boundary condition on solute transport in lysimeters, *Soil Sci. Soc. Am. J.*, 63(6), 1493–1499.
- Fontes, J. C., and R. Gonfiantini (1970), Composition isotopique et origine de la vapeur d'eau atmosphérique dans la région du lac Léman, *Earth and Planetary Science Letters*, 7(4), 325–329.
- Freitas, L. G., H. Singer, S. R. Müller, R. P. Schwarzenbach, and C. Stamm (2008), Source area effects on herbicide losses to surface waters — a case study in the Swiss Plateau, *Agriculture, Ecosystems & Environment*, 128(3), 177–184.
- Frey, M. P., M. K. Schneider, A. Dietzel, P. Reichert, and C. Stamm (2009), Predicting critical source areas for diffuse herbicide losses to surface waters: Role of connectivity and boundary conditions, *Journal of Hydrology*, 365(1–2), 23–36.
- Frisbee, M. D., J. L. Wilson, J. D. Gomez-Velez, F. M. Phillips, and A. R. Campbell (2013), Are we missing the tail (and the tale) of residence time distributions in watersheds?, *Geophysical Research Letters*, pp. n/a–n/a.

## Bibliography

---

- Galdiga, C. U., and T. Greibrokk (1998), Ultra-trace determination of fluorinated aromatic carboxylic acids in aqueous reservoir fluids using solid-phase extraction in combination with gas chromatography-mass spectrometry, *Journal of Chromatography A*, 793(2), 297–306.
- Gonfiantini, R. (1986), Environmental isotopes in lake studies, *Handbook of environmental isotope geochemistry*, 2, 113–168.
- Guidi, W., E. Piccioni, and E. Bonari (2008), Evapotranspiration and crop coefficient of poplar and willow short-rotation coppice used as vegetation filter, *Bioresource technology*, 99(11), 4832–4840.
- Haggerty, R., S. M. Wondzell, and M. A. Johnson (2002), Power-law residence time distribution in the hyporheic zone of a 2nd-order mountain stream, *Geophysical Research Letters*, 29(13).
- Harman, C. J. (2015), Time-variable transit time distributions and transport: Theory and application to storage-dependent transport of chloride in a watershed, *Water Resources Research*, 51(1), 1–30.
- Harman, C. J., and M. Kim (2014), An efficient tracer test for time-variable transit time distributions in periodic hydrodynamic systems, *Geophysical Research Letters*, 41(5), 1567–1575.
- Harman, C. J., P. S. C. Rao, N. B. Basu, G. S. McGrath, P. Kumar, and M. Sivapalan (2011), Climate, soil, and vegetation controls on the temporal variability of vadose zone transport, *Water Resources Research*, 47(1), W00J13.
- Heidbuchel, I., P. A. Troch, S. W. Lyon, and M. Weiler (2012), The master transit time distribution of variable flow systems, *Water Resources Research*, 48.
- Heidbüchel, I., P. A. Troch, and S. W. Lyon (2013), Separating physical and meteorological controls of variable transit times in zero-order catchments, *Water Resources Research*, 49(11), 7644–7657.
- Henderson, D. E., A. D. Reeves, K. J. Beven, and N. A. Chappell (1996), Flow separation in undisturbed soil using multiple anionic tracers. part 2. steady-state core-scale rainfall and return flows and determination of dispersion parameters, *Hydrological Processes*, 10(11), 1451–1465.
- Herbst, M., W. Fialkiewicz, T. Chen, T. Pütz, D. Thiéry, C. Mouvet, G. Vachaud, and H. Vereecken (2005), Intercomparison of flow and transport models applied to vertical drainage in cropped lysimeters, *Vadose Zone J.*, 4(2), 240–254.
- Horita, J., and D. J. Wesolowski (1994), Liquid-vapor fractionation of oxygen and hydrogen isotopes of water from the freezing to the critical temperature, *Geochimica et Cosmochimica Acta*, 58(16), 3425–3437.

- Hrachowitz, M., C. Soulsby, D. Tetzlaff, J. J. C. Dawson, S. M. Dunn, and I. A. Malcolm (2009a), Using long-term data sets to understand transit times in contrasting headwater catchments, *Journal of Hydrology*, 367(3–4), 237–248.
- Hrachowitz, M., C. Soulsby, D. Tetzlaff, J. J. C. Dawson, and I. A. Malcolm (2009b), Regionalization of transit time estimates in montane catchments by integrating landscape controls, *Water Resources Research*, 45.
- Hrachowitz, M., C. Soulsby, D. Tetzlaff, I. A. Malcolm, and G. Schoups (2010a), Gamma distribution models for transit time estimation in catchments: Physical interpretation of parameters and implications for time-variant transit time assessment, *Water Resources Research*, 46(10), W10,536.
- Hrachowitz, M., C. Soulsby, D. Tetzlaff, and M. Speed (2010b), Catchment transit times and landscape controls—does scale matter?, *Hydrological Processes*, 24(1), 117–125.
- Hrachowitz, M., C. Soulsby, D. Tetzlaff, and I. A. Malcolm (2011), Sensitivity of mean transit time estimates to model conditioning and data availability, *Hydrological Processes*, 25(6), 980–990.
- Hrachowitz, M., H. Savenije, T. A. Bogaard, D. Tetzlaff, and C. Soulsby (2013), What can flux tracking teach us about water age distribution patterns and their temporal dynamics?, *Hydrology and Earth System Sciences*, 17(2), 533–564.
- Hunt, R. J., D. P. Krabbenhoft, and M. P. Anderson (1996), Groundwater inflow measurements in wetland systems, *Water Resources Research*, 32(3), 495–507.
- Jasechko, S., Z. D. Sharp, J. J. Gibson, S. J. Birks, Y. Yi, and P. J. Fawcett (2013), Terrestrial water fluxes dominated by transpiration, *Nature*, 496(7445), 347–350.
- Jaynes, D. B. (1994), Evaluation of fluorobenzoate tracers in surface soils, *Ground Water*, 32(4), 532–538.
- Jeanbourquin, D., D. Sage, L. S. Nguyen, B. Schaeli, S. Kayal, D. A. Barry, and L. Rossi (2011), Flow measurements in sewer systems based on image analysis: automatic flow velocity algorithm., *Water Science and Technology*, 64(5), 1108–1114.
- Juhler, R. K., and A. P. Mortensen (2002), Analysing fluorobenzoate tracers in groundwater samples using liquid chromatography–tandem mass spectrometry: A tool for leaching studies and hydrology, *Journal of Chromatography A*, 957(1), 11–16.
- Jury, W. A., G. Sposito, and R. E. White (1986), A transfer-function model of solute transport through soil .1. fundamental-concepts, *Water Resources Research*, 22(2), 243–247.
- Käss, W. (1998), *Tracing techniques in geohydrology*, 581 pp., A.A. Balkema, Rotterdam, Netherlands.

## Bibliography

---

- Kendall, C., and E. A. Caldwell (1998), *Fundamentals of isotope geochemistry*, 870 pp., Elsevier, Amsterdam, The Netherlands.
- Kendall, C., and T. B. Coplen (2001), Distribution of oxygen-18 and deuterium in river waters across the united states, *Hydrological Processes*, 15(7), 1363–1393.
- Kirchner, J., D. Tetzlaff, and C. Soulsby (2010), Comparing chloride and water isotopes as hydrological tracers in two Scottish catchments, *Hydrological Processes*, 24(12), 1631–1645.
- Kirchner, J. W. (2003), A double paradox in catchment hydrology and geochemistry, *Hydrological Processes*, 17(4), 871–874.
- Kirchner, J. W. (2009), Catchments as simple dynamical systems: Catchment characterization, rainfall-runoff modeling, and doing hydrology backward, *Water Resources Research*, 45.
- Kirchner, J. W., and C. Neal (2013), Universal fractal scaling in stream chemistry and its implications for solute transport and water quality trend detection, *Proceedings of the National Academy of Sciences of the United States of America*, 110(30), 12,213–12,218.
- Kirchner, J. W., X. Feng, and C. Neal (2000), Fractal stream chemistry and its implications for contaminant transport in catchments, *Nature*, 403(6769), 524–527.
- Kladivko, E. J., L. C. Brown, and J. L. Baker (2001), Pesticide transport to subsurface tile drains in humid regions of North America, *Critical Reviews in Environmental Science and Technology*, 31(1), 1–62.
- Klein, A., F. Manco, and R. Charles (2007), Pesticides d'origine agricole dans le bassin versant suisse du léman: Campagne 2006, *Tech. rep.*, Commission internationale de protection des eaux du Léman (CIPEL).
- Knisel, W. G. (1980), CREAMS: A field-scale model for chemicals, runoff and erosion from agricultural management systems, *Tech. rep.*, U.S. Dept. Agric. Conserv. Res. Rep., Washington, D.C., USA.
- Koeniger, P., C. Leibundgut, T. Link, and J. D. Marshall (2010), Stable isotopes applied as water tracers in column and field studies, *Organic Geochemistry*, 41(1), 31–40.
- Kreft, A., and A. Zuber (1978), On the physical meaning of the dispersion equation and its solutions for different initial and boundary conditions, *Chemical Engineering Science*, 33(11), 1471–1480.
- Kung, K.-J. S., E. J. Kladivko, T. J. Gish, T. S. Steenhuis, G. Bubenzer, and C. S. Helling (2000), Quantifying preferential flow by breakthrough of sequentially applied tracers silt loam soil, *Soil Sci. Soc. Am. J.*, 64(4), 1296–1304.
- Lam, Q. D., B. Schmalz, and N. Fohrer (2010), Modelling point and diffuse source pollution of nitrate in a rural lowland catchment using the swat model, *Agricultural Water Management*, 97(2), 317–325.



- Larsbo, M., S. Roulier, F. Stenemo, R. Kasteel, and N. Jarvis (2005), An improved dual-permeability model of water flow and solute transport in the vadose zone, *Vadose Zone Journal*, 4(2), 398–406.
- Larsson, M. H., K. Persson, B. Ulén, A. Lindsjö, and N. J. Jarvis (2007), A dual porosity model to quantify phosphorus losses from macroporous soils, *Ecological Modelling*, 205(1–2), 123–134.
- Lasa, J., and I. Śliwka (1990), Application of gas chromatography with electron-capture detection to trace analysis of halogenated compounds, *Journal of Chromatography A*, 509(1), 115–121.
- Leibundgut, C., P. Maloszewski, and C. Külls (2011), *Tracers in Hydrology*, Wiley.
- Leonard, R. A., and W. G. Knisel (1987), Gleams: Groundwater loading effects of agricultural management systems, *Trans, ASAE*, 30(5), 1403–1428.
- Leu, C., H. Singer, C. Stamm, S. R. Müller, and R. P. Schwarzenbach (2004), Simultaneous assessment of sources, processes, and factors influencing herbicide losses to surface waters in a small agricultural catchment, *Environmental Science & Technology*, 38(14), 3827–3834.
- Leu, C., H. Singer, S. R. Müller, R. P. Schwarzenbach, and C. Stamm (2005), Comparison of atrazine losses in three small headwater catchments, *J. Environ. Qual.*, 34(5), 1873–1882.
- Leu, C., M. K. Schneider, and C. Stamm (2010), Estimating catchment vulnerability to diffuse herbicide losses from hydrograph statistics, *J. Environ. Qual.*, 39(4), 1441–1450.
- Leu, C. M. (2003), Sources, processes and factors determining the losses of atrazine, dimethenamid and metolachlor to surface waters : A simultaneous assessment in six agricultural catchments, Phd. thesis, Eidgenössische Technische Hochschule ETH Zürich, Zürich, Switzerland.
- Lindstrom, G., and A. Rodhe (1986), Modeling water exchange and transit times in till basins using oxygen-18, *Nordic Hydrology*, 17(4-5), 325–334.
- Lindström, G., and A. Rodhe (1992), Transit times of water in soil lysimeters from modeling of oxygen-18, *Water, Air, and Soil Pollution*, 65(1-2), 83–100.
- Luo, Y., X. Zhang, X. Liu, D. Ficklin, and M. Zhang (2008), Dynamic modeling of organophosphate pesticide load in surface water in the northern San Joaquin Valley watershed of California, *Environmental Pollution*, 156(3), 1171–1181.
- Ma, J., L. Xu, S. Wang, R. Zheng, S. Jin, S. Huang, and Y. Huang (2002), Toxicity of 40 herbicides to the green alga *Chlorella vulgaris*, *Ecotoxicology and Environmental Safety*, 51(2), 128–132.
- Malone, R. W., L. R. Ahuja, L. Ma, R. Don Wauchope, Q. Ma, and K. W. Rojas (2004), Application of the root zone water quality model (RZWQM) to pesticide fate and transport: an overview, *Pest Management Science*, 60(3), 205–221.

## Bibliography

---

- Maloszewski, P., W. Rauert, P. Trimborn, A. Herrmann, and R. Rau (1992), Isotope hydrological study of mean transit times in an alpine basin (Wimbachtal, Germany), *Journal of Hydrology*, 140(1-4), 343–360.
- Maloszewski, P., H. Moser, W. Stichler, and P. Trimborn (1995), Isotope hydrology investigations in large refuse lysimeters, *Journal of Hydrology*, 167(1–4), 149–166.
- Martinec, J., U. Siegenthaler, H. Oeschger, and E. Tongiorgi ( ), New insights into the run-off mechanism by environmental isotopes, in *Isotope techniques in groundwater hydrology 1974, Vol. I. Proceedings of a symposium*.
- McCarthy, J. F., K. M. Howard, and L. D. McKay (2000), Effect of pH on sorption and transport of fluorobenzoic acid ground water tracers, *J. Environ. Qual.*, 29(6), 1806–1813.
- McDonnell, J. J., and K. Beven (2014), Debates — the future of hydrological sciences: A (common) path forward? a call to action aimed at understanding velocities, celerities and residence time distributions of the headwater hydrograph, *Water Resources Research*, 50(6), 5342–5350.
- McDonnell, J. J., M. Bonell, M. K. Stewart, and A. J. Pearce (1990), Deuterium variations in storm rainfall – implications for stream hydrograph separation, *Water Resources Research*, 26(3), 455–458.
- McDonnell, J. J., K. McGuire, P. Aggarwal, K. J. Beven, D. Biondi, G. Destouni, S. Dunn, A. James, J. Kirchner, P. Kraft, S. Lyon, P. Maloszewski, B. Newman, L. Pfister, A. Rinaldo, A. Rodhe, T. Sayama, J. Seibert, K. Solomon, C. Soulsby, M. Stewart, D. Tetzlaff, C. Tobin, P. Troch, M. Weiler, A. Western, A. Wörman, and S. Wrede (2010), How old is streamwater? open questions in catchment transit time conceptualization, modelling and analysis, *Hydrological Processes*, 24(12), 1745–1754.
- McGuire, K. J., and J. J. McDonnell (2006), A review and evaluation of catchment transit time modeling, *Journal of Hydrology*, 330(3-4), 543–563.
- McGuire, K. J., M. Weiler, and J. J. McDonnell (2007), Integrating tracer experiments with modeling to assess runoff processes and water transit times, *Advances in Water Resources*, 30(4), 824–837.
- McMillan, H., D. Tetzlaff, M. Clark, and C. Soulsby (2012), Do time-variable tracers aid the evaluation of hydrological model structure? a multimodel approach, *Water Resources Research*, 48.
- Merlivat, L. (1978), Molecular diffusivities of  $H_2^{16}O$ ,  $HD^{16}O$  and  $H_2^{18}O$  in gases, *Journal of Chemical Physics*, 69(6), 2864–2871.
- Merlivat, L., and J. Jouzel (1979), Global climatic interpretation of the deuterium-oxygen-18 relationship for precipitation, *Journal of Geophysical Research-Oceans and Atmospheres*, 84(Nc8), 5029–5033.

- Misiak, K., E. Casey, and C. D. Murphy (2011), Factors influencing 4-fluorobenzoate degradation in biofilm cultures of *Pseudomonas Knackmussii* B13, *Water Research*, 45(11), 3512–3520.
- Mortensen, A. P., K. H. Jensen, B. Nilsson, and R. K. Juhler (2004), Multiple tracing experiments in unsaturated fractured clayey till, *Vadose Zone J.*, 3(2), 634–644.
- Motosugi, K., and K. Soda (1983), Microbial degradation of synthetic organochlorine compounds, *Experientia*, 39(11), 1214–1220.
- Neal, C., M. Neal, A. Warrington, A. Avila, J. Pinol, and F. Roda (1992), Stable hydrogen and oxygen isotope studies of rainfall and streamwaters for 2 contrasting holm oak areas of Catalonia, Northeastern Spain, *Journal of Hydrology*, 140(1-4), 163–178.
- Nguyen, L., B. Schaeli, D. Sage, S. Kayal, D. Jeanbourquin, D. A. Barry, and L. Rossi (2009), Vision-based system for the control and measurement of wastewater flow rate in sewer systems, *Water Science and Technology*, 60(9), 2281–2289.
- Niemi, A. J. (1977), Residence time distributions of variable flow processes, *The International Journal of Applied Radiation and Isotopes*, 28(10–11), 855–860.
- Patil, Y., and P. Rao (2014), *Applied Bioremediation—Active and Passive Approaches*, Intech Open Science Online Publishers, Croatia.
- Persson, G. (1995), Willow stand evapotranspiration simulated for Swedish soils, *Agricultural Water Management*, 28(4), 271–293.
- Peters, A., T. Nehls, H. Schonsky, and G. Wessolek (2014), Separating precipitation and evapotranspiration from noise – a new filter routine for high-resolution lysimeter data, *Hydrol. Earth Syst. Sci.*, 18(3), 1189–1198.
- Queloz, P., L. Carraro, P. Benettin, G. Botter, A. Rinaldo, and E. Bertuzzo (2015a), Transport of fluorobenzoate tracers in a vegetated hydrologic control volume: 2. theoretical inferences and modeling, *Water Resources Research*, 51(4), 2793–2806.
- Queloz, P., E. Bertuzzo, L. Carraro, G. Botter, F. Miglietta, P. S. C. Rao, and A. Rinaldo (2015b), Transport of fluorobenzoate tracers in a vegetated hydrologic control volume: 1. experimental results, *Water Resources Research*, 51(4), 2773–2792.
- Rao, P. S. C., R. E. Green, V. Balasubramanian, and Y. Kanehiro (1974), Field study of solute movement in a highly aggregated oxisol with intermittent flooding: Ii. picloram, *J. Environ. Qual.*, 3(3), 197–202.
- Renaud, F. G., C. D. Brown, C. J. Fryer, and A. Walker (2004), A lysimeter experiment to investigate temporal changes in the availability of pesticide residues for leaching, *Environmental Pollution*, 131(1), 81–91.

## Bibliography

---

- Rinaldo, A., and A. Marani (1987), Basin scale model of solute transport, *Water Resources Research*, 23(11), 2107–2118.
- Rinaldo, A., A. Marani, and A. Bellin (1989), On mass response functions, *Water Resources Research*, 25(7), 1603–1617.
- Rinaldo, A., G. Botter, E. Bertuzzo, A. Uccelli, T. Settin, and M. Marani (2006a), Transport at basin scales: 1. theoretical framework, *Hydrol. Earth Syst. Sci.*, 10(1), 19–29.
- Rinaldo, A., G. Botter, E. Bertuzzo, A. Uccelli, T. Settin, and M. Marani (2006b), Transport at basin scales: 2. applications, *Hydrol. Earth Syst. Sci.*, 10(1), 31–48.
- Rinaldo, A., K. J. Beven, E. Bertuzzo, L. Nicotina, J. Davies, A. Fiori, D. Russo, and G. Botter (2011), Catchment travel time distributions and water flow in soils, *Water Resources Research*, 47(7), W07,537.
- Rodhe, A., L. Nyberg, and K. Bishop (1996), Transit times for water in a small till catchment from a step shift in the oxygen-18 content of the water input, *Water Resources Research*, 32(12), 3497–3511.
- Rodriguez-Iturbe, I., and J. B. Valdes (1979), Geomorphologic structure of hydrologic response, *Water Resources Research*, 15(6), 1409–1420.
- Rodriguez-Iturbe, I., A. Porporato, L. Ridolfi, V. Isham, and D. R. Coxi (1999), Probabilistic modelling of water balance at a point: the role of climate, soil and vegetation, *Proceedings of the Royal Society of London. Series A: Mathematical, Physical and Engineering Sciences*, 455(1990), 3789–3805.
- Roth, K., W. A. Jury, H. Fluhler, and W. Attinger (1991), Transport of chloride through an unsaturated field soil, *Water Resources Research*, 27(10), 2533–2541.
- Schaeffer, S., D. Williams, and D. Goodrich (2000), Transpiration of cottonwood/willow forest estimated from sap flux, *Agricultural and Forest Meteorology*, 105(1-3), 257–270.
- Schoen, R., J. P. Gaudet, and T. Bariac (1999a), Preferential flow and solute transport in a large lysimeter, under controlled boundary conditions, *Journal of Hydrology*, 215(1-4), 70–81.
- Schoen, R., J. P. Gaudet, and D. E. Elrick (1999b), Modelling of solute transport in a large undisturbed lysimeter, during steady-state water flux, *Journal of Hydrology*, 215(1–4), 82–93.
- Schrader, F., W. Durner, J. Fank, S. Gebler, T. Pütz, M. Hannes, and U. Wollschläger (2013), Estimating precipitation and actual evapotranspiration from precision lysimeter measurements, *Procedia Environmental Sciences*, 19(0), 543–552.
- Schudel, B., D. Biaggi, T. Dervev, R. Kozel, I. Müller, J. Ross, and U. Schindler (2002), Utilisation des traceurs artificiels en hydrogéologie – Guide pratique, *Rapp. OFEG, Sér. Géol.*, 3.

- Seeger, S., and M. Weiler (2014), Lumped convolution integral models revisited: on the meaningfulness of inter catchment comparisons, *Hydrol. Earth Syst. Sci. Discuss.*, 11(6), 6753–6803.
- Serres-Piole, C., A. Commarieu, H. Garraud, R. Lobinski, and H. Preud'homme (2011), New passive water tracers for oil field applications, *Energy & Fuels*, 25(10), 4488–4496.
- Setegn, S. G., R. Srinivasan, A. M. Melesse, and B. Dargahi (2010), SWAT model application and prediction uncertainty analysis in the Lake Tana Basin, Ethiopia, *Hydrological Processes*, 24(3), 357–367.
- Sherman, L. K. (1932), Streamflow from rainfall by the unit-graph method, *Eng. News Record*, 108, 501–505.
- Siber, R., C. Stamm, and P. Reichert (2009), Modeling potential herbicide loss to surface waters on the Swiss plateau, *Journal of Environmental Management*, 91(1), 290–302.
- Simic, E., and G. Destouni (1999), Water and solute residence times in a catchment: Stochastic-mechanistic model interpretation of  $^{18}O$  transport, *Water Resources Research*, 35(7), 2109–2119.
- Simunek, J., K. Huang, and M. T. van Genuchten (1998), The HYDRUS code for simulating the one-dimensional movement of water, heat, and multiple solutes in variably-saturated media. version 6.0, *Tech. rep.*, USDA, ARS, Riverside, CA, USA.
- Sklash, M. G., and R. N. Farvolden (1979), The role of groundwater in storm runoff, *Developments in Water Science*, 12, 45–65.
- Soulsby, C., J. Petry, M. J. Brewer, S. M. Dunn, B. Ott, and I. A. Malcolm (2003), Identifying and assessing uncertainty in hydrological pathways: a novel approach to end member mixing in a Scottish agricultural catchment, *Journal of Hydrology*, 274(1–4), 109–128.
- Squillace, P. J., and E. M. Thurman (1992), Herbicide transport in rivers: importance of hydrology and geochemistry in nonpoint-source contamination, *Environmental Science & Technology*, 26(3), 538–545.
- Stalder, P. (2012), Identification des sources de pesticides agricoles dans le bassin versant de la Chamberonne, *Semester project*, EPFL, Lausanne, Switzerland.
- Stamm, C., R. Sermet, J. Leuenberger, H. Wunderli, H. Wydler, H. Flühler, and M. Gehre (2002), Multiple tracing of fast solute transport in a drained grassland soil, *Geoderma*, 109(3–4), 245–268.
- Stetzenbach, K. J., S. L. Jensen, and G. M. Thompson (1982), Trace enrichment of fluorinated organic acids used as ground-water tracers by liquid chromatography, *Environmental Science & Technology*, 16(5), 250–254.

## Bibliography

---

- Stewart, M. K., and J. J. McDonnell (1991), Modeling base flow soil water residence times from deuterium concentrations, *Water Resources Research*, 27(10), 2681–2693.
- Stumpp, C., W. Stichler, and P. Maloszewski (2009a), Application of the environmental isotope  $\delta^{18}\text{O}$  to study water flow in unsaturated soils planted with different crops: Case study of a weighable lysimeter from the research field in Neuherberg, Germany, *Journal of Hydrology*, 368(1-4), 68–78.
- Stumpp, C., P. Maloszewski, W. Stichler, and J. Fank (2009b), Environmental isotope ( $\delta^{18}\text{O}$ ) and hydrological data to assess water flow in unsaturated soils planted with different crops: Case study lysimeter station “Wagna” (Austria), *Journal of Hydrology*, 369(1–2), 198–208.
- Stumpp, C., G. Nützmann, S. Maciejewski, and P. Maloszewski (2009c), A comparative modeling study of a dual tracer experiment in a large lysimeter under atmospheric conditions, *Journal of Hydrology*, 375(3–4), 566–577.
- Susarla, S., V. F. Medina, and S. C. McCutcheon (2002), Phytoremediation: An ecological solution to organic chemical contamination, *Ecological Engineering*, 18(5), 647–658.
- Talebizadeh, M., S. Morid, S. Ayyoubzadeh, and M. Ghasemzadeh (2010), Uncertainty analysis in sediment load modeling using ANN and SWAT model, *Water Resources Management*, 24(9), 1747–1761.
- Tiktak, A., J. J. T. I. Boesten, A. M. A. van der Linden, and M. Vanclouster (2006), Mapping ground water vulnerability to pesticide leaching with a process-based metamodel of EuroPEARL, *J. Environ. Qual.*, 35(4), 1213–1226.
- Topp, G. C., J. L. Davis, and A. P. Annan (1980), Electromagnetic determination of soil-water content - measurements in coaxial transmission-lines, *Water Resources Research*, 16(3), 574–582.
- Treydte, K., S. Boda, E. Graf Pannatier, P. Fonti, D. Frank, B. Ullrich, M. Saurer, R. Siegwolf, G. Battipaglia, W. Werner, and A. Gessler (2014), Seasonal transfer of oxygen isotopes from precipitation and soil to the tree ring: source water versus needle water enrichment, *New Phytologist*, pp. n/a–n/a.
- Vallotton, N., R. Eggen, and N. Chèvre (2009), Effect of sequential isoproturon pulse exposure on *Scenedesmus vacuolatus*, *Archives of Environmental Contamination and Toxicology*, 56(3), 442–449.
- van der Velde, Y., G. H. de Rooij, J. C. Rozemeijer, F. C. van Geer, and H. P. Broers (2010), Nitrate response of a lowland catchment: On the relation between stream concentration and travel time distribution dynamics, *Water Resources Research*, 46.
- van der Velde, Y., P. J. J. F. Torfs, S. E. A. T. M. van der Zee, and R. Uijlenhoet (2012), Quantifying catchment-scale mixing and its effect on time-varying travel time distributions, *Water Resources Research*, 48(6), W06,536.

- van der Velde, Y., I. Heidbüchel, S. W. Lyon, L. Nyberg, A. Rodhe, K. Bishop, and P. A. Troch (2014), Consequences of mixing assumptions for time-variable travel time distributions, *Hydrological Processes*, pp. n/a–n/a.
- Vargas, C., B. Song, M. Camps, and M. M. Häggblom (2000), Anaerobic degradation of fluorinated aromatic compounds, *Applied Microbiology and Biotechnology*, 53(3), 342–347.
- Vrchotová, B., P. Lovecká, M. Drazková, M. Macková, and T. Macek (2013), Influence of root exudates on the bacterial degradation of chlorobenzoic acids, *The Scientific World Journal*, 2013, 8.
- Weidmann, M. (1988), Carte géologique de la Suisse 1:25'000: 85 Lausanne (CN 1243).
- Weiler, M., and J. J. McDonnell (2006), Testing nutrient flushing hypotheses at the hillslope scale: A virtual experiment approach, *Journal of Hydrology*, 319(1–4), 339–356.
- Weiler, M., B. L. McGlynn, K. J. McGuire, and J. J. McDonnell (2003), How does rainfall become runoff? a combined tracer and runoff transfer function approach, *Water Resources Research*, 39(11), 1315.
- Winton, K., and J. B. Weber (1996), A review of field lysimeter studies to describe the environmental fate of pesticides, *Weed Technology*, 10(1), 202–209.
- Wolock, D. M., J. Fan, and G. B. Lawrence (1997), Effects of basin size on low-flow stream chemistry and subsurface contact time in the Neversink River watershed, New York, *Hydrological Processes*, 11(9), 1273–1286.
- Zanardo, S., N. B. Basu, G. Botter, A. Rinaldo, and P. S. C. Rao (2012), Dominant controls on pesticide transport from tile to catchment scale: Lessons from a minimalist model, *Water Resources Research*, 48(4), W04,525.
- Zaitsev, G. M., and I. Karasevich (1981), Utilization of 4-chlorobenzoic acid by *Arthrobacter globiformis*, *Mikrobiologiya*, 50(1), 35–40.
- Zhang, L., W. R. Dawes, P. G. Slavich, W. S. Meyer, P. J. Thorburn, D. J. Smith, and G. R. Walker (1999), Growth and ground water uptake responses of lucerne to changes in groundwater levels and salinity: lysimeter, isotope and modelling studies, *Agricultural Water Management*, 39(2–3), 265–282.





## List of peer-reviewed publications

Queloz, P., E. Bertuzzo, L. Carraro, G. Botter, F. Miglietta, P. S. C. Rao, and A. Rinaldo (2015), Transport of fluorobenzoate tracers in a vegetated hydrologic control volume: 1. Experimental results, *Water Resources Research*, 51(4), 2773–2792, doi:10.1002/2014WR016433.

Queloz, P., L. Carraro, P. Benettin, G. Botter, A. Rinaldo, and E. Bertuzzo (2015), Transport of fluorobenzoate tracers in a vegetated hydrologic control volume: 2. Theoretical inferences and modeling, *Water Resources Research*, 51(4), 2793–2806, doi:10.1002/2014WR016508

Rossi, L., P. Queloz, A. Brovelli, J. Margot, and D. A. Barry (2013), Enhancement of Micropollutant Degradation at the Outlet of Small Wastewater Treatment Plants, *Plos One*, 8(3), doi:10.1371/journal.pone.0058864.

Coutu, S., T. Pouchon, P. Queloz, and N. Vernaz (2015), Integrated stochastic modeling of pharmaceuticals in sewage networks, *Stochastic Environmental Research and Risk Assessment*, Accepted Author Manuscript.

## Conference proceedings

Queloz, P., L. Carraro, E. Bertuzzo, G. Botter, P. S. C. Rao, and A. Rinaldo (2014). Non-stationarity of solute travel time distribution observed in a controlled hydrologic transport volume. Oral presentation at American Geophysical Union (AGU) Fall meeting, San Francisco, California, USA, December 15–19, 2014.

Queloz, P., L. Carraro, E. Bertuzzo, G. Botter, P. S. C. Rao, and A. Rinaldo (2014). Non-stationarity in experimental travel time measured in a lysimeter: theoretical and modeling lessons from a simplified hydrological system. Poster presented at European Geosciences Union (EGU) General Assembly, Vienna, Austria, April 27–May 02, 2014.

Queloz, P., E. Bertuzzo, G. Botter, P. S. C. Rao, and A. Rinaldo (2013). Tracer breakthrough curves in a complex lysimeter system: evidence of non-stationary transport. Poster presented at American Geophysical Union (AGU) Fall meeting, San Francisco, California, USA, December 9–13, 2013.

Queloz, P., E. Bertuzzo, B. Schaefli, G. Botter, and A. Rinaldo (2013). Herbicide export dynamics of a mid-sized lake tributary: lessons from observations and modeling. Poster presented at the 11th Swiss Geoscience Meeting, Lausanne, Switzerland, November 15–16, 2013.

Queloz, P., J. Besuchet, P. S. C. Rao, and A. Rinaldo (2013). Development of a low-cost wireless controller for flexible sampling strategies based on real-time flow monitoring. Poster presented at European Geosciences Union (EGU) General Assembly, Vienna, Austria, April 7–12, 2013.

Queloz, P., P. S. C. Rao, and A. Rinaldo (2012). Non-stationary hydrologic transport in the vadose zone: experimental results of multiple tracer injections in lysimeters. Poster presented at American Geophysical Union (AGU) Fall meeting, San Francisco, California, USA, December 3–7, 2012.

## **Workshops and trainings**

Labview Core 1&2, *National Instruments Switzerland Corp.*, Ecole polytechnique fédérale de Lausanne, Switzerland. October 22–26, 2012.

Third annual Catchment Science Summer School, *University of Aberdeen*, Aberdeen, Scotland. August 19–24, 2012.

## **Teaching activities**

Teaching assistant for the course Hydrology for Engineer (Prof. Andrea Rinaldo) for Civil and Environmental Engineering 3rd-year students at EPFL. Fall semesters 2012–2013, 2013–2014, 2014–2015.

Teaching assistant for Probabilités et Statistiques (Prof. Victor Panaretos) for Civil and Environmental Engineering 2nd-year students at EPFL. Spring semester 2012.

The mountains are calling and I must go.

— John Muir



## Pierre Queloz

Blancherie 17  
CH-1022 Chavannes-Renens  
☎ +41 76 541 55 49  
✉ pierre.queloz@gmail.com

7 June 1986  
Swiss



## WORK EXPERIENCE

---

- 2011 - 2015** **Laboratory of Ecohydrology (ECHO), Swiss Federal Institute of Technology of Lausanne (EPFL)**  
*PhD, research assistant*  
Catchment-scale hydrologic transport of herbicides: theory, observations, ecological risk assessment  
*Hydrologic monitoring and data acquisition, water sampling, tracing techniques, river gaging, chemical analysis, hydrological modeling, supervision of undergraduate students and civilists, teaching assistant for the course 'Hydrology for engineers', international conferences, scientific writing, presentation of research activities to students/schoolers*
- Oct. 2010 - Apr. 2011** **Ecological Engineering Laboratory (ECOL), EPFL and Lausanne University**  
*Civil service*  
Investigation of micropollutants degradation in engineered constructed wetlands  
*Micropollutants extraction and analysis, lab-scale experimentation, water treatment technologies*
- May 2010 - Aug. 2010** **Swiss Federal Office for the Environment (FOEN), Bern**  
*Civil service*  
Section Innovation (environmental research and environmental technology promotion)  
*Environmental technologies in Switzerland (clean-/green- tech), project assessment, environmental research master plan*
- Aug. 2009 - Sept. 2009** **Institute of Geophysics, University of Lausanne**  
*Civil service*  
Georadar data processing, piloting of the research vessel for lacustrine seismic data acquisition  
*Geophysical techniques, data acquisition, program development for GPR data*
- Juil. 2008 - Juil. 2009** **ATB-SA Ingénieurs-conseils SIA USIC, Moutier**  
*Internship*  
Implementation of the new standard STORM (VSA) on wastewater discharges for water drainage program  
Concept and design of a constructed wetland for runoff treatment in a construction waste sorting plant
- Aug. 2007 - Sept. 2007** **Swiss Biological Records Center (CSCF in French), Neuchâtel**  
*Civil service*  
Scientific collaborator for the GBIF project (Global Biodiversity Information Facility)  
*Databases, geographic information systems, geographic thesauri*
- 2005 - 2007** **Bureau technique Jean-Bernard Queloz, official land surveyor, Saignelégier**  
Webmaster, creation of an online map extracts order system (PHP), mensuration campaigns

## EDUCATION

---

- 2011 - 2015** **PhD candidate, Laboratory of Ecohydrology (ECHO), EPFL**  
Civil and Environmental Engineering Doctoral program (EDCE). Supervisor Prof. Andrea Rinaldo.
- 2007 - 2010** **Master of Science MSc in Environmental Sciences and Engineering (SSIE), EPFL**  
Specialization "Water, soils and ecosystems engineering"  
Master thesis on the degradation of micropollutants in engineered constructed wetlands (ECOL laboratory)
- 2006 - 2007** **Erasmus exchange « Environmental Engineering and Sustainable Infrastructure »**  
Royal Institute of Technology (KTH), Stockholm
- 2004 - 2007** **Bachelor of Science BSc in Environmental Sciences and Engineering (SSIE), EPFL**
- 2001 - 2004** **High school scientific diploma (biology-chemistry), Lycée Blaise-Cendrars, La Chaux-de-Fonds**  
Distinction very good, Rotary prize in experimental sciences, SIA prize for diploma thesis



## ACTIVITIES

---

- 2006 - 2007** **Coordinator for SeminApero, Doctoral school in Civil and Environmental Engineering, EPFL**  
Networking event for PhD students with short scientific presentations and buffet
- Polyathlon 2009, 2010, 2011**  
High altitude raid (cross running, cycling, swimming and ski-mountaineering)
- Patrouille des glaciers 2010, 2014**  
International ski mountaineering race, Zermatt-Verbier (Switzerland)
- Since 2012** **Keelboat racing on Lake Geneva**
- 2007 - 2013** **Member of Xchange EPFL committee (ESN—Erasmus Student Network)**  
President of the association
- 2005 - 2006** **Member of EPFL coaching**, coaching certificate (2006)
- Aug. 2005** **Volunteering for mountain farmers (Caritas), Cadenazzo, Switzerland**
- Aug. 2004** **Volunteering for the Service Civil International (SCI), Dreilützw, Germany**  
Upkeep work in a castle for Caritas and events organization for underprivileged children

## LANGUAGE SKILLS

---

<b>French</b>	Mother tongue
<b>German</b>	Spoken (B1) and written (B2)
<b>English</b>	Spoken and written (C1)
<b>Swedish</b>	Basic skills (A2)

## COMPUTER SKILLS

---

MS-Office (incl. Access), LaTeX, ArcGIS, MicroStation, Matlab, R, Aquasim, ASIM, hydro(geo)logical modeling, LabView (Core 1 and 2 certificates), basic skills in Java, HTML, PHP and microcontrollers

**References upon request**

